AN EXPERIMENTAL STUDY OF CONVECTIVE HEAT TRANSFER, FRICTION, AND RHEOLOGY FOR NON-NEWTONIAN FLUIDS: POLYMER SOLUTIONS, SUSPENSIONS OF FIBERS, AND SUSPENSIONS OF PARTICULATES

Thesis by

Eric Francois Matthys

In Partial Fulfillment

of the Requirements for the Degree of

Doctor of Philosophy

Division of Engineering and Applied Science

California Institute of Technology

Pasadena, California 91125

1985

(Submitted May 13, 1985)

ACKNOWLEDGMENTS

First I would like to thank my advisor, Professor R. Sabersky, whose support, patience, and encouragements were limitless over these years. He taught me a lot about research, about teaching, about learning, and, most importantly, about people. Thanks also to Professors A. Acosta and C. Brennen, who were always ready to help when they were needed. All three were educators and friends, not just supervisors. Thanks to all the other members of the Faculty, for the knowledge they are so willing to share, and for making Caltech such a very special place to work in. I would not have made it this far without all of them.

Thanks to Dr. V. Sarohia of the Jet Propulsion Laboratory, who made it possible for me to build the experimental installation in his facilities. This might have been a theoretical thesis without his total support. Thanks also to Drs. P. Parikh, and A. Yavrouian for their help and expertise on AMK mixing and degradation; to Drs. Y. Cho and D. Dipprey for their interest in this project; and to Messrs. W. Bixler, J. Godley, B. Green, S. Kikkert, and R. Smither for their fine shop work.

Thanks to Professor A. Jaumotte of the "Universite Libre de Bruxelles" for encouraging me to pursue Ph.D. studies and providing his continuous support ever since. I would not have been able to start without him.

Thanks to Mr. H. Ahn, for his help with the acquisition of data. I would still be running around the lab without him.

Thanks to my good buddies Drs. L. d'Agostino, B. Jery, and S. Patton

for sharing the good times and huddling when the going got tough. These years would have been far less enjoyable without them.

Thanks to Ms. S. Berkeley and M. Haddad for their great help with word processing, and to Ms. C. Lin and N. Tomer for their fine illustrations. This prose (sic) would still be only a twinkle in the screen of this computer without them.

Thanks to Messrs. J. Cullen and J. Grenard from Carnation Research Laboratory, and to Dr. T. Nguyen from Chevron Oil Field Research Company for supplying some of the test materials.

Last, but most important as the reader doubtlessly knows, financial assistance by the U.S. Federal Aviation Administration, the California Institute of Technology, and the "Fonds National de la Recherche Scientifique" is gratefully acknowledged.

ABSTRACT

An experimental investigation was conducted on the convective heat transfer, friction, and rheological properties of various types of non-newtonian fluids in circular tube flows.

If an apparent Reynolds number is used and if the temperature and degradation effects are properly taken into account, the reduced turbulent friction and heat transfer results, respectively, are then shown to be well correlated by the same expressions for different fluids, regardless of the nature of the fluids and whether they are shear-thinning or shear-thickening. This representation can also separate the reductions in turbulent heat transfer and friction that are induced by viscoelasticity from those induced by pseudoplasticity.

Polyacrylamide solutions inducing asymptotic and intermediate drag reduction regimes were investigated over a broad range of Reynolds numbers. The minimum heat transfer asymptote was determined for fully-developed conditions and for the very long (up to x/D=600) entrance region observed. Solutions subjected to various degrees of intentional pre-degradation were studied to separate this effect from that of the degradation induced in the test tube itself.

A kerosene-based antimisting polymer solution was also studied. It was found to exhibit a complex viscous behavior involving time-dependency, shear-thickening beyond a critical shear rate, high susceptibility to degradation, and large sensitivity to temperature variations. The unusual friction and heat transfer results obtained with this fluid

were, however, reduced to simple correlations for asymptotic drag reduction if an appropriate computational model is used.

Suspensions of bentonite of various concentrations were investigated in laminar and turbulent regimes, and the results for fully-developed and entrance flows were well correlated by newtonian relationships when an adequate wall viscosity concept was used. A combination of bentonite and polymer was found to be unusually susceptible to mechanical degradation, which affected significantly the viscosity and the level of drag and heat transfer reductions obtained.

A suspension of organic pulp based on tomato puree was shown to exhibit up to 40% of viscoelastic-type reduction in heat transfer and friction coefficients with respect to newtonian fluids in the turbulent regime. For laminar flow, however, these coefficients were larger than expected. Combinations of pulp and polymer were investigated as well.

A method was developed to predict the "diameter effect" for viscoelastic fluids.

TABLE OF CONTENTS

LIST OF FIGURES

NOMENCLATURE

A_m: Parameter (eq. 3.51)

A_t: Cross-sectional area of test tube wall (eq. B.6) [m^2]

A_0, A_1: Polynomial coefficients (eq. 4.3)

a: Reduced thermal conductivity (eq. A.7) [$W/m°K$]

a': Temperature coefficient for thermal conductivity (eq. A.7) [$°C^{-1}$]

B: Arrhenius-type exponent (eq. 4.5) [$°K^{-1}$]

b: Parameter (eq. 3.60)

b: Reduced electrical conductivity (eq. A.8) [Ohm m]

b': Temperature coefficient for electrical conductivity (eq. A.8) [$°C^{-1}$]

C_f: Friction coefficient (eq. 3.9)

$C_H = h/\rho Cp V$: Stanton number

Cp: Specific heat capacity [$Ws/kg°K$]

D: Diameter [m]

$De = \lambda V^2/\nu$: Deborah number

DF: Damping factor (eq. 3.42)

f(x/D): Entrance correction factor (eq. 5.21)

Gz: Graetz number (eq. 3.55)

g = 9.81:	Gravity acceleration [m/s^2]
H_t:	Height of liquid in tank (eq. B.9) [m]
h:	Film coefficient (eq. 3.50) [$W/m^{2\circ}K$]
I:	Current intensity through the tube walls [A]
$j_H = C_H Pr^{2/3}$:	Colburn factor
K:	Consistency (eq. 3.2) [$N(s)^n/m^2$]
K:	Constant in Prandtl mixing length theory (eq. 3.19)
K':	Consistency (eq. 3.24) [$N(s)^{n'}/m^2$]
k:	Thermal conductivity [$W/m^\circ K$]
L:	Length of tube or capillary [m]
L_e:	Entrance length (eq. 3.11) [m]
$\dot{L}$:	Linear displacement of piston (eq. B.2) [m/s]
ℓ:	Prandtl mixing length (eq. 3.19) [m]
m:	Various Prandtl number exponents in Colburn factor (for graphs)
m:	Constant in Deissler's expression (eq. 3.20)
m:	Summation index (eq. 3.51)
m:	Sieder and Tate's correction exponent (eq. 3.68)
$\dot{m}$:	Mass flow rate [kg/m^3]
Nu:	Nusselt number (eq. 3.49)

Nu_∞: Fully-developed Nusselt number (eq. 3.48)

n: Power-law exponent (eq. 3.2)

n': Power-law exponent (eq. 3.24)

P: Electric heating power [W]

Pe: Peclet number (eq. 3.71)

$Pr = \eta\, Cp / k$: Prandtl number

Pr': Generalized Prandtl number (eq. 3.72)

Pr_a: Apparent Prandtl number (eq. 3.73)

Pr_t: Turbulent Prandtl number (eq. 3.57)

p_a: Atmospheric pressure (eq. B.9) [N/m^2]

p_ℓ: Heat production per unit length (eq. A.11) [W/m]

p_t: Pressure in the tank (eq. B.9) [N/m^2]

Q: Heat source per unit volume (eq. A.1) [W/m^3]

$\dot{Q}$: Volumetric flow rate from pump (eq. B.1) [m^3/s]

q: Heat flux [W/m^2]

R=8314 Gas constant [$J/kmole\ °K$]

Re: Reynolds number (eq. 3.8)

Re_a: Apparent Reynold number (eq. 3.35)

Re': Generalized Reynolds number (eq. 3.31)

R_{el}: Total electrical resistance of test tube [ohm]

RPM: Speed of motor [rev. per min.]

r: Radius [m]

$St = h / \rho\, Cp\, V$: Stanton number

T: Temperature [$^{\circ}C$]

T^{+}: Reduced temperature (eq. 3.59)

$\overline{T}$: Local time-averaged temperature in turbulent flow [$^{\circ}K$]

u_{max}: Centerline velocity [m/s]

$u_{\tau} = (\tau_w / \rho)^{\frac{1}{2}}$: Shear velocity [m/s]

$u^{+} = u / u_{\tau}$: Velocity in the law of the wall representation

$\overline{u}$: Local time-averaged velocity in turbulent flow [m/s]

V: Average velocity [m/s]

V: Voltage drop along the test tube [V]

We: Weissenberg number (eq. 3.47)

x: Distance from the entry of the pipe [m]

x^{+}: Non-dimensional distance (eq. 3.52)

$\dot{x}_p$: Displacement speed of piston (eq. B.12) [m/s]

x_v: Volume fraction (eq. 3.74)

y: Distance from the wall [m]

$y^{+} = y\, u_{\tau} / \nu$: Distance from the wall in the law of the wall representation

Greek symbols

$\alpha = k / \rho\, Cp$: Thermal diffusivity [m^2/s]

α: Damping factor parameter (eq. 3.43)

$\dot{\gamma}$: Shear rate (eq. 3.1) [s^{-1}]

$\dot{\gamma}_c$: Critical shear rate for AMK [s^{-1}]

γ_m: Parameter (eq. 3.51)

$\dot{\gamma}_n$: Newtonian laminar wall shear rate (eq. 4.2) [s^{-1}]

ΔE: Activation energy (eq. 5.7) [W s/mole]

Δu^+: Shift in logarithmic profile (eq. 3.40)

Δp: Pressure drop [N/m^2]

ε_M: Eddy diffusivity for momentum (eq. 3.18) [m^2/s]

ε_H: Eddy diffusivity for heat (eq. 3.56) [m^2/s]

ζ: Factor (eq. A.14) [W/m]

η: Dynamic viscosity (eq. 3.1) [Ns/m^2]

η_a: Apparent viscosity (eq. 3.34) [Ns/m^2]

$\eta_{eff} = \nu_{eff}\, \rho$: Effective dynamic viscosity (eq. 4.5) [Ns/m^2]

η_∞: Parameter (eq. 3.6) [Ns/m^2]

η_{ref}: Reference viscosity (eq. 4.5) [Ns/m^2]

η_0: Parameter (eq. 3.5) [Ns/m^2]

λ: Relaxation time (eq. 3.5) [s]

$\nu=\eta/\rho$: Kinematic viscosity [m^2/s]

$\nu_{eff}=\tau_w/\rho(8V/D)$: Effective viscosity [$m^2/s$]

ξ: Factor (eq. A.10) [$°K$]

ρ: Density [kg/m^3]

ρ_{el}: Electrical resistivity of stainless steel (eq. A.8) [ohm m]

τ: Shear stress (eq. 3.1) [N/m^2]

τ_0: Yield stress (eq. 3.4) [N/m^2]

Subscripts

a: In the apparent Reynolds number representation

b: Bulk of the fluid

c: Capillary

el: Electrical

ent: At the entry

ex: At the exit

f: Film

i: Inside wall

m: At midlength of test tube

o: Outside wall

par: Particulate

s: Solvent

ss: Stainless steel

sus: Suspension

w: At the wall

x: At a given position x

Superscripts

': In the generalized Reynolds number representation

+: Law of the wall representation

Abbreviations

AC: Alternating current

A/D: Analog to digital

AISI: American Iron and Steel Institute

AMK: Antimisting kerosene

AM-1: Polymeric additive (by Conoco)

AP-273: Polyacrylamide (by Dow Chemicals)

API: American Petroleum Institute

ASTM: American Society for Testing and Materials

AVGARD: Base slurry for AMK (by Imperial Chemical Industries)

Avtur: Aviation kerosene

DC: Direct current

e.e.: Estimated error

FM-4: Polymeric additive (by Shell)

FM-9: Base polymer for AMK (by Imperial Chemical Industries)

IC: Integrated circuit

ID: Inside diameter

JA: Jet A (commercial aviation kerosene)

JP-8: Military aviation kerosene

LED: Light-emitting diode

NBS: National Bureau of Standards

OD: Outside diameter

PAA: Polyacrylamide

ppm: Parts per million

RPM: Rotational speed of main motor

ROM: Read-only-memory

SEPARAN: Polyacrylamide (by Dow Chemicals)

s.d.: Standard deviation

T: Tomato puree (6% solids content)

T+20: Combination of tomato (6% solids) and 20 ppm of PAA

T+200: Combination of tomato (6% solids) and 200 ppm of PAA

WT: Wall thickness

Chapter 1.

INTRODUCTION

1.1 THE DRAG REDUCTION PHENOMENON

A large number of research projects have been conducted during the past decade on the subject of non-newtonian Fluid Mechanics. To a large extent this activity was initially motivated by the intriguing and very promising field of drag-reducing solutions. These solutions, in particular the polymeric ones, do indeed pose a particular challenge to the classical (newtonian) fluid mechanicist. The addition of very small quantities of macromolecular agents, for example, may change dramatically the momentum and heat transfer characteristics of a newtonian solvent. The magnitude of these changes, especially in view of the small quantity of solute needed, makes the phenomenon appear particularly interesting, both for practical purposes and for the new information it may add to the current understanding of turbulence mechanisms.

The reduction in drag being only apparent in turbulent flow, it was clear from the start that the influence of the polymer is of a dynamic nature, rather than being a simple modification of the material properties of the fluid. In an approach similar to that adopted for newtonian flows, studies were conducted aiming at the direct measurement of velocity profiles in the layers very close to the walls. These studies appeared to confirm the hypothesis that the macromolecules might modify the turbulence spectra in that region. A model was also proposed, introduc-

ing an additional "elastic" layer between the viscous layer and the logarithmic velocity profile in the "law of the wall" representation.

A correlation was noted between the drag-reduction phenomenon and the viscoelastic character of the solutions. It was then natural indeed to suspect that some of the energy dissipated or transported by the vortices might be somehow affected by the 'elastic' macromolecules, thereby reducing the heat and momentum transfer with respect to the newtonian flows.

One particularly fascinating aspect of this phenomenon is its asymptotic nature : it was shown that there apparently exists a finite limit to the amount by which it is possible to reduce friction in pipes when increasing the concentration of polymer. Furthermore, this limit appears independent of the nature of the polymer if expressed in terms of the Reynolds number and friction coefficient. This asymptote apparently corresponds to the case when, as the concentration is increased, the elastic layer is thickened to the point where it occupies the whole center of the pipe, having eliminated the logarithmic layer altogether.

In parallel with these experimental studies, various mechanistic models were introduced, trying to explain and predict the behavior of these solutions in terms of characteristic times or lengths. Theoretical investigations of individual elastic interactions between coupled molecules or between molecules and vortices were also conducted. Most of these models are complex and usually involve parameters that are not

directly accessible to the experimenter, making the comparison between theory and experiment difficult.

The experimental data themselves usually show a large scatter and significant differences between studies. The highly efficient solutions are indeed very sensitive to factors such as aging, mechanical degradation, mode of preparation, and solvent effects. Contrarily to newtonian fluids, the drag-reducing solutions also exhibit a strong non-linear 'diameter effect', whereby the friction laws are still a function of the diameter of the pipe used for the measurements, even when expressed in function of Reynolds numbers.

The situation at the present time is that, even with sophisticated rheological measurements of the viscoelastic characteristics of these fluids, one is not yet able to predict adequately their behavior. One would clearly hope for some practical correlation that would allow an engineering-type approach to prediction and design. This is presently only possible, to a limited extent, for the solutions that do clearly fall in the asymptotic regime.

1.2. HEAT TRANSFER REDUCTION

As far as the heat transfer goes, one is faced with even more difficulties. Experimental studies showed that typical drag-reducing solutions exhibit a proportionally larger decrease in heat transfer than in friction, when compared to the well-known newtonian relationships. This phenomenon may be interpreted as being in contradiction with the classical Reynolds analogy. The discrepancy has led to some speculation,

and has complicated the still incomplete search for a definitive explanation of what is causing the drag-reduction phenomenon.

One has to be careful, however, when analyzing the experimental heat transfer data. Even for newtonian fluids, heat transfer measurements are usually far less accurate than friction measurements, ten percent accuracy being often considered satisfactory for the former. In the case of our solutions, the problem is particularly complex. Their non-newtonian characteristics, such as the shear rate/viscosity relationships for example, allow for the definition of several different Reynolds and Prandtl numbers, making the comparison with newtonian results sometimes difficult.

Not only are there relatively few existing heat transfer studies, but their validity is also hard to ascertain because of difficulties in reproducing the experimental results. It has been suggested recently, for example, that most of the earlier studies yielded results pertaining to still-developing flows. The entrance regions are indeed unexpectedly much longer for viscoelastic drag-reducing solutions than they are for newtonian fluids. A typical solution inducing asymptotic conditions, for example, might well need 500 diameters or more before the heat transfer may be considered fully-developed.

This implies that a large portion of the data previously collected is not directly usable for formulating general relationships. Relevant data are thus in limited supply, especially if one considers that the information needed for comparison with models, such as characteristic times or

shear rate/viscosity relationships, is usually unavailable.

Additionally, heat transfer studies were often conducted in the recirculation mode to avoid the use of prohibitively large quantities of material if a thermal steady state is desired for a large setup at high Reynolds numbers. Unfortunately, the pumped loop mode also implies greater mechanical degradation, and although this aspect is of practical importance and needs to be studied, one has to be careful to take it into account in order to produce meaningful data. The simultaneous measurement of friction and heat transfer at the same location, for example, is a must in that case.

This problem of relative scarcity of data for heat transfer of non-newtonian fluids of the drag-reducing type is of high importance to scientists and engineers dealing with these fluids. In particular, whereas considerable attention has been paid to the friction asymptote, researchers have started only very recently to study the corresponding heat transfer asymptote under adequate conditions.

1.3. **TEST FLUIDS**

Synthetic polymer solutions have become a standard tool for the study of drag-reducing phenomena, and accordingly, some of these solutions were included as test fluids. Not only was it hoped to be able to gather some information on the heat transfer asymptote, but it was also desired to conduct a detailed investigation of the results using computational tools that allow variations and combinations of parameters (such as temperature, viscosity definition, degradation, and Reynolds number

representation) usually not considered explicitly. It was thought that an analysis of the individual effect of these parameters on the overall results might lead to information that could possibly be applied as well to existing data obtained with simpler computational methods. Additionally, the results for these polymer solutions could also provide a reference for the analysis of the experimental data obtained for the other lesser-known fluids studied during this project.

It is clear that whereas monotype polymer solutions are a convenient medium for study of non-newtonian effects, they are also a somewhat limited set of fluids. Many of the fluids that may exhibit similar effects in real life have not only been far less studied but usually are of a more complicated nature and will also present a less predictable behavior.

Accordingly, a major thrust of this research project was directed towards experimental investigation of fluids that have been very little, or not at all, studied in the past. It was thought to be of interest to find out whether some of these fluids would indeed exhibit characteristics similar to those of the synthetic polymer solutions, or conversely, in what respect they might differ. The distinctive character of additional fluids such as suspensions of particles or fibers might also provide some information on the fundamental nature of the drag-reducing process.

1.3.1. **Polyacrylamide Solutions**

As representative of the synthetic polymer class, aqueous solutions of polyacrylamide were chosen. This particular polymer has been studied intensively in the past along with polyethylene oxide, but is usually

considered to be more resistant to mechanical degradation than the latter, and consequently gives more reproducible results.

Two types of solutions were studied: high concentrations corresponding to the asymptotic regime, and intermediate concentrations with various degrees of pre-degradation. In analyzing the data, attempts were made to find the most physically appropriate reference temperature and viscous representation. It was hoped that this choice would allow the development of correlations of general validity for the experimental heat transfer results.

It was also planned to examine the relationships found between the friction coefficient and the Colburn factor, the latter being usually apparently far lower than expected from the friction data for these fluids. It was thought that the results for the intermediate drag reduction regime could be particularly helpful in that respect, as they might show the variations in discrepancy between heat and momentum transfer when mechanical degradation is present.

1.3.2. **Antimisting Polymer Solution**

A second type of fluid was also investigated, a polymer solution as well, but one exhibiting a far more complex rheological behavior than the polyacrylamide solution. This fluid is an antimisting kerosene (AMK). In particular, contrarily to most drag-reducing solutions, this fluid is shear-thickening. It is currently being evaluated by the Federal Aviation Administration for possible use in commercial airplanes, presenting the advantage of reduced flammability in case of survivable crash landing.

This kerosene, based on commercial jet engine fuel (Jet A), is modified by the introduction of a combination of polymeric additives. Several qualitative studies of flammability were conducted on this fuel, but the basic mechanisms involved in the reduction of misting are still largely unknown, and no detailed friction and heat transfer data are available for this fluid.

A technique of capillary measurements has been developed in order to investigate the viscosity/shear rate relationships of this viscoelastic fluid. With this technique, the study of the friction and heat transfer properties of this fluid was conducted in a manner similar to that used for polyacrylamide. The interpretation of data beyond simple comparisons with the Jet A solvent is far more difficult, however.

It will be shown for example that, depending on the shear rate experienced at a given radius across the tube and given location along its length, the viscosity of the fluid may vary by more than a factor of ten. This variation, in turn, may introduce dramatic differences in the values of computed local Reynolds and Prandtl numbers, depending on the definitions used for these quantities, thereby complicating the development of meaningful correlations and relationships.

Such correlations for friction and heat transfer were nevertheless computed for this fluid, using various temperatures and different approximations for the variations in degradation along the length of the pipe. Interestingly, the results indicate that the fluid apparently behaves much like a drag-reducing solution in the asymptotic regime, as can be

shown if the proper parameters are used in the analysis. This behavior was not anticipated considering the complex manner in which the viscosity of this fluid is dependent on the shear rate. Other tests were also conducted using aged solutions, various concentrations and previously degraded material.

1.3.3. **Suspensions of Particulates**

Clay suspensions were used as another test fluid. Although suspensions of bentonite have been studied by mineralogists, there is only limited data available for them on the heat transfer aspects in turbulent flow, and it seemed worthwile to investigate this class of fluids using the computational methods developed for the polymer solutions. Whereas it is clear that these suspensions will exhibit a lower friction coefficient than water because of their expected purely viscous non-newtonian behavior, additional drag reduction has been claimed at times as well. It was thought interesting to check this possibility, because, if it proved to be true, the mechanism responsible for this drag reduction would probably be quite different from that associated with polymer solutions.

The rheology of bentonite solutions is complex, involving colloidal mechanisms and being dependent on a large number of factors such as dispersion, hydration, availability of exchange ions, and pH. Bentonite suspensions typically exhibit a strongly pseudoplastic behavior, and this rheological characteristic was investigated in the context of these heat transfer studies.

Suspensions also have very important practical applications. Bentonite muds, in particular, are used extensively as drilling fluids by the petroleum industry for the lubrication and cooling of the drilling bits, caking of the wellbore walls, and removal of the cuttings. Heat transfer and friction are thus critical phenomena that deserve further study and have motivated the choice of bentonite as test fluid.

Some solutions involving a combination of polymers and bentonite were also tested for heat and drag reduction. Similar solutions are indeed sometimes used as drilling muds as well. This study yielded unexpected results, the heat transfer and friction showing a much larger susceptibility to mechanical degradation than is usual for the original polymer solution.

1.3.4. **Suspension of organic pulp**

Fiber suspensions constitute another type of fluid having demonstrated drag and heat transfer reduction properties. Most of the few previous studies on fibers were conducted with asbestos or artificial fibers such as nylon, however. Accordingly, it was also decided to use a fluid containing organic fibers for this project. These organic fibers may indeed possibly induce different viscoelastic-type non-newtonian flow characteristics if factors such as aspect ratios are critical for the mechanisms involved.

Fiber suspensions are very common in the food, paper, and chemical industries and present thus important applications. Food rheology has paid attention to non-newtonian pipe flows but the laboratory work has

usually been of a very practical nature and interpretations were often based on simple assumptions. We have chosen tomato puree as a representative test fluid containing natural fibers. Heat transfer and friction experiments were conducted for this fluid as well as for a mixture of tomato puree and polymers.

1.4. OBJECTIVES OF THIS STUDY

The purpose of this work was to collect a rather broad base of experimental data on the friction and heat transfer properties of various non-newtonian fluids, including rheological information. These results might serve a double purpose. On the one hand, they might make possible the development of empirical correlations that could prove accurate and general enough to be useful for practical design problems. On the other hand, they might also be used for the testing of mechanistic models based on theoretical considerations.

Emphasis was placed on the acquisition of accurate data and their detailed numerical processing. It was also attempted to gain sufficient insight into the physical problem in order to be able to conduct meaningful computations and to provide the best representation for the results. This report was written with the aim to provide enough information so that these results may also be used by other investigators.

1.5. OVERVIEW

The material presented here is organized into chapters as follows:

In this first chapter, the background for this study is presented and an explanation is given for the selection of the test fluids.

The second chapter deals with a bibliographical review of previous work. It is hoped that this compilation may be used for reference, in particular for the recent work of direct relevance to this project. The main goal here, however, was to introduce in general terms all the concepts necessary for this study, with their specific references.

The third chapter is a review of all the equations that will be used in the processing or in the discussion of the experimental results. They have been organized in a systematic manner in the hope that they might constitute a fairly complete review of the theoretical and numerical considerations on which this study is based.

The fourth chapter is a description of the experimental installation and procedures, and also of the data processing method. It refers to appendices for more detailed descriptions and derivations.

The fifth chapter involves the presentation and discussion of the results. It was thought more convenient to conduct both at the same time, because the parameters chosen for the presentation and computation of the results may indeed depend on comparisons with other fluids or on further analyses, or may have to be justified step by step.

Most of the major conclusions or findings are then summarized in the

sixth chapter.

CHAPTER 2

BIBLIOGRAPHICAL REVIEW OF PREVIOUS WORK

A rather large number of research projects on non-newtonian fluid mechanics have been conducted over the last 25 years, especially in the field of drag-reducing polymer solutions. Consequently, the present review has been limited to a general account of the major lines of research developed over the years. This review is also intended to introduce the various concepts that will be used in the interpretation and discussion of the data.

2.1. DRAG-REDUCING POLYMER SOLUTIONS

2.1.1. Introduction

It is well-known that one of the early observations of the drag reduction phenomenon was made by Toms (1948,1977), who noticed that the friction exhibited by solutions of poly(methyl methacrylate) in monochlorobenzene was lower than expected from newtonian theory. A similar observation was also made by Mysels (1949) who worked with thickened gasoline. Since then, a great number of studies were conducted in order to find an explanation for this phenomenon. However, although both the physical and theoretical grasp of the concept have improved markedly, a definitive consensus on the mechanism responsible for this reduction does not appear to have yet been reached. Nevertheless, the many experimental studies conducted so far have permitted gathering enough information for these solutions to be effectively used in indus-

trial or commercial situations.

It may be appropriate to mention first some of the most notable review articles published over the years on the subject of drag-reducing solutions. These articles trace the major thrusts of the relevant investigations and they emphasize the most important concepts developed by the researchers.

The idea that the polymer affects the sublayers close to the wall was developed and shown experimentally early on, and has since motivated theoretical studies of the interactions between molecules or between molecules and the flow (Lumley 1967). It was also pointed out (Patterson, Zakin, and Rodriguez 1969) that other fluids besides polymer solutions and soap solutions might also exhibit drag reduction.

Review articles by Hoyt (1972a, 1974), in particular, summarize the state of the art at the time. In these reviews, Hoyt discusses the effects of concentration, roughness, and diameter, presents velocity profiles and molecular-eddy interaction theories, and lists a number of applications intended for the polymer solutions. Major contributions by Virk included his specification of a maximum drag reduction asymptote and his model of the corresponding velocity profiles (Virk 1975).

Thorough up-to-date reviews of the literature were conducted by Granville (1975, 1976, 1978a) and Hoyt (1977). Berman (1978) discussed additions to the existing molecular and turbulent models. Recently, an excellent article by Cho and Hartnett (1982) reviewed very clearly all the concepts necessary for studying the heat transfer and friction in tubes

for non-newtonian fluids of the type in question. Additionally, Cho and Hartnett also introduced some results on entrance flows, solvent effects, and eddy diffusivities of major importance for the field and the present study.

Numerical methods for the dynamics of non-newtonian fluids were reviewed by Crochet and Walters (1983). Bird and Curtiss (1984) described elegantly both the practical flow manifestations of polymeric liquids and the molecular theories attempting to explain their behavior. Finally, a review of the industrial applications of drag-reducing polymers was conducted by Sellin (1984).

Several books were also devoted to the study of non-newtonian fluid dynamics, among others, by Skelland (1967), by Astarita and Marucci (1974), by Bird, Armstrong, and Hassager (1977), and by Schowalter (1978).

2.1.2. **Drag Reduction**

The study of drag-reducing additives seems to have gathered its impetus in the early sixties. For example, the interactions between hydrodynamic forces and macromolecular structures were investigated by Tulin (1966), who suggested ways in which the molecular response to strain might explain the reduction of turbulent energy and the thickening of the viscous sublayer. Gadd (1965) measured dilute solutions of polyethylene oxide and found that, although the solutions had a viscosity close to that of water, they nevertheless showed significant normal stress differences and were susceptible to degradation. Chou and Zakin

(1967), on the other hand, investigated the effect of concentration on the viscosities of solutions, whereas Virk and Baher (1970) examined the concentration effect on the drag reduction itself. The use of pitot tubes and hot film measurements was shown to be problematic in dilute polymer solutions by Smith et al. (1967), and by Mochimaru and Tomita (1974).

In their review, Patterson, Zakin, and Rodriguez (1969) suggested that it may be necessary to introduce the Deborah number in order to correlate the effect of concentration. Seyer and Metzner (1969), studied velocity profiles and turbulence intensities, and proposed that viscoelastic fluids lead to a reduction in the rate of production of turbulence.

Nicodemo, Acierno, and Astarita (1969) also studied velocity profiles with pitot tubes, and Astarita, Greco, and Nicodemo (1969) used dimensionless parameters to correlate their data for various concentrations and diameters. This important type of correlation was reviewed later by Katsibas et al. (1974). The relationship between molecular weight and degree of drag reduction or degradation was investigated by Paterson and Abernathy (1970). McCarthy (1970) addressed the problem of the prediction of drag reduction for flat plates with polymer injection.

The important concept of a maximum drag reduction asymptote was developed by Virk, Mickley, and Smith (1970). In this connection they also defined an "ultimate layer" as part of their three-zone model of the velocity profile close to the wall. This limit to the possible reduction in friction has proved to be a major and most interesting feature of these

fluids.

A study of physical models for the wall turbulence led Ruckenstein (1971, 1973), and Ruckenstein and Popadic (1971) to propose an explanation on how the viscoelasticity causes drag reduction. This was done by evaluating the instantaneous wall shear stresses and by modeling the replacement of liquid elements near the wall. Drag curves were also predicted by Berman (1973) on the basis of estimates regarding the concentration and the distribution of molecular weight. Mizushina, Usui, and Yoshida (1974) used a viscoelastic damping factor model to predict drag reduction, and Huang (1974) examined velocity similarity laws. Mizushina and Usui (1977) also measured the decrease in diffusivities of momentum and heat near the wall.

The eddy viscosity concept was reviewed by Edwards and Smith (1980) for the prediction of velocity profiles and drag reduction. Kubo (1979) measured mean velocity profiles and fluctuations of velocity with a laser-Doppler velocimeter, whereas Durst and Rastogi (1977) used numerical computation for boundary layer studies. Boundary layer calculations were also conducted by Granville, who addressed the problem of the prediction of drag on rough surfaces (Granville 1977a), and characterized their roughness with a similarity law approach (Granville 1978b). The friction in pipe was measured for concentrated solutions of polyacrylamide by Tung, Ng, and Hartnett (1978) who found the friction factors to be somewhat lower than predicted by Virk's expression.

The formation of strings after mixing of the solutions was observed by

Hinch and Elata (1979), who suggested that they might lead to the formation of networks. By introducing additives in a polyethylene oxide solution, Kwack, Hartnett, and Cho (1980) found that the friction and heat transfer of these solutions are very sensitive to the water chemistry. This effect might have been partly responsible for the discrepancies between results found by different authors.

The effect of solvent chemistry on the viscosity and first normal stress difference was also investigated by Cho, Hartnett, and Park (1983) in a capillary and a Weissenberg rheometer. In their study of solvent effects, Kwack and Hartnett (1982b) found no influence on the Weissenberg number corresponding to the minimum asymptote. They also suggested (1983a) that the use of Weissenberg numbers to characterize the fluids might make possible the determination of characteristic times from pressure drop measurements if a friction factor/Weissenberg number relationship is already available for the corresponding Reynolds number.

A different mechanism of drag reduction involving non-homogeneous flows has been recently studied as well. Bewersdorff (1984), Berman and Sinha (1984), and El-Riedy and Latto (1984) all examined the consequences of localized injection of polymer. The drag reduction mechanism observed in that case appears quite different from that corresponding to homogeneous pre-mixed solutions. Fruman (1984) investigated also the effect of a layer of polymer solution close to the wall. Other studies dealing with injection of polymer were conducted by Maksimovic (1984), who compared the diffusion of a passive tracer with that of a drag-reducing one; and by Latto and El-Riedy (1984) who examined the

dispersion from a wall slit injection.

The mechanism of drag reduction was related to elongation of the polymer molecules by Gyr (1984), whereas a correlation for prediction was developed (Darby and Chang 1984, Darby 1984) which used an energy dissipation model with viscoelasticity parameters. Velocity profiles and fluctuations near the walls were measured by Abernathy and He (1984), and by Schmid (1984).

2.1.3. **Mechanistic Theories**

In parallel with these studies of a rather experimental nature, an extensive effort has also been devoted to theoretical approaches to the viscoelasticity problem. As the present study is largely experimental, only a few examples of these theoretical approaches will be reviewed. (More details on recent molecular theories may be found in Bird, Armstrong, and Hassager (1977), for example, and in the proceedings of the 8th (1980) and 9th (1984) International Congresses on Rheology.

One of the early investigations of dilute solutions of coiling polymers was conducted by Rouse (1953) using a linear viscoelasticity theory. The relaxation process of molecules under stress was studied and used to explain non-newtonian flow and diffusion in condensed systems (Ree, Ree, and Eyring 1958). Generalized newtonian models with a zero shear viscosity and a characteristic time were tested by Bird (1965), and Rivlin and Sawyers (1971) used a non-linear continuum mechanics theory for viscoelastic fluids.

Molecular network theories were applied by Carreau (1972) to describe the viscoelastic behavior, complex viscosity, and stress growth and relaxation. Hassager (1974) examined the kinetic theory and rheology of bead-rod models, whereas Bird and Deaguiar (1983) extended the dumbbell molecular theory for dilute solutions to concentrated solutions. An elastic dumbbell model with conformation-dependent hydrodynamic properties was also used by Phan-Tien, Manero, and Leal (1984) to make predictions of rheological behavior for shear and extensional flows.

Typical studies relating these theories to experiments include that by Argumedo, Tung, and Chang (1978) who determined the parameters of the Carreau model by rheological measurements. Similarly, Elbirli and Shaw (1978) derived characteristic times from shear viscosity data using viscosity functions with various parameters, and concluded that the 2 parameter models are better.

2.1.4. **Extensional Flows**

Whereas most of the studies mentioned above dealt mainly with shear flows, viscoelastic fluids in extensional flows also exhibit dramatic differences in behavior with respect to newtonian fluids. The study of extensional flows is consequently important although this area of research has been comparatively neglected.

Porous media flows were investigated by Sadowski (1965), and by Jones and Maddock (1969), who found no drag reduction for polymer solutions in granular beds. The very high elongation to shear viscosity

ratios typical of viscoelastic fluids were observed by Metzner and Metzner (1970), who measured stess levels in rapid extensional flow. Such high ratios were also found by Oliver and Bragg (1973) in jet thrust measurements. Packed beads were used by James and McLaren (1975) for laminar flow measurements of dilute polymer solutions, and they found a higher pressure drop than for newtonian fluids.

The tensile viscosity of polymer solutions was also measured with tubeless siphons by Peng and Landel (1976), who found it to be up to a thousand times larger than the newtonian tensile viscosity as determined by the Trouton ratio. They later investigated in a similar fashion the effects of temperature and concentration on the tensile viscosity (Peng and Landel 1980). A comparison of extensional and shearing flows for polyacrylamide was conducted by Baid and Metzner (1977), who used the results for the testing of constitutive equations. Cogswell (1978), also reviewed converging and stretching flows for non-newtonian fluids.

The extensional flows of dilute polymer solutions were studied in conical channels and stacks of beads by James and Saringer (1980, 1982). More recently they also studied these flows in relation to turbulent bursting (James et al. 1984). Flows in conical nozzles were also investigated by Schummer and Xu (1984). The extensional flow due to sudden contractions was examined by Durst and Schierholz (1984), with the help of Laser-Doppler anemometry and numerical computations. Some non-newtonian effects in porous media were reviewed recently by James (1984).

Entrance effects in tubes involve extensional flows to a certain extent as well, and were studied in that respect. Ouibrahim (1978, 1979) found an excess pressure drop at the entrance of capillary tubes in laminar flow of polymer solutions if a critical shear rate is exceeded. This excess was related to elasticity in the elongational flow at the entrance (Moan, Chauveteau, and Ghoniem 1979; Ouibrahim and Fruman 1980).

2.1.5. **Mechanical Degradation**

Another characteristic aspect of polymer solutions of major importance for experimentalists is their susceptibility to mechanical degradation. This problem was addressed in some of the review articles mentioned at the beginning of this chapter and, among others, in the following references.

Brennen and Gadd (1967), for example, investigated the effect of aging and degradation on pitot pressure loss and viscosities, and concluded that elastic effects such as normal stress differences are lost before drag reduction is fully affected. Ellis (1970) studied shear-induced degradation for polyethylene oxide and asbestos fibers. Polyacrylamide solutions were found less sensitive to degradation than polyethylene oxide by Fischer and Rodriguez (1971). Mechanical degradation may also be caused by rotational mixers as investigated by Stenberg et al. (1977), and by Agarwal and Porter (1980). The latter used gel permeation chromatography to measure the influence of high speed stirring on molecular configuration.

Additionally, aging may also influence the viscosity of the solutions (Gardner, Murphy, and Geehan 1978). The major cause of degradation is usually the friction in the pipe itself (Sedov et al. 1979), but valve throttling can be damaging as well (Lee, Irvine, and Kwack 1980). The mechanical degradation encountered by semi-dilute solutions in laminar capillary flow was described as occuring in the entrance region and above a critical shear rate (Ghoniem et al. 1981).

A molecular model involving chains consisting of both compact and extended bundles was used by Brostow (1983) for the study of degradation. The monitoring of molecular weights in degraded samples suggested a mechanism of chain-halving in extensional flows (Odell and Keller 1984). The rate of shear degradation was also studied recently by Patterson (1984), and the influence of concentration on the susceptibility to shear was compared for various polymers by Layec-Raphalen (1984). Thermal degradation may also be important at times, and was studied by Martischius and Heide (1984).

2.1.6. **Diameter Effect**

A problem typically exhibited by drag-reducing polymer solutions is the dependence of the degree of drag reduction on the diameter of the pipe (even for the same Reynolds number and fluid). The diameter effect is, of course, absorbed entirely in the Reynolds number for newtonian fluids, so that this non-newtonian effect implies that another parameter is needed to describe the flow besides the Reynolds number.

A Deborah or Weissenberg number relating the elasticity of the fluid to the shear, for example, could be appropriate for this purpose. In most cases, however, the direct determination of relaxation times is not easy to achieve for the dilute solutions used for drag reduction. Accordingly, most of the efforts on predicting the diameter effect have been limited to methods involving extrapolations for a unique fluid whose characteristics are assumed constant for the various diameters considered.

Vleggaar, Dammers, and Tels (1968), for example, have related the diameter effect to the characteristic frequency of the small scale dissipative eddies. Elliott and Stow (1971) observed that a solution would induce the same drag reduction in a small tube whether highly or moderately sheared, whereas in a larger tube, the highly sheared solution would exhibit the lowest reduction. Consequently, they suggested that a supermolecular structure or aggregation of polymer molecules might be related to the diameter effect.

The velocity profile studies having shown that the logarithmic layer is displaced for drag-reducing solutions, Huang (1974) observed that this shift is independent of the diameter for a given shear stress. The shear velocity based on the wall shear stress was indeed used in several correlations for the diameter effect. Some of these were reviewed by Katsibas et al. (1974), and later by Savins and Seyer (1977). Using a logarithmic approximation for the velocity profile, Taylor and Sabersky (1974) used this shear velocity in an iterative procedure to predict the diameter effect.

Ting (1976) proposed that the minimum molecular weight for the existence of drag reduction might be a function of the pipe diameter. The effect of flow time scales on the drag reduction was investigated by Berman (1977), because of the correlation between pipe diameter and eddy size. Velocity similarity laws were also chosen by Granville (1977) who used the logarithmic shift as the parameter for his scaling-up method. Using capillary tubes in the laminar regime, Ouibrahim (1978) observed an influence of the diameter on the transitional shear rates. The effect of diameter on the minimum Weissenberg numbers necessary for asymptotic friction and heat transfer was investigated by Kwack and Hartnett (1982a), who concluded that it was not important.

A set of experiments covering a large range of diameters, including the large sizes used in the industry, was conducted by De Loof et al. (1977). Other comprehensive experiments in various diameters were conducted by Sellin and Ollis (1983), who tested some scaling-up methods and concluded that they did not entirely account for the difference in reduction of drag between large and small pipes.

In a previous article (Matthys and Sabersky 1982, also in app. C.1.), a method of predicting the diameter effect on friction and heat transfer was developed. This method is based on the concept that the logarithmic velocity profile shift is principally function of the shear velocity. A three-layers velocity profile model, including the viscous and elastic layers was then integrated numerically to compute various families of friction coefficients and Reynolds numbers characterized by constant values of the logarithmic shift. These results were then used in a simple

iterative procedure to predict the friction and heat transfer for various diameters.

This introduction of the buffer layer in the integration is, of course, critical for high levels of drag reduction. Indeed, Granville (1984) later modified his method to take this layer into account, and found the corresponding predictions to be more accurate. Recently, scale-up correlations methods were also reviewed by Havlik (1984), and by Mironov and Shishov (1984).

2.1.7. **Specialized Problems and Applications**

Some of the other characteristic problems typical of drag-reducing solutions are briefly mentioned in this section.

Jets of non-newtonian fluids have also been studied because they exhibit a behavior markedly different from that of newtonian fluids. The stability of laminar non-newtonian viscoelastic jets was investigated by Goldin et al. (1969), who found a more rapid growth of wave disturbances than for newtonian fluids of the same viscosity. Pownall and Kiser (1970), on the other hand, observed that the corrected rate of spread for polyacrylamide was the same as that of water. The improvement of jet performance by additives was also examined by Hoyt and Taylor (1979), and Hoyt, Taylor, and Altman (1980). Laminar jets, in particular, were recently studied by Adachi and Yoshioka (1984).

The problem of cavitation in non-newtonian fluids has been studied very little so far, although the dynamics of bubbles and droplets in such a liquid may be quite different than in a newtonian fluid, especially in a

shear flow situation (Schowalter and Hara 1980). Some recent studies include cavitation inception around bodies (Gates 1977), ultrasonic cavitation (Malinsky and Myska 1984), bubble dynamics (Schowalter 1984b), and bubble motion (De Kee and Dajan 1984).

It is interesting to note that, in addition to the measurement of the viscosity of these viscoelastic fluids by traditional means such as capillaries, cone-and-plate arrangements, and concentric cylinders, a method using a falling ball has also been recently proposed (Cho and Hartnett 1979; Cho, Hartnett and Kwack 1980; Cho and Hartnett 1983; Cho, Hartnett, and Lee 1984). Optical methods may also be used to study polymeric fluids, such as birefringence for example, which can be very useful to investigate flow-induced conformation changes in strong flows (Leal 1984).

The use of polymer solutions has also been frequent in the oil industry: for oil recovery (Mungan, Smith, and Thompson 1966; Martin and Kuntamukkula 1984; Vargas-Jarillo 1984), for hydraulic fracturing (Veatch 1982), and for mixing with drilling muds. Recently they have also been used in pipeline transport of crude oil for their drag-reducing properties (Burger, Chorn, and Perkins 1980; Burger, Munk, and Wahl 1980; Beaty et al. 1984; Motier and Prilutski 1984; Motier et al. 1984).

Although the emphasis has been put on synthetic polymers such as polyethylene oxide or polyacrylamide, many other substances may exhibit a drag-reducing character as well. Besides the well-known soaps and guar gum, one can also find, for example, deoxyribonucleic acid (Hoyt

1966), polymers created by microbial and algae cultures (Kenis 1968), and fish slime (Rosen and Cornford 1970).

2.2. HEAT TRANSFER REDUCTION BY POLYMER SOLUTIONS

The number of studies dealing with the heat transfer aspects of these polymer solutions flows is, of course, far smaller than for the fluid mechanics aspects. A general discussion of the subject may be found in one of the recent reviews, such as that by Dimant and Poreh (1976) or Cho and Hartnett (1982). Some of the important original papers will, however, be mentioned separately in the following paragraphs.

Very early on, it became obvious that the phenomenon of drag reduction in turbulent flow was accompanied by a similar reduction in convective heat transfer. A detailed description and explanation of the latter was naturally even more difficult to achieve than for purely isothermal drag-reducing flows, especially because it was not entirely clear whether or not the friction-heat transfer analogies are applicable. This last problem was pointed out early, in studies such as that by Marucci and Astarita (1967), who found that viscoelastic fluids will show a reduction in heat transfer proportionally larger than the reduction in drag. This is clearly unlike the case of purely viscous non-newtonian fluids for which the Colburn analogy is valid.

Gupta, Metzner, and Hartnett (1967) suggested that the reduction in heat transfer for polyacrylamide solutions might be related to a suppression of turbulence close to the wall. Polyethylene oxide solutions were also studied by McNally (1968) in smooth and rough tubes, and by

Smith et al. (1969) who gave an estimate of the maximum heat transfer asymptote. Measurements of heat transfer and drag were conducted by James and Acosta (1970) for laminar flow of dilute polymer solutions around small cylinders.

The effect of the solvent nature, such as the difference found between solutions in fresh or salt water was examined by Howard (1970), and the solution properties were also introduced for the correlation of momentum and heat transfer (Howard and McCrory 1971). A significant effect of metallic salts on the reduction of heat and momentum transfer was found by Monti (1972), who noted also that the use of the Colburn analogy overestimated the heat transfer.

A turbulence model consisting of a succession of laminar boundary layers near the wall was used by Ruckenstein (1972) to compute the heat transfer for power-law and viscoelastic fluids. Laminar heat transfer for pseudoplastic fluids was studied by Fito and Requeni (1974), and turbulent heat transfer for both power-law and viscoelastic solutions by Yoo (1974). Debrule and Sabersky (1974) investigated rough pipes and determined that these would result in even lower heat transfer and drag reduction than smooth pipes. They suggested that the presence of the polymer would lead to a damping of turbulence near the wall.

A mixing length model with variable damping was chosen by Dimant and Poreh (1974) for the prediction of momentum and heat transfer. They also observed a large effect of temperature-dependent fluid properties. This problem may be particularly critical for heat transfer-

reducing solutions, because the temperature difference between the core of the fluid (which is the temperature commonly used for reference) and the wall (the critical region) may be far larger at the same heat flux than it is for a newtonian fluid. Simple newtonian corrections such as that by Sieder and Tate (1936) or the use of different base temperatures for the Nusselt, Reynolds, and Prandtl numbers (Sleicher and Rouse 1975) may not be sufficient in that case. Probably most appropriate as reference, but usually unknown in the simpler experiments, is the wall temperature.

The proportionally larger decrease in heat transfer with respect to friction was also investigated by Mizushina, Usui, and Yamamoto (1975) using a damping factor model. Kale (1977), on the other hand, used a modified Deissler velocity profile and extended Reichardt's analysis to drag-reducing fluids. In another comparison, McConaghy and Hanratty (1977) found a proportionally larger change (with respect to newtonian fluids) in the mass transfer than in the pressure gradient for a drag-reducing solution.

The heat transfer reduction for polyacrylamide solutions was found to be more sensitive to mechanical degradation than the friction reduction (Ng and Hartnett 1979). The value of the minimal Deborah number necessary for asymptotic conditions was also determined to be larger for heat transfer than for friction reduction. It was suggested by Cho and Hartnett (1980) that the analogy between momentum, heat, and mass transfer might be inapplicable for viscoelastic fluids. The thermal entrance length was also noted to be much longer for concentrated

polymer solutions than for newtonian fluids (Ng, Cho, and Hartnett 1980). A heat transfer correlation for this entrance region was developed (Cho, Ng, and Hartnett 1980), and the mass transfer entrance length and asymptote evaluated as well (Cho and Hartnett 1981).

The transient response to a step increase in surface temperature was computed by Gorla (1980) for the laminar boundary layer of a power-law fluid near a transition point. The heat transfer to a shear-thickening fluid between plates was investigated by Suckow, Hrycak, and Griskey (1980), whereas Joshi and Bergles (1980a, 1980b, 1981) examined the laminar heat transfer to a pseudoplastic fluid in a tube. Surprisingly, Tiu and Low (1981) found no reduction of heat transfer for polyacrylamide in a flat plate heat exchanger although drag reduction was observed. The thermal conductivity of semi-dilute polyacrylamide and polyethylene oxide aqueous solutions was found identical to that of water by Lee, Cho, and Hartnett (1981).

Smith and Edwards (1981) reviewed eddy viscosity correlations for the heat transfer of drag-reducing fluids. Kawase and Ulbrecht (1982a), on the other hand, used a Levich three-zone model for power-law fluids and a periodic transitional sublayer model for drag-reducing fluids (Kawase and Ulbrecht 1982b). The eddy diffusivity was estimated to be smaller for heat than for momentum by Kwack, Cho, and Hartnett (1981a), in support of the suggestion that the momentum-heat analogy might be invalid. They also investigated the effects of degradation, solvent effects, and entrance region on the heat transfer during their study of the minimum heat transfer asymptote (Kwack, Hartnett, and Cho 1982).

Empirical correlations were then developed for heat transfer and friction as a function of the Reynolds and Weissenberg numbers (Kwack and Hartnett 1983b).

Recently, the problem of thermal convection in non-newtonian fluids was reviewed by Shenoy and Mashelkar (1982), including the effects in pipes used for convection studies. The laminar heat transfer to a power-law fluid in a rotating disk was investigated by Tsay and Chou (1983); and Kawase and De (1984) used a surface renewal concept for heat and mass transfer in rough pipes. Kwack and Hartnett (1984) computed the eddy diffusivities for momentum and heat and found them to be functions of the Weissenberg number. Also function of this number representative of the elasticity of the fluid, were the entrance length and the turbulent Prandtl number. Finally, a model of heating system taking into account both the pumping power saving and the decrease in heat transfer was examined by Leca and Leca (1984), and Rose et al. (1984) investigated the heat transfer characteristics of a viscoelastic surfactant.

2.3. **ANTIMISTING KEROSENE**

Antimisting additives designed to reduce the possibility of crash landing fires for airplanes have been studied for the past decade. Most of these studies have concentrated either on practical aspects such as engine compatibility, filtration, ignition, quality control, and blending; or on more basic rheological characterization of viscoelasticity and non-newtonian viscosity. Very little information is available on turbulent friction and particularly heat transfer properties of the modified fuels.

One of the early studies (Mannheimer and Weatherford 1975) dealt with AM-1 (a Conoco product) dissolved in JP-8 (a military version of Jet A kerosene). The properties of this fluid were investigated with porous media, and it was found that whereas the shear viscosity of this viscoelastic solution is a constant essentially independent of shear rate, the solution nevertheless exhibits a large resistance to flow in filters, which is an indication of a high extensional viscosity. Several other polymer additives were also available that had a similar antimisting character. Some of these were investigated by Hoyt, Taylor, and Altman (1980) by photography of jet break-up and by correlation with the drag reduction which is sometimes associated with the polymers.

A study of heat transfer for modified fuel was conducted (Medani and Hayes 1978) with FM-4 (a Shell Co. product) in 'Avtur' fuel. Surprisingly, very little difference in behavior was found between the solvent, the modified fuel, and a sheared modified fuel.

A new type of additive (FM-9 by Imperial Chemical Industries), which is characterized by the gelation it induces above a critical shear rate, was also investigated in parallel with AM-1. Mannheimer (1977) studied the critical flow rate through porous media that some of these polymeric solutions exhibit. He also examined (Mannheimer 1979) the possibility of degrading the modified fuel and designed a small-scale spinning disk atomizer for flammability studies. Large scale tests were conducted as well (San Miguel and Williams 1978; Salmon 1981), confirming the viability of the antimisting additive approach to the flammability problem.

A comprehensive research program was started, focusing on the FM-9-based solution as a standard. This particular additive exhibits a well defined shear-induced thickening that may be related to a shift from intramolecular to intermolecular hydrogen bonding. Similar phenomena were suggested by Eliassaf, Silverberg, and Katchalsky (1955), Eliassaf and Silverberg (1962), and Ono and Murakami (1977) for polymethacrylic acid, and by Savins (1968) who examined the thickening of poly(vinyl) alcohol-borate complexes. For a comparison of some shear-thinning and shear-thickening systems, see for example Hadjistamov (1984).

The solutions of FM-9 proved to be highly viscoelastic and to exhibit a large extensional viscosity. It is not entirely clear whether it is the shear-thickening or this extensional viscosity that is directly responsible for the antimisting properties of the modified kerosene. Accordingly, Sarohia and Landel (1980) studied the break-up of droplets and jets for AM-1 and FM-9 solutions and evaluated their extensional viscosity through the elongation of pendant drops. In parallel, a thorough investigation of the shear-induced thickening was conducted by Peng and Landel (1981, 1983) in a cone-and-plate rheometer and the results correlated with flammability data.

A study of various practical problems related to the use of FM-9 as antimisting agent was simultaneously conducted. Mannheimer (1981, 1982) examined screen and tube flows, the ignition and filtration characteristics of the fluid, and the feasibility of intentional degradation by flow restrictors and pumps. A preliminary attempt at measuring skin friction and heat transfer was undertaken (Wat and Sarohia 1982), as

well as studies of flammability and atomization by image processing techniques (Sarohia 1981; Fleeter et al. 1982).

A full-scale degrader using a pump and a needle valve was developed by Mannheimer (1983a), who also pursued his studies of flammability with a spinning disk atomizer, and correlated these results with a Darcy viscosity obtained in packed tubes (Mannheimer 1983b). The compatibility of water with the dissolved additive was an important problem to evaluate (Yavrouian, Sarboluki, and Sarohia 1983), as were the blending process, the quality control techniques, and the effect of the base fuel (Yavrouian, Ernest, and Sarohia 1984).

In parallel, more fundamental studies were recently pursued to investigate the basic rheology of the antimisting FM-9 solution. These were conducted using die-swell and torsional balance measurements (Mannheimer 1984), and capillary tube viscometers (Matthys 1984, 1985).

2.4. SUSPENSIONS OF PARTICLES

2.4.1. Fluid Mechanics Aspects

The study of particulate suspensions dates back to early experimental projects such as that by Gregory (1927), for example, who evaluated the friction losses in pipes for clay slurries encountered in cement processing. He found that a minimum pumping power could be achieved through the use of a critical velocity. Clays, and in particular bentonite, were studied extensively by mineralogists (Ries 1927). Hauser and Reed

(1936b) found evidence of rheopexy in bentonite when studying particle size distribution by centrifugation (Hauser and Reed 1936a). This effect of particle size on the thixotropic nature of bentonite is very important for studies of gel structure aspects such as clusters and networks (Hauser and Reed 1937). Similarly, sedimentation and dilatancy of various concentrated solutions and pastes were also investigated by Freundlich and Jones (1936).

The use of clays, in particular bentonite, as drilling fluids in the oil industry, provided some impetus to the rheological study of these suspensions. Their thixotropic properties, for example, are of major importance for cuttings removal, and the study of the variations of their viscosity is vital for pumping systems (Rogers 1948, Zaba and Doherty 1956). For more complex situations, clays will sometimes be mixed with polymer to create an adequate drilling mud. On the other hand, when encountered naturally during drilling and exposed to water, clays might induce permeability problems because of the swelling they experience when hydrated (Hower 1974). Clays come in many varieties with distinct properties, and their study by mineralogists may often be applied to flow problems (Grim 1968; Grim and Gruven 1978).

The flow of clay suspensions and muds in pipes was also investigated by Caldwell and Babbitt (1941), who distinguished plastic from turbulent flow for these fluids, and studied their thixotropic character with a Stormer viscometer. The conditions for the existence of dilatancy in concentrated suspensions of particles such as titanium oxide and glass beads were examined by Metzner and Whitlock (1958) with capillary and

cup-bob viscometers. They studied in particular the effects of carrier viscosity, particle size, and concentration.

The introduction by Metzner and Reed (1955) of generalized Reynolds numbers based on the power law constituted a major advance towards the correlation of friction factors for non-newtonian fluids of the purely viscous type such as clay suspensions. In particular, it became then possible to predict turbulent velocity profiles and to generalize the newtonian friction laws (Dodge and Metzner 1959; Bogue and Metzner 1963).

Interestingly, Vanoni and Nomicos (1959) determined that reductions of friction factors up to 30% could be achieved with suspended sediments in their flume experiments on channel bed shapes. Eissenberg and Bogue (1964), on the other hand, observed by experimental study of aqueous thoria suspensions that, for dilute solutions, the friction factor and velocity profile would follow the newtonian laws if a viscosity estimated at the wall shear stress is used. For concentrated suspensions, the friction factor would be lower than for newtonian fluids. Up to 50% drag reduction at the same flow rate was also found by Zandi (1967) for various concentrations and particle sizes of clay, coal, and ash. Gyr (1968) suggested similar mechanisms of vortex stretching for the drag reduction induced by both polymer solutions and sand suspensions.

A review of turbulent pipe drag reduction by Patterson, Zakin, and Rodriguez (1969) compared the effects of polymer solutions, soap solutions, and particle suspensions, whereas Cox and Mason (1971) examined

the behavior of suspended particles, drops, and bubbles in a newtonian fluid. To reduce pipe friction in solid transport, Poreh et al. (1970) added complex soaps to particle suspensions of moderate concentrations, and Ghassemzadeh and Carmi (1982) studied the effect of the addition of carboxymethylcellulose to a mixture of coal and oil. Recently, the addition of polymer to coal-liquid mixtures for drag reduction purposes was investigated by Golda (1984), and the influence of a polymer on the settling velocities of particles studied by Pollert (1984).

Schowalter (1984a) investigated the stability and kinetics of coagulation processes for colloids under shear, and the friction in tubes of bentonite suspensions in salt water was studied by Ippolito and Sabatino (1984). The viscosity functions of concentrated suspensions of coal in oil were studied experimentally by Gleissle and Baloch (1984). Coal and water slurries, on the other hand, were shown to be shear-thickening by Hanks (1984), even for fairly dilute solutions.

Several theoretical studies were also conducted on the problem of particle suspensions. Among others, Batchelor (1970a) investigated the properties of the bulk stress for non-spherical particles, and applied the slender body theory to the calculation of the forces parameters by distribution of Stokeslets on the body boundaries (Batchelor 1970b). He also studied the interactions in straining motion for concentrated elongated particles (Batchelor 1971). Russel (1978) computed the stress generated under shear by charged particles and the effect on viscosity: non-newtonian in shear flow but newtonian in extensional flow. He also reviewed the various colloidal effects on the rheology of suspensions

(Russel 1980), and the effect of brownian motion on small particles in liquids (Russel 1981).

2.4.2. **Heat Transfer Aspects**

The heat transfer aspects of particle suspensions were studied only to a lesser extent. Orr and Dallavalle (1954) found the newtonian Dittus-Boelter expression applicable if the viscosity (as measured in a capillary) and conductivity (as determined by Maxwell's law) of the suspension are used. In a similar fashion, Thomas (1960) noted that the heat transfer found experimentally for aqueous thorium oxide suspensions was the same as that predicted by newtonian correlations if a high shear viscosity (measured in a tube) is used. With this high shear viscosity, the data found for various diameters were correlated uniquely but not in the case an effective viscosity (corresponding to the actual wall shear stress) was used. He also found that the Martinelli analogy between heat and mass transfer was applicable for the suspension. Particles suspensions were also considered in the excellent review of friction and heat transfer of non-newtonian fluids by Metzner (1965).

In parallel to liquid studies, the heat transfer in pipe for suspensions of solids in air was investigated by Sadek (1972), who found an increase in heat transfer. However, Boothroyd and Walton (1973) determined that the presence of solid particles in a gas reduced the turbulence near the wall and led to decreased friction and heat transfer.

Correlations for suspensions of clays among other purely viscous non-newtonian fluids were developed by Yoo (1974). The heat transfer

between parallel plates for dilatant suspension systems was reviewed by Suckow, Hrycak, and Griskey (1980), who solved the corresponding energy equation using a power-law relationship. The problem of heat transfer to various settling particles and beads in a vertical pipe was studied by Smith and Paradi (1982), who found a good correlation with the Colburn relationship if the water properties alone were used.

2.5. SUSPENSIONS OF FIBERS

Fiber suspensions have also been of interest to researchers due in part to the problems encountered in the wood and paper industry. One such typical study is that by Bugliarello and Daily (1961), who examined laminar and transition flow of wood and nylon fibers. They noted significant viscoelastic effects, formation of networks and entanglements, and in particular the presence of a water annulus by segregation of the suspended phase. This latter point is important as it could lead to erroneous viscosity measurements. Bobkowicz and Gauvin (1965) also investigated nylon fibers in water, but in the turbulent range. They observed drag reduction, and studied the effects of concentration and aspect ratio. Aspect ratio was indeed later proved to be of crucial importance for drag reduction.

Morrison and Harper (1965) examined suspensions of cellulose fibers, and in particular, the non-newtonian effects induced in the wall vicinity. Drag reduction of up to 50% was also found experimentally for short nylon fibers by Kerekes and Douglas (1972), who determined the limiting conditions for this reduction in terms of viscosities and aspect ratios. It

was shown by Vaselesky and Metzner (1974) that the drag reduction induced by fibers suspensions involves turbulent core processes and is thus independent of the scale of the system. This is not true of polymer solutions which involve principally wall effects.

The relationship between drag reduction and aspect ratio was emphasized by the studies of asbestos fibers with high aspect ratios (commonly of several thousands). These fibers were investigated, among others, by Hoyt (1972b) who correlated better drag reduction with higher aspect ratio in rotating disk and pipe experiments. Moyls and Sabersky (1977) conducted experiments on the effect of asbestos fibers on friction and heat transfer, and found drastic reductions for both smooth and rough tubes. Recently, the study of turbulent energy spectra by McComb and Chan (1981) showed indeed marked changes with respect to newtonian results for asbestos fiber suspensions.

Another interesting field of study for suspensions is the one dealing with combinations of polymers and fibers in solution. It was noted, in particular, that when one combined the two materials, the drag reduction obtained (up to 95%) was larger than expected from the respective individual contributions (Lee, Vaselesky, and Metzner 1974; Metzner 1977). This synergism probably stems from the different zones respectively influenced by the fibers and polymer.

It was nevertheless shown by the study of velocity profiles that in polymer and fiber mixtures the fibers also affect the sublayer region (Kale and Metzner 1976; Sharma, Seshadri, and Malhotra 1979).

Recently Singh et al. (1984) also studied the effectiveness and stability of combinations of polymer and fibers as drag-reducing agents. The drag reduction exhibited by fiber suspensions is of course of major interest if a minimum pumping power is desired, which may be attained through design based on an optimum pulp consistency (Higgins and Wahren 1982).

2.6. FOOD RHEOLOGY

Studies of the viscous properties of non-newtonian fluids were also conducted in the field of food rheology. Typically, the fluids encountered in this area are pseudoplastic, often involving significant yield stresses in the high concentrations. Thixotropic behavior is sometimes also observed.

In these studies, viscoelasticity has apparently not been considered as playing an important role, although guar gum, investigated in the early stages of the research on drag reduction, is sometimes used in the food industry. Tomato purees may contain fibers and accordingly might present a behavior normally associated with drag reduction, but that aspect does not seem to have been considered either.

The early stages of fundamental research on the problems associated with food products consisted primarily in recognizing the fact that many of these fluids were indeed exhibiting a strong non-newtonian behavior and in trying to determine quantitatively this character. Accordingly, it was proposed by Eolkin (1957) to include automatic measurements of viscosity at 2 different shear rates for the monitoring of production

lines. Charm (1960) investigated the computation of flow constants from shear stress vs. shear rate relationships obtained from tube viscometers. He also reviewed systematically the various models and expressions of viscosity useful for a study of the food materials (Charm 1962).

One of the few studies of heat transfer for those pseudoplastic fluids was also conducted at that stage, using an overall thermal balance in a concentric laminar pipe heat exchanger (Charm and Merrill 1959). This study also proposed to predict the heat transfer coefficients using corrected velocity profiles. Harper (1960) recognized that a power-law is a good approximation for many of these fluids, and examined the relationship between their viscosity and the performance of evaporators.

Harper and El Sahrigi (1965) used a coaxial cylinder viscometer to confirm the usefulness of the power-law model for pseudoplastic food products, and studied the influence of temperature and concentration on the consistency of tomato concentrates. Saravacos (1970), in a similar fashion, investigated the temperature effect on the viscosity for fruit purees, using correlations of the Arrhenius-type. An experimental study of laminar flow heat transfer in a plate exchanger was also conducted by Jowitt and McCarthy (1974) for highly pseudoplastic food liquids. The pseudoplasticity of hydrocolloids or gum additives was then experimentally determined by Krumel and Sarkar (1975).

Rha (1978) reviewed the influence of chemical contents on hydrodynamic properties and structural effects. Recently, Rao and Anantheswaran (1982) published a review of non-newtonian flow

phenomena. Various models involving yield stresses, some initially developed for suspensions, were also tested with tomato concentrates by Rao and Cooley (1983). It was also shown that some fruit juices exhibit yield stresses because of the presence of pulp particles (Van Vliet and Van Hooijdonk 1984).

Food rheology seems to be concerned mostly with simple models related to the power-law representation and sometimes involving yield stresses. Little attention has apparently been paid to heat transfer problems, however, even though food materials often require thermal processing. Accordingly, a better fundamental understanding of the non-newtonian heat transfer and friction phenomena exhibited by these fluids may well benefit the development of food processing systems, especially if a drag-reducing behavior is involved.

CHAPTER 3

THEORETICAL CONSIDERATIONS

This chapter is devoted to a review of the definitions and equations used for the computation and discussion of the experimental results.

3.1. CLASSIFICATION OF FLUIDS AND CONSTITUTIVE EQUATIONS

The fluids we are interested in may be classified for our purposes in 4 categories: newtonian, purely viscous non-newtonian, viscoelastic, and time-dependent.

3.1.1. Newtonian Fluids

Newtonian fluids are characterized by a ratio (the viscosity) between shear stress and shear rate that is independent of time and shear rate, although it can be a strong function of temperature. For simplicity, we will only consider shear flows in circular pipes in the following discussion. For a newtonian fluid, we have thus:

$$\tau = \eta \dot{\gamma} \tag{3.1}$$

where η is the dynamic viscosity, τ is the shear stress, and $\dot{\gamma}$ is the shear rate. Water and kerosene are examples of newtonian fluids that have been used in this study.

3.1.2. Purely Viscous Non-Newtonian Fluids

The viscosity of a purely viscous non-newtonian fluid can be a func-

tion of the shear rate. If the viscosity decreases with increasing shear rate, the fluid is called pseudoplastic (or shear-thinning), in the opposite case it is designated as dilatant (or shear-thickening). A simple type of shear rate dependency is the important power-law (known also as Ostwald-de Waele) relationship, which is a good representation of the behavior of many fluids:

$$\tau = K\dot{\gamma}^n \tag{3.2}$$

which gives an equivalent viscosity of

$$\eta = K\dot{\gamma}^{n-1} \tag{3.3}$$

where K (the consistency) and n are independent of the shear rate. Using this representation, we see that n, the power-law exponent, which is a measure of the non-newtonian character of the fluid, will be smaller than one for the pseudoplastic fluids (the most common), larger than one for dilatant fluids, and obviously equal to one for newtonian fluids. Other fluids may well have a shear stress that is a more complex function of the shear rate, but it could still be conveniently represented by this relationship, provided K and n are regarded as a function of the shear rate themselves. This representation will be used frequently in the present study.

Fluids such as Bingham plastics may be considered part of this category as well. These are characterized by a minimum shear stress that has to be exceeded in order to make any motion possible. A simple representation of this behavior might be:

$$\tau = \tau_0 + K\dot{\gamma}^n \quad . \tag{3.4}$$

Certain suspensions may pertain to this category.

3.1.3. **Viscoelastic Fluids**

The viscoelastic fluids, because of their component of elasticity, do have a "memory." That is, their instantaneous shear stress is not only a function of the current deformation, but is also a function of the past history of motion. This type of phenomenon is clearly far more difficult to model.

One could use differential or integral constitutive equations (see Carreau 1972, or Bird and Deaguiar 1983 for example), but these models are complicated (and somewhat impractical for our purposes). These equations attempt to describe not only the simple shear viscosity functions, but also the elongational viscosity, normal stress differences, stress relaxation etc.

More simply, it is possible to describe the elasticity of the fluid in terms of a characteristic time, a material property function of the molecular configuration. Many such models have been presented in the literature (see Chapter 2) which are good examples of simple empirical relations for the shear viscosity of these fluids. Eyring's equation (Ree, Ree, and Eyring 1958), in particular, is given by

$$\eta = \eta_0 \left(\frac{\sinh^{-1}\lambda\dot{\gamma}}{\lambda\dot{\gamma}} \right) \quad , \tag{3.5}$$

and Carreau's (1968) by

$$\frac{\eta - \eta_\infty}{\eta_0 - \eta_\infty} = \left[1 + (\lambda\dot{\gamma})^2\right]^{\frac{n-1}{2}} \quad . \tag{3.6}$$

Models such as these present the advantage, if they prove applicable, that the characteristic time of the solution may then be determined from simple shear viscosity experiments. For more complex fluids, the direct determination of the elasticity with the aid of sophisticated equipment such as computerized rheometers might be necessary. If the characteristic time is known, it can be used to construct non-dimensional numbers (such as the Weissenberg or Deborah numbers) in order to provide an additional parameter for a better description of the flow and of the fluid.

Some of the most commonly studied viscoelastic fluids are solutions of polymers. The elasticity of this type of fluid is considered responsible for such typical non-newtonian phenomena as recoil, rod-climbing, die swell, tubeless siphon, and drag and heat transfer reduction.

Polymer solutions often present a viscosity function consisting of a newtonian region at low shear rates, a pseudoplastic region for intermediate shear rates, and finally another newtonian region for the high shear rates. For the type of experiments conducted in this study, the range of shear rates encountered usually corresponds to the latter two regions.

It is also possible to encounter fluids that would exhibit a combination of the various characteristic behaviors mentioned in these sections. The antimisting kerosene studied, for example, is viscoelastic but also

discontinuously shear-thickening and time-dependent.

3.1.4. **Time-Dependent Fluids**

Time-dependent fluids exhibit a viscosity that may decrease (thixotropic fluids) or increase (rheopectic fluids) with time under a constant shear. This behavior is typical of some suspensions and polymer solutions, and may be encountered in conjunction with other non-newtonian characteristics. This time-dependency naturally complicates significantly the representative equations for these fluids.

3.2. **FRICTION**

3.2.1. **Newtonian Fluids**

3.2.1.1. *Laminar flow*

In the laminar regime, up to a Reynolds number of about 2000, it is well-known that for fully-developed flow, the friction coefficient and the Reynolds number are related by the simple expression

$$C_f = \frac{16}{\mathrm{Re}} \tag{3.7}$$

where the Reynolds number is defined as

$$\mathrm{Re} = \frac{\rho V D}{\eta} \tag{3.8}$$

and the friction coefficient is

$$C_f = \frac{\tau_w}{\frac{1}{2}\rho V^2} \tag{3.9}$$

(τ_w is the wall shear stress). This result stems from a straightforward integration of the momentum equation. The corresponding velocity profile is parabolic. The wall shear rate is then

$$\dot{\gamma}_w = \frac{8V}{D}. \tag{3.9a}$$

For the flow in the entrance region, one may solve a linearized momentum equation or use other methods (see the review by Shah and London, 1978) to determine the velocity profile and the pressure drop. These are usually presented as numerical results for simplicity. In addition to the friction-induced pressure drop, one has to take into account extra losses. These losses are often added to the kinetic energy term in empirical expressions such as:

$$\Delta p_{ent} = 1.12\rho V^2 \tag{3.10}$$

for a flush tube with slightly rounded entrance.

The entrance length for newtonian fluids may be approximated by expressions such as (Kays and Crawford 1980)

$$\frac{L_e}{D} = \frac{\mathrm{Re}}{20} . \tag{3.11}$$

This would amount to a maximum of about 100 diameters for the case of

Re = 2000.

3.2.1.2. *Turbulent flow*

The study of turbulence is clearly a very complicated problem, and there has been a large number of experimental and theoretical studies devoted to finding the best representation of the mechanisms involved. Semi-empirical studies have been very successful for pipe flows, and the results are not much contested, although the accuracy of the simpler expressions may be off by a few percent over certain ranges of Reynolds numbers. For fully-developed flows the well-known expressions by Prandtl

$$\frac{1}{\sqrt{C_f}} = 4.0 \log(Re\sqrt{C_f}) - 0.4 \tag{3.12}$$

and Blasius

$$C_f = 0.079\ \mathrm{Re}^{-0.25} \tag{3.13}$$

are often used. Good approximations for smooth pipes were also found by White (1974)

$$C_f = 0.255(log\ Re)^{-2.5} \tag{3.14}$$

and Petukhov (1970)

$$\frac{C_f}{2} = (2.236\ \ln \mathrm{Re} - 4.639)^{-2}\ . \tag{3.15}$$

More sophisticated expressions may be developed based on elaborate representations of velocity profiles and turbulence. These may also sometimes be used for studies of friction and heat transfer of

viscoelastic fluids, as will be shown later. One of the simplest representations of the velocity profile is the 2-layer model. In the law of the wall nomenclature, it consists of a viscous sublayer

$$u^+ = y^+ \tag{3.16}$$

for $y^+ < 12$, and a logarithmic or turbulent profile

$$u^+ = 2.5 \ln y^+ + 5.5 \tag{3.17}$$

for the rest of the pipe.

The latter layer corresponds to a K= 0.4 constant in the Prandtl mixing length theory (and leads to Prandtl's expression mentioned above). As a reminder, this theory is based on the concept of eddy diffusivity, obtained from the turbulent equation of momentum. A commonly used version of this equation is

$$\frac{\tau}{\rho} = (\nu + \varepsilon_M) \frac{\partial \overline{u}}{\partial y} \quad . \tag{3.18}$$

The eddy diffusivity for momentum (ε_M) is approximated by

$$\varepsilon_M = \ell^2 \left| \frac{\partial \overline{u}}{\partial y} \right| \tag{3.19}$$

where it was suggested that "ℓ" may be proportional to the product "Ky" near the wall.

This rather simple approach has been improved by the use of expressions for the eddy diffusivity that would give a smooth profile in the overlap region. As these concepts are of importance for the modeling of drag reduction, they will be reviewed briefly. Continuous expressions for the

eddy diffusivity include contributions by Deissler (1954) for $y^+ < 26$ (with m = 0.124)

$$\frac{\varepsilon_M}{\nu} = m^2 u^+ y^+ \left(1 - e^{-m^2 u^+ y^+}\right) , \tag{3.20}$$

Reichardt (1951,1957), with K = 0.4

$$\frac{\varepsilon_M}{\nu} = \frac{K y^+}{6}\left(1 + \frac{r}{r_i}\right)\left(1 + 2\left(\frac{r}{r_i}\right)^2\right) , \tag{3.21}$$

and the damping model of Van Driest (1956), with K = 0.4 and $A^+ = 26$

$$\frac{\varepsilon_M}{\nu} = K^2 y^{+2}\left(1 - e^{-y^+/A^+}\right)^2 \left|\frac{\partial u^+}{\partial y^+}\right| . \tag{3.22}$$

This type of expressions leads, after integration, to velocity profiles that are smoother than the 2-layer model, and some of them, more accurate at the center of the pipe (zero velocity gradient). As illustration, Deissler's expression would give after integration of Equation 3.18

$$u^+ = \int_0^{y^+} \frac{dy^+}{1 + m^2 u^+ y^+ (1 - e^{-m^2 u^+ y^+})} \tag{3.23}$$

for $y^+ < 26$ and could be combined with Prandtl's logarithmic profile for the turbulent core.

More importantly maybe, the models that do not assume a zero diffusivity in the viscous sublayer will give better results for heat transfer. A simple approximation sometimes used for these velocity profiles is based on a power-law with a 1/7 exponent, and gives after integration an expression very close to Blasius's.

The hydrodynamic entrance region for turbulent flows is fairly short, and 20 diameters are usually sufficient to obtain a fully-developed velocity profile.

3.2.2. **Purely Viscous Non-Newtonian Fluids**

3.2.2.1. *Laminar flow*

The case of purely viscous non-newtonian fluids has been extensively investigated by Metzner and coworkers (Metzner and Reed 1955, Dodge and Metzner 1959, Bogue and Metzner 1963), who defined the concept of generalized Reynolds number, based on a power-law representation. They proposed that for a laminar tube flow of these fluids

$$\frac{D\,\Delta p}{4L} = K'\left(\frac{8V}{D}\right)^{n'} \tag{3.24}$$

or

$$n' = \frac{d\left(log\ \frac{D\,\Delta p}{4L}\right)}{d\left(log\ \frac{8V}{D}\right)}\ , \tag{3.25}$$

and

$$\dot{\gamma}_w = \left(\frac{3n'+1}{4n'}\right)\frac{8V}{D}\ . \tag{3.26}$$

If we have a fluid representable by a power-law, then

$$\tau = K\dot{\gamma}^n \tag{3.27}$$

and

$$\tau_w = K\left(\frac{3n + 1}{4n}\,\frac{8V}{D}\right)^n \quad . \tag{3.28}$$

Accordingly, if n is constant

$$n' = n \tag{3.29}$$

and, because

$$\tau_w = \frac{D\,\Delta p}{4L} \tag{3.29a}$$

for laminar pipe flow, we have also

$$K' = K\left(\frac{3n + 1}{4n}\right)^n \quad . \tag{3.30}$$

Metzner then defined the generalized Reynolds number as

$$\mathrm{Re}' = \frac{\rho\, V^{2-n'} D^{n'}}{K' 8^{n'-1}} \quad . \tag{3.31}$$

This definition has the great advantage that for laminar flow

$$C_f = \frac{16}{\mathrm{Re}'} \tag{3.32}$$

whatever the value of n (the power-law exponent) is. All the friction coefficients for laminar flow of power-law fluids would thus collapse on this one curve (which is not necessarily the case with other definitions of the Reynolds number).

3.2.2.2. *Turbulent flow*

For turbulent flow, basing themselves on velocity profiles similar to those of newtonian fluids, Metzner then derived the following correlation (determining experimentally the exponents of n)

$$\frac{1}{\sqrt{C_f}} = \frac{4}{n^{0.75}} \log\left[\mathrm{Re}' C_f^{1-(n/2)}\right] - \frac{0.4}{n^{1.2}} \qquad (3.33)$$

which is similar to Prandtl's expression except for the presence of n. This correlation is often used, although it has been suggested later that the resulting values for C_f might be too low (Metzner 1965). The transition was observed to be slightly higher than for newtonian fluids (between Re = 2000 and 4000).

The entrance length for purely viscous fluids was estimated (Yoo, 1974) to be roughly similar to that of newtonian fluids.

3.2.3. **Viscoelastic Fluids**

3.2.3.1. *Laminar flow*

The study of friction in tubes is somewhat more complicated for viscoelastic fluids of the drag-reducing type. As mentioned above, these fluids exhibit a much lower friction than Newtonian fluids do at the same flow rate. Interestingly, this phenomenon is limited to turbulent flow, however, and it is thus possible in the case of laminar flow to use the same expression as that used for the purely-viscous non-newtonian fluids. Another definition of Reynolds number is often used for viscoelastic fluids, and seems sometimes more adequate than the generalized Reynolds number. This definition is based on an apparent newtonian viscosity (η_a) at the wall defined as

$$\tau_w = \eta_a \dot{\gamma}_w \tag{3.34}$$

and consists simply of

$$\mathrm{Re}_a = \frac{\rho V D}{\eta_a} \ . \tag{3.35}$$

This approach is acceptable because it is believed that the most important phenomena for drag reduction do occur very close to the wall, and also because for the high shear rates considered in these flows the viscosity does not vary much in general with shear rate. This definition of the apparent Reynolds number does not lead to a unique laminar relationship, however. We have in laminar tube flow

$$\tau_w = \eta_a \frac{3n + 1}{4n} \frac{8V}{D} \tag{3.36}$$

and consequently

$$C_f = \frac{3n + 1}{4n} \frac{16}{\mathrm{Re}_a} \tag{3.37}$$

which is now a function of n.

3.2.3.2. *Turbulent flow*

In turbulent flow, the friction coefficient may be significantly smaller than for a newtonian fluid, and depends on both the flow and the polymer characteristics (graphs illustrating the concepts mentioned in these sections on viscoelastic fluids may be found in app. C.1). This reduction is, however, limited to a minimum value which appears to be remarkably independent of the type of polymer and solvent used. An expression for this minimum asymptote has been compiled by Virk, Mickley, and Smith

(1969) using experimental data of various sources

$$\frac{1}{\sqrt{C_f}} = 19.0 \log(Re\sqrt{C_f}) - 32.4 \quad . \tag{3.38}$$

Virk inferred from this expression for the friction coefficient a velocity profile for asymptotic flow conditions

$$u^+ = 11.7 \ln y^+ - 17.0 \tag{3.39}$$

corresponding to an "elastic" layer. This logarithmic form implies a mixing length constant of K = 0.085 rather than the value of 0.4 found for newtonian fluids. Another interesting characteristic of this profile is that it is close to intersecting the linear and newtonian logarithmic profiles at their own intersection, namely for approximately $y^+ = 12$.

Based on the experimental studies of velocity profiles for intermediate drag reduction, Virk proposed a three-layer model for these fluids that consists of the viscous sublayer, the elastic sublayer and a logarithmic profile parallel to that for newtonian fluids (see app. C.1., fig. 3). The latter might be represented by

$$u^+ = 2.5 \ln y^+ + 5.5 + \Delta u^+ \tag{3.40}$$

where Δu^+, the shift, is a function of the polymer and of the flow characteristics. The asymptotic flow would then correspond to the case where the ultimate profile extends to the center of the pipe, effectively cancelling the turbulent logarithmic core. This model is consistent with the early idea that the viscous sublayer is somehow thickened by the action of the polymer.

In a fashion similar to that used for the case of newtonian fluids, it has been attempted to improve on this simple model by the use of more sophisticated expressions for the eddy diffusivity.

Out of the several models existing, the one by Mizushina, Usui, and Yoshida (1974) will be used as an illustration. These authors followed an analysis similar to the Van Driest model, but with a viscoelastic damping factor involving a characteristic time. The mixing length obtained was

$$\ell = DF\left[0.4\,y^{+} - 0.44\,\frac{y^{+2}}{r_i^{+}} + 0.26\,\frac{y^{+3}}{r_i^{+2}} - 0.06\,\frac{y^{+4}}{r_i^{+3}}\right] \tag{3.41}$$

where DF, the damping factor, is

$$DF = 1 - e^{-\frac{y^{+}}{26}\left(-\alpha + (1+\alpha^2)^{\frac{1}{2}}\right)^{\frac{1}{2}}} \tag{3.42}$$

and α is a function of the characteristic time of the fluid:

$$\alpha = 2\,\frac{\lambda}{\nu}\left[\frac{u_\tau}{26}\right]^2 . \tag{3.43}$$

For the asymptotic regime, they determined that α is equal to about 60, whereas for intermediate drag reduction they correlated its value in function of the Weissenberg number. Using this expression it is possible to determine the velocity profile by integration in the usual newtonian manner. A model also based on Van Driest's method, but incorporating a law of the wake to describe more accurately the velocity at the center of the pipe, was used by Dimant and Poreh (1976).

A representation based on Deissler's expression (eq. 3.20) but with lower values of m, was adopted by Debrule and Sabersky (1974) who

found that a value of m = 0.040 would fit their data. Several other expressions based on eddy viscosity have also been used for drag-reducing fluids, and some were reviewed by Edwards and Smith (1980).

In summary, the models used for the drag-reducing fluids are mostly extensions of traditional newtonian turbulence models with additional parameters introduced to represent the viscoelasticity, or more simply, with modified values of the existing parameters.

In a more practical approach, empirical correlations for the drag-reducing asymptotes have been reported (Cho and Hartnett 1982) that do make the distinction between generalized and apparent Reynolds number:

$$C_f = 0.332\ \mathrm{Re}'^{-0.55} \tag{3.44}$$

for $6000 < Re' < 40000$, and

$$C_f = 0.20\ \mathrm{Re}_a^{-0.48} \tag{3.45}$$

for $6000 < \mathrm{Re}_a < 60000$. These equations lead to friction factors which are somewhat lower than Virk's.

Whereas it is possible to represent the friction in this simple fashion for asymptotic drag reduction, for intermediate cases another parameter, such as the Weissenberg number (We), may be needed. Empirical correlations for C_f as a function of We have thus been developed for given Reynolds numbers (Kwack and Hartnett 1983). It may also be possible to evaluate Δu^+ (eq. 3.40) as a function of We (Kwack and Hartnett 1984). It is not clear, however, whether the diameter present in the

expression of

$$We = \frac{\lambda V}{D} \tag{3.47}$$

might account properly for the diameter effect observed for these polymer solutions.

As mentioned earlier, for a concentration and a Reynolds number that do not correspond to asymptotic conditions, the friction curve will be located somewhere between the newtonian curve and Virk's asymptote (app. C.1., fig. 1). Exactly where is not fully predictible at this time, especially because for a given solution the amount by which the friction is reduced is also a function of the pipe diameter (app. C.1., fig. 2). Of course, the flow characteristics of a given solution will also depend on the degree of degradation to which the fluid has been exposed, but this is measurable and could be expressed by a lower value of the Weissenberg number. The solvent effects may have a similar influence.

The hydrodynamic entrance lengths for viscoelastic fluids in the laminar regime are similar to those of purely viscous fluids because the elasticity apparently does not play a role in laminar flow. For turbulent flows, however, the entrance lengths appear to be longer than those for purely viscous non-newtonian fluids. According to Tung, Ng, and Hartnett (1978), up to 100 diameters may be needed to establish equilibrium profiles.

3.3. HEAT TRANSFER

3.3.1. Newtonian Fluids

3.3.1.1. *Laminar flow*

In fully-developed laminar flow, it is well-known that for the constant heat flux boundary condition one finds a value of the local Nusselt number that is independent of the Reynolds and Prandtl numbers

$$Nu_\infty = 4.364 \tag{3.48}$$

with the usual assumptions (no axial conduction, no viscous dissipation). (For a complete discussion of laminar flow, see the review by Shah and London 1978.) The Nusselt number is defined as

$$Nu = \frac{h\,D}{k} \tag{3.49}$$

where k is the thermal conductivity of the fluid and h is the convective heat transfer coefficient, itself defined as

$$h = \frac{q_w}{T_w - T_b} \tag{3.50}$$

(q_w being the wall heat flux).

For a thermally-developing but already hydrodynamically-developed flow, the results are more complicated, and are often expressed as the solution of an eigenvalue problem. We find, for example, (Kays and Crawford 1980):

$$Nu = \left[\frac{1}{Nu_\infty} - \frac{1}{2} \sum_m \frac{e^{-\gamma_m^2 x^+}}{A_m \gamma_m^4} \right]^{-1} \tag{3.51}$$

with

m = 1	γ_m^2 = 25.68	A_m = 7.630 10^{-3}
2	83.86	2.058
3	174.2	0.901
4	296.5	0.487
5	450.9	0.297

etc, and where

$$x^+ = \frac{2 \frac{x}{D}}{\mathrm{Re}\ Pr} \quad . \tag{3.52}$$

A first approximation for the entrance region length might be taken as $x^+ = 0.1$ for which the difference with the fully-developed value of Nu is about 3%. In that case, we have for this length

$$\frac{L_e}{D} = 0.05\ \mathrm{Re}\ Pr \quad . \tag{3.53}$$

Typical conditions for some of the fluids used in this study might be, for example, Re= 1000 and Pr= 10. We see that in this case the thermal entrance length would be of the order of 500 diameters, which is fairly long indeed.

If the hydrodynamic conditions are not yet fully-developed at the entry of the heated section, the temperature and velocity profiles will develop simultaneously and the problem to solve is accordingly more

complex. For Pr > 5 , however, the velocity profile grows much more rapidly than the temperature profile, and the approximation of hydrodynamically-developed flow is usually acceptable.

Simpler expressions approximating these results are sometimes used, in particular (Bird, Armstrong, and Hassager 1977)

$$Nu = 1.41\ Gz^{1/3} \tag{3.54}$$

where the Graetz number is defined as

$$Gz = \frac{\pi}{4} \mathrm{Re}\ Pr\ \frac{D}{x} \ . \tag{3.55}$$

3.3.1.2. *Turbulent flow*

For turbulent flow, the heat transfer problem is solved using the turbulence concepts described above for friction. The turbulent energy equation may be reduced to a form very similar to that for the turbulent shear stress (eq. 3.18):

$$\frac{q}{\rho\, Cp} = (\alpha + \varepsilon_H)\ \frac{\partial \overline{T}}{\partial y} \tag{3.56}$$

where ε_H is the turbulent diffusivity for heat.

Following the Reynolds analogy, the turbulent diffusivities for heat and momentum are often assumed to be equal, because both are representative of the same mechanism of turbulent exchange. This assumption appeared quite successful for many analyses. It has been suggested, however, that the analogy might not be true in general, particularly close to the wall. For large Prandtl number though, it is probably acceptable.

Using the universal velocity profiles described earlier, it is possible to integrate the previous expression to obtain the temperature profile, as a function of both the Prandtl number and the turbulent Prandtl number. The latter is defined as

$$Pr_t = \frac{\varepsilon_M}{\varepsilon_H} \quad . \tag{3.57}$$

We get

$$T^+ = \int_0^{y^+} \frac{dy^+}{\frac{1}{Pr} + \frac{\varepsilon_M}{\nu\, Pr_t}} \tag{3.58}$$

where

$$T^+ = \frac{(T_w - T)\rho\, Cp\, u_\tau}{q_w} \quad . \tag{3.59}$$

This integral can be evaluated if we use one of the expressions for the eddy diffusivity of momentum, and it is then a simple matter to evaluate the Nusselt number.

The well-known Reichardt's analysis (Reichardt 1951,1957), for example, with the additional assumptions that $Pr_t = 1$, that the ratio of the mean to maximum temperature difference between fluid and wall is one as well, and that the shear stress and shear rate are linear functions of the radius, would give (Friend and Metzner 1958)

$$Nu = \frac{\frac{C_f}{2}\,\mathrm{Re}\,Pr}{1.2 + b\sqrt{\frac{C_f}{2}}\,(Pr - 1)} \tag{3.60}$$

where

$$b = \int_0^{\frac{u_{max}}{u_\tau}} \frac{du^+}{1 + Pr\,\frac{\varepsilon_M}{\nu}} \tag{3.60a}$$

and u_{max} is the centerline velocity.

Many correlations have been developed based on the form of the results of analyses conducted as explained above, but better fitted to experimental data. For example, (Petukhov 1970) found that

$$Nu = \frac{\frac{C_f}{2}\mathrm{Re}\,Pr}{1.07 + 12.7\frac{\sqrt{C_f}}{2}(Pr^{2/3} - 1)} \tag{3.61}$$

is adequate over a large range of Pr and Re numbers if his expression for the friction coefficient (eq. 3.15) is used.

Another interesting correlation is that by Sleicher and Rouse (1975) :

$$Nu = 5 + 0.015\,\mathrm{Re}^a\,Pr^b \tag{3.62}$$

where

$$a = 0.88 - \frac{0.24}{4 + Pr}$$

and

$$b = 1/3 + 0.5\,e^{-0.6\,Pr} .$$

Other convenient correlations are (Kays 1966) for 1<Pr<20

$$Nu = 0.0155\ \mathrm{Re}^{0.83}\ Pr^{0.5} \tag{3.63}$$

and for Pr>20

$$Nu = 0.0118\ \mathrm{Re}^{0.9}\ Pr^{0.3}\ . \tag{3.64}$$

These expressions are all considered somewhat more accurate than the well-known Dittus-Boelter equation for heating (Dittus and Boelter 1930)

$$Nu = 0.023\ \mathrm{Re}^{0.8}\ Pr^{0.4}\ . \tag{3.65}$$

The Colburn analogy (Colburn 1933) between heat and momentum transfer is usually expressed as

$$C_H\ Pr^{2/3} = \frac{C_f}{2} \tag{3.66}$$

and is a fair approximation for newtonian tube flows. It can also be written as

$$Nu = \frac{C_f}{2}\ \mathrm{Re}\ Pr^{1/3}\ . \tag{3.67}$$

If the properties of the fluid do vary with temperature and the temperature difference between the wall and the bulk of the fluid is not small, these expressions involving the bulk temperature must be corrected. A popular type of correction is based on property ratios, where a factor such as (Sieder and Tate 1936)

$$\left(\frac{\eta_w}{\eta_b}\right)^m \tag{3.68}$$

may be used to correct the values of Nu and C_f based on the assumption of constant properties. For the heating case, common values are

$m = -0.14$ for laminar heat transfer, m=0.58 for laminar friction, m=-0.11 for turbulent heat transfer, and m=0.25 for turbulent friction (Kays and Crawford 1980).

Another suggestion for reducing this problem is the proposal by Sleicher and Rouse (1975) to use in their formula Nu computed at bulk temperature, Re based on film temperature, and Pr calculated at wall temperature.

The problem of the turbulent thermal entry region can be solved in the same fashion as the laminar problem. The entry lengths are shorter, however, and for Pr>5, 20 diameters should be sufficient for the local Nu to approach its fully-developed value within 1%.

3.3.2. **Purely Viscous Non-Newtonian Fluids**

3.3.2.1. *Laminar flow*

For laminar flow, it is easy to modify the existing equations for newtonian fluids. For example, assuming power-law velocity profiles, we can use (Bird, Armstrong, and Hassager 1977)

$$Nu = 1.41\ Gz^{1/3}\left(\frac{3n+1}{4n}\right)^{1/3} \tag{3.69}$$

for the thermal entry region, and

$$Nu_{\infty} = \frac{8(3n+1)(5n+1)}{31n^2+12n+1} \tag{3.70}$$

for the fully-developed thermal problem. The entrance lengths are similar to those of newtonian fluids.

If the difference between bulk and wall temperature is large, corrections of the Sieder-Tate type (eq. 3.68) are sometimes used. Other correlations are reviewed in Cho and Hartnett (1982), some including corrections for natural convection as well.

For non-newtonian fluids, the non-standard Reynolds and Prandtl numbers have to be consistent. The Prandtl number may be defined in such a way (Cho and Hartnett 1982) that the product of Re and Pr is equal to the Peclet number which is only a function of the material properties and of the velocity, but not of the non-newtonian character of the fluid

$$Pe = \frac{V D \rho Cp}{k} \quad . \tag{3.71}$$

We have then, based on the definitions of generalized (eq. 3.31) and apparent (eq. 3.35) Reynolds numbers,

$$Pr' = \frac{Cp\ K'(\frac{8V}{D})^{n-1}}{k} \tag{3.72}$$

and

$$Pr_a = \frac{\eta_a Cp}{k} \quad . \tag{3.73}$$

The thermal conductivity of solid suspensions in liquid may be approximated by an analogy with the electrical equations of Maxwell (Metzner 1965). This gives us for low concentrations

$$\frac{k_{sus}}{k_s} = \frac{2k_s + k_{par} - 2x_v(k_s - k_{par})}{2k_s + k_{par} + x_v(k_s - k_{par})} \tag{3.74}$$

where k_{sus} is the thermal conductivity of the suspension, k_s that of the solvent, k_{par} that of the particles, and x_v is the volume fraction of particles.

The heat capacity may be approximated simply by a weighted average.

3.3.2.2. *Turbulent flow*

For the turbulent flow of purely viscous fluids, it was suggested (Friend and Metzner 1958) to use a correlation based on Reichardt's treatment of the analogy between momentum and heat transfer. The correlation is

$$Nu = \frac{\mathrm{Re}\, Pr\, \frac{C_f}{2}}{1.2 + 11.8\sqrt{\frac{C_f}{2}}(Pr - 1)\, Pr^{-1/3}} \tag{3.75}$$

for $Pr\ \mathrm{Re}^2 C_f > 5\ 10^5$, C_f being given by Metzner's expression for purely viscous fluids (eq. 3.33).

Another correlation has been developed empirically by Yoo (1974) for purely viscous fluids

$$C_H\, Pr_a^{2/3} = 0.0152\, \mathrm{Re}_a^{-0.155} \quad . \tag{3.76}$$

3.3.3. **Viscoelastic Fluids**

In laminar flow, the viscoelastic fluids behave like purely viscous non-newtonian fluids, because the elastic character they exhibit is apparently of no influence in this regime.

In turbulent flow, however, the differences are considerable, even more so for heat transfer than for friction. It is well-known that the drag reduction experienced by these solutions is accompanied by an even greater reduction in convective heat transfer (see section 2.2).

A major characteristic of these viscoelastic fluids is the very large thermal entrance lengths they exhibit in turbulent flow (it may be pointed out that the hydrodynamic entrance region was also somewhat larger than for newtonian fluids). Ng, Cho, and Hartnett (1980), for example, found that the thermal entry region extends to 430 diameters in some cases. This important fact has not been fully explained yet, but it has to be concluded that the results of most of the previous experimental heat transfer studies probably do not correspond to fully-developed conditions.

For fully-developed turbulent flow, most of the investigators have proposed models based (as was the case for friction) on classical newtonian expressions with either the introduction of new parameters, or a modification of the old ones.

An example of a correlation based on the implicit use of the Reynolds analogy, but with the introduction of a viscoelastic parameter, is that by Kale (1977). His correlation is based on Reichardt's analysis for heat transfer and Deissler's expression for the velocity profile. It is

$$Nu = \frac{\frac{C_f}{2} \mathrm{Re}\, Pr}{1.2 + \sqrt{\frac{C_f}{2}}(Pr - 1)(9.2\, Pr^{-0.258} + 1.2\, De\, Pr^{-0.236})} \quad . \quad (3.77)$$

This expression for intermediate heat transfer reduction is thought to represent the asymptotic case when the Deborah number ($De = \lambda u_\tau^2 / \nu$) is larger than 20. Other similar semi-empirical correlations are reviewed in Cho and Hartnett (1982).

One study in particular that did not strictly assume the equality of eddy diffusivities of heat and momentum is that by Mizhushina, Usui, and Yamamoto (1975). They proposed that

$$\frac{\varepsilon_H}{\varepsilon_M} = 1.5\, \frac{1 - e^{-y^+/(42+(120/\sqrt{Pr}))}}{1 - e^{-y^+/26}} \quad (3.78)$$

where ε_M is their modified expression for the eddy diffusivity of momentum (from eq. 3.41). The exponential factor on the numerator is their expression for the heat transfer damping factor as evaluated from a polyethylene oxide solution.

According to this expression, the eddy diffusivity of heat would be significantly smaller than that of momentum for $y^+ < 50$. Using these values for the eddy diffusivities, these authors were able to predict a heat transfer reduction larger than the friction reduction (Mizushina and Usui 1977).

Using their experimental data for the minimum heat transfer asymptote and Virk's velocity profile, Cho and Hartnett (1982) determined an expression for the asymptotic eddy diffusivity of heat

$$\frac{\varepsilon_H}{\nu} = 2.5\ 10^{-6} y^{+3} \tag{3.79}$$

This expression gives a value smaller than the eddy diffusivity of momentum calculated from Virk's profile, suggesting again a deviation from Reynolds's analogy. Using this result, they also evaluated the entrance lengths to be much larger than for newtonian fluids.

Their expression for the minimum heat transfer asymptote is

$$C_H\ Pr^{2/3} = 0.03\ \mathrm{Re}_a^{-0.45} \tag{3.80}$$

for $4000 < \mathrm{Re}_a < 40000$, whereas in the entrance region ($x/D < 430$) they proposed

$$C_H\ Pr^{2/3} = 0.13(\frac{x}{D})^{-0.24}\mathrm{Re}_a^{-0.45} \tag{3.81}$$

In the intermediate regime, the diffusivities might be estimated as a function of the Weissenberg number. Kwack and Hartnett (1984) attempted to evaluate this effect, but, surprisingly, they found that the turbulent Prandtl number would be about equal to- or smaller than unity for most of the Weissenberg number range wich corresponds to friction coefficients above the asymptote. They also examined the effect of Weissenberg number on the entrance length and velocity profile shift.

3.4. THE DIAMETER EFFECT

An important point that is to be emphasized for some non-newtonian fluids, and viscoelastic polymer solutions in particular, is that the diameter of the pipe in which the measurements are conducted may have a significant influence on the friction and heat transfer results. This

problem was introduced in section 2.1.6, with a review of some of the important related studies.

A theoretical study was conducted on this subject, and has led to a prediction method for the influence of the diameter effect on the friction and heat transfer properties of viscoelastic fluids. These results were published (Matthys and Sabersky 1982), and this article has been reproduced in Appendix C.1. Consequently, the results will not be repeated here in detail. However, a few of the findings will be summarized.

The method is based on a three-layer model of velocity profile (section 3.2.3.2.). A key feature of this model is the displacement of the logarithmic layer by an amount Δu^+. The assumption is made that this displacement is a unique function of the friction velocity (independently of the diameter), and that this relationship Δu^+ vs u_τ is a property of the particular solution considered.

This prediction method is based on the determination of the value of Δu^+ for a given polymer and flow conditions. If the three layers are taken into account, however, it is not feasible to find a closed analytical solution for Δu^+ as a function of the friction coefficient and Reynolds number. As Δu^+ is therefore not known a priori, the following approach was used.

By numerical integration of the velocity profiles, families of values are derived which give C_f as a function of Re for any Δu^+. Several such standard families were determined for various values of Δu^+ as the parameter, and are applicable for any polymer or flow conditions. With

the aid of these relationships, an iterative interpolation procedure allows then the determination for any diameter of a consistent set of Δu^+ , Re, and C_f which also satisfies the Δu^+ vs u_τ relationship for the solution. This procedure was verified using experimental results, and the values predicted were in rather good agreement with these results.

It should be emphasized that the need for this procedure arises from the fact that the asymptotic layer is included in the integration over the radius. Most of the earlier studies used only the logarithmic layer which made it possible to develop analytical solutions. It is evident, however, that such results are not acceptable for more than a slight drag reduction, the asymptotic layer soon playing an important role. Naturally, for cases where the asymptotic velocity layer extends to the center of the pipe, the displaced logarithmic layer disappears, the value of Δu^+ becomes then indetermined, and there is no more effect of the diameter on friction and heat transfer. The value of the friction coefficient in these cases is, of course, uniquely determined by the expression for the friction asymptote.

CHAPTER 4

EXPERIMENTAL INSTALLATION AND PROCEDURES

4.1. INTRODUCTION

In order to address the objectives of this research project as outlined earlier, a complete experimental installation had to be designed and built for friction, heat transfer, and rheological measurements. This system had to be designed taking into account the following constraints and requirements.

The degradation induced by the system itself has to be minimal in order to be able to study the fluids in an unaltered state. The best way to avoid degradation is to use a single-action hydraulic cylinder (the "pump" for simplicity) in a once-through system, rather than rotary or reciprocating pumps and recirculating loops. This concept is also advantageous in the sense that it provides an accurate and convenient way of measuring mass flow rates, a sometimes difficult proposition for non-newtonian fluids. The disadvantage of this method is the large quantity of fluid needed for high Reynolds number measurements and the associated necessary increase in size for the pump itself and the reservoirs.

The largest available cylinder allowed only relatively short runs at the high Reynolds numbers, which made the manual collection of the large number of necessary measurements impossible. Consequently, a direct connection between the installation and a computerized data acquisition system was essential. This method of data collection was also most

convenient as it made possible measurements as a function of time, and allowed the averaging and direct processing of a great number of data. This feature significantly increased the accuracy and versatility of the installation.

For the present experiments, it was desired to obtain a region of fully-developed flow, and as pointed out earlier this may require a length to diameter ratio of as much as 500. Taking into account the constraints on laboratory space, this led to the selection of a pipe of approximately 0.8 cm inside diameter. This diameter was thought to be sufficiently large to avoid problems with suspensions of even relatively large fibers. It also allowed the drilling of pressure taps proportionally small enough to limit the possible errors introduced by the non-newtonian fluids. In order to be able to study both the entrance flow and the degradation in the tube, sets of pressure transducers and thermocouples were positioned along its length. The dimensions of the installation typically allowed the study of flows involving Reynolds numbers of up to 100000 for water.

A constant heat flux mode was chosen for the heat transfer measurements, an accurate control of the power and temperature distributions being obtained by direct Joule heating of the stainless steel tube walls. Two DC generators delivering up to 750 A were connected to provide the necessary currents. The high currents used also required special precautions to isolate the system for personnel safety and for the protection of the electronic equipment. Local heat transfer and friction measurements were conducted simultaneously in the same test section.

In view of the large dimensions of the pump and the relatively high pressures involved (up to 7 atm), an external hydraulic system was connected to the chamber on the rear side of the piston. In this way the back of the piston was also exposed to pressure, thereby eliminating bypass leaks in the cylinder and also reducing the mechanical force that had to be transmitted to the piston rod by the main electric motor.

Separately from the main installation, two capillary viscometers were constructed, one of the vacuum and pressure tank variety and the other one based on the single-action hydraulic cylinder principle. These are used for the rheological measurements of the solutions studied and had to be designed to provide shear stress/shear rate relationships in the ranges covered by the fluids in the main heat transfer tests.

4.2. DESCRIPTION OF THE EXPERIMENTAL INSTALLATION

(For more details on the installation, the reader is referred to app. B on hardware description and calibration.)

4.2.1. The pump

A schematic diagram of the test installation is shown in Fig. 4.1. As mentioned in section 4.1, in order to limit the degradation of the fluid by the system itself, a large single-action hydraulic cylinder (the "pump") was used. The brass cylinder, carefully honed and polished before the start of the experiments, has an inside diameter of approximately 0.25 m and a usable length of about 1 m, i.e. a volume of about 0.05 m^3. The flow rate deliverable by the pump, limited on the one hand by the

minimum readable speed of the motor and on the other hand by the maximum pressure allowable for the system, ranges between $3\ 10^{-5}$ and $6\ 10^{-4}\ m^3/s$.

The piston is moved primarily by a variable speed DC electric motor, through a gear box and a ball screw shaft driven by a recirculating ball system. Rails and casters were added to prevent the shaft from spinning under heavy loads. A pair of course-limiting switches was introduced in series with the power supply to prevent the piston from bottoming out. An electromagnetic pick-up is used to measure the rotational speed of the motor (see app. B.2.). The signal produced is converted by an electronic circuit to a square wave of constant amplitude and sent to the analog/digital converter for frequency measurement. This measurement can be easily translated, after calibration, to a linear displacement speed for the piston, making it possible to compute very accurately the volumetric flow rate delivered by the pump (see app. B.1.).

During these flow rate calibrations, it was discovered that, at the high pressure settings, a substantial leak developed from the front (high pressure side) to the back of the piston. This problem was not prevented even after the piston was fitted with a set of new "scraper" O-rings, and the cylinder further polished. This leak is attributed to the thinness of the cylinder walls which probably allowed for a small distortion under pressure. Additionally, for these high pressures, a significant bending of the motive shaft was also noticed.

In order to alleviate both problems, a regulated pressurized hydraulic

system was connected to the back side of the piston. It consisted of a small tank pressurized by nitrogen and containing water or jet fuel according to the fluid being tested. (The use of jet fuel was made necessary by the polymer separation problems induced if the antimisting kerosene (AMK) tested is allowed to contact water.) It was then a simple matter to equalize the pressures on the front and back side of the piston during the runs, thereby effectively cancelling the leak as was indeed verified by calibration. This also relieved substantially the load on the electric motor and the shaft, adding the side benefit of a much more constant displacement speed. The cylinder and the secondary tank were of course fitted with various pressure relief and purge valves.

The side of the cylinder containing the test fluid was connected through a system of large feed pipes (2 inches diameter to avoid degradation) to either the main supply tank or independent 50-gallon drums. The drums were used only for the kerosene and AMK runs. The main supply tank (1 m^3) was built out of sheet metal and coated with acid-resistant tank paint in order to prevent contamination of the fluids. A large size adjustable-speed stirrer was mounted in the tank, as were electric heating coils when needed for high-temperature runs. The tank was left open for easier mixing and homogeneity checks of the solutions.

The pump cylinder was filled by aspiration directly from the supply tank or drums. This was done at low speed in most cases to prevent degradation. In the case of the clay suspensions, however, no degradation is expected but sedimentation on the other hand might well occur. For these suspensions, the filling was therefore done at higher speed for

better mixing, and the fluid was not allowed to stand in the cylinder for more than one or two minutes in order to avoid any deposition of particles. The cylinder has its output line positioned at the bottom for easier emptying and cleaning. It was also fitted with air purge vents and lines for nitrogen or solvent flushing.

The main line (2 inches diameter) connects the cylinder to the test tube with only two 90° elbows and no intermediate constriction. The mixing seemed to be adequate, and no mixing chamber was introduced upstream of the test tube. The temperature of the incoming fluid was measured at that location directly by a thermocouple probe in the pipe. A bell reducer was used to decrease as smoothly as possible the diameter of the line to that of the test tube (see fig. 4.2). All these features were adopted in order to minimize degradation.

Between the test tube and the feed line, an electrical and thermal insulator was inserted. This isolator consists of a disk of half-inch thick Teflon positioned between the adjacent circular flanges (fig. 4.2). Assembly bolts, themselves encased in Teflon bushings, were inserted through the 3 disks. This configuration is very convenient as it isolates electrically the test tube from the rest of the system, limits the heat lost by conduction at its extremities, and allows the tube to be readily slid in or out of the system without modification of its final positioning.

4.2.2. **The test tube**

The test tube is made of extruded seamless stainless steel. Its inner diameter is approximately 8 mm and its length about 5 m (see app. B.3.).

This diameter was chosen as a compromise between the corresponding necessary length for fully-developed flow, the largest diameter possible to avoid anisotropy effects, the desired range of Reynolds numbers of 5000 to 100000 for water-like fluids, and the availability of tubing.

The heat transfer measurements are conducted under the constant heat flux mode by direct Joule heating. This is done by short-circuiting a DC generator through the tube itself. The copper electrode disks are silver soldered to the end of the tube and connected to the generator by heavy duty welding cables. The generators are adjustable for currents between zero and 750 A (see app. B.9.). The voltage drop along the tube is measured directly by the analog-digital converter, whereas the value of the current intensity is obtained from a calibrated resistor in series with the DC circuit. The whole system was carefully grounded, and the leads to the A/D converter were shielded to avoid parasitic signals.

Pressure taps were drilled at various locations along the length of the tube. At each axial station 3 holes were drilled 120° apart. The holes are approximately 0.8 mm in diameter. This is the smallest size that allows deburring, chosen to minimize non-newtonian pressure hole errors that may become significant for large holes. It was nevertheless decided, as an additional precaution, to use only differential pressure measurements, this procedure likely cancelling any remaining error.

In order to isolate the electrically live tube from the pressure transducers, a cylindrical Teflon sleeve fitting over the tube was designed. This sleeve incorporates an inner coaxial cylindrical chamber in order to

connect the 3 holes for averaging of the pressure (fig. 4.3). A couple of metal outer liners, one of them connecting the pressure transducer to the inner chamber could then be securely clamped over the Teflon sleeve for a leakproof fit.

Difficulties were encountered at first because of the presence of burrs on the inside wall after drilling of the taps. Indeed, tests showed variations in measured pressure drops of more than 25% depending on the finish of the hole. The length of the tube preventing any accurate deburring from the ends, a tool had to be designed for insertion in the pressure taps themselves. This tool, essentially a sharp angular reamer was positioned with a sleeve in the hole in order to scrape off any burr on the inside wall. This procedure made it possible to clean the holes adequately for repeatable pressure measurements.

The pressure taps were connected to high-accuracy transducers that, fitted with a power supply and bridge, could be connected directly through shielded leads to the A/D converter (see app. B.9.). Unfortunately, these transducers were not available in large numbers, especially because the pressure drops to be measured were overlapping the ranges of several of the existing models. Because of this limited availability, it was not possible to obtain sets of more than 4 interchangeable transducers for each desired range of pressure.

Accordingly, it was decided to position the pressure taps at approximately 0.6 m apart, on the downstream half of the tube (because the primary interest of the friction studies was in fully-developed flows). This

separation distance was thought to be small enough for the actual pressure drop per unit length not to vary greatly between the taps. On the other hand, it permitted covering approximately half of the tube, making possible the evaluation of degradation in the tube itself.

The lines between the pressure taps and the transducers were bent and positioned in such a way as to prevent the accumulation of test fluid in the lines, and were filled with solvent prior to the tests. They also had to be carefully purged of all air for repeatable results, even after it was found out that 1/4 inch lines gave far better results than the 1/8 inch lines initially used.

A series of custom E-type thermocouples (see app. B.5.) was fixed on the outside wall of the tube at 9 different locations using high-thermal conductivity epoxy. The thermocouples were positioned at roughly 0.6 m apart, midway between the pressure taps, with an extra thermocouple close to the entrance of the tube to allow for a better investigation of the thermal entrance effects.

In the early stages of the thermocouple performance evaluation, various combinations of 2 and 3 thermocouples at a given axial location were tried. After several trial-and-error procedures involving the thickness of the epoxy layer, its width, and the substitution of thermal greases, it was concluded that the difference in measured temperature depending on the circumferential location was small. Accordingly, it was possible to use only one thermocouple at each axial location, provided a thin layer of epoxy was deposited around the tube to average the tem-

perature of the outside wall. This fact was of great help in reducing the number of channels necessary on the A/D converter.

The thermocouples were chosen to be of the E-type because of their high output and good match with the narrow range of temperature covered in the experiments. Tests were conducted with thermistors as well, but the difficulties encountered in the procurement of interchangeable high-accuracy and high-stability thermistors prevented their use.

It was shown that the epoxy electrically isolated the thermocouples adequately, and no effect of the current in the test tube on the temperature readings was noticed after a proper guarding procedure. The DC power mode was also chosen with the problem of induced currents in mind, being far less inconvenient than AC in that respect, especially with the long leads used in the installation.

The thermocouples were directly connected to the A/D converter, the junction reference temperature being measured very accurately. The correction to the measured voltages was made through software. Both thermocouple probes used for the measurement of entry and exit bulk temperatures were custom-built and of the ungrounded E-type. All the thermocouples were fabricated by inert arc bead-welding out of the same calibrated spool of high-quality thermocouple wires, and were calibrated in hot baths (see app. B.5.).

The leads were one piece from the measuring junction to the A/D converter in order to avoid additional junction problems and poor quality extension wires. The accuracy of the temperature measurements was

limited by the resolution of the microvoltmeter to 0.01 $^{\circ}C$. Additionally, of course, other errors were introduced through the use of the software compensation, epoxy, outer insulation etc. However, it is estimated that the temperature differences measurements were likely correct within 0.05 $^{\circ}C$, and this accuracy should be more than adequate for most of the measurements. The test tube, mixing chamber, and feed lines were all insulated with special foam to prevent heat loss to the atmosphere. The test tube, was placed under tension, and was carefully straightened out horizontally by several adjustable suspension lines fitted with porcelain isolators.

The end of the test tube was connected to a mixing chamber fitted with baffles to provide an efficient mixing for the exit bulk temperature measurement. This measurement was done with a probe at the end of the mixing chamber. Before this chamber and right after the end of the test tube, a side outlet makes possible the collection of samples for degradation studies. After the mixing chamber, the fluid is sent to a drain for disposal, or to drums for collection.

The various measurements mentioned: heating voltage and current intensity, temperatures, pressure drops, and speed of the motor, were all processed by the A/D converter in real time and stored in the computer memory for further processsing. During one run, as soon as a thermal steady state was achieved (as evidenced by constant wall temperature measurements), several sets of all the necessary data were taken. This precluded the possibility of use of non-steady measurements resulting from a change of conditions during a given run. It also greatly enhanced

the possible accuracy through averaging of a large number of data.

4.2.3. **The viscometers**

The samples collected both before and after use in the test section were analyzed with a couple of custom-built capillary viscometers. These are shown in Figs. 4.-4 and 4.-5 and are described in detail in Appendix B.8. More information can also be found in other articles (Matthys 1984, 1985; see also app. C.2. and C.3.). The purpose of these viscometers was to obtain the viscosity/shear rate relationships for the samples.

These non-newtonian relationships characteristic of these fluids are then used in the data processing. They were also used to monitor the solutions for mixing repeatability and aging. For these relationships to be useful for the large size tests, the shear rates encountered in the test tube have to be covered by the viscometers. This was possible through the use of various tubes of adequate length and diameter.

One of the viscometers is of the pressurized-tank variety (fig. 4.-4) and allowed very high ranges of flow rates and shear rates to be covered (up to 100000 s^{-1} for water under laminar conditions). Its tubes are positioned vertically and the flow rates are measured by collecting and weighing the exiting fluid. This viscometer could also be used with a vacuum in order to cover very low shear rates. A drawback of this design is that it is difficult to make measurements at the same shear rate for fluids of different viscosities. It is also very time-consuming to use.

Consequently, a second viscometer (fig. 4.-5) was built, using a cylinder and a piston activated by a variable-speed electric motor. The

pressure in the tank was measured, as in the case of the other viscometer, with a pressure transducer. The adjustments being made directly on the flow rate, instead of on the pressure as with the other viscometer, it was then easy to make measurements at constant shear rate with this viscometer. The flow rate being limited by the speed of the motor, and a minimum diameter being judged necessary to avoid problems with fibers and particles, the maximum shear rate obtained in these cases with this viscometer was 30000 s^{-1}. The use of high sensitivity transducers allowed the measurement of shear rates as low as 50 s^{-1} for both viscometers.

4.3. EXPERIMENTAL PROCEDURES

4.3.1. **Preparation of the solutions**

Except for Jet A and AMK, the solutions were prepared in the main supply tank using tap water. This tank was fitted with a variable-speed mechanical stirrer consisting of 2 large inclined paddles. The stirrer was used vigorously for both the clay suspensions (to provide good hydration and suspension of the clay particles), and for the tomato purees (for good dilution purposes). For the low concentration (20 ppm) of polyacrylamide (Separan AP-273 by Dow Chemicals), however, it was found that if the stirrer was left overnight at a speed of more than about 10 rpm, significant degradation would occur. Fortunately, the 20 ppm solution is fairly easy to mix with proper preparation and does not need strong stirring.

The polymer solutions were all prepared in a similar fashion: the necessary quantity of polymer powder was first mixed with methanol until thoroughly wetted (the polyacrylamide is soluble in water but not in methanol), and then added to the water in the tank. This method contributed to a far better dispersion of the powder, especially if poured slowly under a jet of water.

Whereas this worked well for the 20 ppm solution, the larger quantity of powder necessary for the 200 ppm solution created some problems. Indeed, after a certain amount of powder was added to the water, the viscosity of the solution increased so rapidly that subsequent additions were confined to the surface of the liquid and formed big blobs of gel-like material. With gentle stirring, the solution, if left overnight, would nevertheless be homogeneous the next day and would present no trace of any residual unmixed powder.

This stirring did not result in any modification to the drag-reducing capability of the 200 ppm solution, because of the buffer effect provided by its saturated asymptotic nature, and there was no measurable influence on the viscosity either. The waiting period of one day was also thought advantageous for stabilization of the solutions. All the tests showed that, although aging could be a factor after long periods of time, all the solutions nevertheless gave repeatable results at the same age, thereby validating the mixing procedure. No solution was used for tests that was more than a few days old, unless purposely so for aging studies. The pH of the polymer solution and water used were monitored throughout the study.

The AMK solution (nominally 0.3% by weight) was prepared separately in drums, using an in-line mixing procedure developed at the Jet Propulsion Laboratory (Yavrouian, Ernest, and Sarohia 1984). This procedure consists of injecting minute quantities of polymer slurry in a flow of Jet A under steady-state conditions, the mixing rate being controlled by a pump. The use of kerosene-like fluids for the experiments required enhanced safety precautions as a well as special cleaning of the system before and after the runs.

The clay suspensions were prepared with bentonite and tap water. The mixing presented no particular problem because of the higher rate of stirring permitted. The pH of the various suspensions was also monitored. It was observed that the settling speeds were a strong function of the concentration of clay. A suspension of 1% of bentonite by weight would, for example, settle to half-height within less than half an hour. For 2%, it would take several hours, for 3% several days, and for concentrations above 4%, there was no sign of sedimentation at all, even after 2 weeks. This phenomenon is likely related to the minimum concentration necessary for the build-up of sufficient yield stress and thixotropy.

Accordingly, it was decided to test bentonite suspensions of concentration ranging between 1% and 5%. The 1% solutions were found difficult to handle, especially during the viscosity measurements, because of their rapid settling time. Suspensions much above 5%, on the other hand, were so viscous that a turbulent regime was not within the capabilities of the system. The 5% fluid, however, provided an interesting look at the laminar and transitional regime, which was not readily possible

with the polymer solutions.

When polymer (20 ppm) was added to the clay suspensions, the mixture immediately flocculated, and distinct unmixable zones of pure water also became apparent. This fluid was not only impossible to homogenize without violent stirring, but became also extremely sensitive to degradation, up to the point that the simple pouring out of a bottle would reduce the viscosity by more than 10% (see section 5.6.1).

The suspensions of pulp were prepared with canned industrial tomato puree that was diluted to 6% of solid contents. This concentration was chosen for its relative fluidity to minimize system pressure and plugging, and because it is a concentration used by the food industry for tomato juices. The mixing of the solutions was uneventful and no significant sedimentation was observed. There was no problem with the pressure transducers, thanks to the small size of the pressure taps and to the water-filled transducer lines.

Difficulties arose, however, when the viscosity of the pulp suspension was measured. Its fibers were noted to be as long as one millimeter, a fact that prevented the use of the smaller capillaries available. Even in the largest capillary, however, some non-homogeneity was observed at times. The addition of polymer to the suspension presented no difficulty.

4.3.2. **System cleaning**

Adequate cleaning of the system proved to be important. For all the tests involving water-based solutions, vigorous flushing with water for a couple of hours, followed by compressed air or nitrogen, seemed more

than adequate for a thorough cleaning. After each series of tests, the system was rechecked with water in any case to ensure that no residual test fluid would influence the following test.

Between water and AMK tests, a more complicated cleaning procedure was necessary, because of the extreme sensitivity of AMK to water. Indeed, the polymer may well come out of its kerosene solution if enough water is present, thereby thoroughly plugging everything up. To avoid this problem, before undertaking AMK or Jet A tests, the system was flushed first with water, then air, then methanol to remove all remaining humidity, and finally with Jet A to remove the methanol. After these tests, the reverse procedure had to be followed.

During AMK or Jet A tests, the hydraulic system on the back side of the piston was filled with Jet A rather than with water for the same reason. Except for the test tube, the system consisted mostly of galvanized steel pipes, with the temporary addition of kerosene-resistant flexible tubing for the drum connections. No damage to any of the parts in contact with the fluids was observed.

4.3.3. **Data collection procedure**

The step by step procedure may be summarized as follows:

- Connection of appropriate transducers for the expected pressure drop.
- Introduction of transducer data in data acquisition programs.
- Flushing of the system.
- Preparation of the solutions.
- Stabilization waiting period.

- Measurement of viscosity functions of unused samples with viscometers before start of test.
- Filling of the system by aspiration from supply tank or drum.
- Purge of air left in the system.
- Purging and zeroing of transducers, adjustment of their power supplies.
- Pressurization of secondary hydraulic system.
- Start of motor.
- Adjustment of desired motor speed.
- Start of generators.
- Adjustment of generators for desired heating power.
- Equalization of back and front pressures.
- Check of constancy of displacement speed and temperature with the computer.
- In steady-state, data collection and storage in memory.
- Collection of samples from test tube (with system running).
- Turn-off
- Emptying of cylinder, the system remaining filled.
- The data and all necessary information are stored on disks.
- Other runs are conducted.
- The system is depressurized, emptied, and cleaned.
- The degraded samples are analyzed with the viscosimeters.
- The viscometric functions for the samples are introduced in the programs, allowing further processing and plotting of results.

4.3.4. **Comments**

A typical test at the lowest measurable speed would take two or three minutes overall for the system to reach steady-state and for the computer to complete 10 sets of data collection. Very little fluid would be used in that case. At the highest possible speed, on the other hand, it would not take more than 15 s to reach steady state, but that would leave only about another 20 s before the cylinder would be empty, permitting only 5 sets of data to be taken for averaging. These fast runs were thus more difficult to complete and required a lot of fluid.

This constraint on the overall duration of the test put a limitation on the maximum running speed for the asymptotic drag-reducing fluids. For less effective drag-reducers, the maximum speed would be generally determined by the highest pressure the system was capable of handling safely in a routine fashion (approximately 7 atm).

The transducers had to be carefully chosen, and sometimes changed during a set of runs, because they would tend to give erratic results for pressure drop measurements in the low end of their range. They could also be thrown off calibration by excessive pressures. In order to obtain good accuracy, it was always attempted to select the transducers in such a way that they would read in the upper half of their range.

In most cases the fluids were used at room temperature. The non-newtonian character of the fluids did indeed introduce variations in viscosity larger than those that could have been achieved by modifying the overall bulk temperature of the fluid. A few runs were nevertheless

conducted at higher temperature to test the correlations developed.

Adequate choice of the heating power was crucial for the experiments. It was decided not to exceed an overall increase in bulk temperature of more than $2°C$ for the total length of the tube. This limit was selected in order to avoid major differences in properties along the length of the tube. Such differences would indeed have complicated the comparison of the various stations for degradation and entrance effect studies.

It is to be noted that the heat transfer measurements were made locally, most of them corresponding to the location of a pressure drop measurement. These measurements were not simply taken across the whole tube as it is commonly done when heat exchangers are used. Accordingly, if taken individually by location, the measurements are usable even for large temperature differences between the entrance and the exit of the pipe, because the associated variations in properties are bypassed. Indeed, this procedure was adopted for some of the water runs with high power setting.

If large heat fluxes had been used for the drag-reducing fluids, the difference between the bulk temperature of the fluid and the wall temperature would have become very large. In that case, the heat losses would have increased significantly and the viscometric functions corresponding to those temperatures would not have been readily measurable.

Incidentally, an interesting aspect of the experimental installation is that it was designed with drag-reducing solutions in mind. Under nomi-

nal conditions, temperature differences of up to 20 °*C* between fluid bulk and inside wall are possible for these solutions. The accuracy of the heat transfer measurements for these solutions is thus far better than for water under the same conditions. This is because the corresponding bulk/wall temperature difference for the latter would only be less than 1 °*C*, and thus far more dependent on possible temperature measurement errors of, say, 0.05 °*C*.

The increase in temperature along the length of the pipe was measured directly with the probes. For fluids of well-known properties such as water, it was possible to compare this measurement with the increase in temperature computed from electrical power, mass flow rate, and heat capacity of the fluid (see app. A.2.). In most cases, the difference was small, of the order of 1%. This shows that the power and mass flow rate measurements are acceptable, and that the losses to the environment are not important (see app. A.4.).

For some of the non-newtonian fluids, however, the measurement of the exit temperature became at times unreliable. This might have been due to physical problems such as accumulation of fibers or gelled polymer on the probe, or possibly to non-newtonian heat transfer problems similar to those preventing the use of hot-wire anemometers for those fluids. For the AMK, the thermal properties are not known with as much accuracy as those of water, therefore introducing some uncertainty on the computed increase of bulk temperature. The exit temperature measurements, however, even if erratic, would nevertheless generally agree after averaging with predicted values, thereby confirming the

general validity of the heat capacity values used.

4.4. OUTLINE OF THE DATA PROCESSING METHOD

4.4.1. Viscosity functions

In order to evaluate the parameters necessary for the treatment of the raw data, the viscosity of the fluid has to be first measured. This is accomplished with the capillary viscometers, which allow the measurement of the viscosity in the laminar regime over the range of shear rates covered in the main test tube. These relationships between viscosity and shear rates ("viscosity functions" in short) were measured for the range of temperatures of interest in the heat transfer experiments, namely from the bulk temperature in the coldest case to the wall temperature in the hottest one. (As mentioned earlier, the difference between bulk and inside wall temperature can amount to 20 $^{\circ}C$ for the drag-reducing fluids under standard conditions.)

The results are expressed in terms of an effective kinematic viscosity

$$\nu_{eff} = \frac{\tau_w}{\rho(8V/D)} \tag{4.1}$$

where τ_w, the wall shear stress, is computed with Equation 3.29a. This viscosity is expressed as a function of an associated newtonian laminar wall shear rate

$$\dot{\gamma}_n = \frac{8V}{D}. \tag{4.2}$$

For easier computations, these relationships are transformed to a polynomial expression of the form

$$ln(8V/D) = A_0 + A_1 \ln\tau_w + A_2(ln\,\tau_w)^2 + \cdots \quad . \tag{4.3}$$

This expression is equivalent to the viscosity function and will be designated either by this name or by "polynomial" for simplicity. The order of the polynomial is selected so as to give the best fit with the least oscillating character.

It is then possible to compute an equivalent power-law exponent from this expression. However, in contrast to the case of most of the pseudoplastic purely viscous fluids, this exponent will not be a constant, but instead may be a strong function of the shear rate itself. Letting n be a variable justifies the use of a power-law representation even for viscoelastic fluids, for which this representation is clearly often inadequate if a constant exponent is used. With expression 4.3. for the shear rate, it is easy (eq. 3.25) to compute

$$n = (A_1 + 2A_2 \ln\tau_w + 3A_3(ln\,\tau_w)^2 + \ldots)^{-1} \tag{4.4}$$

as a function of the wall shear stress or wall shear rate. This expression is obtained by differentiation of Equation 4.3.

The values of the coefficients of the polynomial are all that is needed to determine the viscosity functions at a given temperature or degree of degradation. (It is also possible to compute the characteristic times corresponding to various models (see section 3.1.3) with these expressions). The actual wall shear rate for the fluid measured can be computed with Equation 3.26.

To take the temperature variations into account, the polynomials corresponding to various temperatures may be introduced in the

programs. Alternatively, in some cases a correction factor designed to account for the temperature effect on viscosity may be determined. Only one polynomial is then necessary if used in conjunction with this factor. The correlation chosen for this purpose is of the Arrhenius-type

$$\eta_{eff}(T,\dot{\gamma}) = \eta_{ref}(\dot{\gamma})\, e^{B/T} \tag{4.5}$$

where T is expressed in $^{\circ}K$. In other words, to compute the viscosity at one temperature from that at another temperature, one uses

$$\eta_{eff}(T_1,\dot{\gamma}) = \eta_{eff}(T_2,\dot{\gamma})\, e^{\left(\frac{B}{T_1}-\frac{B}{T_2}\right)}. \tag{4.6}$$

The factor B is not necessarily the same for different concentrations and degrees of degradation. To account for the degradation effect, for example, all the polynomials corresponding to the various samples collected during the tests under different conditions of mass flow rates were introduced in the programs.

The viscoelasticity of the fluid, if there is any, might introduce slight errors in the viscosity measurements, notably because of end effects (die swell primarily). This problem has been addressed in a separate article (Matthys 1984, see also app. C.2.). The extent of the error can be evaluated, and a correction devised, by the use of capillary tubes of various lengths. The antimisting kerosene was used for illustration of this phenomenon in the reference mentioned, because of the high elasticity and viscosity associated with the gelated material. This effect, however, was estimated to be small for the solutions of polyacrylamide, and is certainly negligible for the non-elastic fluids.

4.4.2. **The fundamental concept behind the data processing method**

The basic idea behind the treatment of data for these non-newtonian fluids is to apply the information gained from the measurements of viscosity functions to the main experiment results. The relationships between the non-newtonian viscosity and the shear rate were obtained in a laminar experiment in a small capillary tube. The apparent difficulty is that most of the heat transfer and friction experiments pertained to a turbulent regime in the larger test tube.

It is thought that the region most affected by the non-newtonian effects is the region very close to the wall. Furthermore, and especially for Prandtl numbers larger than one, the heat transfer coefficient is determined principally by the mechanisms very close to the wall, even for newtonian fluids. As an approximation, it seems thus reasonable to expect that the relationship between the wall shear rate and the wall shear stress (as determined in the laminar regime with the viscometer), might apply fairly well to the region very close to the wall in the test tube (region of a pseudo-laminar type itself). This assumption is related to the "law of the wall" which is the basis for many analyses of heat transfer and friction in pipes for newtonian fluids (see section 3.2.1.2.).

In other words, all the predominant effects being probably localized close to the wall, it seems reasonable to base all the computations on the viscous properties determined by the wall conditions.

The only quantity that is actually measured in the test tube is the wall shear stress. The shear rate varies with the radius and is not known a

priori because of the uncertainty on the velocity profile due to the non-newtonian nature of the fluid. However, basing oneself on the concept outlined above, one can compute the associated wall shear rate corresponding to the measured wall shear stress by using the viscosity functions determined with the viscometers. This shear rate, of course, will then be representative of the wall region only, but, once again, this is the region presumed most important for the effects investigated. The computation of this shear rate is in practice the most critical part of the procedure, because the non-newtonian effects are at times very large and the numerous interpolations necessary require adequate viscosity data over large ranges of parameters.

Subsequently, using this wall shear rate and wall shear stress, one can compute the power-law exponent (eq. 4.4), and the corresponding apparent viscosity (eq. 3.34) and consistency (eq. 3.28). One can then determine the associated Prandtl and Reynolds numbers, either of the generalized or apparent type (eqs. 3.31, 3.35, 3.72, and 3.73).

The Reynolds numbers obtained in this fashion will be representative in some cases of rather large changes in viscosity. These changes result from the fact that the viscosity may be a strong function of the shear rate for these fluids, especially at low shear rates. Furthermore, when other phenomena such as discontinuous shear-induced thickening are present (for antimisting kerosene for example), the viscosity may vary by a factor of ten between, say, $\dot{\gamma}_w$=4000 and 5000 s^{-1}. Of course, this in turn would show as a decrease of the Reynolds number by a factor of ten as well, a rather significant jump to be taken into account.

The choice of an appropriate Reynolds number is thus critical. Certain combinations of computational parameters and Reynolds number definition will indeed be shown to be suitable for correlating the experimental data - much more so than might have been expected. The antimisting kerosene, because of the abrupt discontinuity in viscosity it exhibits, is particularly suited for a test of the concepts and methods outlined above. It will be shown that a representation may be developed for this unorthodox fluid that takes this discontinuity well enough into account for the results to be reduced to correlations typical of much simpler polymer solutions.

Another indirect way of checking the soundness of the concepts used, would be to compare the results obtained in isothermal and non-isothermal conditions. Indeed, the temperature used as reference for the computation of the viscosity is a critical parameter, because the difference in temperature between the bulk of the fluid and the wall may be quite large for certain fluids. The viscosity obtained may then vary by more than 50% depending on the temperature used in the computations, with all the corresponding modifications to the values of the Reynolds and Prandtl numbers. This is again particularly true of the antimisting kerosene, for which, depending on the temperature, one could find the computed wall shear rate to be on one or the other side of the discontinuity.

In other words, if, according to the concept outlined above, one computes the viscosity based on wall conditions, the temperature to be used in the computations should be that of the inner wall or possibly of the

interface temperature, certainly not of the bulk temperature. Therefore, if the results for the isothermal case, and those for the non-isothermal case computed at the wall temperature, are indeed represented by the same relationship, it is a strong indication that the concept of the wall predominance is correct. These aspects of the choice of reference temperature and definition of viscosity will be illustrated in the chapter devoted to experimental results (see section 5.2.2. for example).

4.4.3. **Treatment of data**

A detailed numerical example of the processing of the raw data is presented in Appendix D. To illustrate the general ideas behind this treatment, however, an outline of the procedure will be given here.

The quantities measured at a given location are the average pressure drop, and the outer wall temperature (see app. B on the measurement methods and hardware). The bulk temperature of the fluid can be determined for any location after measurement of electrical heating power and mass flow rate (see app. A.2.). The temperature drop across the wall of the tube is also computed (see app. A.1.). Therefore, the difference in temperature between the bulk of the fluid and the inner wall is known. One can then compute the Nusselt number at that location, having chosen a reference temperature for the evaluation of the material properties and knowing the convective heat transfer coefficient based on the inner wall heat flux.

The pressure drop measured directly gives the wall shear stress. Using this value, the wall shear rate and the value of the corresponding viscosities and power-law exponent are determined as outlined in sections 4.4.1 and 4.4.2. Also computed are the friction coefficient and the various Reynolds and Prandtl numbers needed. Again all these computations are based on the chosen reference temperature (wall, interface, or bulk).

The viscosity functions used for this purpose depend on the local temperature, and also on the degree of degradation. This latter factor can be taken into account for any location by interpolation between the viscosity functions corresponding to the undegraded fluid at the entry of the test tube on the one hand, and to the degraded fluid at the exit on the other hand. This exit viscosity function is, of course, a function of the shear to which the fluid has been subjected, and can be itself obtained by interpolation between the known viscosity functions corresponding to the various samples collected at selected flow rates.

It is then a simple matter to compute all the other necessary quantities, such as the Stanton number, Colburn factor, or any of the values obtainable from the pertinent theoretical or empirical correlations available.

For better comparison and assessment of the validity of computational parameters and procedures, the data processing programs were used systematically to evaluate the results for all locations, and corresponding to all the possible combinations of the various reference

temperatures, types of viscosity, and types of degradation interpolation used. Additionally, as explained earlier, the bulk temperature may also be obtained from a direct measurement of the exit probe, and all the computations were also conducted for that case.

CHAPTER 5.

DISCUSSION OF EXPERIMENTAL RESULTS

5.1. WATER

5.1.1. Material Properties

The inner diameter of the capillaries used in the viscometers having been calibrated with distilled water (see app. B.8.), it is to be expected that subsequent viscosity measurements of water will give results very close to the tabulated values. This was indeed verified later on, and the repeatability of the measurements was usually better than 0.5%. Similarly, the tabulated density of distilled water was used in the calibration of the containers used for density measurements (see app. B.6.). The repeatability of density measurements was of the order of 0.1%. The values of the different properties of water used in the computations have been reproduced in Appendix B.7. for reference. Necessary interpolations on water properties were conducted in the programs by polynomial fitting or linear estimates.

5.1.2. Verification of the Experimental Installation

The experimental installation for heat transfer and friction measurements was tested with water to verify the general validity of the concepts and formulae used. A large number of tests with water were also subsequently conducted to check the calibration of the instruments or the cleanliness of the system before and after runs with other fluids. These

tests were conducted with various levels of heating power and various configurations of thermocouples.

Consequently, for an illustration of the validity of the methods used, a small number of results have been randomly selected among those obtained over a 5 months period in the way just mentioned. For a better comparison of the heat transfer results, however, the selection includes only test runs and locations corresponding to a Prandtl number of 5.55 +/- 6%.

It is important to remember that the scatter present in the results may correspond to variations in properties of the fluid tested as well as to random errors inherent to the experimental installation. Furthermore, it would be incorrect to assess the accuracy of the whole procedure based on the water results alone. Indeed, the difference in temperature between the bulk of the fluid and the inside wall (under the standard power levels used) is far smaller for water (less than 1 $^{\circ}C$) than for the polymer solutions for example (up to 20 $^{\circ}C$). This discrepancy is caused by the lower heat transfer coefficient under drag reduction conditions.

The calculated Nusselt numbers will thus be more accurate for the other fluids than they are for water. These Nusselt numbers are indeed computed with this bulk-wall difference in temperature, and the thermocouple errors will thus be proportionally less important if this difference is large. Naturally, for the heat transfer-reducing fluids, the fluid properties will also greatly vary with radius because of this large difference

in temperature, an effect that has to be evaluated adequately for accurate results.

5.1.2.1. *Friction*

The data used here for illustration of the friction measurements correspond to various locations along the tube, not to an average for its total length. The difference in measured friction between stations was equal to- or smaller than the general scatter, however, the hydrodynamic entrance length for turbulent newtonian fluids being too short to be of influence to these stations (see section 3.2.1.2). All the water friction data pertain to the turbulent regime; they cover a range of Reynolds numbers from about 10000 to 100000.

All the values for water have been computed at bulk temperature, because the difference in temperature between the bulk of the fluid and the inner wall was in all cases less than 1 $^{\circ}C$. Consequently, a correction of the Sieder-Tate type (eq. 3.68) would amount to less than 0.5%.

The measured friction coefficients are presented as functions of Reynolds number in Fig. 5.1.-1, along with the values of several common expressions for the friction of newtonian fluids in circular pipe. It is apparent that the experimental data fit very well inside the bracket delimited by the other expressions. The scatter exhibited by these expressions is approximately 3%. Consequently, it appears safe to assume that the friction measured by the present installation for water is probably accurate within 2% (with respect to average accepted values). The use of different fluids should not affect much this estimate, because the

transducers were changed and matched to the pressure ranges covered, and there was no observed instance of plugging or similar problems for any of the test fluids.

A simplified correlation has been obtained for these data

$$C_f = 0.0726\,\mathrm{Re}^{-0.242} \quad . \tag{5.1}$$

The other expressions used for comparison are those by Prandtl (eq. 3.12), Blasius (eq. 3.13), White (eq. 3.14), and Petukhov (eq. 3.15).

5.1.2.2. *Heat transfer*

As was the case for the hydrodynamic entrance region, the thermal entrance region could not be observed either, being very short for newtonian fluids in turbulent regime (see section 3.3.1.2). All the data chosen for illustration correspond to test runs and locations yielding Prandtl numbers of 5.55 +/- 6% (for better comparison of the Nusselt numbers). The empirical correlation obtained for these data is

$$Nu = 0.0353\,\mathrm{Re}^{0.830} \quad . \tag{5.2}$$

Assuming a Prandtl number exponent of 0.5 for comparison with Kays's expression (eq. 3.63), this gives

$$Nu = 0.0150\,\mathrm{Re}^{0.830} Pr^{0.5} \quad . \tag{5.3}$$

The coefficient found is very close to that of Kays's correlation, and the Reynolds number exponents are identical. Overall, these experimental values are only 3% smaller than Kays's.

The experimental data have been plotted in Fig. 5.1.-2, together with

correlations by Kays (eq. 3.63), Sleicher and Rouse (eq. 3.62), Petukhov (eq. 3.61), Dittus-Boelter (eq. 3.65), Friend-Metzner (eq. 3.75), Yoo (eq. 3.76), Kale (eq. 3.77), and Colburn (eq. 3.67).

The experimental results match well with the values obtained with these correlations. The maximum spread of these values is quite large (approximately 20%), as expected for heat transfer results. It is noticeable that the values of Nu obtained by the Colburn analogy are lower than all the others but Yoo's. If these values as well as those obtained by Yoo's correlation (developed with experiments for purely non-newtonian fluids) are neglected, the total spread between correlations decreases to approximately 10%.

The experimental data are close to the average of the values predicted by these remaining expressions. Furthermore, the data appear to be approximately within 3% of the values predicted by the correlation of Sleicher and Rouse (identical in value to Kale's), which is considered to be one of the most accurate correlations. Both Sleicher's and Kale's correlations are somewhat inconvenient to use, so that in practice Kays's may be preferred, being simpler and giving similar values for this range of Prandtl numbers.

Although the Colburn analogy (eq. 3.66) is only an approximation, it is often used for a check of the correspondence between turbulent heat transfer and friction. Accordingly, both $C_f/2$ and the Colburn factor are shown in Fig. 5.1.-3. Also shown for comparison is a modified Colburn factor based on a Prandtl number exponent of 0.5. It appears that the

heat transfer results would require a Prandtl exponent between 0.5 and 2/3 for the best possible fit with friction results. These results may be correlated by

$$\frac{C_f}{2} = 0.0363\ \mathrm{Re}^{-0.242}\ , \tag{5.4}$$

$$C_H\ Pr^{2/3} = 0.0199\ \mathrm{Re}^{-0.170}\ , \tag{5.5}$$

$$C_H\ Pr^{0.5} = 0.0150\ \mathrm{Re}^{-0.170}\ . \tag{5.6}$$

In conclusion, the heat transfer experimental results for water seem to be acceptable, their values being close to the average of existing correlations for newtonian fluids and being within 3% of some of the correlations considered most accurate.

5.2. POLYACRYLAMIDE SOLUTIONS

5.2.1. Material Properties

The solute used for preparation of all the polyacrylamide solutions is Separan AP-273 (by Dow Chemical Company). It is water soluble, anionic and of high molecular weight (for more information on this polymer, see Dow bulletins No. 192-762-80 and 192-425-80).

The concentration of the solutions discussed here is 200 ppm or less by weight. Because of these very low concentrations, the density, thermal conductivity, and heat capacity of the solution were taken to be identical to that of water for these cases. Indeed, the thermal conductivity of solutions of this polymer was measured by Lee, Cho and Hartnett (1981) for different concentrations and temperatures. It appears from their results that, for the concentrations and temperatures used in this study, the thermal conductivity of the solution should be very close to that of water (differences smaller than 1%). Cho and Hartnett (1982) have also verified that for these low concentrations, the density and specific heat of the solutions could be taken to be the same as those of water.

The viscosity of the solutions, however, is dependent on the concentration, temperature, and degree of degradation. This viscosity was measured with the capillary viscometers for each solution and its degraded samples. The results, necessary for the computations of the non-newtonian viscosity functions, are presented in the following sec-

tions.

5.2.2. **Asymptotic Regime**

Solutions of 200 ppm of Separan were chosen as representative of the saturated (i.e. asymptotic) regime. It was verified that this concentration was large enough for a fully-saturated regime. Indeed, with adequate precautions to avoid degradation, it was even possible to reach the minimum friction asymptote for as little as 20 ppm of solute. Furthermore, there was no difference noticed in the heat and friction reduction for concentrations larger than 200 ppm. The higher viscosity of these latter solutions led to high pressures in the system and reduced the maximum Reynolds number that could be obtained under the present conditions. From this point of view, higher concentrations were therefore undesirable for our purposes in any case.

5.2.2.1. *Viscosity Functions*

The viscosity functions (i.e. the relationships between the effective viscosity and the associated newtonian wall shear rate) were obtained with the motor-driven capillary viscometer, fitted with tube T-20 (see appendix B.8.). The viscosity of the unused solution was measured, as was that of various samples obtained from the exit of the test tube during the actual runs (see section 4.4.1). The solutions were used no later than 2 or 3 days after preparation. During that period, no effect on the viscosity of inadequate stabilization or of aging was observed.

In Fig. 5.2.-1 the measured effective viscosity (eq. 4.1) of the unde-

graded (unused) solution is shown as a function of an associated newtonian laminar wall shear rate (eq. 4.2) for a range of temperature covering those encountered in the test section during the actual runs. The temperature was usually maintained during the viscosity measurements within 1 $°C$ of the desired value. The 3 curves shown correspond to average temperatures of 25, 35, and 45 $°C$.

Using the temperature correction scheme described in section 4.4.1., all the data were reduced to values corresponding to a temperature of 35 $°C$. As shown in Fig. 5.2.-2, the 3 curves collapse nicely together, implying that the temperature effect is well represented by the Arrhenius-type expression. The value of the exponent found for the temperature correction factor (eq. 4.6) is B= 1631 $°K^{-1}$. If an equivalent activation energy is computed as ΔE in

$$e^{\frac{B}{T}} = e^{\frac{\Delta E}{RT}} \tag{5.7}$$

where R=8314 J/Kmole $°K$ is the universal gas constant, we find ΔE = 3.239 Kcal/gmole in the usual units. Note that for pure water one would find an exponent B= 1902 $°K^{-1}$ or ΔE = 3.777 Kcal/gmole.

In Fig. 5.2.-2 the effective viscosity ν_{eff} is given in terms of the associated laminar newtonian wall shear rate (8V/D). The same information may also be given more conveniently for computations in terms of 8V/D as a function of the wall shear stress τ_w. This relationship could be expressed in terms of a polynomial (see section 4.4.1). For illustration, the best fit for the viscosity data of this undegraded solution (after reduction to values at 35 $°C$) was obtained with a third order polynomial

of the form

$$\ln(8V/D) = 6.504 + 1.165\ln\tau_w - 0.03115(\ln\tau_w)^2 + 0.002187(\ln\tau_w)^3 \quad (5.8)$$

Various samples were also taken during the course of the experiments. In particular, one sample taken during a run at close to the maximum possible speed for this fluid was subjected to an average wall shear stress of 38 N/m^2 over the length of the tube. This in turn is roughly equivalent to Re_a =78000 and a wall shear rate of 38000 s^{-1}, computed at the wall temperature (which averaged 37 °C for the pipe) and under degraded conditions. The wall shear rate and Reynolds number are smaller, of course, if computed at the bulk temperature (avg: 25 °C). The corresponding values would then be approximately Re_a= 59000 and $\dot{\gamma}_w = 30000\, s^{-1}$.

These shear rates require slight extrapolations of the viscosity data for their computations. This extrapolation is, however, handled easily by the polynomial which is practically a straight line for the high shear rates. No extrapolation is ever necessary for the low end of the shear rates, for which the procedure would be far more uncertain.

The temperatures at which the viscosity of this sample was measured were also 25, 35, and 45 °C. The data can be reduced to values corresponding to a temperature of 35 °C as explained above, and the collapsed curves after reduction to 35 °C are shown in Fig. 5.2.-3, together with the undegraded fluid for comparison. The Arrhenius exponent obtained in this case was B= 1757 °K^{-1}., a value closer to that of water.

The difference between the viscosity of the undegraded solution and that of this sample (which corresponds to close to the maximum possible degradation in the system) is of the order of 7%. This difference is fairly small, as expected because of the relatively high shear rates used during the measurements with the viscometers. Indeed, the reduction in viscosity due to mechanical degradation is more apparent for viscosity measurements at very low shear rates, say under 10 s^{-1} for example (see Cho and Hartnett 1982).

Several other samples were also collected for intermediate speeds. Interestingly, most of them gave values of viscosity close to that of the Re_a =78000 sample. This seems to imply that, although a significant sensitivity of the solution to induced mechanical degradation is apparent at fairly low values of shear rates, this sensitivity decreases thereafter for larger shear rates. Furthermore, it was observed from pressure drop measurements in the test tube that this degradation process likely occurred at the beginning of the pipe. Indeed, no variations in pressure drop could be observed in the second half of the pipe.

For clarity, only one of those samples (for Re_a =38000) has been reproduced in Fig. 5.2.-3, together with the undegraded results and those corresponding to the Re_a =78000 sample for comparison. One sees easily on this graph that the viscosity of this sample is closer to that of the high speed sample than it is to the intermediate values one might expect. The data shown were measured at 35 $^{\circ}C$ as well, and correspond to average values in the test tube of about Re_a =38000, $\dot{\gamma}_w$ =15000 s^{-1}, and τ_w = 16 N/m^2 (all computed at wall temperature and with degraded

viscosity).

The viscosity function polynomials corresponding to all the samples (both the undegraded one and those subjected to maximum and intermediate degradation) were entered in the data processing programs together with their respective exponents B (for the evaluation of the temperature effect). The particular solution used for the data of Fig. 5.2.-3 is designated as batch #3. Other batches of same concentration were tested as well during earlier experiments. The viscosity functions for batch #1 were within 3% of those of batch #3, and for batch #2 they were within 6%. These viscosity results are not reproduced here, the trends exhibited being very similar to those of batch #3.

The solution was sufficiently concentrated to give results in the asymptotic regime. In this regime, changes in concentration or degradation level do not influence the actual friction and heat transfer experienced by the fluid. An error on the viscosity, however, could lead to inaccurate computations of Reynolds and Prandtl numbers, and the viscosity measurement of samples from each batch is, therefore, necessary.

The measured pH for batch #1 was 7.8, for batch #2 it was 7.2 (water: 7.1), and for batch #3 it was 7.2 (water: 6.8). The differences are probably due to variations in the nature of the city tap water used. The influence of the pH on the viscosity of the solution was observed (Cho and Hartnett 1982) to be very slight for shear rates above 100 s^{-1} and for pH around 7, however, so that the solvent effect was not expected to be of great

importance in this case.

5.2.2.2. *Friction*

As mentioned earlier, the computations of Reynolds and Prandtl numbers are dependent on the various possible choices of viscosity definition and of temperature reference. In this section the influence of these choices on the friction results will be illustrated. The trends discussed are similar for the heat transfer results, and are applicable also to most of the other fluids studied. It will therefore not be necessary to repeat this discussion for these cases.

5.2.2.2.1. Choice of Viscosity Function

The choice of the viscosity function used for the various computations is important. As explained in section 5.2.2.1., the viscosity of various samples directly obtained from the test runs was measured. These viscosity relationships are used in the computation programs in various interpolations. For these 200 ppm solutions the decrease in viscosity due to degradation amounted to no more than 7%, and consequently the effect on the calculated Reynolds number is approximately of the same magnitude. However, for other fluids, taking the degradation into account may indeed prove important for accurate data processing.

Fig. 5.2.-4 shows the friction data for batch #3 computed with on the one hand viscosity functions of the undegraded fluid, and on the other hand, using the viscosity functions of the degraded samples with the corresponding interpolations on location and flow rate. (Also shown for

reference is Virk's asymptote (eq. 3.38).) As expected, the difference due to the choice of viscosity function is more noticeable for the higher flow rates, but is fairly small overall. Subsequent computations were conducted with the viscosity functions corresponding to degraded conditions ("degraded viscosity functions" in short).

These computations were conducted at film temperature (the friction data were taken simultaneously with heat transfer measurements). The results shown for these asymptotic solutions all correspond to the transducer positioned at the end of the tube. They are based on the pressure drop measured between x/D=517 and x/D = 601 (in short: at x/D = 560). There was no variation of pressure drop observed between the various transducers along the tube for these runs, a verification that the flow is hydrodynamically fully-developed in a short distance (see section 3.2.3.2.).

5.2.2.2.2. Choice of Reynolds Number Definition

It was explained earlier (section 3.2.) that there are two definitions of Reynolds number often used for non-newtonian fluids: the generalized Reynolds number (eq. 3.31) and the apparent Reynolds number (eq. 3.35). In order to evaluate how important is the choice of the definition used for this polymer solution, Fig. 5.2.-5 shows the friction results for the same batch, computed at the film temperature, but expressed in terms of both generalized and apparent Reynolds numbers.

It appears that the difference is quite small in this case, especially when compared to the overall reduction in friction with respect to the

newtonian fluids (as illustrated by the Prandtl curve, also shown). The reason for this small difference is that the value of the power-law exponent varies only between n=0.9 and n=1 for the shear rates covered in these runs. Indeed, one can see that for the highest flow rates (where n=1), the two types of Reynolds number give identical results, whereas the difference increases for the low flow rates.

Again, for other fluids the difference may be larger than in this case, and the problem of the most appropriate representation will be reexamined when necessary. Apparent Reynolds numbers will be used for these polymer solutions, this definition appearing to be the most adequate for viscoelastic fluids (see section 5.5.3.).

5.2.2.2.3. Choice of Reference Temperature

As explained earlier, the difference of temperature between fluid bulk and inner wall may be large for drag-reducing solutions. Consequently, depending on which temperature is chosen for the computations, the values used for the material properties (the viscosity primarily) may greatly vary. This in turn could affect the values of the Reynolds and Prandtl numbers. In Fig. 5.2.-6 the friction results are shown, the computations being based on bulk-, film-, and wall temperature.

The difference between the curves is rather large. For the highest flow rate, for example, the apparent Reynolds number based on bulk temperature is about 65000, whereas the one based on wall temperature is about 85000, a difference (30%) hardly to be ignored when developing correlations. Expressed in terms of friction coefficient at Re_a = 70000,

for example, the ratio of the C_f for these 2 cases is about 20%.

The difference between bulk and wall temperatures for this case being approximately 10 $^{\circ}C$, the ratio of viscosities, based on an exponent B= 1757 $^{\circ}K^{-1}$ (sections 4.4.1. and 5.2.2.1.), would be 1.21. With a correction of the Sieder-Tate type (eq. 3.68), one would only correct the values of C_f by 5%, clearly underestimating the effect of reference temperature. This problem will become even more critical for the antimisting kerosene, for example, because of the larger variations of viscosity with temperature and shear rate.

Clearly, an adequate reference temperature has to be chosen, not only for more accurate results, but also to make sure that the concepts behind the computations are coherent. As explained in section 4.4.2., the point of view taken in this study is based on the assumption that the properties in the region close to the wall will be the principal ones influencing the flow and heat transfer mechanisms. If this model is physically sound, the reference temperature for computations should likely be that of the inner wall, rather than that of the film (as usually assumed for newtonian fluids), and certainly not that of the core.

One way of assessing the effect of selecting a certain reference temperature is to conduct isothermal friction experiments. Indeed, if the computations are representative of the relevant physical mechanism, one would expect all the friction results to collapse on the same curve, whether obtained in isothermal flow or not. The results of the isothermal (no heating power) runs are plotted in Fig. 5.2.-6 as well. It can be

easily seen that they do indeed match closely with the friction curve based on the inner wall reference temperature. The temperature of the fluid during the isothermal experiments being even lower than that corresponding to the bulk condition of the power-on runs, the inner wall temperature appears to be the correct reference for the computations.

To further verify this assumption, similar computations were done with the data obtained from earlier tests (batch #1). These tests were conducted with much larger variations in power settings than the later ones were. Accordingly, the temperature differences between wall and bulk varied from almost zero to more than 20 $^{\circ}C$ for those runs. This fact was expected to lead to far more scatter in the results. These results are presented in Fig. 5.2.-7, for computations based on both bulk and wall temperature. It is obvious that the large scatter present in the results corresponding to the bulk temperature reference is greatly reduced when the wall temperature is used for the computations, which is a good indication that the wall temperature serves as a more adequate reference temperature.

Additionally, 2 runs were also completed with no heating power. These isothermal results are also presented in Fig. 5.2.-7, and match perfectly with the wall temperature reference computations.

Consequently, it appears that the wall temperature is indeed the one to be used as reference for this type of fluid, in support of the wall viscosity concept used in this study. Accordingly, all the following

results have been computed on the basis of the wall temperature.

5.2.2.2.4. Repeatability and Correlation of Data

All the results corresponding to the 3 batches of 200 ppm solution tested are shown in Fig. 5.2.-8. The scatter is small, even though the solutions appear to have been slightly different after mixing and stirring (see section 5.2.2.1.). As the viscosity function was measured for each solution separately, one may conclude that these differences have been properly taken into account in the computations.

The results are shown together with Virk's asymptote for comparison. The friction coefficients measured appear to be slightly larger than the values obtained from Virk's expression for Re_a<30000. They are somewhat smaller for Re_a>40000, however. The differences with respect to Virk at the extremes of the range of Reynolds numbers covered are +5% at Re_a = 6000 and -13% at Re_a=90000.

The experimental results expressed in log-log axes do exhibit a slight curvature, indicating that the relationship between the friction coefficient and the Reynolds number is not exactly a power-law. This departure from a power-law is, however, smaller than for Virk's expression. For simplicity, one may nevertheless approximate the results with a best fitted power-law expression

$$C_f = 0.624\ Re_a^{-0.585} \quad . \tag{5.10}$$

(It should be recalled that this expression corresponds to results obtained with interpolations on degraded viscosity functions and with all

the computations conducted at wall temperature.) This expression approximating the experimental results gives values that are too low by 3% for Re_a = 6000, too high by 3% for Re_a=30000, and too low again by 2 % for Re_a=90000.

Of course, Virk's relationship is an average of data obtained from various sources affording only somewhat undetermined definitions of the viscosities used, and consequently a comparison with his results may not be entirely meaningful. If one compares the results with the expression found by Cho and Hartnett (eq. 3.45), the trends are rather different. For Re_a= 6000 the present results are 25% higher and for 60000, 2% lower.

For further illustration of the points addressed in the preceding sections, the corresponding correlations obtained for batch #3 will be presented here.

A correlation expressed in terms of generalized Reynolds number, and corresponding to wall temperature reference and degraded viscosity functions is

$$C_f = 0.508\ Re'^{-0.567} \qquad (5.11)$$

(-5% with respect to eq. 5.10 at Re'=6000, 0% at Re'=90000). The difference is small because 0.9<n<1 for this solution and shear rates.

A correlation for the apparent Reynolds number, and based on degraded viscosity functions, but all computations conducted at bulk temperature is

$$C_f = 0.836\ Re_a^{-0.627} \qquad (5.12)$$

(-8% at $Re_a = 6000$, -20% at $Re_a = 90000$ with respect to eq. 5.10). This confirms the importance of mentioning the reference temperature, when using or comparing results.

A correlation based on wall temperature, but using only viscosity functions corresponding to fresh fluid is

$$C_f = 0.706\ Re_a^{-0.601} \qquad (5.13)$$

(-2% at $Re_a = 6000$, -6% at $Re_a = 90000$ with respect to eq. 5.10). As mentioned above, this effect is small for these dilute solutions at high shear rate.

5.2.2.3. *Heat Transfer*

5.2.2.3.1. Fully-developed Conditions

As expected, the heat transfer for these solutions has been dramatically reduced with respect to water. As an illustration of this reduction, experimental results for batch #3 are presented in terms of Nusselt and apparent Reynolds numbers in Fig. 5.2.-9 (wall temperature reference, degraded viscosity functions). The measurements presented (as are all those in this section), were conducted at x/D= 560. Also shown for comparison, are data obtained with water.

The difference is significant, the Nusselt number being reduced from 70 to 9.5 (85%) for Re_a=9000, and from 475 to 25 (95%) for Re_a=90000. (This large reduction in Nusselt numbers appears even more remarkable

if one recalls that the Prandtl number of the polymer solution is up to twice as large as that of the water for the low shear rate.)

Results are shown in Fig. 5.2.-10 in terms of Colburn factors in order to be able to compare these results to those of Cho and Hartnett (1982) which is, perhaps, the only experimental study comparable to the present one (because of the problems of entrance lengths and non-asymptotic conditions for most of the previous studies). In this figure, the values of Cho's expression for the heat transfer asymptote (eq. 3.80), are shown together with the present results for the 3 batches, including a special set conducted at high temperature (to increase the variations on Prandtl numbers). (The present data are computed with a wall temperature reference and with degraded viscosity functions.)

Although reservations are sometimes expressed as to the validity of the 2/3 Prandtl exponent in the Colburn factor for newtonian fluids (see section 5.1.2.2.), the choice of such a representation apparently takes care fairly well of the variations in Prandtl number. Indeed, the scatter appears proportionally rather small when compared to the variations in apparent Prandtl numbers (eq. 3.73) corresponding to these runs. These variations are due to differences in experimental conditions, such as average temperature, and also to the effect of the shear rate on the viscosity. These Prandtl numbers are shown in Fig. 5.2.-11 to give an idea of the range covered in these experiments. Limitations on the maximum temperature allowed in the system, however, restricted the range to $5 < Pr_a < 10$.

A power-law correlation has been developed for these results obtained for $6000 < Re_a < 90000$, and corresponding to the heat transfer asymptote

$$C_H Pr_a^{2/3} = 0.0510\ Re_a^{-0.506} \quad . \tag{5.14}$$

This expression gives values of the Colburn factor close to those found by Cho and Hartnett (eq. 3.80): +4% at Re_a=6000, and -6% at Re_a=40000. The agreement is rather good. It is not clear, however, if Cho's computations take into account the effect of degradation on the viscosity and the influence of temperature, which indeed have been shown earlier to have a significant influence on the results. The present results were also obtained at a larger value of x/D. In any case, the fact that the expressions give results of the same order, and furthermore that the present results are lower than Cho's over most of the range covered, confirms the belief that the 200 ppm solution used in the present study was concentrated enough to reach asymptotic conditions for heat transfer.

It is interesting, however, to note that the Prandtl numbers measured in this study are smaller than those in Cho's, because the concentrations he used were higher (500 to 5000 ppm). The fact that the values of the Colburn factor for the two studies are nevertheless very similar, seems thus to indicate that an exponent of about 2/3 for the Prandtl number in the Colburn factor is indeed adequate to absorb the Prandtl number effect, even though the usual analogies are possibly be invalid for these fluids.

It is believed that the scatter present in the data shown in Fig. 5.2.-10

is due in part to the fact that the viscosity measurements for the first two batches of solution were not as good as those for batch #3. Furthermore, less viscosity data having been collected during these earlier tests, the interpolations in the programs probably gave less accurate results as well. Consequently, for simplicity and very possibly for better predictions, the correlations obtained for batch #3 alone will be used hereafter. We have for this batch alone (with wall temperature reference, x/D=560, degraded viscosity functions)

$$C_H Pr_a^{2/3} = 0.0596\ Re_a^{-0.523} \quad . \qquad (5.15)$$

This equation is proposed as the expression for the heat transfer asymptote for $6000<Re_a<90000$. The difference with eq. 5.14 is small : +1% at Re_a=6000 and -4% at 90000. With respect to Cho's results (eq. 3.80) it would give +5% at Re_a=6000 and -9% at 40000.

As mentioned earlier, although used frequently in the form shown above, the Colburn factor would probably give better results for newtonian fluids if an exponent between 0.5 and 2/3 would be used rather than 2/3 itself. Because of this uncertainty, and to give an idea of the effect of different exponents, the results (batch #3, usual conditions) are presented in Fig. 5.2.-12 for both 0.5 and 2/3 exponents. Shown also is $C_f/2$, and for comparison, similar results for water. (It is noticeable, as explained in section 5.1.2., that the repeatability is not as good for heat transfer in water, because of the smaller temperature differences.)

As expected, it is obvious that the heat transfer not only has been

dramatically reduced, but has been also reduced proportionally far more than the friction. It is clear that whereas $C_f/2$ falls neatly between $C_H Pr_a^{2/3}$ and $C_H Pr_a^{0.5}$ for water, this is not the case for the polyacrylamide solution (PAA).

A correlation for the results obtained with a modified Prandtl exponent is

$$C_H Pr_a^{0.5} = 0.0330\ Re_a^{-0.497} \quad . \tag{5.16}$$

Interestingly, the Reynolds number exponent is not the same as that for the original Colburn factor: -0.497 instead of -0.523. This is related to the fact that the Prandtl numbers are larger at low Reynolds numbers (i.e. at low shear rates) for this solution. Of course, the relationship between the last 2 correlations is dependent on the average Prandtl number used in this study. Had the overall Prandtl number been much larger, the difference between the 2 correlations would have been larger as well. This difference, however, is only proportional to $Pr_a^{1/6}$, and for Prandtl numbers of the order of those generally found in the case of the semi-dilute solutions used for asymptotic regimes, it will not be excessive.

It is interesting to see for what exponent of the Prandtl number we would have an equality with the values of $C_f/2$. Surprisingly, if an exponent of 1.2 is used, not only do the values become similar, but the curves would be also parallel, unlike for the case of water. In other words, we have a good match with

$$C_H Pr_a^{1.2} = \frac{C_f}{2} \tag{5.17}$$

for these solutions. This 1.2 exponent is dependent, however, on the average values of Prandtl number used to compute it (that is, at least, if we assume that the correlation involving the usual Colburn factor is indeed truly independent of the Prandtl number).

In order to evaluate the effect of temperature reference, let me mention here a correlation corresponding to results computed at the bulk temperature of the fluid

$$C_H Pr_a^{2/3} = 0.0536\ Re_a^{-0.508}\ . \tag{5.18}$$

With respect to eq. 5.15, this expression gives values that are different by +2.5% at Re_a=6000, and by +7% at 90000. Unlike for friction, in the case of the heat transfer the results would thus be overvalued if computed at bulk temperature.

For comparison with results computed using generalized Reynolds numbers (but at wall temperature again), we have

$$C_H Pr'^{2/3} = 0.0538\ Re'^{-0.514} \tag{5.19}$$

giving -2% at Re'=6000 and 0% at 90000, with respect to eq. 5.15. The difference would be larger for solutions of higher concentrations which would exhibit smaller values of the power-law exponent.

Additionally, it was found interesting to evaluate another one of the expressions found previously for the asymptote, but based on theoretical concepts, however. Kale's expression (eq. 3.77), for example, would give (with the present expression for the friction asymptote, eq. 5.10)

$$Nu = \frac{0.312\, Pr_a\, Re_a^{0.415}}{1.2 + 0.559\, Re_a^{-0.292}(Pr_a - 1)(9.2\, Pr_a^{-0.258} + 24\, Pr_a^{-0.236})} \quad (5.20)$$

Assuming Pr_a=7.5 at Re_a=20000, this expression gives us Nu=27, which is too high (by 100%), the measured value being Nu=13. This large difference could be explained if Reynolds's analogy is indeed invalid for these fluids as has been suggested, because Kale assumed its validity in the development of his expression.

5.2.2.3.2. Entrance Region

In order to evaluate the influence of the entrance effects for these asymptotic solutions, the heat transfer computations were conducted for all the thermocouple locations along the length of the tube. These results correspond to the same runs that were presented in the previous section (with computations made at wall temperature and degraded viscosity functions). A sample of the results obtained are shown in Fig. 5.2.-13, in terms of Nusselt number and x/D.

The whole range of Reynolds number covered in the experiments (from Re_a= 6000 to 90000) is shown here, with only a few intermediate runs for clarity, however, the other runs presenting very similar trends. These runs correspond respectively (by increasing Nu) to values of the apparent Reynolds number of 6280, 14400, 27100, 39500, 55600, 68900, and 84300 (at x/D=560). (The results for two of the thermocouple locations are not included because of electrical connection problems during these measurements.)

It is clear that the heat transfer cannot be considered fully-developed until approximately x/D=500, a very long entrance region indeed, when compared to the 20 diameters necessary for newtonian fluids in the turbulent regime. As a matter of fact, for the highest Reynolds number covered, the entrance region defined by, say, 5% off the fully-developed value, may even extend to more than x/D= 600. These entrance regions are longer than the x/D=430 mentioned by Cho and Hartnett (1982) for higher concentrations, probably because of the larger Reynolds numbers covered in the present study. Other factors may also influence the Nusselt number besides the entrance effect, namely the fact that the temperature increases with the distance (an increase limited to $2°C$ in this case, however) and also the degradation. The Reynolds and Prandtl numbers vary of course correspondingly a little along the length of the pipe.

As mentioned earlier, the correlations developed for this solution in the previous section were all obtained with measurements at x/D=560. It is now desired to evaluate how these correlations should be modified to be valid in the entrance region. Let us find a correction factor $f\,(x/D)$ such that

$$C_H Pr_a^{2/3} = f\,(x/D)\,0.0596\,\mathrm{Re}_a^{-0.523} \qquad (5.21)$$

for x/D < 560. This form implies that the correction factor is not a function of Prandtl and Reynolds numbers, which is of course an approximation.

Considering two locations, including one at x/D= 560 (where f=1), this

expression gives

$$\frac{Nu(x/D)}{Nu(560)} = f(x/D)\left[\frac{Re_a(x/D)}{Re_a(560)}\right]^{0.477}\left[\frac{Pr_a(x/D)}{Pr_a(560)}\right]^{1/3} \quad (5.22)$$

Pending further detailed analyses of these data taking into account the actual variations of Prandtl and Reynolds numbers, it is assumed here that if one of these numbers has increased by a certain amount along the length of the tube, the other one will have decreased by approximately the same amount at the same location (because of the inverse respective effect of the viscosity variation with temperature). Because of the similarity of the exponents and with only small variations to be considered, one has approximately

$$\frac{Nu(x/D)}{Nu(560)} = f(x/D) \quad (5.23)$$

with $f(560)=1$ by definition.

In order to be able to evaluate the correction factor, this ratio of experimental Nusselt numbers as a function of x/D has been plotted in Fig. 5.2.-14. All the runs conducted with batch #3 are included in this figure. The results show a good coherence (except for x/D=35) despite the large variation in conditions for these runs. It is to be mentioned that the scatter is apparently not directly representative of a Reynolds number influence, the ratio of the Nusselt numbers showing a somewhat random correlation (possibly a slight increasing trend) with the Reynolds number within the envelope at each location. The approximation that this correction factor is independent of the Reynolds number is thus apparently acceptable.

The increasing scatter for lower x/D is probably caused by the fact that the Prandtl and Reynolds number variations along the tube were not taken into account in this preliminary analysis, as mentioned above. The larger scatter for x/D=35 may also be related to the fact that the phenomena at the very beginning of the pipe are also, of course, inherently unrepeatable, because of their sensitivity to many uncontrollable factors such as turbulence triggering or the existence of pseudo-laminar regions.

A simple power-law correlation has been developed by best fit for the correction factor using these results. The power-law seems to be a very adequate representation for this function, and is also shown in Fig. 5.2.-14. The expression found is

$$f(x/D) = 6.32\left(\frac{x}{D}\right)^{-0.293} \tag{5.24}$$

for 35<x/D<560. This correction factor, together with

$$C_H Pr_a^{2/3} = 0.0596\, f(x/D)\, \mathrm{Re}_a^{-0.523} \tag{5.25}$$

constitutes the expression proposed for the heat transfer reduction asymptote, for 6000 < Re_a < 90000 and 35< x/D < 560. In first approximation, and certainly for the lower part of the Reynolds number range covered, one may take this expression (with f =1) to represent fully-developed flow for x/D>560. Interestingly, Cho and Hartnett (1982) proposed an exponent relatively similar (-0.24) for the entrance region (eq. 3.81), based on results at x/D=83, 236, and 430, and for 6000< Re_a< 40000. Their analytical study, however, predicted entrance lengths at

high Reynolds number somewhat shorter than those observed here (200 diameters predicted at $Re = 10^5$ for the present range of Prandtl numbers for example, versus the 600 diameters observed in this study).

5.2.3. **Intermediate regime**

By intermediate regime, it is meant the region in which the drag and heat transfer correspond to values that are intermediate between those given by newtonian and asymptotic relationships. This regime is generally encountered with solutions which are of low concentration, or which have been significantly degraded. The polymer used in the present experiments is Separan AP-273 (see section 5.2.1.). Several concentrations were investigated that could possibly fall in this regime, ranging from 10 to 100 ppm. The results presented here correspond to the 20 ppm solution. This particular concentration was found to be particularly interesting because, although very sensitive to degradation, it could nevertheless exhibit reductions close to those represented by the asymptotic regime if precautions against degradation were taken.

5.2.3.1. *Viscosity functions*

The viscosity of both the undegraded and degraded samples were measured with the capillary viscometers at various temperatures (see section 5.2.2.1.) for the three batches used. These batches were tested within 2 or 3 days after mixing. During this period, no significant effect of aging on the viscosity was observed. The respective pH of the solutions were: 7.2 for batch #1, 7.2 for batch #2, and 7.0 for batch #3 (pure water: 6.5).

Contrarily to the viscosity results for the 200 ppm solution, no marked dependence of the viscosity on the shear rate could be observed for the 20 ppm solutions. Consequently, the viscosity was taken as being independent of the shear rate in the computations corresponding to these fluids. Accordingly, there is no distinction to be made between Re_a and Re' for these solutions (because n=1).

For batch #3 (the least degraded), for example, the kinematic viscosity reduced to 25 $°C$ was found to be $\nu=0.960\ 10^{-6} m^2/s$. This is only 7% more than water at the same temperature. The viscosity measurements covered a range of temperature from 20 to 50 $°C$. The value of the exponent in the temperature correction factor (eq. 4.6) was found to be B=1844 $°K^{-1}$.

It is interesting to note that for the undegraded 200 ppm solution B=1631 $°K^{-1}$ (see section 5.2.2.1.), for the degraded 200 ppm B=1757 $°K^{-1}$, and finally for water B=1902 $°K^{-1}$. A trend towards higher value of the exponent for lower concentration or higher degradation is apparent for all the solutions used. These variations in the value of the exponent are large, and have to be carefully taken into account to avoid imprecisions during the computations involving large temperature differences.

Several samples were collected during the runs for subsequent viscosity measurements. As illustration of this effect, for batch #3 (viscosity of unused sample: 0.960 $10^{-6} m^2/s$ at 25 $°C$) it was determined that the viscosity at 25 $°C$ was $\nu=0.937\,10^{-6}$ for a sample collected during a run at RPM=350, and $\nu=0.930\,10^{-6}$ for samples collected at RPM>550 (water:

ν=0.893 10^{-6} m^2/s). These speeds correspond respectively to Re_a=50000 and $\dot{\gamma}_w$ =19850 s^{-1} (computed at x/D=560, wall temperature of 33 °C, and with degraded viscosity functions), and to Re_a =80400 or $\dot{\gamma}_w$=55700 s^{-1} (same conditions, 32.5 °C).

The differences found in the measured viscosities (-3%) are small compared to the large effect that the degradation has on the drag-reducing ability of the fluid (see next section). This rather small decrease in viscosity was expected because of the low concentration of the solutions and of the high shear rates used for the viscosity measurements.

The viscosities of the 2 other batches were found to be smaller by 3% for unused batch #1 and by 4% for unused batch #2. Degraded samples for these batches showed decreases in viscosity similar to those for batch #3. The reason why batches #1 and #2 exhibit a lower viscosity than #3 is that they were subjected to a far more intense stirring during mixing (see section 4.3.1.), and were thus pre-degraded before use.

The 20 ppm batches were stirred overnight with a large mechanical agitator (2 paddle blades of 0.01 m^2, at 0.1m from axis) to ensure complete solution of the polymer, and to vary the degree of pre-degradation. The approximate stirring speeds were: 20 rpm for batch #1, 10 rpm for batch #2, and 5 rpm for batch #3. After this initial stirring period, precautions were taken to limit any further unwanted degradation, particularly for batch #3, which was hoped to be used for tests in as minimally degraded a condition as possible. These precautions included slow filling

of the cylinder and minimal additional stirring in the supply reservoir.

5.2.3.2. *Friction*

The procedure described for the 200 ppm solution (section 5.2.2.2.) was also used for computation of the friction coefficient for these 20 ppm solutions, with the simplification of constant viscosities. All the results presented correspond to x/D=560. As was the case for the asymptotic solution, no variation in pressure drop could be observed in the second half of the pipe, even for the runs inducing high mechanical degradation in the tube itself. This suggests that the hydrodynamic entrance region is short, and that all the shear-induced degradation is exerted at the beginning of the pipe.

The viscosity functions for the 20 ppm solution indicating that the power-law exponent is n=1, there is no difference between generalized and apparent Reynolds numbers, but these Reynolds numbers are nevertheless smaller than the solvent Reynolds numbers. Consequently, all results are presented in terms of apparent Reynolds numbers to allow better comparison with the 200 ppm solution for which the distinction has to be made.

The effect of the use of degraded or undegraded viscosity functions in the computations is similar to that discussed in section 5.2.2.2.1 and is of the order of 5% or less (the viscosity showing a decrease of less than 5% for the degraded samples). The results presented here all correspond to computations done with degraded viscosities.

The effect of the choice of temperature reference is similar to that mentioned in section 5.2.2.2.3. The difference in temperature between bulk and wall being smaller (for the same heating and flow conditions) in this case, however, this effect has a smaller influence. The results shown in this section were also computed at the wall temperature for better comparison with the 200 ppm solutions. In addition, tests were also conducted under isothermal conditions, and the corresponding friction coefficients did again match best with the results for the non-isothermal cases for which the wall temperature was used as the reference temperature (see section 5.2.2.2.3).

These friction results are presented in Fig. 5.2.-15 for the 3 batches of 20 ppm solution, together with results for water and the 200 ppm solution (batch #3) for comparison. It is apparent that the 20 ppm batch #3 solution (the least pre-degraded) exhibited friction characteristics of an asymptotic nature for the lower Reynolds numbers. This solution, however, being of marginally low concentration, was not sufficiently buffered against in-tube degradation, as it appears clearly from the fact that the friction coefficient departs from the asymptote for Re_a>30000.

The other two pre-degraded batches showed, as expected, friction results intermediate between the newtonian and the asymptotic drag reduction cases. The characteristically sharp increase of friction coefficient observed when the in-tube degradation became significant and caused the #3 solution to become non-asymptotic, is reduced for the more highly pre-degraded batches. The greater scatter for batches #1 and #2 is probably not representative of actual phenomena influencing

the measurements. It is more likely due to the fact that these runs were conducted in the early stages of the experiments, when adequate measurement and cleaning procedures had not yet been perfected.

It is noteworthy to emphasize the fact that the amount of predegradation to which these batches have been subjected, are by no means unusually high. Indeed, these relatively low stirring speeds are commonly used during preparation of solutions. The effect this moderate stirring had on the drag-reducing potential of the fluid was far from negligible, however, as is evident from the apparent changes in behavior. It is also interesting to point out that, with adequate precautions, this concentration usually considered far too dilute for asymptotic drag reduction has been shown to be capable of sustaining this regime for a significant range of Reynolds numbers.

These particular conditions of degradation being somewhat non-reproducible in other experiments, there is no point in developing correlations for these results. Indeed, to be possibly of any use, these correlations would have to be accompanied by direct measurements of the viscoelasticity for samples of fluid collected during each run, and expressed as intricate functions of the shear rate to which the samples have been subjected in the test tube. A comparison with the corresponding heat transfer results may, however, prove instructive, even if conducted in a qualitative fashion only.

5.2.3.3. *Heat transfer*

5.2.3.3.1. Fully-developed conditions

The measurements at x/D=560 have been used as representative of the thermally fully-developed flow for these solutions. (This is certainly the case as will be shown in the next section.) The Nusselt numbers are shown in Fig. 5.2.-16, as a function of the Reynolds number for the 3 batches of 20 ppm solution (as well as for water and for the 200 ppm batch #3 for comparison). As expected, the Nusselt numbers do follow trends similar to those of the friction coefficients. The Prandtl numbers of the 20 ppm solutions are close (within +7%) to those of water, a fact allowing a better comparison of the Nusselt numbers at the same Re_a.

One feature particularly striking in this graph, is the fact that even for low Re_a, the 20 ppm #3 solution does not present evidence of an asymptotic behavior for heat transfer (whereas it does for friction). Indeed, even though its Prandtl numbers are lower than those of the 200 ppm #3 solution, its Nusselt numbers are higher. It is therefore clearly incorrect to assume that because the drag reduction is asymptotic, the heat transfer reduction will be as well. This is consistent with the greater sensitivity to degradation exhibited by the heat transfer with respect to the friction that was observed by Cho and Hartnett (1982).

The heat transfer results (expressed as Colburn factors) are compared with the friction results (as $C_f/2$) for the 20 ppm #3 and the 200 ppm #3 in Fig. 5.2.-17. This graph clearly shows that even though the friction exhibited by the 20 ppm #3 at low Reynolds number is almost

identical to that of the 200 ppm #3, this similarity does not apply to heat transfer. The Colburn factor relationships at low Re_α are parallel for the 20 and the 200 ppm solution, but the discrepancy between heat transfer and friction is much smaller for the 20 ppm solution.

Both friction and heat transfer for the 20 ppm solution seem to depart from their low Reynolds numbers relationships (no in-tube degradation) at approximately the same point: for Re_α=30000. The heat transfer reduction, however, is degraded more rapidly at high Reynolds numbers, and it appears that the Colburn factor might become equal to $C_f/2$ for approximately Re_α=120000.

In order to evaluate how the non-conformity to the Colburn analogy decreases with degradation, results are presented in Fig. 5.2.-18 for both 20 ppm #1 and #3, and for water. It is apparent that the 20 ppm #1 solution (the most pre-degraded) shows close to identical values of $C_f/2$ and Colburn factors for as low as Re_α=40000, and still rather similar values for Re_α<40000. In contrast, for the 20 ppm #3 solution, these values are significantly different for most Reynolds numbers. It appears that (considering that the Colburn factor is actually greater than $C_f/2$ for water) an extrapolation of these trends would indeed confirm that for even further degradation, the 20 ppm solution would reach a water-like match between these 2 quantities.

Finally, all these results, with the addition of those for 20 ppm #2, are shown in Fig. 5.2.-19. The results for batch #2 fall in between the curves for #1 and #3 as expected. It is noticeable on this graph that all the

curves stay parallel to the asymptotes until the departure due to degradation in the test tube itself.

5.2.3.3.2. Entrance region

The heat transfer results for the 20 ppm #3 solution, obtained as a function of the distance along the tube, are shown in Fig. 5.2.-20 for various Reynolds numbers. It is evident from this graph that the very long entrance region observed in the case of the 200 ppm solution is no longer apparent. In all cases, 150 diameters seem sufficient for obtaining close to fully-developed thermal conditions. These shorter thermal entrance regions are probably related to the lower concentration and to the fact that the heat transfer for these conditions are not asymptotic.

The apparent Reynolds numbers (computed at x/D=560) for these curves are Re_a=14100, 44800, 67300, 72100, 86300, and 95500 respectively, starting with the lowest curve. As explained earlier, the scatter is larger for these solutions because of the smaller temperature differences used in the computations.

Upon closer examination, an interesting pattern seems to emerge from results obtained at small x/D. It is apparent that for Re_a <50000, the Nusselt numbers decrease continuously from the entry to the value of fully-developed flow. This was clearly the case for the 200 ppm solution as seen in Fig. 5.2.-13. This fact may be attributed to a normal drag-reducing (somewhat laminar-like) entrance region.

For Re_a >50000, however, the heat transfer in that region seems to decrease initially in a similar fashion, but will immediately increase

again before reaching the fully-developed value. This may be attributed to the degradation induced in the test tube itself, especially because Re_a=50000 was seen to be one of the values at which the friction and heat transfer were already significantly affected by degradation. As pointed out earlier, friction and pressure drop measurements show that the in-tube degradation occurs to a large extent at the beginning of the pipe, and these heat transfer results seem indeed to support that conclusion.

Furthermore, it may be noted that, for the highest Reynolds number covered in Fig. 5.2.-20 (Re_a=95500), the Nusselt number seems to increase noticeably over the rest of the pipe as well, whereas it was roughly constant for all the lower flow rates. This increase is probably caused by some slight additional degradation induced in the tube beyond the immediate entrance region, because of the very high flow rate.

The results corresponding to batches #1 and #2 were very similar, but the decrease at low x/D was reduced for #2, and not observed at all for #1 (that is, could not be seen with only 2 thermocouple locations at x/D= 35 and 75). Additionally, the accompanying slight increase in the downstream region of the pipe became noticeable for lower Reynolds numbers (about 50000) in the case of #2, and was apparent from the lowest Reynolds number on for #1. Clearly then, the pre-degradation had a significant effect on the entrance region behavior.

5.3. KEROSENE

5.3.1. Material properties

The kerosene used in these experiments is "Jet A", a type commonly used in commercial aviation. Its composition and properties varying somewhat (Yavrouian, Ernest, and Sarohia 1984), especially the viscosity, this latter property and the density were measured before the friction and heat transfer tests.

The density was measured in function of the temperature with calibrated flasks (see app. B.6.). The results are presented in Fig. 5.3.-1 for illustration of the scatter, and clearly indicate a linear relationship between these quantities. We have

$$\rho = 820.1 - 0.7278\ T \tag{5.26}$$

where the temperature is expressed in degree centigrades, and the density in kg/m^3.

The viscosity was also measured in function of the temperature, using the standard viscometer procedures described earlier (see also app. B.8.). The results are shown in Fig. 5.3.-2 , and are well correlated by

$$\eta = 1.01\ 10^{-5}\, e^{\frac{1490}{(273+T)}} \tag{5.27}$$

where $\eta(Ns/m^2)$ is the dynamic viscosity and the temperature is expressed in degree centigrades. This kerosene appears to be a newtonian fluid, no influence of the shear rate on the viscosity being observed.

The other quantities necessary for our computations are the thermal conductivity and the specific heat. The expressions being used (from a compilation of various sources) are

$$Cp = 1940 + 4.74\,T \tag{5.28}$$

and

$$k = 0.140 - 7.41\,10^{-5}\,T \tag{5.29}$$

where T is expressed in degree centigrades, k in W/m $^{\circ}K$, and Cp in J/kg $^{\circ}K$.

5.3.2. **Friction**

The friction was measured for Jet A in order to have a reference for the antimisting kerosene tests. It was verified that the flow was indeed hydrodynamically fully-developed, as expected because of the newtonian nature of the fluid Both the friction and heat transfer results shown represent the average of results for the last 3 measurements stations (i.e. for 350<x/D<600). These tests were conducted under various conditions of heating power, they include large increases in bulk temperature as well as small ones, thereby inducing large variations in Prandtl number.

The friction results are presented in Fig. 5.3.-3 together with the values of Prandtl's expression for newtonian fluids and Virk's expression for asymptotic drag reduction. The experimental results do match very nicely with Prandtl's values. The scatter is small despite the large variations in temperature conditions, because the temperature effect is ade-

quately absorbed by the use of the Reynolds number for newtonian fluids. The results (computed at wall temperature) are well correlated by

$$C_f = 0.0779\,\mathrm{Re}^{-0.249}\,. \qquad (5.30)$$

This expression is very close to that of Blasius (eq. 3.13). The difference is -0.5% at Re=5000 and -0.3% at Re=50000.

5.3.3. **Heat transfer**

The heat transfer results are presented in Fig. 5.3.-4 in terms of the Colburn factor and of a modified version with a Prandtl number exponent of 1/2. The Prandtl numbers covered in these experiments vary randomly from 19.2 to 21.2 (at wall temperature), adding to the scatter (inherently large because of the small difference in temperature between wall and bulk, typical of newtonian fluids for the power settings used).

The measured Colburn factors match very well with $C_f/2$. However, when compared to the values predicted by Friend and Metzner's correlation for heat transfer (eq. 3.75) for example, they appear slightly smaller. This difference may be due in part to the values used for the thermal conductivity and specific heat (these quantities were not measured, but taken from tables and graphs, and are additionally dependent of the exact composition of the particular kerosene used).

Rather than to correct the expressions for k and Cp in any artificial way based on these results, the values for these quantities described in section 5.3.1 were conserved. Most importantly, the Reynolds numbers

and viscosities are known accurately for our tests. It is then indeed a simple matter of multiplication by a correction factor (involving ratios of k and Cp) to modify the final heat transfer results for comparison with any other kerosene of known characteristics, if so desired.

Simple correlations developed for these results (computed at wall temperature) are

$$Nu = 0.0308\,Re^{0.881} \tag{5.31}$$

and

$$C_H Pr^{2/3} = 0.0108\,Re^{-0.114} \tag{5.32}$$

(the average Prandtl number at wall temperature for these runs is 20.1).

5.4. ANTIMISTING KEROSENE

The antimisting kerosene (AMK) studied here consists of Jet A kerosene modified by the introduction of a polymeric additive ("FM-9" by Imperial Chemical Industries). This modified fuel, designed to reduce the possibility of fire during crash landing of airplanes, is less likely to form very small droplets of fuels under high relative air velocity. This phenomenon is usually credited to high extensional viscosities and viscoelastic characteristics. For general information on this AMK, see Appendix C.2. and C.3., and the references mentioned in section 2.3.

This AMK, unlike the polyacrylamide solutions, was found to exhibit a remarkably complex viscous behavior in tubes (see Matthys 1984, also in app. C.2.). It is slightly pseudoplastic until a critical shear rate $\dot{\gamma}_c$ is reached. At this point, the viscosity of the fresh undegraded solution increases sharply by a factor of ten or so (this phenomenon will be referred to as gelation for simplicity). As the shear rate increases beyond $\dot{\gamma}_c$ the viscosity remains initially about constant at its maximum value, and then decreases because of mechanical degradation for high shear rates (see fig. 1 in app. C.2.).

This gelation phenomenon is caused by a shear-induced and time-dependent thickening of the solution in the tube if the critical shear rate is exceeded. This thickening is thought to reflect a shift from intra- to intermolecular hydrogen bonding of the polymeric additive.

This particular solution was investigated, not only for the direct information on friction and heat transfer that may be necessary for actual

use of this fuel, but also because the complexity of its viscosity functions proves to be a challenge and a test for the methods and concepts used in this study. As mentioned earlier, the complexity of the viscosity function of this fluid complicates the data processing and interpretation so much that, to obtain any reasonable results at all, probably means that the concepts used are at least adequate.

5.4.1. **Material properties**

The standard concentration used in the study of these modified fuels is 0.3% by weight. The AMK tested was prepared by in-line blending with a master slurry ("AVGARD" by Imperial Chemical Industries), using a method and mixer developed at the Jet Propulsion Laboratory (Yavrouian, Ernest, and Sarohia 1984). The polymer's exact composition is proprietary information, but it is considered somewhat of a standard and has been studied before by rheologists. The solvent used is the Jet A described in section 5.3. The thermal conductivity and specific heat are taken to be the same as those of the solvent, the difference probably being small.

The density was measured and the results (similar in scatter and number of data to those shown in fig. 5.3.-1 for Jet A) are well correlated by

$$\rho = 821.4 - 0.7317\, T \qquad (5.33)$$

where the temperature is expressed in $^{\circ}C$. When compared to the density of Jet A (eq. 5.26), this expression gives slightly larger values (+0.15% at 20 $^{\circ}C$). This difference is likely due to the presence of the polymer

and also of the water that can be retained in small quantities in the modified fuel.

The measurement of the viscous properties of this fluid is critical for this study and is described in detail in the following section.

5.4.2. **Viscosity functions**

The shear viscosity of the solution is measured in laminar flow with the viscometers described in section 4.2.3. and Appendix B.8. The resulting viscosity curves (fig. 5.4.-1) clearly illustrate the remarkably abrupt thickening of the fluid for shear rates exceeding $\dot{\gamma}_c$. The length of the tube is an important parameter because of the influence of the residence time in the tube on the extent of gelation. There may also be degradation induced in the viscometer's capillary itself. Finally, because of the viscoelasticity of the fluid, especially after gelation, end effects (such as die swell) may influence the measurements. This effect may be evaluated using tubes of different lengths. Very short tubes were also used to estimate the pressure loss at the entrance. All these aspects are examined in Appendix C.2.

The solution is very susceptible to mechanical degradation, and considerable care has to be observed to avoid unintentional degradation before use. This AMK is also sensitive to aging and photodegradation. The latter effects were studied for up to 50 days, and are described in Matthys (1985) (also in app. C.3.). The conclusion was that the photodegradation is probably caused by chain-scission of the polymer molecules, and exerts a larger influence on the viscosity than the aging alone. This

photodegradation effect is not a factor in the present heat transfer experiments, however, the solutions being stored in the dark and used no later than about a week after mixing.

Three batches of AMK were tested for friction and heat transfer. The first batch was tested after 8 days, during which its viscosity decreased significantly, probably because it was exposed to high environment temperatures. The second batch was tested after one and a half days, which is enough for full stabilization of the solution but insufficient for significant aging. Thirdly, part of the second batch was intentionally fully-degraded in a special mechanical system, to verify whether the solution would subsequently behave as normal Jet A, which is a desirable feature for injection in turboreactor engines.

Repeatable mixing of the polymer is difficult, and the in-line system for its injection in Jet A is fairly complicated. The concentration of polymer in various batches produced at different times may thus vary somewhat. During the present investigation, the concentration estimated by solid content measurement after mixing indicated values of 0.275% by weight for the first batch and 0.315% for the second batch. The concentration having a strong effect on the viscosity, this factor in addition to the aging of the first batch makes a direct comparison of the viscosity functions corresponding to the two batches rather difficult.

As was done for the polyacrylamide solutions, the viscosity of the AMK was measured for both unused and degraded samples. Because of the sharp increase in viscosity at $\dot{\gamma}_c$, however, the temperature effect can

not be easily taken into account with an Arrhenius-type expression. Indeed, an increase in temperature does not only significantly decrease the overall viscosity, but also greatly affects the value of $\dot{\gamma}_c$. Consequently, separate viscosity function polynomials had to be determined for various temperatures in order to permit subsequent interpolations during the computations. This procedure was followed for all samples of both batches of AMK.

A large number of polynomials had thus to be determined, and only some of the viscosity data will be presented here to illustrate a few points of direct importance for the heat transfer measurements. All the results presented in this section were measured with the motor-driven viscometer, fitted with tube T-20.

The temperature effect on the viscosity is very noticeable. Typical results for the unused AMK (batch #2, 2 days old) are presented in Fig. 5.4.-1. The temperatures at which these viscosities were measured are 26.3, 35.5, 44.8, and 53.1 $^{\circ}C$. It is clear that with such large variations, not only in the value but also in the shape of the viscosity functions, the choice of the reference temperature (bulk, film, or wall) at which the computations are conducted will be even more critical than for the polyacrylamide solutions (section 5.2.2.2.3.).

The shape of the curves, for example, is such that depending on the temperature, if the shear stress measured in the test tube is close to that corresponding to the critical shear rate, a difference of 1 or 2 degrees could be enough to shift the computed shear rate from one side

of $\dot{\gamma}_c$ to the other. In other words, at this shear stress, it would be possible for the fluid to show an equivalent viscosity of $3\ 10^{-6} m^2/s$ for, say, 30 $^\circ C$ and $25\ 10^{-6} m^2/s$ for 32 $^\circ C$. This large difference, although limited to a narrow region of shear rate, is of course far greater than is usual for other fluids, and had to be taken carefully into account in order to avoid problems in the critical region.

Another problem apparent with these curves, especially for low temperatures is the fact that for shear rates close to critical, the computed value of n will be very large, in some cases more than 10. With such high values of the power-law exponent, it is clear that the selection of an appropriate Reynolds number may be crucial to a meaningful representation of the experimental results.

The polynomials representing the viscosity functions (see section 4.4.1.) will naturally need to be of a high order to be able to represent adequately the jump in viscosity. For illustration, the best-fitting polynomial for the unused AMK at 26.3 $^\circ C$ would be

$$\ln (8V/D) = 6.856 - 1.894 \ln \tau_w + 2.519 (ln\ \tau_w)^2 - 0.6996 (ln \tau_w)^3$$

$$-0.07476 (ln \tau_w)^4 + 0.06507 (ln\ \tau_w)^5 - 0.01055 (ln \tau_w)^6 + 0.0005659 (ln \tau_w)^7 \qquad (5.34)$$

In some cases, polynomials of order 8 or 9 had to be used for good fit.

Several samples were taken during the tests. Some of the results are

presented in Fig. 5.4.-2. The apparent Reynolds numbers, wall shear rates, and wall shear stresses (computed at x/D=560 with wall temperature reference and degraded viscosity function) for the used samples are: Re_a=4000, $\dot{\gamma}_w$=1800 s^{-1}, τ_w=3.5 N/m^2; Re_a=11700, $\dot{\gamma}_w$=8400 s^{-1}, τ_w=17.0 N/m^2; and Re_a=13200, $\dot{\gamma}_w$=17300 s^{-1}, τ_w=65.0 N/m^2. These results were measured at 25.0, 28.0, and 28.1 $°C$ respectively. The viscosity of the unused fluid is also shown for comparison (measured at 26.3 $°C$).

It is important to note that the Reynolds numbers do not necessarily increase with increasing mass flow rate in the case of AMK because of the possible sudden increase in viscosity if the shear rate becomes large enough. Additionally, because the gelation is time-dependent at a given flow rate, the viscosity may also vary with the distance along the pipe. Finally, of course, mechanical degradation induced in the test tube itself will also have an influence on the viscosity.

It is noticeable on this graph that the degradation induced during the test is very small for the $\dot{\gamma}_w$= 1800 s^{-1} sample (the curve is superposed to that of the unused fluid because the latter corresponds to a slightly higher temperature). The $\dot{\gamma}_w$ = 17300 s^{-1} sample (which corresponds to close to maximum flow rate) shows viscosities reduced by almost 50% , however, and a noticeably larger critical shear rate is apparent as well in that case. The increase in viscosity is also somewhat less abrupt than for the unused fluid.

To further illustrate the large variations in viscosity that have to be

taken into account for the computations, results for the $\dot{\gamma}_w = 17300\ s^{-1}$ sample are shown at the same scale in Fig. 5.4.-3 for 28.1, 42.0, and 55.1 $^{\circ}C$. On the other hand, results for the unused, $\dot{\gamma}_w = 1800\,s^{-1}$, and $\dot{\gamma}_w = 17300\,s^{-1}$ samples are shown (measured at 53.1, 56.5, and 55.1 $^{\circ}C$ respectively) in Fig. 5.4.-4. It is apparent from these graphs that a combination of high temperature and degradation about eliminates completely the gelation phenomenon.

As mentioned above, the AMK batch #1 was of somewhat lower concentration, and was also used 8 days after mixing. All the viscosity measurements were also conducted for unused and degraded samples of this solution at various temperatures. These viscosity results were significantly smaller than for batch #2 (because of lower concentration and aging), but the trends were similar. Accordingly, these results are not presented here, except for one example in order to show the reader how different the solutions were.

In Fig. 5.4.-5, the viscosity function of unused AMK #2 measured 2 days after mixing (at 26.3 $^{\circ}C$) is shown together with the viscosity of unused AMK #1 after 2 days as well (at 24.5 $^{\circ}C$). (Also shown for comparison is the viscosity of AMK #1 at 25.0 $^{\circ}C$ after 8 days.) The large difference between #1 and #2 after 2 days is due only to the variation in concentration of FM-9. The critical shear rates are the same for both solutions at the same age, but the maximum viscosities are quite different (approximately 21 and 26 $10^{-6} m^2/s$, or 24%).

After 8 days, the maximum viscosity of batch #1 decreased from 21 to

about 17.5 $10^{-6} m^2/s$ (another 20%), and its $\dot{\gamma}_c$ increased from 3000 s^{-1} to 4000 s^{-1}. Consequently, as tested, the viscosities of the 2 batches were different by about 48% at 25 $°C$. The heat transfer tests conducted with batch #1 thus permitted covering higher Reynolds numbers than was possible with #2. Additional studies of the viscous characteristics of this fluid were also conducted. Parameters such as concentration, intermediate intentional degradation, addition of chemicals, and post-blending transient history were investigated. These results, not directly relevant to the present friction and heat transfer tests, are not presented here and will be published separately.

5.4.3. **Friction**

As explained in the previous section, the main characteristics of this AMK solution are its complex viscous behavior and its large sensitivity to temperature variations and mechanical degradation. Accordingly, depending on the choice of parameters and conditions used in the computations, the results may vary by a larger amount than is usually encountered in this type of analysis. The goal here is to illustrate the effects of the various parameters, and particularly to show how it is possible, by selection of the appropriate concepts, to reduce the results to a simple form surprisingly close to relationships valid for less complex fluids.

For the purpose of illustration, a number of possible ways to reduce the data will be discussed, starting with the simplest ones up to those that are felt to give the best representation of friction characteristics of

this fluid. All the results presented here were obtained by averaging those corresponding to the last 4 pressure drop stations on the test tube (i.e. for 265<x/D<600)

An inspection of the individual station results reveals small differences with what seems to be somewhat of a repeatable pattern as to which stations measure higher or lower friction. This trend shows slightly lower Reynolds numbers at the intermediate stations, which would be consistent with the assumption of a progressive development of the thickening followed by relaxation or degradation. The differences are too small, however, to be interpreted as conclusive evidence for this hypothesis.

As was the case for the other fluids, all the computations were conducted under various combinations of different conditions. Clearly, for example, these computations should be done with the viscosity function of the degraded fluid (interpolated for flow rate and location), and not with that of the unused material as is done in most studies (or worse, with that of the solvent). Some results for AMK #2 are presented in Fig. 5.4.-6 that show the difference between results computed with unused and degraded viscosity functions. The results are computed at bulk temperature and are expressed in terms of generalized Reynolds numbers. Shown for comparison are also Prandtl and Virk relationships.

The effect of the gelation phenomenon is very apparent on this graph. The results corresponding to pre-critical shear rates follow approximately Virk's asymptote, but as soon as the critical shear rate is

exceeded, the thickening and the resulting increase in viscosity cause the Reynolds number to decrease dramatically. Apparently, the solution is thus potentially an asymptotic drag-reducer in its pre-gelation state, but no further conclusion at this point can be drawn for the thickened state. The results computed with the degraded viscosity functions should be the more meaningful ones, and they naturally show an increase of Reynolds numbers for the high flow rates, bringing them closer to Virk's asymptote.

In Fig. 5.4.-7 the results are computed in terms of both apparent and generalized Reynolds numbers (for bulk temperature and degraded viscosity functions). The use of the apparent Reynolds numbers seems to reduce the scatter away from Virk's asymptote. The results come out in this latter case as a continuous curled curve (with increasing flow rate), expressing the initial sharp thickening and the subsequent decrease in viscosity and loss in drag-reducing potential caused by degradation. Accordingly, the use of apparent Reynolds numbers is thought to be more appropriate than generalized Reynolds numbers. This will be verified again further on.

The most critical factor, as expected, is the choice of the temperature at which the computations are conducted. The results for both bulk and inner wall temperature references, are shown in Fig. 5.4.-8 (these and all results shown subsequently correspond to degraded viscosity functions). The results for film temperature (not shown) gave intermediate values. Clearly, the choice of the reference temperature is far more critical than for the polyacrylamide solutions (fig. 5.2.-6), the shape of the curves

being fundamentally different in this case depending on the reference chosen. The choice of the wall temperature for the computations was favored as physically most appropriate (see section 5.2.2.2.3.), and indeed, the corresponding curve is seen to match almost perfectly with Virk's asymptote, even for the gelated fluid.

Having chosen the wall temperature as reference for the computations, it is then verified in Fig. 5.4.-9 that the choice of apparent Reynolds number is the most suitable for this case as well. Indeed, the results based on the generalized Reynolds numbers show a sharp departure from Virk's asymptote for high flow rates, whereas those based on the apparent Reynolds numbers do not. Interestingly, whereas for bulk temperature the generalized Reynolds numbers were smaller than the apparent ones for the gelated fluid, it is the opposite in this case.

Having shown that for this batch (#2) the computations (conducted at wall temperature and expressed in terms of apparent Reynolds number) give a relationship very close to that of the familiar drag reduction asymptote, the next step was to verify that the results for the other batch would be compatible. Indeed, the AMK #1 (as explained in section 5.4.2.) exhibited a much lower viscosity.

Results are shown in Fig. 5.4.-10 for both batches with wall temperature reference. Because of its lower viscosity, the results corresponding to batch #1 gave much larger Reynolds numbers, but clearly the values are again very close to those of the drag reduction asymptote. This good match for 2 rather different batches of the fluid supports the assump-

tion that the AMK is indeed physically an asymptotic drag reducer, the collapse of the results on the asymptote being likely more than just a coincidence. Also shown for comparison are the experimental data obtained for Jet A.

A simple correlation of the power-law type has been worked out to approximate the friction data

$$C_f = 0.654\,\mathrm{Re}_a^{\,-0.584} \quad . \tag{5.35}$$

As expected, this expression is very similar to that for the asymptotic polyacrylamide solution (eq. 5.10), the difference in value being only +5%, and the exponents being identical. This difference is small indeed considering the numerous steps necessary to formulate the AMK results in the present form.

Finally, as an illustration of the progression covered during the steps previously described, in Fig. 5.4.-11 the results are shown for both batches for the 2 extreme procedures used for computations: generalized Reynolds number, bulk temperature, and unused viscosity functions on the one hand; and apparent Reynolds number, wall temperature, and degraded viscosity functions on the other hand. The difference is surprisingly large, emphasizing the importance of the adequate choice of computational parameters for this type of fluid.

5.4.4. **Heat transfer**

5.4.4.1. *Fully-developed conditions*

As explained in the previous section, the simultaneous thickening, relaxation, and degradation phenomena contribute to make the flow rather complicated in the downstream part of the pipe. Consequently, to minimize the uncertainties on what may be considered to be the location of thermally fully-developed flow, the following results represent the average of heat transfer measurements at the last 4 thermocouple stations on the tube (i.e. from x/D= 307 to 560). As will be seen in the next section, there are indeed only small differences between the results respectively corresponding to these 4 stations.

The Prandtl numbers corresponding to these 2 AMK batches ranged from 30 to 70 (as computed at wall temperature), the variation being mainly due to the increase in viscosity due to gelation. The tests were conducted for various heating rates as well. The temperature difference between fluid bulk and inner wall may be as high as 20 $^{\circ}C$ or more for this fluid under the usual heating conditions of 2 $^{\circ}C$ increase in bulk temperature over the length of the pipe.

Nusselt number results computed at the wall temperature are presented in Fig. 5.4.-12 for both AMK batches and for Jet A. As illustration of a different representation, the "solvent Reynolds number" used here is based on the viscosity of Jet A. This is indeed the representation of major interest to the engineer concerned with these fuels, the mass flow rate being the critical parameter for combustion related studies.

Clearly, the difference in heat transfer between pure Jet A and the modified kerosene is very large. This is of course a serious concern in practice because of the common use of fuel as coolant in turboreactor engine heat exchangers.

For better comparison with the polyacrylamide solutions, the heat transfer results are also shown in Fig. 5.4.-13. In this graph, both $C_f/2$ and the Colburn factor are presented for Jet A, AMK #1, and AMK #2. In each case, the results for the 2 batches of AMK are very coherent despite their large differences in viscosity and Prandtl numbers. As was the case for the polyacrylamide solutions and water, it is apparent that the Colburn factor of the AMK solution is no longer equal to $C_f/2$ (as it is for Jet A). A modified Colburn factor with a Prandtl number exponent of 0.5 is also shown for comparison.

The results for the asymptotic 200 ppm polyacrylamide solutions are also shown as curves (1), (2), and (3) for comparison with the AMK results, they correspond respectively to $C_f/2$, and to 2/3 and 0.5 exponent for Prandtl in the Colburn factors. As mentioned in the previous section, the AMK friction results match very nicely with the polyacrylamide asymptote. Amazingly, the AMK Colburn factors are very close to those given by the heat transfer asymptote, despite the complicated viscosity functions for AMK, and the great difference in Prandtl number between the two types of solutions. That the results match, even if only approximately, adds considerable weight to the assumption that the present expression for the heat transfer asymptote (eq. 5.15) is correct. A simple power-law correlation for these results is

$$C_H Pr_a^{2/3} = 0.0991\,\mathrm{Re}_a^{-0.566}. \qquad (5.36)$$

When compared to the expression for the heat transfer asymptote, the difference is +14% at $\mathrm{Re}_a = 6000$ and +2% at $\mathrm{Re}_a = 90000$.

Another interesting observation is the fact that the AMK Colburn factor with a 0.5 Prandtl exponent does not match its equivalent for polyacrylamide quite as well as the Colburn factor with a 2/3 exponent. The results for the 0.5 exponent are also smaller than the corresponding polymer asymptote instead of slightly larger as are the 2/3 exponent. That the AMK results should be larger than the polyacrylamide ones is also physically more likely because the asymptote represents a minimum. What this confirms is that, as supposed earlier, the 2/3 exponent (or a slightly smaller one) is indeed apparently more appropriate for absorbing the variations in Prandtl number. The difference between the original and modified Colburn factors is naturally larger for AMK than for polyacrylamide, because the Prandtl numbers are larger.

5.4.4.2. *Entrance region*

The Nusselt numbers for batch #2 are presented in Fig. 5.4.-14 as a function of x/D for typical runs covering the whole range of flow rates studied during the tests. Starting with the lowest one, the curves correspond respectively, to $\mathrm{Re}_a = 2217$ ($\dot{\gamma}_w = 957\ s^{-1}$, $\tau_w = 2.2\ N/m^2$), $\mathrm{Re}_a = 9180$ ($\dot{\gamma}_w = 5170\ s^{-1}$, $\tau_w = 9.91\ N/m^2$), $\mathrm{Re}_a = 8870$ ($\dot{\gamma}_w = 10600\,s^{-1}$, $\tau_w = 43.1\,N/m^2$), and $\mathrm{Re}_a = 25900$ ($\dot{\gamma}_w = 32500\,s^{-1}$, $\tau_w = 75.3\,N/m^2$); all computed at wall temperature and for x/D=560. It is apparent that the last 4 stations give similar results in most cases, with some fluctuations

probably caused by a combination of gelation and degradation.

The thermal entrance length seems to be a strong function of the flow rate, apparently more so than for the case of the polyacrylamide solution (fig. 5.2.-13). For the lowest speed, 100 diameters seem to be sufficient for fully-developed thermal conditions, whereas for the highest speed, 400 diameters seem necessary. The Reynolds numbers not being a continuously increasing function of the flow rate, it is difficult to find a direct correlation between the Reynolds number and the entrance length, especially if one considers the unknown additional influence of gelation, degradation, and possibly relaxation in the tube. The heat transfer results in the thermal region for the AMK #1 show identical trends.

5.4.5. **Fully-degraded antimisting kerosene**

The idea behind the antimisting kerosene concept is to store this modified fuel in the airplane tanks to avoid fire in case of rupture of these tanks. Because of the high viscosity and viscoelasticity of the AMK, it would be difficult to inject it as a properly reactive spray in the combustion chamber, however. Consequently, before this injection the fuel should be processed through a mechanical degrader in order to bring the AMK back to a state as close as possible to that of Jet A. Such an intentional degradation was obtained in this study by forcing some AMK (batch #2) at very high pressure through a needle valve (pressure drop: 5000 psi), the extremely high extension and shear rates involved inducing the rupture of the polymeric chains.

It is easy to check if the viscosity after degradation becomes constant with shear rate and close to that of the solvent (Jet A), but this does not imply necessarily that the viscoelastic character of the fluid has been eliminated (as the 20 ppm polyacrylamide solution clearly showed). Additionally , it was also thought interesting to investigate the friction and heat transfer properties of the degraded fuel, and tests were conducted accordingly with this degraded batch.

The viscosity of the degraded AMK was measured with the viscometers (tube T-20) at various temperatures. (There was of course no need to take samples during the heat transfer runs because of the already extremely high degree of degradation before use.) As expected, the viscosity appeared constant with shear rate, with no indication of gelation over the range covered. The effect of temperature was well correlated by an expression of the Arrhenius type, and the results may be expressed as

$$\eta = 1.43\,10^{-5}\, e^{\frac{1430}{273+T}} \tag{5.37}$$

with the temperature expressed in $^{\circ}C$, and η in Ns/m^2.

When compared to the results for Jet A (eq. 5.27), it is apparent, however, that the difference is not so negligible: +18% between 25 $^{\circ}C$ and 50 $^{\circ}C$. This slightly larger viscosity is understandable, because the original concentration is rather high (3000 ppm) and the polymer cannot be totally eliminated by the degradation procedure. On the other hand of course, when compared to the viscosity of the undegraded AMK, this is proportionally close enough to Jet A. Nevertheless, the important

question is whether all viscoelasticity has been eliminated from the solution, so that there will be no problem with injection.

The friction results are shown in Fig. 5.4.-15, together with the results for Jet A (all are computed at wall temperature, and are averages of the last 4 stations). The material properties (ρ, k, Cp) are taken to be the same as those of AMK. The results for degraded AMK appear close indeed to those of Jet A when compared to Virk's asymptote, confirming that the drag-reducing behavior has been essentially eliminated. The results for fully-degraded AMK are well correlated by

$$C_f = 0.107\,\mathrm{Re}^{-0.285} \quad . \tag{5.38}$$

When compared to the results for Jet A (eq. 5.30), the difference is small: +1% at Re= 5000 and -6% at Re=40000.

The heat transfer results are shown in Fig. 5.4.-16 together with Jet A, all in terms of Colburn factor. Again, it is clearly seen that the results for both fluids give essentially identical values of the Colburn factor for the range of Reynolds numbers covered. The results may be correlated with

$$C_H Pr^{2/3} = 0.0123\,\mathrm{Re}^{-0.128} \quad . \tag{5.39}$$

The comparison with the expression for Jet A (eq. 5.32) gives +1% at Re=5000 and -2% at Re=40000, a rather good match.

The Nusselt numbers when expressed in function of x/D are approximately constant over the whole length of the tube, confirming the newtonian nature of this fluid.

In conclusion, the polymer solution can be successfully brought back by high mechanical degradation to an essentially newtonian behavior for friction and heat transfer, despite a slightly higher shear viscosity.

5.5. SUSPENSIONS OF PARTICULATES

The material used in these tests is bentonite, a type of clay well-known for its structure that consists of layers of platelets inducing significant swelling when hydrated. Aqueous suspensions of bentonite exhibit typical colloidal characteristics and their viscosities are strongly dependent on factors such as pH and presence of foreign ions. The suspensions are typically pseudoplastic, and may exhibit a yield stress and a thixotropic character. Of course, the concentration of bentonite is a crucial parameter for this type of behavior. For more information and references see section 2.4., and in particular Rogers (1948) for a description of some of the viscosity characteristics of bentonite suspensions.

The suspensions were rapidly agitated for at least a day before use in order to maximize the dispersion and hydration of the clay. In all cases the carrier fluid was tap water. The mixing procedure offered no problem, except for the case of the suspension with added polyacrylamide (see section 5.6). The quantity of unsuspended foreign material found in the tank was very small (typically no more than, say, 2 tablespoons out of 15 kg of bentonite). These fine particles, appearing to be sand or ash, were not aspirated in the system because of sedimentation in the main supply tank.

The sedimentation of the bentonite particles themselves proved to be an interesting problem. Various tests were conducted to estimate the speed of sedimentation and it was found that the sedimentation time

increased sharply as the concentration was increased above 3%. The sedimentation time is defined here as the time required to obtain clear water in the upper half of a column of fluid that was initially mixed to homogeneity. This time increased from less than one hour for concentrations smaller than 3% up to several days for larger concentrations (see section 4.3.1.). This critical concentration probably corresponds to interparticular distances small enough for the molecular or electric forces to effectively lock the particles in a gel-like structure (if no shear is present).

Accordingly, it was decided to test suspensions in this range of concentration to investigate whether a similar discontinuity might be observed for friction and heat transfer. During the measurements, the 1% suspension proved difficult to handle repeatably because of its rapid rate of sedimentation, and consequently, the friction and heat transfer data for this fluid were discarded.

The thixotropic behavior of these suspensions is beneficial for their use as drilling fluids, because of the resulting reduced settling of the cuttings in the case of interruption of the mud circulation. Other functions of the drilling muds beside removal of the cuttings are cooling and lubrication of the bit, control of subsurface pressure, and walling up and support of the wellbore. In order to obtain the high viscosity necessary for these applications, the concentrations of solids required for the muds are higher than those used in this study. The present investigations were limited to a concentration of 5% by weight to insure that the pressure drops would be small enough to permit measurements in the

turbulent regime.

Rather large reductions in friction with respect to newtonian fluids have been mentioned in the past for this kind of suspension. Consequently, a question also addressed in this study was whether or not these suspensions might possibly exhibit any drag-reducing behavior in turbulent flow beyond the reductions induced by pseudoplasticity. The nature of these fluids, however, does not appear to suggest the existence of a potential mechanism that could impart a large enough viscoelasticity to the fluid to induce viscoelastic drag reduction. Consequently, the reductions mentioned in the literature probably correspond only to the lowered friction typical of pseudoplastic purely viscous non-newtonian fluids (which is best characterized in the generalized Reynolds number representation). The latter decrease in friction is not considered as "drag reduction" according to the usual definition which implies modifications of the turbulence characteristics because of viscoelasticity (and which is best characterized in the apparent Reynolds number representation).

5.5.1. **Material properties**

The bentonite studied here (manufactured by American Colloid Co.) satisfies the API 13A specification for oil-well drilling fluid materials. The measured pH after mixing was: 7.8 for the 2% suspension, 8.0 for the 3% batch, 7.6 for the mixture of 3% clay and 20 ppm polyacrylamide, and 7.8 for the 5% batch (the pH of the tap water used varied from 6.2 to 7).

The density of the 5% suspension was measured directly as a function of the temperature. The results are well correlated by

$$\rho = 1043 - 0.480\ T \tag{5.40}$$

where T is expressed in $^{\circ}C$, and ρ in kg/m^3.

The heat capacity and thermal conductivity of the clay could not be measured and had to be taken from published values. The thermal conductivity of dilute suspensions can then be approximated using Maxwell's formula (eq. 3.74). Assuming a value of k=1.28 $W/m\,^{\circ}C$ at 20 $^{\circ}C$ for solid clay, we find a value of thermal conductivity for the 5% suspension that is 1.025 times that of water. The heat capacity is taken to be additive, and using a value of Cp= 877 J/kg $^{\circ}C$ for clay, we find that for the 5% suspension, the heat capacity of the fluid is 0.960 times that of water. For lower concentrations, the density, heat capacity, and thermal conductivity are interpolated linearly.

5.5.2. **Viscosity functions.**

The viscosity of the suspensions was measured in the usual manner as a function of temperature and shear rate. As degradation is not a factor for these suspensions, there was no need to take samples during the heat transfer tests. This problem does, however, have to be considered for the clay and polymer combination (see section 5.6). The viscosity of the 1% batch is presented for illustration but these results were not used because the sedimentation time to "half-height" was only about 15 minutes for this fluid, which was not enough to ensure the homogeneity of the fluids during the tests.

The effect of temperature could not be correlated by a unique Arrhenius-type exponent for the 3% and 5% batches, the exponent being slightly dependent on the shear rate. Consequently, the viscosity function polynomials were entered in the programs separately for different temperatures, thereby permitting the necessary interpolations during the processing of data. For illustration, typical numbers would be B=1208 $^{\circ}K^{-1}$ at 5500 s^{-1} for the 5% batch, and B=1611 $^{\circ}K^{-1}$ at 20000 s^{-1} for the 3% one. The temperature effect for the 2% batch, however, was represented adequately over the whole range of shear rates by B=1800 $^{\circ}K^{-1}$. The relative order of these values of B with decreasing concentration is consistent, the value for water being 1902 $^{\circ}K^{-1}$.

The values of viscosity for the 4 batches tested are shown in Fig. 5.5.-1 as a function of shear rate, the data corresponding to 25.4 $^{\circ}C$ for the 1% batch, 25.0 $^{\circ}C$ for the 2%, 25.1 $^{\circ}C$ for the 3%, and 25.2 $^{\circ}C$ for the 5% batch. It is apparent that the viscosity for the 5% solution is far larger than that of water (35 times at 100 s^{-1}), and that the values of the power-law exponent are quite low for this fluid (as low as n=0.55 for the smallest shear rate used in the experiments). The viscosity functions for other temperatures are not shown.

5.5.3. **Friction**

There was no noticeable difference between pressure transducer measurements as a function of the position, implying that the hydrodynamic entrance region was small. The heat transfer measurements were a function of the position for low Reynolds numbers, however, and

consequently the station at x/D=560 was used to evaluate fully-developed thermal conditions. Accordingly, for better comparison, the friction results presented in this section correspond to x/D=560 as well.

The results shown correspond to computations conducted at inner wall temperature, in accordance with the conclusions reached for other fluids (in any case, the difference between bulk and wall temperature is small for these suspensions). The values of the power-law exponent corresponding to the test conditions are $0.55<n<0.75$ for the 5% batch, $0.75<n<0.85$ for the 3%, and about $n=0.9$ for the 2% batch.

The friction results for the 3 batches are shown in Fig. 5.5.-2 as a function of Re'. It is apparent that because of the large viscosity of the 5% suspension, several of the runs conducted with this fluid corresponded to laminar conditions. These laminar friction results match well with eq. 3.32, a proof that the viscosity and friction measurements are adequate. (The lowest Reynolds number result is a bit off, very likely because the corresponding RPM and pressure drop measurements were conducted at the minimum of the instrument ranges.) The first 2 runs for the 3% batch also pertain to the laminar regime. For both cases, the transition occurs at about Re'=3000.

The laminar results for the 5% batch are correlated by

$$C_f = 9.15\,\mathrm{Re}'^{-0.926} \tag{5.41}$$

which differs from eq. 3.32 by +0.5% at Re'=2000, and by -5% at Re'=1000.

The turbulent results are about parallel to Prandtl's expression for newtonian fluids, as expected for purely-viscous non-newtonian fluids.

Metzner's eq. 3.33 is also shown for n=0.7 for reference. (For larger values of n, the curves are parallel to Prandtl's, and located in between these two.) The experimental results are in good agreement with the values given by these expressions.

The same results are also presented in Fig. 5.5.-3, but in terms of apparent Reynolds numbers. The laminar results are now, as expected, larger than the values of $16/Re_a$, because of the presence of a factor dependent on n in eq. 3.37. In this representation, the turbulent friction coefficients for all 3 batches collapse very close to Prandtl's expression for newtonian fluids, however. The turbulent results for the three batches are well correlated by

$$C_f = 0.0781\, Re_a^{-0.252} \qquad (5.42)$$

which, with respect to Prandtl's expression (eq. 3.12), differs by -1% at Re_a=10000, and by -2% at Re_a=50000, an excellent match.

This verifies that, as suspected, these suspensions do not exhibit drag reduction beyond the purely viscous pseudoplatic effect.

The large difference between the two Reynolds number representations illustrates rather well why the apparent Reynolds numbers are often better suited for viscoelastic fluids: they absorb the effect of the power-law exponent, isolating the remaining viscoelastic drag reduction.

5.5.4. **Heat transfer**

5.5.4.1. *Fully-developed flow*

It will be shown in the next section that the thermal entrance region extends in certain cases to large values of x/D, and consequently all results shown here correspond to x/D=560. These computations were conducted at the wall temperature. The values of the generalized Prandtl numbers for these runs are 20<Pr'<90 for the 5% batch, 13<Pr'<25 for the 3% batch, and 8<Pr'<12 for the 2% batch.

Heat transfer results for the 3 batches are shown in Fig. 5.5.-4 in terms of Nusselt and generalized Reynolds numbers. The difference between batches is caused by the spread due to the definition of Re' (as was the case for friction), and also by the variations in Prandtl number. Also shown as curve (1) is eq. 3.70 for values of n corresponding to those of the 5% batch in the laminar regime, and as curve (2) is eq. 3.75 for the values of n of the 2% batch for the turbulent case. In both regimes, the experimental results are larger than the values given by these relationships. If these expressions are correct, this difference could be caused by influence of the thermal entrance region or possibly by regions of plug flow or because of thixotropic behavior.

These heat transfer results are presented in terms of Colburn factors (with Prandtl number exponents 2/3 and 0.5) and $C_f/2$ as a function of apparent Reynolds numbers in Fig. 5.5.-5. Water results are also shown for comparison. The values of $C_f/2$ for all 3 batches were shown in Fig. 5.5.-3 to coincide with those for water under turbulent conditions. The

$C_f/2$ curve is located neatly in between $C_H Pr_a^{2/3}$ and $C_H Pr_a^{0.5}$ for the clay suspensions in turbulent flow (as in the case of water). Interestingly, the relative positions of these 3 curves in laminar regime are similar to those of asymptotic polymer solutions in turbulent regime (itself a somewhat laminar-like regime if asymptotic drag reduction is present).

It appears that $C_H Pr_a^{2/3}$ absorbs the effect of variation of Prandtl numbers better than $C_H Pr_a^{0.5}$, the difference between values corresponding to the various batches being smaller for the former. These results are larger than those for water, however, whereas $C_H Pr_a^{0.5}$ for clays and water match somewhat better. The Colburn factors in the turbulent regime show a distinctive curvature in this log-log graph. A simple power-law function of the Reynolds number would thus be a poor approximation for these results. When compared with eq. 5.5 , however, we find approximate differences of 0% at Re_a=5000, +30% at Re_a=20000, and +20% at Re_a=50000. These results, if presented in terms of generalized Reynolds numbers, give very similar curves and trends, with slightly smaller Reynolds numbers and Colburn factors.

The Colburn factors for the 5% batch in laminar flow are correlated by

$$C_H Pr_a^{2/3} = 0.127\, Re_a^{-0.613} \quad . \tag{5.42a}$$

Whereas, for comparison, water at 27 $^\circ C$ in fully-developed laminar flow would give (eq. 3.48)

$$C_H Pr^{2/3} = 2.423\, Re^{-1} \quad . \tag{5.42b}$$

The two expressions give identical values for Re_a=2000 but for lower Re_a, the value of the Colburn factor for clay is much smaller than for water

despite larger Nu, because of the larger values of Pr_a for the clay.

5.5.4.2. *Entrance region*

The heat transfer results for the 5% batch are shown as a function of x/D in Fig. 5.5.-6 for the whole range of Re' covered in the tests. The particular runs chosen for illustration (starting with the lowest curve) correspond to Re'=530 (Pr'=90), Re'=2460 (Pr'=50), Re'=2730 (Pr'=46), Re'=3230 (Pr'=40), and Re'=9650 (Pr'=22), all computed with properties evaluated at wall temperature and at x/D=560. These results constitute an interesting illustration of the transition from laminar to turbulent regime.

The Nusselt numbers corresponding to the lowest Reynolds number (curve 1) show that the entrance region extends to more than x/D=600. The value of the Nusselt number for x/D=610 is 6.3, somewhat larger than the Nu=4.7 value for fully-developed flow according to eq. 3.70. The difference is probably due to non-yet fully-developed thermal conditions. Indeed, according to eq. 3.53 , the laminar thermal entrance region would extend to x/D= 2400 for newtonian fluids under the same conditions.

The results corresponding to Re'=2460 (curve 2) show the beginning of an apparent instability development in the pipe at x/D=300, but interestingly, the flow seems to return to a laminar condition further in the tube, and exhibits another increase in heat transfer at the very end. This is likely corresponding to the onset of the transition to turbulent regime.

The run (curve 3) at Re'=2730 (note the small increase in Re') corresponds in turn to fully transitional conditions. The heat transfer starts as in a laminar flow, showing a decrease in Nusselt number up to x/D=100, then, with turbulence developing, starts to increase continuously in the remainder of the test tube.

The next run (curve 4), at Re'=3230 (again very small increase in Re') shows constant values of Nu for x/D>75 indicating a fully-developed turbulent flow for most of the pipe. The first thermocouple (at x/D=35) gave a much lower Nu, implying that it still pertains to the entrance region. The highest Re' covered here (curve 5) shows Nu constant for the whole length of the pipe, however, showing that the entrance region extends to even less than x/D=35 in that case, as is typical for newtonian turbulent flows.

The results for the 3% batch show very similar trends. The 2% batch shows Nu constant for the whole length of the pipe for all the runs, however, all these runs corresponding to fully-developed turbulent flow.

In order to investigate the entrance region for the laminar runs, the Nusselt numbers have been plotted in terms of Graetz number in Fig. 5.5.-7. The runs corresponding to fully-laminar conditions (without evidence of transitional behavior) are Re_a=580, 1080, and 1420 for the 5% batch; and Re_a=1450 and 2200 for the 3% batch. The values of the power-law exponent n for these runs vary with location, the range covered being 0.55<n<0.63 for the 5% batch (with $56<Pr_a<76$), and 0.72<n<0.78 for the 3% batch (with $23<Pr_a<27$). Eq. 3.69 is also shown

on the graph for the average value n=0.66 for comparison.

The agreement with this equation is good, the experimental data being all within 10% of the values given by this expression. The results are rather on the large side for the 5% batch and on the low side for the 3% batch. (In contrast, Cho and Hartnett (1982) observed values that are generally smaller.)

5.6. COMBINATION OF POLYMER AND PARTICULATES

It was thought interesting to investigate the properties of a combination of 20 ppm of polyacrylamide and 3% bentonite in water, these materials having been studied separately for these concentrations. The material properties, except viscosity, were taken to be the same as those of the 3% bentonite suspension. The pH of the fluid after mixing was 7.6 (the pH of the tap water used as solvent being 6.1).

5.6.1. Viscosity functions

The fluid was prepared by mixing the clay first and subsequently adding the polymer under stirring. Immediately after addition of the polyacrylamide, however, the mixture showed signs of flocculation (clusters of 1 or 2 mm).

Both the unused fluid and the samples taken during the runs were tested for viscosity as a function of temperature in the motor-driven capillary viscometer (with tube T-20). These measurements proved unrepeatable until it was observed that the unused fluid showed an extreme sensitivity to handling-induced degradation, thereby necessitating precautions even against mere sloshing in the bottles during filling of the viscometers. The degraded samples did share this problem, but to a lesser degree only.

In order to illustrate the unusual sensitivity to degradation of this fluid, the viscosity of an unused sample is shown in Fig. 5.6.-1 as curve (1). For comparison, curves (2), (3), and (4) correspond to the same sample but shaken manually in its container (respectively one, three,

and several times). It is apparent that the viscosity of the samples decreased very significantly with agitation (not a much more vigorous handling than that occurring during normal filling and transport), namely by 12%, 28%, and 34%. The temperature at which these samples were tested are respectively 23.2, 23.2, 23.8, and 23.8 °*C*.

Amazingly, the viscosity (curve 5) of a sample taken during heat transfer tests at an intermediate flow rate (Re_a=17500, x/D=560, wall temperature of 32.6 °*C*) is still larger (i.e. less degraded), despite the shear-induced degradation in the test tube, than that of the unused samples having been roughly "handled." The temperature at which the viscosity of this sample was measured is 23.5 °*C*. Other samples taken during runs at higher Reynolds numbers exhibited viscosities similar to that of the sample shown in the graph.

It is important at this point to emphasize that the use of the term "degradation" should not be limited in this context to the rupture of polymer molecules. Indeed, it is possible that the shear might additionally affect the size or nature of the flocculated clusters of polymer and clay, which in turn could possibly have a strong influence on the flow characteristics of the suspension, and therefore have a significant effect on the viscosity or drag reduction. In other words, by the term degradation it is meant the overall modification of the fluid, possibly by rupture of polymer molecules and by alteration of flocculated clusters.

Naturally, these viscosities might also have been influenced by other phenomena unaccounted for here, such as chemical reactions or

recombination after degradation for example. A more comprehensive study of this problem is thus necessary before definitive conclusions may be drawn, but these viscosities were nevertheless used in the programs, for qualitative illustration, and for want of any better information.

For better comparison with other fluids, the viscosity data for the unused sample are shown together with the viscosity of the pure clay suspensions in Fig. 5.6.-2 (see section 5.5.2. for details on the latter fluids). It is apparent that the viscosity of the combination of 3% clay and 20 ppm polymer is significantly larger than that of the pure 3% clay suspension ($3.75\ 10^{-6}$ vs $2.62\ 10^{-6} m^2/s$ at 22000 s^{-1}, i.e. +43%). As reference, the addition of 20 ppm of polymer to water would only increase its viscosity from $0.893\ 10^{-6}$ to $0.960\ 10^{-6} m^2/s$ at 25 $^{\circ}C$ i.e. +7.5%, a much smaller effect.

In conclusion, the addition of polyacrylamide to this bentonite suspension has modified dramatically its properties by impairing its homogeneity, increasing its viscosity, and most importantly, making it highly susceptible to degradation during handling. These phenomena should be taken into account if practical use or study of this type of mixture are contemplated.

5.6.2. **Friction**

The friction results are presented in terms of apparent Reynolds numbers in Fig. 5.6.-3, together with the results corresponding to the

pure 3% bentonite suspension and to the 20 ppm polyacrylamide solution (batch #3). All the results are based on wall temperature, correspond to x/D=560, and are computed with degraded viscosity functions if needed.

It is apparent that the friction exhibited by the mixed fluid is very different from that corresponding to either one of the 2 pure fluids. The friction at intermediate Reynolds numbers for the mixed fluid reaches close to asymptotic levels, but at Re_a=10000 it already shows characteristic signs of in-tube mechanical degradation. This degradation occurs at a much lower Re_a than for the 20 ppm solution (Re_a=10000 vs 60000), confirming the fact that the mixed fluid is much more sensitive to degradation than normal polymer solutions. This shear-induced degradation causes the friction coefficient to increase very rapidly towards newtonian values.

For low values of the Reynolds number, the friction coefficient seems to depart from the asymptote. This could be representative of a typical onset phenomenon for the drag reduction. It may also be due to the difficulties encountered during the viscosity measurements. Results computed at bulk temperature and with undegraded viscosity functions show similar trends.

Interestingly, these friction measurements do vary with the location along the tube, unlike the case of all the other fluids studied, and these variations are very much a function of the flow rate. These results are shown below in tabular form for illustration.

Re_a(x/D=560)	C_f(306)	C_f(390)	C_f(474)	C_f(559)
1560	1.87 10^{-2}	1.83 10^{-2}	1.83 10^{-2}	1.80 10^{-2}
2540	1.14	1.11	1.10	1.07
3330	8.00 10^{-3}	7.70 10^{-3}	7.61 10^{-3}	7.47 10^{-3}
4390	6.60	6.32	6.18	6.06
6370	4.66	4.39	4.35	4.29
9300	3.11	2.85	2.87	2.93
11200	2.59	2.45	2.52	2.81
15500	2.11	2.09	2.40	2.99
16900	1.92	1.84	2.03	2.63
17500	1.98	1.87	2.29	2.78
22100	2.46	3.22	3.44	3.63
24500	2.63	3.28	3.55	3.74
31000	3.38	3.57	3.75	3.87
35600	3.57	3.72	3.83	3.96
35700	3.56	3.70	3.83	3.96

It is apparent that for the low Reynolds numbers, the C_f decreases slightly with increasing x/D: by 4% for Re_a=1560 up to a maximum of 9% for Re_a=4390 and 6370. Starting at Re_a=9300 and up to 17500, C_f first decreases and then increases again (by only 3% at Re_a= 9300, and up to 49% at Re_a=17500). Very likely, the increase in the last part of the pipe is due to shear-induced mechanical degradation in the test tube itself. For Re_a>22100, C_f increases over the whole length under observation,

greatly at first (48%) down to 11% for the highest Re_a covered. The last 2 runs show the good repeatability of the measurements.

In other words, at low Reynolds numbers, the friction apparently decreases slightly in the pipe. For larger Reynolds numbers, at a certain location the friction starts increasing again, probably because of mechanical degradation induced in the tube that reduces the effectiveness of the drag reduction. Naturally, this degradation becomes more important with increasing velocity, balancing the initial decrease in viscosity earlier in the pipe.

Finally, at the highest Reynolds number, most of the degradation seems to occur at the beginning of the pipe with only reduced susceptibility farther downstream. (Note that for the pure polymer solutions, all the degradation was observed to occur at the beginning of the pipe with no variation in friction in the second half.) Strikingly similar trends for the heat transfer as a function of location are discussed in the next section.

There is no clear explanation as to why the friction should initially decrease with distance in the pipe. Possible reasons might be: the effect of entrance flow, decrease in viscosity due to degradation, homogeneization of the fluid, or thixotropy. Clearly, this combination of polymer and particulates exhibits an unexpectedly far more complex behavior than the separate component fluids, and would deserve further study.

5.6.3. **Heat transfer**

The heat transfer results for the combination fluid are shown in Fig. 5.6.-4 in terms of Nusselt numbers. Also shown are results for the pure 20 ppm solution, and for the 3% suspension. The results are all computed with properties evaluated at wall temperature. Degraded viscosity functions were used when necessary and the data correspond to the location x/D=560. The apparent Prandtl numbers for the combination fluid range from 13 to 33.

As was the case for friction, the heat transfer results for the combination fluid are intermediate between the results for its constituents, and again show very clearly the strong influence of mechanical degradation induced in the tube. The results for the 20 ppm solution and for the combination fluid appear to be perfectly matching before degradation. Very likely this is only a coincidence, however, because the Prandtl numbers are different for the two fluids, and because the degradation induced by stirring before the tests is probably not the same either.

The same results are presented in Fig. 5.6.-5 in terms of Colburn factors. Also shown is $C_f/2$ for the combination fluid. The Colburn factor for this fluid appear lower before in-tube degradation than for the extrapolated 20 ppm solution, indicating that, although the mixed fluid is more sensitive to degradation, it probably was less degraded before the tests. This is consistent with the results shown in Fig. 5.6.-4 where the extrapolated Nusselt numbers for the 20 ppm solution appear similar for $Re_a < 10000$, despite larger Prandtl numbers for the combination fluid.

The $C_f/2$ results for the combined fluid show the usual viscoelastic discrepancy with the Colburn factor for low Reynolds numbers, but they become very similar for the degraded fluid at high Reynolds number. The Colburn factors for the pure 3% clay suspension are naturally much higher.

It was mentioned in the previous section that the friction data showed dramatic differences according to location. It is then natural to suspect that the situation will be similar for heat transfer results. Indeed, Fig. 5.6.-6, a graph of the Nusselt numbers as a function of x/D, shows unexpectedly large variations of heat transfer with distance along the pipe. These results were computed as usual at wall temperature. The results correspond, starting with the lowest curve, to Re_a=1560 (Pr_a=30.2), 9300 (20.8), 17500 (17.1), 24500 (15.0), and 35600 (13.1), all evaluated at x/D= 560. (Although the Nusselt number varies significantly with x/D, the Reynolds numbers, however, change relatively little along the tube as the viscosity remains fairly constant.)

When these results are examined in light of friction and heat transfer as a function of Reynolds number, it is confirmed that the main reason for variation with distance is probably the degradation induced in the test tube.

Indeed, for the run at Re_a=1560, the variation of Nu with x/D is typical of drag-reducing solutions. For that at Re_a=9300, which is the highest Re_a before degradation affects the friction, the Nusselt number does still decrease overall over the length of the pipe. As can be seen,

however, there is a slight increase towards the middle. This small bump is very similar to the partial destabilization seen with the 5% suspension, which was interpreted as an aborted transition to turbulence. In the present case, such an instability might be due to a decrease in the drag-reducing character of the fluid because of degradation.

For higher Re_α, the Nusselt numbers start increasing dramatically, first at the end of the pipe, and then earlier if the flow rate is increased. At the highest Reynolds number, the degradation appears to take place at the beginning of the pipe, with the heat transfer varying much less towards the end.

These heat transfer trends are surprisingly similar to those pointed out for the friction as a function of the distance. It is not unreasonable, of course, to expect some correspondence between the two phenomena, but it should be emphasized that for the pure polymer solutions, the turbulent friction and heat transfer entrance regions were generally uncoupled. The heat transfer was seen to vary up to x/D=500 for the asymptotic solutions, for example, whereas, for the same runs, the friction was stabilized very early in the pipe.

Clearly, the behavior of this combination fluid is quite different from those encountered normally in the study of either newtonian fluids or pure polymer solutions.

5.7. SUSPENSION OF ORGANIC PULP

It was decided to use an organic pulp for the investigation of the heat transfer and friction of a fluid containing fibers. The material chosen was a tomato puree ("1.06" puree from Contadina Foods Inc.), diluted with tap water to 6.0% of total solids. The original puree was tested at 15.2% total solids, 14.8% soluble solids, pH=4.25, and a Bostwick number of 1.75 cm/30 s. The manufacturing process includes a passage through a "045" finisher screen in order to limit the size of particles and fibers. Visual inspections have shown that a large number of fibers measuring 1 mm were present, with a maximum of about 2 mm. This material is not a fiber suspension in the usual sense, however, because it contains a significant amount of small particles and other substances as well. Additionally, the fibers present are of small aspect ratio. This material is thus significantly different from the artificial fiber suspensions generally studied such as of asbestos or nylon, which contain only discrete fibers (of aspect ratio up to 10^5 for asbestos) immersed in a pure solvent. Another organic material somewhat similar to this puree that has been studied as well is wood pulp. (See the references mentioned in section 2.5. for more information on fiber suspensions.)

Wood pulp was shown to exhibit a viscoelastic-type of drag reduction to a significant degree, and it was thus thought possible that the puree might also present evidence of such non-newtonian behavior. It has been suggested for asbestos fibers that the greater their aspect ratio is, the larger the drag reduction they induce will be. Consequently, it was expected that if a drag reduction phenomenon due to fibers is present at

all for the tomato puree, it would probably be less important than for the case of asbestos fibers, which can cause a reduction in friction of well over 50%. It should be emphasized that the puree also contains other natural substances such as gums, for example, which could very well contribute significantly to any drag reduction observed for this fluid.

5.7.1. **Material properties**

The density of the diluted puree was measured as a function of the temperature in the same fashion as for the other fluids. Over the range of 20 to 40 $^{\circ}C$, the density was found to be

$$\rho = 1027 - 0.307\,T \tag{5.43}$$

(with the temperature expressed in $^{\circ}C$) or approximately 2% larger than that of water. The fluid did not show evidence of sedimentation over the small periods necessary for the experiments.

The values of the thermal conductivity and heat capacity of this fluid being unknown, it was decided to use the values for water in the computations. These values were expected to be very close to those of the actual fluid because of the low concentration and of the organic nature of the material. The final heat transfer results can also be easily modified for arbitrary values of these quantities, if it is so desired for better comparison.

5.7.2. **Viscosity functions**

As usual, the viscosity is a critical factor in the computations, and accordingly, it had to be directly measured. A few studies of viscosity for similar types of fluids have been conducted in the past (see section 2.5) and have indicated that pseudoplastic behavior is frequent, with an influence of yield stresses in the case of high concentrations and low shear rates.

The viscosity of the pulp suspension was measured in the pressurized viscometer with tube T-2. The diameter of this tube (the largest available) being only 2 mm, there was some concern that the fibers might interfere with the isotropy of the flow during viscosity measurements. Indeed, at very low flow rate, the fluid in the tube showed at times evidence of slight anisotropy, fibers grouping themselves in slightly more concentrated clusters separated by clearer fluid. (No particular alignment of the fibers in the tube was observed, however.) Very likely the effect this anisotropy might have on the results is reduced in any case because of the time-averaging over long periods used in this measurement method.

A more serious problem for this type of fluid is the possibility that because of their size and relative rigidity, the fibers will not readily penetrate the region very close to the wall. If there is in that case a zone of less concentrated fluid, or possibly pure water, in this region which is critical for pressure drop measurements, it is then possible that the

viscosity results might be affected. This problem is unavoidable unless tubes of impractically large diameter are used. Naturally, this same phenomenon might also have an influence in the test tubes and might modify the friction in a similar manner, but the diameter and the flow conditions being different in this case, it is not possible to assume that this factor will be eliminated entirely.

The viscosity was measured for this 6% suspension at various temperatures between 15 and 45 $°C$. The results have been corrected for temperature using the Arrhenius-type relation mentioned earlier (section 4.4.1), with B=2710 $°K^{-1}$. This value is larger than that for water (1900 $°K^{-1}$) and that by Harper and El Sarighi (1965) for tomato concentrates (1710 $°R^{-1}$), but is similar to some found by Saravacos (1970) for other juices and purees.

The viscosity results are presented in Fig. 5.7.-1 after reduction to 25 $°C$, the use of the Arrhenius exponent having collapsed the results for different temperatures on one curve. The larger scatter at low shear rates is probably due to the difficulties in measurements at very low flow rates or possibly because of the influence of yield stresses. This range of shear rates is not used in the computations, however.

The value of the power-law exponent computed for the experiments varies slightly around a mean of n=0.62. This value and the viscosity agree very well with those by Harper and El Sarighi (1965). (For example, with a 5.8% concentration of tomato at 90 $°F$ (32 $°C$) and 500 s^{-1}, they found n=0.59, and η=17.5 cpoise whereas the present experimental

value at 500 s^{-1} and 25 $^{\circ}C$ is about ν=16.8 $10^{-6} m^2/s$ or η=17.2 cpoise). As expected, this fluid is strongly pseudoplastic.

5.7.3. **Friction**

The friction results are shown in Fig. 5.7.-2 in terms of generalized Reynolds numbers, and were computed with properties evaluated at the wall temperature. The difference with results computed on the basis of the bulk temperature is fairly small, because the temperature difference between bulk and wall is only 3 or 4 $^{\circ}C$. A couple of runs were also conducted under isothermal conditions, and they are seen to give results which match well with those for non-isothermal cases computed at wall temperature. The results are obtained by averaging of those corresponding to the last two stations on the test tube. The measured friction was not a function of x/D for this fluid, implying that the flow was hydrodynamically fully-developed early in the pipe.

The friction coefficients are seen to be somewhat larger than the laminar prediction in that regime, although the curves are parallel. It is possible that this difference may be caused by imprecisions in the measurement of the viscosity due to the macroscopic size of the fibers. Indeed if, as mentioned above, there is a layer of water devoid of fibers very close to the wall, the overall measured viscosity might be closer to that of water. If the viscosity is underestimated for this reason, the Reynolds numbers will in turn be overestimated, which would cause the laminar friction curve to be shifted towards high Reynolds number, as it is observed on graph 5.7.-2. (Friction results of a combination of tomato

and polymer (section 5.8) seem to indicate that the viscosity measurements might be adequate, however, in which case these large friction results might be correct after all.)

In the turbulent regime, it is apparent that the friction coefficient is not only significantly smaller than for newtonian fluids, but also smaller than the values predicted by Metzner's relation (eq. 3.33) for purely viscous non-newtonian fluids (which are also shown for the average n=0.62). The experimental results appear to be intermediate between this expression for n=0.62 and Virk's asymptote, being almost parallel to the former relationship. If a correction on the viscosity were to be introduced as mentioned above, the friction coefficient in the turbulent regime would appear even lower. These results seem thus to show that this suspension does indeed exhibit drag reduction to a very significant degree.

The same results are shown in Fig. 5.7.-3 expressed as a function of the apparent Reynolds number. The difference between the two representations is large, as expected, because of the small value of the power-law exponent. In the apparent Reynolds number representation, the friction coefficient should be very close to the Prandtl values for newtonian fluid if the reduction in turbulent friction were due to pseudoplasticity only. The fact that the friction coefficient is significantly lower than Prandtl's confirms that the drag reduction might be similar to that of typical fiber or polymer systems, possibly involving a viscoelastic-type of behavior.

In terms of apparent Reynolds number, the reduction in friction coefficient with respect to newtonian fluids might be evaluated at about -40% at Re_a=10000, and -34% at Re_a=35000, a significant decrease. In terms of generalized Reynolds numbers, on the other hand, the reduction would be -50% at Re'=6500 and -46% at Re'=14000. The use of apparent Reynolds numbers is believed to be more meaningful for comparison of viscoelastic drag reduction, however, because it absorbs the contribution of non-elastic pseudoplasticity to the overall reduction (see section 5.5.3.).

The friction results may be correlated by the following expressions

$$C_f = \frac{24.3}{Re'^{1.01}} \tag{5.44}$$

and

$$C_f = \frac{36.5}{Re_a^{1.02}} \tag{5.45}$$

for laminar flow, and

$$C_f = 0.0310\, Re'^{-0.220} \tag{5.46}$$

and

$$C_f = 0.0179\, Re_a^{-0.149} \tag{5.47}$$

for the turbulent regime.

5.7.4. **Heat transfer**

The heat transfer results for this fluid are shown in Fig. 5.7.-4 in terms of Nusselt and generalized Reynolds numbers. These results were

computed on the basis of the wall temperature and correspond to an average of results from stations x/D= 475 and 560. (It will be shown that the heat transfer is no longer a function of position at these locations.) The range of Prandtl numbers covered in these runs is 18<Pr'<78. The difference between these results and those computed at bulk temperature is small, because the difference between this temperature and that of the inner wall is only 3 or 4 °C.

The Nusselt numbers appear to be significantly larger than normal for laminar flow, reaching a value of 63 for Re'=4000 (a value still appearing to pertain to this regime). For comparison, the value of fully-developed flow for purely viscous non-newtonian flow, according to eq. 3.70, would be only Nu=4.61 for n=0.62. It is not clear what phenomenon might cause such a large difference. (Note that the friction results were also larger than for newtonian fluids in laminar flow.)

For comparison, the values given by Metzner for turbulent flow as eq. 3.75 (using actual values of n) are shown as well. These values are somewhat smaller than the experimental results, but it is suspected that the former are probably underestimated even for the purely viscous particulate suspensions for which they were designed (see section 5.5.4.1.). Also shown are values computed by Sleicher and Rouse's relationship (eq. 3.62) for a newtonian fluid of the same Prandtl and Reynolds number. The experimental results are close to, or slightly larger than these values. As mentioned in several instances, however, the generalized Reynolds number does not appear to give a good representation for drag-reducing fluids, and conclusions should be preferably drawn from results

expressed in terms of apparent Reynolds numbers.

Accordingly, the heat transfer results are shown in the latter representation in Fig. 5.7.-5 (same conditions for computations). The Prandtl numbers covered are $15<Pr_a<68$. Again, Nusselt numbers for an equivalent newtonian fluid with the same Prandtl number and for a purely viscous non-newtonian fluid with the same Pr_a and n are shown for comparison, and it is apparent that the experimental results are smaller than both these values. This seems to indicate that the heat transfer has indeed been reduced with respect to newtonian and purely viscous non-newtonian fluids, as was expected because of the accompanying friction reduction.

For better comparison with other fluids and with friction data, the results are shown in Fig. 5.7.-6 in terms of Colburn factors, $C_f/2$, and apparent Reynolds numbers. Also shown are similar results for water. It is immediately apparent that the $C_f/2$ for turbulent flow of tomato puree is intermediate between the Colburn factor and $C_H Pr_a^{0.5}$, as was the case for water.

The absolute values of the Colburn factor indicate a decrease with respect to water. At Re_a=10000 the reduction in Colburn factor is approximately -25%, and at Re_a=34000 it is -35% , with the corresponding reductions in $C_f/2$ being -40% and -34%. The trends are opposite for the friction (which shows a difference with water decreasing with increasing Re_a) and for the Colburn factor (for which this difference increases).

More data in the turbulent region are necessary before the conclu-

sions may be extended to high Reynolds numbers, but the results present little scatter in the turbulent regime, and seem to be very well represented by a power-law relationship. Such a correlation could be expressed as

$$C_H Pr_a^{2/3} = 0.0471\, Re_a^{-0.291} \tag{5.48}$$

for the turbulent regime, and

$$C_H Pr_a^{2/3} = 0.0795\, Re_a^{-0.371} \tag{5.49}$$

for laminar flow (all with wall temperature reference). It is possible that the diameter of the test tube is a significant parameter for friction and heat transfer of this type of fluid, but it is probably less so than for the viscosity measurements.

These laminar results are much higher than for clays (eq. 5.42a) despite similar Prandtl numbers. At Re_a=500 we have +182% for the Colburn factor of the tomato puree with respect to the 5% bentonite suspension, and +294% at Re_a=2000.

Characteristic heat transfer results are shown in Fig. 5.7.-7 as a function of x/D. These runs correspond respectively, by increasing Nusselt numbers, to Re_a=880 (Pr_a=61.9), Re_a=2590 (Pr_a=45.8), Re_a=5810 (Pr_a=34.1), Re_a=10900 (Pr_a=26.2), and Re_a=33800 (Pr_a=15.4), all computed at wall temperature and x/D=560. These results confirm that in most cases the heat transfer is not changing significantly with x/D.

For the low Reynolds numbers, the Nusselt number appears to decrease slightly with x/D. This is common for newtonian fluids of high

Prandtl numbers and for slightly drag-reducing solutions. At Re_α=10900, the Nusselt number is seen to decrease at the beginning of the pipe but after x/D=150 starts to increase again until it stays approximately constant for x/D>300. This increase in heat transfer is attributed to transition to turbulence. Indeed, this Reynolds number corresponds, as evidenced by friction results, to the beginning of the turbulent region. For higher Reynolds numbers, the Nusselt number appears approximately constant from the beginning of the pipe on, as is to be expected for turbulent flow.

In conclusion, this fluid appears to show friction and heat transfer coefficients that are larger than for newtonian fluids in the laminar regime, but are significantly reduced in the turbulent regime. The good correspondence between the Colburn factor and $C_f/2$ in turbulent regime, and the heat transfer coefficient trends as a function of location, both appear somewhat more consistent with the behavior of newtonian fluids than with intermediate efficiency drag-reducers, however. It is therefore not excluded that the significant reductions in turbulent friction and heat transfer might be partly caused by other phenomena besides a viscoelastic type of drag reduction. Additionally, it is possible that any such viscoelastic drag reduction might not only be caused by the presence of fibers in suspension, but also by other natural substances found in this organic material, such as gums for example.

5.8. COMBINATION OF POLYMER AND PULP

In order to investigate the properties of a fluid combining polymer and fibers, the pulp suspension described in the previous section has been modified by the addition of polyacrylamide. The concentrations of added polymer were the same as those studied in the pure polymer solutions cases, namely 20 ppm and 200 ppm.

The addition of polymer to the suspension induced no problem during the mixing and the measurement of viscosity properties. In particular, no unusual sensitivity to degradation was observed, contrarily to the case of the polymer and bentonite combination. The stirring speeds used were the same as for the pure polymer solutions, and the fluids were used one day after mixing.

The material properties of the combination fluid were taken to be the same as those of the pure pulp suspension, because the influence of the polymer at low concentration on these properties is known to be very small. Additionally, this choice allows a better comparison with the unaltered suspension for which the thermal conductivity and specific heat were assumed to be similar to those of water.

5.8.1. Viscosity functions

Following the usual procedure, the viscosity of the samples was measured for various temperatures with the T-2 capillary. The results are shown in Fig. 5.8.-1, together with the viscosity curves for the pure 20 ppm #3 (+7.5% with respect to the viscosity of water) and 200 ppm #3 solutions, all reduced to 25 $^{\circ}C$ by Arrhenius-type relationships (only

best-fitting curves are shown for clarity). The Arrhenius exponent for the modified purees is about B=2070 $^{\circ}K^{-1}$, close to that of water (1900 $^{\circ}K^{-1}$).

The viscosity of the suspension with 20 ppm added (T+20) is very similar to that of the pure suspension (T). The viscosity of the T+20 fluid appears smaller than that of the pure tomato batch, however, and not slightly larger as was expected because of the addition of the polymer. The difference was rather small though, and it might possibly have been dismissed as experimental error were it not for the even more surprising behavior of the T+200 fluid.

Indeed, the viscosity of this latter fluid appears to be even smaller than that of the T+20 fluid for low shear rates, but becomes larger than that of the pure T fluid for the high shear rates. These differences seem too large to be explained by errors in the measurements, but it is not clear what might be the reason for these trends. Possibly, the polymer exerts an influence on the surmised heterogeneous character of the suspensions during viscosity measurements. There might also be a direct influence of chemical reactions between the polymer and the organic material on the viscosity of the fluids.

5.8.2. **Friction**

The friction results for the 3 batches are presented in Fig. 5.8.-2 in terms of apparent Reynolds numbers. All the results are computed evaluating the properties at the wall temperature, and are averages from x/D=430 to 600. There was no significant difference observed between

the friction coefficients as measured by the various stations. Also shown for comparison are the results for the pure 200 ppm polyacrylamide solution. The values of the power-law exponent are $0.57<n<0.77$ for T+20, and $0.68<n<0.87$ for T+200 over the covered range of shear rate.

In the laminar region, the results are distinct for the 3 batches. This was expected because of the influence of the power-law exponent in the apparent Reynolds number representation. In the generalized Reynolds number representation, the 3 curves are superimposed, but, as pointed out in section 5.7., for the pure tomato suspension the values are not equal to 16/Re' as they would be for particulate suspensions.

In the turbulent regime, the friction coefficients for T+20 and T+200 match surprisingly well with the results obtained for the friction asymptote as determined by the pure 200 ppm polymer solution. This fact could imply that the viscosity measurements for the tomato-based fluids were adequate after all. It would then follow that the difference in laminar flow between C_f and 16/Re' may well be a characteristic of the fluid or of the flow, and not merely a consequence of possible uncertainties in the viscosity measurements as was conjectured in section 5.7.3.

Indeed, if a correction of the measured viscosity were justified and the Reynolds numbers were reduced to match the laminar results with Equation 3.37, the values of C_f for the turbulent flow would be much smaller than the asymptote. This would also be the case in the generalized Reynolds number representation (in fact they are already smaller even without reduction of the Reynolds number). It is thought that there

exists a synergism between combined fibers and polymer that reduces the friction more than would be expected from the separate constituents alone. However, it is unlikely that the friction could drop to levels far lower than the asymptote. Consequently, the good match between the turbulent results for the T+20 and T+200 fluids and those for the asymptotic polymer solution provides some indication that the viscosity measurements may be correct after all, and again that the apparent Reynolds number representation is indeed the most adequate for these fluids.

The two runs at the highest Reynolds numbers for T+20 show a slight departure from the results for T+200. This could well be a sign of in-tube degradation. Although the friction results are not entirely conclusive in that respect (the difference being small and the data insufficiently numerous in that region), the heat transfer results seem to confirm this hypothesis (see next section).

The friction results of the T+200 solution in the turbulent region are well correlated (maximum experimental deviation: 3%) by

$$C_f = 2.60\,\mathrm{Re}_a^{-0.741} \quad . \tag{5.30}$$

This result is mentioned for illustration only, the covered range of apparent Reynolds number being only $7000<Re_a<20000$. When compared with the results for the 200 ppm solution (eq. 5.10), these results show a difference of +4% at Re_a=7000 and -12% at Re_a=20000, which is rather good considering the drastically different nature and viscosity of the

fluids.

5.8.3. **Heat transfer**

The heat transfer results computed at wall temperature are presented in Fig. 5.8.-3 in terms of Nusselt and apparent Reynolds numbers. All results are averages for x/D=475 and 560. The variations in Prandtl numbers are $30<Pr_a<75$ for T+20 and $35<Pr_a<80$ for T+200. These Prandtl numbers are about similar for the 3 batches, which makes for better comparison of the Nusselt numbers. Also shown are the Nusselt numbers for the pure 200 ppm polymer solution, for which the Prandtl numbers are much lower, however.

It is to be noted that the scatter is not principally due to inaccuracies in the measurements. It mainly results from differences in heating conditions that induce variations in the overall temperature of the system and thus in the Prandtl numbers. These variations in Prandtl numbers, of course, in turn influence the Nusselt numbers.

A comparison of friction ($C_f/2$) and heat transfer (Colburn factor) is illustrated in Fig. 5.8.-4 for the 3 batches (same conditions as above), as well as for the pure 200 ppm solution and for water. It may be noted that the scatter for the heat transfer results has been significantly reduced with respect to Fig. 5.8.-3, because of the absorption of the Prandtl number effect in the Colburn factor.

It is apparent that although the friction in the laminar regime is very similar for the 3 batches, this is not the case for the heat transfer. The Colburn factor for the T+200 fluid appears slightly higher than for the

200 ppm solution, indicating that, although the friction asymptote is reached, the heat transfer is not quite reduced to asymptotic condition. The difference is small, however, and could be caused by the large difference in Prandtl number between the T+200 and 200 ppm batches (the Colburn factor was shown previously to absorb the Prandtl number well, but not perfectly).

The T+20 batch which shows friction coefficients very close to those of T+200, has higher heat transfer coefficients, however. This is very similar to the behavior of pure polymer solutions. The Colburn factor for the T+20 batch is not parallel to that of T+200 in the turbulent zone, an indication that the former fluid might start to degrade in that region, which is not surprising in view of the low concentration of polymer, and the stirring to which it was subjected before testing. As usual for degraded drag-reducers, $C_f/2$ and the Colburn factor become equal at one point for the T+20 fluid, rather than exhibiting the constant difference they show under asymptotic conditions. The pure tomato batch, however, shows a $C_f/2$ smaller than the Colburn factor for the turbulent regime, but both are still lower than the water results.

The Colburn factors for the T+200 batch are well correlated by

$$C_H Pr_a^{2/3} = 0.0308 \, Re_a^{-0.429} \tag{5.51}$$

in turbulent regime, and

$$C_H Pr_a^{2/3} = 0.362 \, Re_a^{-0.717} \tag{5.52}$$

in laminar regime.

The heat transfer results for the T+20 solution are shown as a function of x/D in Fig. 5.8.-5, all computed with properties evaluated at wall temperature. The curves correspond, by increasing Nusselt numbers, to Re_a=745 (Pr_a=59.2), 7890 (28.8), 11000 (28.7), 15500 (25.6), and 21100 (24.9), all computed at x/D=560.

The first and second curves are quite different in shape, probably because these runs respectively correspond to laminar and turbulent conditions. Naturally, the low speed turbulent runs are not characterized by constant Nusselt numbers over the whole pipe, because of the drag-reducing character of the fluid. Typically, and for the same reason, the decrease in heat transfer at low x/D is larger for turbulent conditions than for laminar ones, despite the lower Prandtl numbers.

For the highest Reynolds number, it can be seen that the Nusselt number starts to decrease rapidly, but after x/D=150 is practically constant. It is believed that the reason for this constancy is the mechanical degradation induced in the test tube.

Heat transfer results for the T+200 batch are shown in Fig. 5.8.-6 as a function of the distance. The Reynolds numbers for these runs are Re_a=1130 (Pr_a=54.2), 3680 (38.8), 7380 (31.3), and 17670 (27.6). It is apparent that, for the turbulent runs (curves 3 and 4), the Nusselt number curves are very similar in trend to those for pure asymptotic polymer solutions, showing the usual continuous decrease up to very large x/D (section 5.2.2.3.2.). For laminar flow (curve 1), the shape is flatter, and is more representative of high Prandtl number laminar flow

for non-viscoelastic fluids.

CHAPTER 6.

SUMMARY AND CONCLUSIONS

6.1. OVERVIEW

Although a large number of projects have been devoted to the study of friction in tube for non-newtonian fluid flows, particularly those of the drag-reducing type, there are far less adequate data available for the convective heat transfer aspects of these flows. Accordingly, this study aimed at obtaining a systematic set of heat transfer data for fluids of this kind.

The design of the experimental installation used in this study took into account recent findings, such as the need for large entrance lengths, that have shed doubts on the general applicability of most of the previous experimental heat transfer studies of drag-reducing non-newtonian fluids. The test tube used in the present study is, therefore, over 600 diameters long. The installation is of the once-through type and is based on a single-action hydraulic cylinder in order to reduce as much as possible any unintentional degradation that could be induced during the measurements. It also allows simultaneous heat transfer and friction measurements. Additionally, viscometers were custom-built to measure the non-newtonian viscosities of the fluids and of their degraded samples. Particular care was taken to ensure that the data and results obtained would be of a high enough accuracy to serve as a basis for future analyses.

The computations were conducted in a rather detailed and systematic way in order to study the influence of parameters generally not considered separately. For example, the effect of the degradation induced in the test tube itself, and the influence of both the temperature reference and the viscosity definition used in the computations were investigated in detail. It was shown that certain representations were clearly superior to most others, and allowed the reduction of results for complex fluids to correlations obtained for much simpler cases.

Tests were conducted first with the well-known polyacrylamide solutions in order to compare the data obtained in the present study with earlier ones. It was also hoped to be possible to collect more consistent information on this fluid, which seemed feasible because of the particular characteristics of the installation and of the computational procedures.

Next, suspensions of clay particles were studied in order to ascertain whether any reduction in friction and heat transfer beyond that induced by pseudoplasticity might be present. Fluids involving a combination of clay and polymer were also investigated and showed a significantly different behavior.

Finally, two other types of fluid for which very limited information has been available were studied in order to find out if they could induce drag reduction: an antimisting polymer solution in kerosene exhibiting a complex shear-thickening viscous behavior, and an aqueous suspension of organic pulp. Fluids such as these are used more and more in industrial

and commercial applications, and to provide information on their transport characteristics would therefore be most valuable for practical purposes. Additionally, the rather complex behavior of this antimisting polymer solution ensures that the processing of results obtained for this fluid will constitute an unforgiving test of the validity of the concepts and computational procedures used for these investigations.

A theoretical study was conducted in parallel with these experimental investigations that led to the development of a prediction method for the influence of the "diameter effect" on the friction and heat transfer exhibited by drag-reducing polymer solutions.

6.2. SUMMARY OF FINDINGS

The installation was checked with water, and the results showed excellent agreement with the best correlations available for newtonian fluids. The friction and heat transfer results were well correlated through the use of the Colburn factor by selecting an exponent between 2/3 and 1/2 for the Prandtl numbers.

6.2.1. Polyacrylamide solutions

Solutions of polyacrylamide corresponding to the asymptotic and intermediate regimes were investigated. Both samples subjected to in-tube degradation and unused samples were investigated under a wide range of temperature conditions and for several levels of intentional pre-degradation. These results are subsequently used for the data processing. The temperature effect on the viscosity of these solutions was well

correlated by an Arrhenius-type correction factor. Both the apparent and the generalized Reynolds numbers representations were used throughout the study but it was concluded that the apparent viscosity is the most appropriate for drag-reducing fluids.

The selection of the reference temperature at which the properties are evaluated was shown to be crucial, and the wall temperature was found to be the best reference for these fluids, in accordance with the wall viscosity concept used for the computations. The friction asymptote was computed for various combinations of computational parameters under well-defined conditions, and in some of these cases was expressed by correlations close to Virk's.

The respective influences of the viscosity definition, temperature reference, and degradation on the heat transfer asymptote were also investigated. The Colburn factor was shown to take rather well into account the effect of variations in Prandtl number on the heat transfer characteristics of these fluids.

The minimum heat transfer asymptote correlation developed here under the present preferred representation is close to the correlation obtained by Cho and Hartnett in what is believed to be the most comparable experimental study. For the high Reynolds number range which was not covered by these investigators, however, the present experimental results are significantly lower than the extrapolated values predicted by their correlation. The proportionally greater length of the tube used in the present study appears necessary for these high Reynolds numbers

for which the thermal entrance region was found to extend up to about 600 diameters, which is longer than was expected. Heat transfer results were obtained in this entrance region and were well correlated down to low values of x/D.

Solutions of lower concentration in the intermediate regime were intentionally pre-degraded to various degrees to differentiate this effect from the influence of in-tube degradation. The pre-degradation clearly influenced the overall levels of drag and heat transfer reduction, whereas the degradation induced in the tube itself was characterized by an increase of these quantities if a certain Reynolds number is exceeded. Both friction and heat transfer were found to depart from the low flow rate trends at about the same Reynolds numbers. For highly pre-degraded batches, this departure was less abrupt.

For "asymptotic" solutions the heat transfer was reduced more than the friction. For high enough levels of degradation, however, these two quantities were affected about equally, although the absolute values were still far below those for a newtonian fluid. The effects of degradation induced in the test tube itself were found to be localized at the beginning of the pipe. With precautions to avoid pre-degradation, concentrations as low as 20 ppm of polymer were shown to cause the friction to be reduced to asymptotic levels, although the heat transfer asymptote was not necessarily reached under the same conditions.

6.2.2. **Antimisting polymer solutions**

Aviation kerosene was studied as a reference for the antimisting polymer solutions using it as solvent, and was shown to exhibit a newtonian behavior. A systematic study of the viscous characteristics of the antimisting kerosene (AMK) in tubes showed these characteristics to include a discontinuous shear-thickening at a critical shear rate, a high susceptibility to mechanical and photodegradation, a high dependency on variations in temperature, and time-dependency. The influence of aging and end effects on the viscosity measurements was also investigated.

All the computational aspects mentioned for polyacrylamide solutions such as the selection of the temperature reference, the choice of a suitable Reynolds number representation, and the accounting for degradation had an even greater effect on the data processing for AMK. Despite the very complex viscous characteristics of this fluid, a representation similar to that used for the polyacrylamide solutions permitted the reduction of the rather unusual friction and heat transfer results obtained for AMK to relationships very close to the simple asymptotic forms developed for drag-reducing solutions. Results for significantly different batches matched also remarkably well in that representation involving apparent viscosities, wall temperature reference, and degraded viscosity functions. In other words, the AMK samples still maintained sufficient drag-reducing capabilities, even after gelation, for asymptotic results to be obtained. When intentionally highly-degraded, this fluid was

brought back to an essentially newtonian nature.

6.2.3. **Suspensions of particulates**

Several suspensions with concentrations ranging from 1% to 5% of bentonite in water were studied as representative of the purely-viscous non-newtonian fluids. These suspensions showed good agreement in laminar and turbulent flow with the friction values predicted by pseudoplastic correlations in Metzner's generalized Reynolds number representation. It was shown, however, that in the apparent Reynolds number representation using the apparent wall viscosity concept, the turbulent results could more conveniently be accurately represented by newtonian relationships.

This fact suggests that the pseudoplasticity-induced reductions in friction and heat transfer can be effectively taken into account, and in a sense removed, from the results by the use of apparent Reynolds numbers if proper computational procedures are used. It is thus possible to separate these reductions from the remaining ones that are induced by viscoelasticity. This is why the apparent Reynolds numbers are thought more appropriate for drag-reducing solutions.

The heat transfer results for these suspensions were found to give values of Nusselt number somewhat larger than expected. In the laminar regime, this is probably due to the long thermal entrance region, in which case the experimental data obtained may not have corresponded to fully-developed flow within the tube. These laminar entrance region results were indeed well correlated in terms of Graetz numbers. The

heat transfer in the transition regime was clearly illustrated by the changes in the Nusselt number as a function of distance along the tube. The turbulent heat transfer results expressed in terms of Colburn factor and apparent Reynolds number were also reduced to values close to those for newtonian fluids.

The addition of polyacrylamide to the bentonite suspension resulted in flocculation of the fluid, which also became inhomogeneous on a larger scale. The addition of these small quantities of polymer increased the viscosity of the fluid much more than expected. More importantly, the resulting fluid apparently became extremely susceptible to mechanical degradation, as suggested by the accompanying dramatic decreases in viscosity. This susceptibility was also apparent from the reduced friction and heat transfer results vs apparent Reynolds number graph which showed a sharp degradation-induced increase starting at rather low Reynolds numbers. The change of the friction and heat transfer coefficients along the length of the tube were also found to be significantly influenced by the degradation induced in the tube itself. This behavior was quite different from that observed for other fluids.

6.2.4. **Suspension of organic pulp**

The suspension of organic fibers and particles based on tomato puree was found to be highly pseudoplastic. Although the laminar friction and heat transfer results were shown to be signficantly higher than for newtonian fluids, the turbulent results were lower by about 40%, a reduction equivalent to that induced by viscoelastic polymer solutions in the

intermediate regime. When polymer was added to the puree, the friction and heat transfer were reduced even more, down to asymptotic values.

6.3. CONCLUSIONS

- An installation has been built that eliminates the experimental problems (such as too short a test section and significant unintentional mechanical degradation) that have shed doubts on the general applicability of most of the previous experimental studies of heat transfer and friction for drag-reducing non-newtonian fluids.

- The turbulent friction and heat transfer results for various types of drag-reducing non-newtonian fluids could be correlated by similar expressions regardless of the nature of the fluid if an apparent wall viscosity is used. This apparent viscosity must be evaluated at the wall temperature and be determined by taking into account the degradation induced in the test tube. The fluids correlated include a discontinuously shear-thickening antimisting kerosene, shear-thinning polyacrylamide solutions, and pseudoplastic combined polymer and pulp suspensions.

- The same representation also allowed turbulent friction and heat transfer results for purely viscous non-newtonian fluids (such as suspensions of particulates) to be correlated by newtonian relationships.

- A detailed investigation of the viscous characteristics of the fluids studied as a function of the temperature and the degradation was therefore shown to be indispensable for the development of adequate correlations for friction and heat transfer of non-newtonian fluids of the foregoing

type.

- The corrections that are often applied to the friction and heat transfer correlations of newtonian fluids in order to account for the variations of properties across the radius due to temperature gradients were insufficient for the non-newtonian fluids studied. For adequate correlations, the properties of these fluids had to be directly evaluated at the wall temperature.

- The effect of the temperature on the non-newtonian viscosity of most of these fluids could be well correlated by an Arrhenius-type exponential factor.

- The minimum heat transfer asymptote for polymer solutions was determined for fully-developed flow and for the entrance region. The thermal entrance region was observed to extend up to 600 diameters or more.

- An investigation of the rheological nature of an antimisting kerosene showed it to be time-dependent, discontinuously shear-thickening beyond a critical shear rate, highly susceptible to mechanical and photo-degradation, and very sensitive to temperature variations. Friction and heat transfer results, when reduced with the aid of the apparent viscosity, were nevertheless found to be characteristic of an asymptotic drag-reducing behavior.

- The combination of a polymer and bentonite in suspension proved to be unusually susceptible to degradation.

- A pulp suspension based on a pseudoplastic tomato puree was shown to exhibit up to about 40% of viscoelastic-type reduction in turbulent friction and heat transfer, whereas laminar results were found to be significantly larger than expected.

- Heat transfer results expressed in terms of Colburn factors were observed to be satisfactorily independent of the Prandtl number for the fluids studied.

- For the majority of the fluids studied, the entrance region of the test tube was found to be the location where most of the mechanical degradation is induced.

- A theoretical method developed for drag-reducing fluids was shown to adequately predict the "diameter effect" for their friction and heat transfer in pipes.

REFERENCES

Abernathy, F.H., and Z. He. 1984. Polymer-induced velocity fluctuations in dilute drag reducing pipe flows. In Proc. of 3d Int. Conf. on Drag Reduction, paper B8. Eds.: R.H. Sellin and R.T. Moses. Bristol, England: University of Bristol.

Adachi, K., and N. Yoshioka. 1984. Tube exit flows and laminar newtonian jets in the atmosphere. In Advances in Rheology, vol. 2, 329-337. Eds.: B. Mena, A. Garcia-Rejon, and C. Rangel-Nafaile. Mexico: Universidad Nacional Autonoma de Mexico.

Agarwal, S.H., and R.S. Porter. 1980. Shear degradation of poly(vinyl acetate) in toluene solutions by high-speed stirring. J. of Applied Polymer Science 25:173-185.

Argumedo, A., T.T. Tung, and K.I. Chang. 1978. Rheological property measurements of drag-reducing polyacrylamide solutions. J. of Rheology 22 (5): 449-470.

Astarita, G., and G. Marrucci. 1974. Principles of Non-newtonian Fluid Mechanics. London: McGraw-Hill.

Astarita, G., G. Greco, and L. Nicodemo. 1969. A phenomenological interpretation and correlation of drag reduction. AIChE J. 15 (4): 564-567.

Bagley, E.B. 1957. End corrections in the capillary flow of polyethylene. J. of Applied Physics 28 (5): 624-627.

Baid, K.M., and A.B. Metzner. 1977. Rheological properties of dilute polymer solutions determined in extensional and in shearing experiments. Trans. of the Society of Rheology 21 (2): 237-260.

Batchelor, G.K. 1970a. The stress system in a suspension of force-free particles. J. Fluid Mech. 41 (part 3): 545-570.

_____. 1970b. Slender-body theory for particles of arbitrary cross-section in Stokes flow. J. Fluid Mech. 44 (part 3): 419-440.

_____. 1971. The stress generated in a non-dilute suspension of elongated particles by pure straining motion. J. Fluid Mech. 46 (part 4): 813-829.

Beaty, W.R., R.L. Johnston, R.L. Kramer, L.G. Warnock, and G.R. Wheeler. 1984. Offshore crude oil production increased by drag reducers. In Proc. of 3d Int. Conf. on Drag Reduction, paper F1. Eds.: R.H. Sellin and R.T. Moses. Bristol, England: University of Bristol.

Berman, N.S. 1973. The interpretation of polymer data. NOSC report No. TM 73-53. Washington, D.C.: U.S. Department of Navy.

_____. 1977. Flow time scales and drag reduction. The Physics of Fluids 20 (10): S168-S174.

_____. 1978. Drag reduction by polymers. Ann. Rev. Fluid Mech. 10:47-64.

Berman, N.S., and P.K. Sinha. 1984. Drag reduction in pipe flow for non-homogeneous injection of polymer additives. In Proc. of 3d Int. Conf. on Drag Reduction, paper B3. Eds.: R.H. Sellin and R.T. Moses. Bristol, England: University of Bristol.

Bewersdorff, H. 1984. Effect of centrally injected polymer thread on turbulent properties in pipe flows. In Proc. of 3d Int. Conf. on Drag Reduction, paper B4. Eds.: R.H. Sellin and R.T. Moses. Bristol, England: University of Bristol.

Bird, R.B. 1965. Experimental tests of generalized newtonian models containing a zero-shear viscosity and a characteristic time. The Canadian J. of Chemical Engineering (August): 161-168.

Bird, R.B., and C.F. Curtiss. 1984. Fascinating polymeric liquids. Physics Today (January): 36-43.

Bird, R.B., and J.R. Deaguiar. 1983. An encapsulated dumbbell model for concentrated polymer solutions and melts. J. of Non-newtonian Fluid Mechanics 13:149-160.

Bird, R.B., R.C. Armstrong, and O. Hassager. 1977. Dynamics of Polymeric Liquids. 2 vols. New York: John Wiley and Sons.

Bobkowicz, A.J., and W.H. Gauvin. 1965. The turbulent flow characteristics of model fibre suspensions. The Canadian J. of Chemical Engineering (April): 87-91.

Bogue, D.C., and A.B. Metzner. 1963. Velocity profiles in turbulent pipe flows. I. & E. C. Fundam. 2 (2): 143-149.

Boothroyd, R.G., and P.J. Walton. 1973. Fully developed turbulent boundary-layer flow of a fine solid-particle gaseous suspension. Ind. Eng. Chem. Fundam. 12 (1): 75-82.

Brennen, C., and G.E. Gadd. 1967. Aging and degradation in dilute polymer solutions. Nature 215 (September 23): 1368-1370.

Brostow, W. 1983. Drag reduction and mechanical degradation in polymer solutions in flow. Polymer 24 (May): 631-638.

Bugliarello, G., and J.W. Daily. 1961. Rheological models and laminar shear flow of fiber suspensions. TAPPI 44 (12): 881-893.

Burger, E.D., L.G. Chorn, and T.K. Perkins. 1980. Studies of drag reduction conducted over a broad range of pipeline conditions when flowing Prudhoe bay crude oil. J. of Rheology 24 (5): 603-626.

Burger, E.D., W.R. Munk, and H.A. Wahl. 1980. Flow increase in the Transalaska pipeline using a polymeric drag-reducing additive. Society of Petroleum Engineers report No. SPE9419. New York, NY: American Institute of Mining, Metallurgical, and Petroleum Engineers.

Caldwell, D.H., and H.E. Babbitt. 1941. The flow of muds, sludges, and suspensions in circular pipe. Trans. Am. Inst. Chem. Eng. 37:237-266.

Carreau, P.J. 1968. Rheological equations form molecular network theories. Ph.D. Dissertation, University of Wisconsin - Madison.

_____. 1972. Rheological equations from molecular network theories. Trans. of Soc. of Rheology 16 (1): 99-127.

Charm, S.E. 1960. Viscometry of non-newtonian food materials. Food Research 25:351-362.

_____. 1962. The nature and role of fluid consistency in food engineering applications. In Advances in Food Research, 355-435. New York: Academic Press.

Charm, S.E., and E.W. Merrill. 1959. Heat transfer coefficients in straight tubes for pseudoplastic food materials in streamline flow. Food Research 24:319-331.

Cho, Y.I., and J.P. Hartnett. 1979. The falling ball viscometer - a new instrument for viscoelastic fluids. Letters in Heat and Mass Transfer 6:335-342.

_____. 1980. Analogy for viscoelastic fluids - momentum, heat and mass transfer in turbulent pipe flow. Letters in Heat and Mass Transfer 7:339-346

_____. 1981. Mass Transfer in turbulent pipe flow of viscoelastic fluids. Int. J. Heat Mass Transfer 24 (5): 945-951.

_____. 1982. Non-newtonian fluids in circular pipe flow. Advances in Heat Transfer 15:59-139.

_____. 1983. Drag coefficients of a slowly moving sphere in non-newtonian fluids. J. of Non-newtonian Fluid Mechanics 12:243-247.

Cho, Y.I., J.P. Hartnett, and E.Y. Kwack. 1980. A study of wall effect

for viscoelastic fluids in the falling ball viscometer. Chem. Eng. Com. 6:141-149.

Cho, Y.I., J.P. Hartnett, and W.Y. Lee. 1984. Non-newtonian viscosity measurements in the intermediate shear range with the falling-ball viscometer. J. of Non-newtonian Fluid Mechanics 15:61-74.

Cho, Y.I., J.P. Hartnett, and Y.S. Park. 1983. Solvents effects on the rheology of aqueous polyacrylamide solutions. Chem. Eng. Com. 21:369-382.

Cho, Y.I., K.S.Ng, and J.P. Hartnett. 1980. Viscoelastic fluids in turbulent pipe flow : a new heat transfer correlation. Letters in Heat and Mass Transfer 7:347-351.

Chou, L., and J.L. Zakin. 1967. The effect of concentration on the viscosities of solutions of linear flexible high polymers. J. of Colloid and interface Science 25:547-557.

Cogswell, F.N. 1978. Converging flow and stretching flow: a compilation. J. of Non-newtonian Fluid Mechanics 4:23-38.

Colburn, A.P. 1933. A method of correlating forced convection heat transfer data and a comparison with fluid friction. Trans. AIChE 29:174-210.

Cox, R.G., and S.G. Mason. 1971. Suspended particles in fluid flow through tubes. Ann. Review Fluid Mechanics 3:291-316.

Crochet, M.J., and K. Walters. 1983. Numerical methods in non-newtonian fluid mechanics. Ann. Review Fluid Mechanics 15:241-260.

Darby, R. 1984. The influence of viscoelastic properties on turbulent drag reduction in dilute polymer solutions. In Advances in Rheology, vol. 2, 51-58. Eds.: B. Mena, A. Garcia-Rejon, and C. Rangel-Nafaile. Mexico: Universidad Nacional Autonoma de Mexico.

Darby, R., and H.D. Chang. 1984. Prediction of turbulent drag reduction in polymer solutions from rheological properties. In Proc. of 3d Int. Conf. on Drag Reduction, paper A4. Eds.: R.H. Sellin and R.T. Moses. Bristol, England: University of Bristol.

Debrule, P.M., and R.H. Sabersky. 1974. Heat transfer and friction coefficients in smooth and rough tubes with dilute polymer solutions. Int. J. Heat and Mass Transfer 17:529-540.

Deissler, R.G. 1954. Analysis of turbulent heat transfer, mass transfer, and friction in smooth tubes at high Prandtl and Schmidt numbers. Report No. NACA TN 3145. Washington, D.C.: National Advisory Committee for Aeronautics.

De Kee, D., and A. Dajan. 1984. On the motion of gas bubbles in polymer solutions. In Advances in Rheology, vol. 2, 97-101. Eds.: B. Mena, A. Garcia-Rejon, and C. Rangel-Nafaile. Mexico: Universidad Nacional Autonoma de Mexico.

De Loof, J.P., B. De Lagarde, M. Petry, and A. Simon. 1977. Pressure drop reduction in large industrial ducts by macromolecular additives. In Proc. of 2d Int. Conf. on Drag Reduction, paper B2. Cranfield, England: BHRA Fluid Engineering.

Dimant, Y., and M. Poreh. 1974. Momentum and heat transfer in flows with drag reduction. Faculty of Civil Engineering publ. No. 203. Haifa, Israel: Technion-Israel Institute of Technology.

_____. 1976. Heat transfer in flows with drag reduction. Advances in Heat Transfer 12:77-113.

Dittus, F.W., and L.M. Boelter. 1930. Heat transfer in automobile radiators of the tubular type. University of California Publications in Engineering 2 (13): 443-461.

Dodge, D.W., and A.B. Metzner. 1959. Turbulent flow of non-newtonian systems. AIChE J. 5 (2): 189-204.

Durst, F., and A.K. Rastogi. 1977. Calculations of turbulent boundary layer flows with drag reducing additives. The Physics of Fluids 20 (12): 1975-1985.

Durst, F., W. Schierholz, and A. Wunderlich. 1984. Numerical and experimental studies of elongational flow fields for refined studies of flows with additives. In Proc. of 3d Int. Conf. on Drag Reduction, paper A1. Eds.: R.H. Sellin and R.T. Moses. Bristol, England: University of Bristol.

Eckert, E.R., and R.M. Drake. 1972. Analysis of heat and mass transfer. New York: McGraw-Hill.

Edwards, M.F., and R. Smith. 1980. The use of eddy viscosity expressions for predicting velocity profiles in newtonian, non-newtonian, and drag-reducing turbulent pipe flow. J. of Non-newtonian Fluid Mechanics 7:153-169.

Eissenberg, D.M., and D.C. Bogue. 1964. Velocity profiles of thoria suspensions in turbulent pipe flow. AIChE J. 10 (5): 723-727.

Elbirli, B., and M.T. Shaw. 1978. Time constants from shear viscosity data. J. of Rheology 22 (5): 561-570.

Eliassaf, J., A. Silverberg, and A. Katchalsky. 1955. Negative thixotropy of aqueous solutions of polymethacrylic acid. Nature

4493:1119.

Eliassaf, J., and A. Silverberg. 1962. The gelation of aqueous solutions of polymethacrylic acid. Polymer 3:555-564.

Elliott, J.H., and F.S. Stow. 1971. Solutions of drag-reducing polymers, diameter effect and rheological properties. J. of Appl. Pol. Sc. 15:2743-2748.

Ellis, H.D. 1970. Effects of shear treatment on drag-reducing polymer solutions and fibre suspensions. Nature 226 (April 25): 352-353.

El-Riedy, O.K., and B. Latto. 1984. Energy spectra and turbulent intensity in polymer injection flows. In Proc. of 3d Int. Conf. on Drag Reduction, paper B5. Eds.: R.H. Sellin and R.T. Moses. Bristol, England: University of Bristol.

Eolkin, D. 1957. The plastometer, a new development in continuous recording and controlling consistometers. Food Technology (May): 253-257.

Fischer, D.H., and F. Rodriguez. 1971. Degradation of drag-reducing polymers. J. of Appl. Pol. Sc. 15:2975-2985.

Fito, P.J., and V. Requeni. 1974. Heat transfer coefficients and pressure losses in non-newtonian fluids flowing in tubes. Proc. 4th Int. Cong. Food Sci. and Tech., 4:337-349.

Fleeter, R., R.A. Petersen, R.D. Toaz, A. Jakub, and V. Sarohia. 1982. Antimisting kerosene atomization and flammability. Federal Aviation Administration report No. DOT/FAA/CT-82/19. Washington, D.C.: U.S. Department of Transportation.

Foldin, M., J. Yerushalmi, R. Pfeffer, and R. Shinnar. 1969. Break-up of a laminar capillary jet of a viscoelastic fluid. J. Fluid Mech. 38 (part 4): 689-711.

Freundlich, H., and A.D. Jones. 1936. Sedimentation volume, dilatancy, thixotropic and plastic properties of concentrated suspensions. J. Phys. Chem. 40:1217-1236.

Friend, W.L., and A.B. Metzner. 1958. Turbulent heat transfer inside tubes and the analogy among heat, mass and momentum transfers. AIChE J. 4 (4): 393-402.

Fruman, D.H. 1984. Rheologically inhomogeneous flows. In Proc. of 3d Int. Conf. on Drag Reduction, paper B7. Eds.: R.H. Sellin and R.T. Moses. Bristol, England: University of Bristol.

Gadd, G.E. 1965. Turbulence damping and drag reduction produced by

certain additives in water. Nature 206 (4983): 463-467.

Gardner, K.L., W.R. Murphy, and T.G. Geehan. 1978. Polyacrylamide solution aging. J. of Appl. Pol. Sci. 22:881-882.

Gates, E.M. 1977. The influence of freestream turbulence, freestream nuclei populations, and a drag-reducing polymer on cavitation inception on two axisymmetric bodies. Ph.D. thesis. California Institute of Technology.

Ghassemzadeh, M.R., and S. Carmi. 1982. Drag reduction in flow of coal-oil suspensions. J. of Fluids Engineering 104:92-93.

Ghoniem, S., G. Chauveteau, M. Moan, and C. Wolff. 1981. Mechanical degradation of semi-dilute polymer solutions in laminar flows. The Canadian J. of Chemical Engineering 59:450-454.

Gleissle, W., and M.K. Baloch. 1984. Reduced flow functions of suspensions based on newtonian and non-newtonian liquids. In Advances in Rheology, vol. 2, 549-556. Eds.: B. Mena, A. Garcia-Rejon, and C. Rangel-Nafaile. Mexico: Universidad Nacional Autonoma de Mexico.

Golda, J. 1984. Drag reduction in the hydraulic transport of coal in pipes. In Proc. of 3d Int. Conf. on Drag Reduction, paper D2. Eds.: R.H. Sellin and R.T. Moses. Bristol, England: University of Bristol.

Goldin, M., J. Yerushalmi, R. Pfeffer, and R. Shinnar. Break-up of a laminar capillary jet of a viscoelastic fluid. J. Fluid Mech. 38 (part 4): 689-711.

Gorla, R.S. 1980. Unsteady thermal boundary layers in non-newtonian fluids. AIChE Symposium Series 76 (199); 264-269.

Granville, P.S. 1975. Progress in frictional drag reduction : summer 1974 to summer 1975. DTNSRDC report No. SPD 569-03. Washington,D.C.: U.S. Department of Navy.

_____. 1976. Progress in frictional drag reduction : summer 1975 to summer 1976. DTNSRDC report No. SPD 569-04. Washington, D.C.: U.S. Department of Navy.

_____. 1977a. A prediction method for the viscous drag of ships and underwater bodies with surface roughness and/or reducing polymer solutions. DTNSRDC report No. SPD 797-01. Washington, D.C.: U.S. Department of Navy.

_____. 1977b. Scaling-up of pipe flow frictional data for drag-reducing polymer solutions. In Proc. 2d Int. Conf. on Drag Reduction, paper B1. Cranfield, England: BHRA Fluid Engineering.

_____. 1978a. Frictional drag reduction - a literature survey of progress from summer 1976 to fall 1977. DTNSRDC report No. 78-SPD 569-05. Washington, D.C.: U.S. Department of Navy.

_____. 1978b. Similarity-law characterization methods for arbitrary hydrodynamic roughnesses. DTNSRDC report No. 78-SPD-815-01. Washington, D.C.: U.S. Department of Navy.

_____. 1980. Frictional drag reduction - a literature survey of progress from spring 1979 to spring 1980. U.S. Navy report No. 80-SPD-569-07. Washington, D.C.: U.S. Department of Navy.

_____. 1981. Frictional drag reduction - a literature survey of progress from spring 1980 to spring 1981. U.S. Navy report No. 81-SPD-569-08. Washington, D.C.: U.S. Department of Navy.

_____. 1984. A method for predicting additive drag reduction from small-diameter pipe flows. In Proc. of 3d Int. Conf. on Drag Reduction, paper C3. Eds.: R.H. Sellin and R.T. Moses. Bristol, England: University of Bristol.

Gregory, W.B. 1927. Pumping clay slurry through a four-inch pipe. Mech. Eng. 49 (6): 609-615.

Grim, R.E. 1968. Clay mineralogy, 2d ed. New York: Mc Graw Hill.

Grim, R.E., and N. Guven. 1978. Bentonites: geology, mineralogy, properties and uses. Amsterdam: Elsevier.

Gupta, M.K., A.B. Metzner, and J.P. Hartnett. 1967. Turbulent heat transfer characteristics of viscoelastic fluids. Int. J. Heat Mass Transfer 10:1211-1224.

Gyr, A. 1968. Analogy between vortex stretching by drag-reducing additives and vortex stretching by fine suspensions. Nature 219 (August): 928-929.

_____. 1984. Direct evidence that drag reduction is an effect of the elongation of the polymer molecules. In Proc. of 3d Int. Conf. on Drag Reduction, paper B10. Eds.: R.H. Sellin and R.T. Moses. Bristol, England: University of Bristol.

Hadjistamov, D. 1984. Rheological characterization of systems with shear-thinning and systems with shear-thickening flow behavior. In Advances in Rheology, vol. 2, 277-284. Eds.: B. Mena, A. Garcia-Rejon, and C. Rangel-Nafaile. Mexico: Universidad Nacional Autonoma de Mexico.

Hanks, R.W. 1984. Laminar tube flow of dilatant fluids: Cross model rheology. In Advances in Rheology, vol. 2, 355-360. Eds.: B. Mena, A. Garcia-Rejon, and C. Rangel-Nafaile. Mexico: Universidad Nacional

Autonoma de Mexico.

Harper, J.C. 1960. Viscometric behavior in relation to evaporation of fruit purees. Food Technology (November): 557-561.

Harper, J.C., and A.F. El Sahrigi. 1965. Viscometric behavior of tomato concentrates. J. of Food Science 30 (3): 470-476.

Hassager, O. 1974. Kinetic theory and rheology of bead-rod models for macromolecular solutions. The J. of Chemical Physics 60 (5): 2111-2124.

Hauser, E.A., and C.E. Reed. 1936a. Studies in thixotropy (I). J. Phys. Chem. 40:1169-1182.

_____. 1936b. Rheopexy in bentonite. J. Am. Chem. Soc. 58:1822.

_____. 1937. Studies in thixotropy (II). J. Phys. Chem. 41:911-934.

Havlik, V. 1984. Drag reduction and scale-up methods. In Proc. of 3d Int. Conf. on Drag Reduction, paper C1. Eds.: R.H. Sellin and R.T. Moses. Bristol, England: University of Bristol.

Higgins, B.G., and D. Wahren. 1982. Optimum consistency for pumping pulp. TAPPI 65 (3): 131-133.

Hinch, E.J., and C. Elata. 1979. Heterogeneity of dilute polymer solutions. J. of Non-newtonian Fluid Mechanics 5:411-425.

Howard, R.G. 1970. Heat and momentum transfer in drag-reducing solutions. NSRDC report No. 3226. Washington, D.C.: U.S. Department of Navy.

Howard, R.G., and D.M. McCrory. 1971. The correlation between heat and momentum transfer for solutions of drag-reducing agents. NSRDC report No. 3232. Washington, D.C.: U.S. Department of Navy.

Hower, W.F. 1974. Influence of clays on the production of hydrocarbons. *Society of Petroleum Engineers report No. SPE 4785. New York, NY:* American Institute of Mining, Metallurgical, and Petroleum Engineers.

Hoyt, J.W. 1966. Turbulent-flow properties of deoxyribonucleic acid solutions. Nature 211 (5045): 170-171.

_____. 1972a. The effect of additives on fluid friction. J. of Basic Engineering (June): 258-285.

_____. 1972b. Turbulent flow of drag-reducing suspensions. Naval Undersea Center report No. TP 299. Washington, D.C.: U.S. Department of Navy.

_____. 1974. Recent Progress in polymer drag reduction. NUC report No. TP 433. Washington, D.C.: U.S. Department of Navy.

_____. 1977. Polymer drag reduction - A literature review : 1975-76. In Proc. 2nd Int. Conf. on Drag Reduction, paper A1. Cranfield, England: BHRA Fluid Engineering.

Hoyt, J.W., and J.J. Taylor. 1979. Effect of nozzle shape and polymer additives on water jet appearance. J. of Fluids Engineering 101 (September): 304-308.

Hoyt, J.W., J.J. Taylor, and R.L. Altman. 1980. Drag reduction - jet breakup correlation with kerosene based additives. J. of Rheology 24 (5): 685-699.

Huang, T.T. 1974. Similarity laws for turbulent flow of dilute solutions of drag-reducing polymers. The Physics of Fluids 17 (2): 298-309.

Ippolito, M., and C. Sabatino. 1984. Rheological behavior and friction resistance of colloidal aqueous suspensions. In Advances in Rheology, vol. 2, 683-690. Eds.: B. Mena, A. Garcia-Rejon, and C. Rangel-Nafaile. Mexico: Universidad Nacional Autonoma de Mexico.

James, D.F. 1984. Non-newtonian effects in porous media flow. In Advances in Rheology, vol. 1, 279-283. Eds.: B. Mena, A. Garcia-Rejon, and C. Rangel-Nafaile. Mexico: Universidad Nacional Autonoma de Mexico.

James, D.F., and A.J. Acosta. 1970. The laminar flow of dilute polymer solutions around circular cylinders. J. Fluid Mech. 42 (part 2): 269-288.

James, D.F., and D.R. McLaren. 1975. The laminar flow of dilute polymer solutions through porous media. J. Fluid Mech. 70 (part 4): 733-752.

James, D.F., and J.H. Saringer. 1980. Extensional flow of dilute polymer solutions. J. Fluid Mech. 97 (4): 655-671.

_____. 1982. Flow of dilute polymer solutions through converging channels. J. of Non-newtonian Fluid Mechanics 11:317-339.

James, D.F., J.H. Saringer, A.B. Welch, and B. McLean. 1984. Extensional rheology and extensional bursts. In Proc. of 3d Int. Conf. on Drag Reduction, paper A2. Eds.: R.H. Sellin and R.T. Moses. Bristol, England: University of Bristol.

Jones, W.M., and J.L. Maddock. 1969. Relaxation effects in the flow of dilute polymer solutions through tubes and granular beds. Brit. J. of Appl. Phys. 2:797-808.

Joshi, S.D., and A.E. Bergles. 1980a. Experimental study of laminar heat

transfer to in-tube flow of non-newtonian fluids. J. of Heat Transfer 102:397-401.

_____. 1980b. Analytical study of heat transfer to laminar in-tube flow of non-newtonian fluids. AIChE Symposium Series 76 (199): 270-281 .

_____. 1981. Analytical study of laminar flow heat transfer to pseudoplastic fluids in tubes with uniform wall temperature. AIChE Symposium Series 77 (208): 114-122.

Jowitt, R., and O.J. McCarthy. The experimental determination of laminar flow heat transfer coefficients for newtonian and non-newtonian food liquids in tubular and plate exchangers. Proc. 4th Int. Congress Food Sci. and Technol. 4: 350-360.

Kale, D.D. 1977. An analysis of heat transfer to turbulent flow of drag- reducing fluids. Int. J. Heat Mass Transfer 20:1077-1081.

Kale, D.D., and A.B. Metzner. 1976. Turbulent drag reduction in dilute fiber suspensions: mechanistic considerations. AIChE J. 22 (4): 669-674.

Katsibas, P., C. Balakrishnan, D. White, and R.J. Gordon. 1974. Drag reduction correlations. In Proc. of Int. Conf. on Drag Reduction, paper B2. Cranfield, England: BHRA Fluid Engineering.

Kawase, Y., and A. De. 1984. Turbulent heat and mass transfer in newtonian and dilute polymer solutions flowing through rough pipes. Int. J. Heat Mass Transfer 27 (1): 142-144.

Kawase, Y., and J.J. Ulbrecht. 1982a. Mass and heat transfer in a turbulent non-newtonian boundary layer. Letters in Heat and Mass Transfer 9:79-97.

_____. 1982b. Turbulent heat and mass transfer in non-newtonian fluids. ASME paper No. 82-HT-57. New York, NY: American Society of Mechanical Engineers.

Kays, W.M. 1966. Convective heat and mass transfer. New York : McGraw-Hill.

Kays, W.M. and M.E. Crawford. 1980. Convective heat and mass transfer (2nd ed.). New York : McGraw-Hill.

Kenis, P.R. 1968. Effects of pH on the production of bacterial extracellular drag-reducing polymers. Applied Microbiology 16 (8): 1253-1254.

Kerekes, R.J., and W.J. Douglas. 1972. Viscosity properties of suspensions at the limiting conditions for turbulent drag reduction. 1972. The Canadian J. of Chemical Engineering 50:228-231.

Krumel, K.L., and N. Sarkar. 1975. Flow properties of gums useful to the food industry. Food Technology (April): 36-44.

Kubo, I. 1979. Turbulence in drag reducing polymer solutions. NSSC report No. TM 79-66. Washington, D.C.: U.S. Department of Navy.

Kwack, E.I., and J.P. Hartnett. 1982a. Effects of diameter on critical Weissenberg numbers for polyacrylamide solutions in turbulent flows. Int. J. Heat Mass Transfer 25 (6): 797-805.

_____. 1982b. Effects of solvent chemistry on critical Weissenberg numbers. Int. J. Heat Mass Transfer 25 (9): 1445-1450.

_____. 1983a. New method to determine characteristic time of viscoelastic fluids. Int. Com. in Heat and Mass Transfer 10:77-82.

_____. 1983b. Empirical correlations of turbulent friction factors and heat transfer coefficients for viscoelastic fluids. Int. Com. in Heat and Mass Transfer 10:451-461.

_____. 1984. Heat transfer to aqueous polyacrylamide solutions in turbulent channel flow. In Advances in Rheology, vol. 2, 17-25. Eds.: B. Mena, A. Garcia-Rejon, and C. Rangel-Nafaile. Mexico: Universidad Nacional Autonoma de Mexico.

Kwack, E.I., Y.I. Cho, and J.P. Hartnett. 1981a. Heat transfer to polyacrylamide solutions in turbulent pipe flow: the once-through mode. AIChE Symposium Series 77 (208): 123-130.

_____. 1981b. Solvent effects on drag reduction of polyethylene oxide solutions in square duct and capillary tube flows. J. of Non-newtonian Fluid Mechanics 9:79-90.

Kwack, E.I., J.P. Hartnett, and Y.I. Cho. 1980. Chemical effects in the flow of dilute polymer solutions. Letters in Heat and Mass Transfer 7:1-6.

_____. 1982. Turbulent heat transfer in circular tube flows of viscoelastic fluids. Warme und Stoffubertragung 16:35-44.

Latto, B., and O.K. El-Riedy. 1984. Dispersion of polymer additives in a developing turbulent boundary layer. In Proc. of 3d Int. Conf. on Drag Reduction, paper B6. Eds.: R.H. Sellin and R.T. Moses. Bristol, England: University of Bristol.

Layec-Raphalen, M.N. 1984. Shear degradation of drag-reducing polymers

- influence of the solutions on the resistance to the degradation. In Proc. of 3d Int. Conf. on Drag Reduction, paper E2. Eds.: R.H. Sellin and R.T. Moses. Bristol, England: University of Bristol.

Leal, L.G. 1984. Birefringence studies of flow-induced conformation changes in polymer solutions. In Advances in Rheology, vol. 1, 191-209. Eds.: B. Mena, A. Garcia-Rejon, and C. Rangel-Nafaile. Mexico: Universidad Nacional Autonoma de Mexico.

Leca, A., and M. Leca. 1984. Drag reduction and heat transfer measurements with polyacrylamides on a model of a district heating system. In Proc. of 3d Int. Conf. on Drag Reduction, paper D8. Eds.: R.H. Sellin and R.T. Moses. Bristol, England: University of Bristol.

Lee, H., T.F. Irvine, and E.Y. Kwack. 1980. Anomalous effects in drag reduction measurements of polymer solutions. Letters in Heat and Mass Transfer 7:7-13.

Lee, W.K., R.C. Vaseleski, and A.B. Metzner. 1974. Turbulent drag reduction in polymeric solutions containing suspended fibers. AIChE J. 20 (1): 128-133.

Lee, W.Y., Y.I. Cho, and J.P. Hartnett. 1981. Thermal conductivity measurements of non-newtonian fluids. Letters in Heat and Mass Transfer 8:255-259.

Little, R.C., R.J. Hansen, D.L. Hunston, O. Kim, R.L. Patterson, and R.Y. Ting. 1975. The drag reduction phenomenon: observed characteristics, improved agents, and proposed mechanisms. Ind. Eng. Chem. Fundam. 14 (4): 283-296.

Lumley, J.L. 1967. The Toms phenomenon: anomalous effects in turbulent flow of dilute solutions of high molecular weight linear polymers. Applied Mechanics Reviews 20 (12): 1139-1149.

Maksimovic, C. 1984. Diffusion of the passive tracer and drag-reducing polymer solution in a developing duct flow. In Proc. of 3d Int. Conf. on Drag Reduction, paper B1. Eds.: R.H. Sellin and R.T. Moses. Bristol, England: University of Bristol.

Malinsky, K., and J. Myska. 1984. The investigation of the ultrasonic cavitation in drag-reducing polymer solutions. In Proc. of 3d Int. Conf. on Drag Reduction, paper E1. Eds.: R.H. Sellin and R.T. Moses. Bristol, England: University of Bristol.

Mannheimer, R.J. 1977. Rheology study of antimist fuels. Federal Aviation Administration report No. FAA-RD-77-10. Washington, D.C.: U.S. Department of Transportation.

_____. 1979. Restoring essential flow and ignition properties to

antimisting kerosene (AMK) for turbine aircraft operations. Federal Aviation Administration report No. FAA-RD-79-62. Washington, D.C.: U.S. Department of Transportation.

_____. 1981. Degradation and characterization of antimisting kerosene (AMK). Paper No. AIAA-81-1423. New York, NY: American Institute of Aeronautics and Astronautics.

_____. 1982. Degradation and characterization of antimisting kerosene (AMK). Federal Aviation Administration report No. DOT/FAA/CT-82/93. Washington, D.C.: U.S. Department of Transportation.

_____. 1983a. Feasibility of a full-scale degrader for antimisting kerosene . AIAA paper No. AIAA-83-1137. New York, NY: American Institute of Aeronautics and Astronautics.

_____. 1983b. Rheological and mist ignition properties of dilute polymer solutions. Chem. Eng. Com. 19:221-241.

_____. 1984. Shear and normal stress measurements of antimisting kerosene at high shear rates. In Advances in Rheology, vol. 2, 1-16. Eds.: B. Mena, A. Garcia-Rejon, and C. Rangel-Nafaile. Mexico: Universidad Nacional Autonoma de Mexico.

Mannheimer, R.J., and W.D. Weatherford. 1975. Investigation of rheological properties of dilute solutions of polymeric antimist agents in hydrocarbons fuels. U.S. Army report No. AFLRL-59. Washington, D.C.: U.S. Department of Defense.

Marrucci, G., and G. Astarita. 1967. Turbulent heat transfer in viscoelastic liquids. I.& E. C. Fundam. 6 (3): 470-471.

Martin, F.D., and M.S. Kuntamukkula. 1984. The influence of mechanical degradation on the viscous, elastic, and elongational flow properties of polymer solutions used in enhanced oil recovery. In Advances in Rheology, vol. 4, 411-419. Eds.: B. Mena, A. Garcia-Rejon, and C. Rangel-Nafaile. Mexico: Universidad Nacional Autonoma de Mexico.

Martischius, F., and W. Heide. 1984. Drag reduction in heating systems: stabilisation of polyacrylamide solutions up to temperatures of 150o. In Proc. of 3d Int. Conf. on Drag Reduction, paper D9. Eds.: R.H. Sellin and R.T. Moses. Bristol, England: University of Bristol.

Matthys, E.F. 1984. A viscometric study of the gelation phenomenon for polymer solutions in kerosene. In Advances in Rheology, vol. 2, 117-125. Eds.: B. Mena, A. Garcia-Rejon, and C. Rangel-Nafaile. Mexico: Universidad Nacional Autonoma de Mexico.

_____. 1985. Influence of photodegradation and aging on the viscosity of antimisting polymer solutions. J. of Non-newtonian Fluid Mechanics

(in press).

Matthys, E.F., and R.H. Sabersky. 1982. A method of predicting the 'diameter effect' for heat transfer and friction of drag-reducing fluids. Int. J. Heat Mass Transfer 25 (9): 1343-1351.

McCarthy, J.H. 1970. Flat plate frictional drag reduction with polymer injection. NSRDC report No. 3290. Washington, D.C.: U.S. Department of Navy.

McComb, W.D., and K.T. Chan. 1981. Drag reduction in fibre suspension. Nature 292 (5823): 520-522.

McConaghy, G.A., and T.J. Hanratty. 1977. Influence of drag-reducing polymers on turbulent mass transfer to a pipe wall. AIChE J. 23 (4): 493-500.

McNally, W.A. 1968. Heat and momentum transport in dilute polyethylene oxide solutions. NUWRES report No. TM 44. Washington, D.C.: U.S. Department of Navy.

Medani, M.S., and K.G. Hayes. 1978. Heat transfer to aviation fuels. J. of Eng. Science (Riyadh, Saudi Arabia) 4 (1): 45-54.

Metzner, A.B. 1965. Heat transfer in non-newtonian fluids. Advances in Heat Transfer 2:357-397.

_____. 1977. Polymer solution and fiber suspension rheology and their relationship to turbulent drag reduction. The Physics of Fluids 20 (10): S145-S149.

Metzner, A.B., and A.P. Metzner. 1970. Stress levels in rapid extensional flows of polymeric fluids. Rheologica Acta 9 (2): 174-181.

Metzner, A.B., and J.C. Reed. 1955. Flow of non-newtonian fluids - correlation of the laminar, transition, and turbulent regions. AIChE J. 1 (4): 434-440.

Metzner, A.B., and M. Whitlock. 1958. Flow behavior of concentrated (dilatant) suspensions. Trans. of the Society of Rheology 2:239-254.

Mironov, B.P., and V.I. Shishov. 1984. Generalization of friction drag dependences for turbulent flows of water - polyethylene oxide solutions in pipes. In Proc. of 3d Int. Conf. on Drag Reduction, paper C4. Eds.: R.H. Sellin and R.T. Moses. Bristol, England: University of Bristol.

Mizushina, T., and H. Usui. 1977. Reduction of eddy diffusion for momentum and heat in viscoelastic fluid flow in a circular tube. The Physics of Fluids 20 (10): S100-S108

Mizushina, T., H. Usui, and T. Yamamoto. 1975. Turbulent heat transfer of viscoelastic fluids flow in pipe. Letters in Heat and Mass Transfer 2:19-26.

Mizushina, T., H. Usui, and T. Yoshida. 1974. Turbulent pipe flow of dilute polymer solutions. J. of Chemical Engineering of Japan 7 (3): 162-167.

Moan, M., G. Chauveteau, and S. Ghoniem. 1979. Entrance effect in capillary flow of dilute and semi-dilute polymer solutions. J. of Non-newtonian Fluid Mechanics 5:463-474.

Mochimaru, Y., and Y. Tomita. 1974. A study on the flows of dilute polymer solutions. Bulletin of the JSME 17 (114): 1594-1601.

Monti, R. 1972. Heat transfer in drag-reducing solutions. Progress in Heat Transfer 5:239-250. Oxford, England: Pergamon Press.

Morrison, S.R., and J.C. Harper. 1965. Wall effects in Couette flow of non-newtonian suspensions. I & E C Fundamentals 4 (2): 176-181.

Motier, J.F., and D.J. Prilutski. 1984. Case histories of polymer drag reduction in crude oil pipelines. In Proc. of 3d Int. Conf. on Drag Reduction, paper F2. Eds.: R.H. Sellin and R.T. Moses. Bristol, England: University of Bristol.

Motier, J.F., D.J. Prilutski, Z. Shanti In, and R.J. Kostelnik. 1984. Polymeric drag reduction in petroleum products. In Proc. of 3d Int. Conf. on Drag Reduction, paper F3. Eds.: R.H. Sellin and R.T. Moses. Bristol, England: University of Bristol.

Moyls, A.L., and R.H. Sabersky. 1978. Heat transfer and friction coefficients for dilute suspensions of asbestos fibers. Int. J. of Heat and Mass Transfer 21:7-14.

Mungan, N., F.W. Smith, and J.L. Thompson. 1966. Some aspects of polymer floods. J. of Petroleum Technology (September): 1143-1150.

Mysels, K.J. 1949. Flow of thickened fluids. U.S. Patent 2492173, December 27.

Nicodemo, L., D. Acierno, and G. Astarita. 1969. Velocity profiles in turbulent pipe flow of drag-reducing liquids. Chemical Engineering Science 24:1241-1246.

Ng, K.S., and J.P. Hartnett. 1979. Effects of mechanical degradation on pressure drop and heat transfer performance of polyacrylamide solutions in turbulent pipe flow. In Studies in Heat Transfer, 297-307. Ed.: T. Irvine. New York, NY: McGraw-Hill.

Ng, K.S., Y.I. Cho, and J.P. Hartnett. 1980. Heat transfer performance of concentrated polyethylene oxide and polyacrylamide solutions. AIChE Symposium Series 76 (199): 250-256.

Odell, J.A., and A. Keller. 1984. Flow-induced polymer degradation: chain halving - a new method for determining molecular weight distributions. In Proc. of 3d Int. Conf. on Drag Reduction, paper A3. Eds.: R.H. Sellin and R.T. Moses. Bristol, England: University of Bristol.

Oliver, D.R., and R. Bragg. 1973. The extensional flow of polymeric solutions through small orifices. The Chemical Engineering J. 5:1-6.

Olson, R.M., and E.M. Sparrow. 1963. Measurements of turbulent flow development in tubes and annuli with square or rounded entrances. AIChE J. 9 (6): 766-770.

Ono, K., and K. Murakami. 1977. Kinetics of gelation of aqueous poly(methacrylic acid) solutions under shear stress. Polymer letters 15:507-511.

Orr, C., and J.M. Dallavalle. 1954. Heat transfer properties of liquid-solid suspensions. AIChE Symposium Series 50 (9).

Ouibrahim, A. 1978. Rheology of polylmer solutions in laminar capillary tube flows. Phys. Fluids 21 (1): 4-8.

_____. 1979. Excess pressure drop of polymer solutions in laminar capillary tube flows. Phys. Fluids 22 (4): 784-785.

Ouibrahim, A., and D.H. Fruman. 1980. Characteristics of HPAM dilute solutions in three elongational flow situations. J. of Non-newtonian Fluid Mechanics 7:315-331.

Paterson, R.W., and F.H. Abernathy. 1970. Turbulent flow drag reduction and degradation with dilute polymer solutions. J. Fluid Mech. 43 (4): 689-710.

Patterson, G.K. 1984. Rates of shear degradation of drag-reducing polymers. In Proc. of 3d Int. Conf. on Drag Reduction, paper E4. Eds.: R.H. Sellin and R.T. Moses. Bristol, England: University of Bristol.

Patterson, G.K., J.L. Zakin, and J.M. Rodriguez. 1969. Drag reduction. Industrial and Engineering Chemistry 61 (1): 22-30.

Peng, S.T., and R.F. Landel. 1976. Preliminary investigation of elongational flow of dilute polymer solutions. J. of Applied Physics 47 (10): 4255-4260.

_____. 1980. Extensional flow of dilute polymer solutions. In Rheology,

vol 2, 385-391. Eds.: G. Astarita, G. Marucci, and L. Nicolais. New York, NY: Plenum Pub. Co.

Peng, S.T., and R.F. Landel. 1981. Rheological behavior of progressively shear-thickening solutions. J. of Applied Physics 52 (10): 5988-5993.

_____. 1983. Rheological behavior of FM-9 solutions and correlation with flammability test results and interpretations. J. of Non-newtonian Fluid Mechanics 12:95-111.

Petukhov, B.S. 1970. Heat transfer and friction in turbulent pipe flow with variable physical properties. Advances in Heat Transfer 6:503-564.

Phan-Tien, N., O. Manero, and L.G. Leal. 1984. A study of conformation-dependent friction in a dumbbell model for dilute solutions. Rheologica Acta 23:151-162.

Pohreh, M., and Y. Dimant. 1972. Velocity distribution and friction factors in pipe flows with drag reduction. Department of Civil Engineering publ. No. 175. Haifa, Israel: Technion-Israel Institute of Technology.

Pohreh, M., J.L. Zakin, A. Brosh, and M. Warshavsky. 1970. Drag reduction in hydraulic transport of solids. J. of the ASCE Hydraulics Division (April): 903-909.

Pollert, J. 1984. Influence of drag-reducing polymers on settling velocity of solid particles in hydrotransport systems. In Proc. of 3d Int. Conf. on Drag Reduction, paper D1. Eds.: R.H. Sellin and R.T. Moses. Bristol, England: University of Bristol.

Powell, R.E., and H. Eyring. 1944. Mechanisms for the relaxation theory of viscosity. Nature 154 (3909): 427-428.

Pownall, R.A., and K.M. Kiser. 1970. Rate of spread of jets of non-newtonian fluids. Ind. Eng. Chem. Fundam. 9 (2): 293-297.

Rao, M.A., and R.C. Anantheswaran. 1982. Rheology of fluids in food processing. Food Technology (February): 116-126.

Rao, M.A., and H.J. Cooley. 1983. Applicability of flow models with yield for tomato concentrates. J. of Food Process Eng. 6:159-173.

Ree, F.H., T. Ree, and H. Eyring. 1958. Relaxation theory of transport problems in condensed systems. Industrial and Engineering Chemistry 50 (7): 1036-1040.

Reichardt, H. 1951. Die Grundlagen des Turbulenten Warmeuberganges. Archiv fur Gesamte Warmetechnik 2 (6/7): 129-142.

_____. 1957. The principles of turbulent heat transfer. Report No. NACA TM 1408. Washington, DC: National Advisory Committee for Aeronautics.

Ries, H. 1927. Clays: their occurrence, properties and uses. New York: Wiley and Sons.

Rivlin, R.S., and K.N. Sawyers. 1971. Nonlinear continuum mechanics of viscoelastic fluids. An. Rev. Fluid Mech. 3:117-146.

Rha, C. 1978. Rheology of fluid foods. Food Technology (July): 77-82.

Rogers, W.F. 1948. Composition and properties of oil well drilling fluids. Houston: Gulf Pub. Co.

Rose, G.D., K.L. Foster, V.L. Slocum, and J.G. Lenhart. 1984. Drag reduction and heat transfer characteristics of viscoelastic surfactant formulations. In Proc. of 3d Int. Conf. on Drag Reduction, paper D6. Eds.: R.H. Sellin and R.T. Moses. Bristol, England: University of Bristol.

Rosen, M.W., and N.E. Cornford. 1970. Fluid friction of the slime of aquatic animals. NUC report No. NUC TP 193. Washington, D.C.: U.S. Department of Navy.

Rouse, P.E. 1953. A theory of the linear viscoelastic properties of dilute solutions of coiling polymers. The J. of Chemical Physics 21 (7): 1272-1280.

Ruckenstein, E. 1970. Mass or heat transfer from a solid boundary to a turbulent fluid. Int. J. Heat Mass Transfer 13:1283-1291.

_____. 1971. On the mechanism of drag reduction in turbulent flow of viscoelastic liquids. Chemical Engineering Science 26:1075-1079.

_____. 1972. Turbulent heat transfer to non-newtonian liquids. Chemical Engineering Science 27:947-957.

_____. 1973. A note on the mechanism of drag reduction. J. of Applied Polymer Science 17:3239-3240.

_____. 1978. Interpolating equations between two limiting cases for the heat transfer coefficient. AIChE J. 24 (5): 940-941.

Ruckenstein, E., and V. Popadic. 1971. Physical model for drag reduction in turbulent pipe flow. Nature Physical Science 233 (September 20): 58-59.

Russel, W.B. 1978. Bulk stresses due to deformation of the electrical double layer around a charged sphere. J. Fluid Mech. 85 (part 4):

673-683.

_____. 1980. Review of the role of colloidal forces in the rheology of suspensions. J. of Rheology 24 (3): 287-317.

_____. 1981. Brownian motion of small particles suspended in liquids. Annual Review Fluid Mechanics 13:425-455.

Sadek, S.E. 1972. Heat transfer to air-solids suspensions in turbulent flow. Ind. Eng. Chem. Process Des. Develop. 11 (1): 133-135.

Sadowski, T.J. 1965. Non-newtonian flow through porous media. Trans. of the Society of Rheology 9 (2): 251-271.

Salmon, R.F. 1981. Wing spillage tests using antimisting fuel. Federal Aviation Administration report No. FAA-CT-81-11. Washington, D.C.: U.S. Department of Transportation.

San Miguel, A., and M.D. Williams. 1978. Antimisting fuel spillage and air shear tests at the Naval Weapons Center. Federal Aviation Administration report No. FAA-RD-78-50. Washington, D.C.: U.S. Department of Transportation.

Saravacos, G.D. 1970. Effect of temperature on viscosity of fruit juices and purees. J. of Food Science 35:122-125.

Sarohia, V. 1981. Fundamental studies of antimisting fuels. Paper No. AIAA-81-1422. New York, NY: American Institute of Aeronautics and Astronautics.

Sarohia, V., and R.F. Landel. 1980. Influence of antimisting polymer in aviation fuel break-up. Paper No. AIAA-80-1287. New York, NY: American Institute of Aeronautics and

Savins, J.G. 1968. Shear thickening phenomena in poly(vinyl) alcohol-borate complexes. Rheologica Acta 7 (1): 87-93.

Savins, J.G., and F.A. Seyer. 1977. Drag reduction scale-up criteria. The Physics of Fluids 20 (10): S78-S84.

Schmid, A. 1984. Experimental investigation of the influence of drag-reducing polymers on a turbulent channel flow. In Proc. of 3d Int. Conf. on Drag Reduction, paper B12. Eds.: R.H. Sellin and R.T. Moses. Bristol, England: University of Bristol.

Schowalter, W.R. 1978. Mechanics of Non-newtonian Fluids. Oxford: Pergamon Press.

_____. 1984a. Stability and coagulation of colloids in shear fields. Annual Review of Fluid Mechanics 16:245-261.

_____. 1984b. Growth and collapse of bubbles in rheologically complex liquids. In Advances in Rheology, vol. 1, 225-242. Eds.: B. Mena, A. Garcia-Rejon, and C. Rangel-Nafaile. Mexico: Universidad Nacional Autonoma de Mexico.

Schowalter, W.R., and S.K. Hara. 1980. A review of approaches to the study of cavitation inhibition by means of polymer additives. ONR report No. 160-6076-1. Washington, D.C.: U.S. Department of Navy.

Schummer, P., and Y. Xu. 1984. Flow of viscoelastic liquids in conical nozzles. In Advances in Rheology, vol. 2, 153-157. Eds.: B. Mena, A. Garcia-Rejon, and C. Rangel-Nafaile. Mexico: Universidad Nacional Autonoma de Mexico.

Sedov, L.I., V.A. Ioselevich, V.N. Pilipenko, and N.G. Vasetskaya. 1979. Turbulent diffusion and degradation of polymer molecules in a pipe and boundary layer. J. Fluid Mech. 94 (part 3): 561-576.

Sellin, R.H. 1984. Industrial applications for drag-reducing polymeric additives: a review. In Proc. of 3d Int. Conf. on Drag Reduction, paper I3. Eds.: R.H. Sellin and R.T. Moses. Bristol, England: University of Bristol.

Sellin, R.H., and M. Ollis. 1983. Effect of pipe diameter on polymer drag reduction. Ind. Eng. Chem. Prod. Res. Dev. 22:445-452.

Seyer, F.A., and A.B. Metzner. 1969. Turbulence phenomena in drag reducing systems. AIChE J. 15 (3): 426-434.

Shah, R.K., and A.L. London. 1978. Laminar flow forced convection in ducts (Advances in Heat Transfer suppl. 1). New York: Academic Press.

Sharma, R.S., V. Seshadri, and R.C. Malhotra. 1979. Drag reduction in dilute fibre suspensions: some mechanistic aspects. Chemical Engineering Science 34:703-713.

Shenoy, A.V., and R.A. Mashelkar. 1982. Thermal convection in non-newtonian fluids. Advances in heat transfer 15: 144-225.

Sieder, E.N., and G.E. Tate. 1936. Heat transfer and pressure drop of liquids in tubes. Industrial and Engineering Chemistry 28 (12): 1429-1435.

Singh, R.P., P. Chand, G.V. Reddy, S.R. Deshmukh, and B. Adinarayana. 1984. Characteristics of some polymer-polymer, polymer-fibre combinations and grafted polymers as drag-reducing agents and their industrial applications. In Proc. of 3d Int. Conf. on Drag Reduction, paper D4. Eds.: R.H. Sellin and R.T. Moses. Bristol, England: University of Bristol.

Skelland, A.H. 1967. Non-newtonian flow and heat transfer. New York: Wiley.

Sleicher, C.A., and M.W. Rouse. 1975. A convenient correlation for heat transfer to constant and variable property fluids in turbulent pipe flow. Int. J. Heat Mass Transfer 18:677-683.

Smith, J.W., and J.C. Paradi. 1982. Heat transfer to settling slurries in vertical transport. J. of Pipelines 3:43-52.

Smith, K.A., E.W. Merrill, H.S. Mickley, and P.S. Virk. 1967. Anomalous pitot tube and hot film measurements in dilute polymer solutions. Chemical Engineering Science 22:619-626.

Smith, K.A., G.H. Keuroghlian, P.S. Virk, and E.W. Merrill. 1969. Heat transfer to drag-reducing polymer solutions. AIChE J. 15 (2): 294-297.

Smith, R., and M.F. Edwards. 1981. Heat transfer to non-newtonian and drag-reducing fluids in turbulent pipe flow. Int. J. Heat Mass Transfer 24 (6): 1059-1069.

Stenberg, L.G., T. Lagerstedt, O. Sehlen, and E.R. Lindgren. 1977. Mechanical mixing of polymer additive in turbulent drag reduction. The Physics of Fluids 20 (5): 858-859.

Suckow, W.H., P. Hrycak, and R.G. Griskey. 1980. Heat transfer to non-newtonian dilatant flluids flowing between parallel plates. AIChE Symposium Series 76 (199): 257-263.

Taylor, D.D., and R.H. Sabersky. 1974. Extrapolation to various tube diameters of experimental data taken with dilute polymer solutions in a smooth tube. Letters in Heat and Mass Transfer 1:103-108.

Thomas, D.G. 1960. Heat and momentum transport characteristics of non-newtonian aqueous thorium oxide suspensions. AIChE J. 6 (4): 631-639.

Ting, R.Y. 1976. Diameter dependence of the cutoff molecular weights of drag-reducing polymers. J. of Applied Polymer Science 20:3017-3023.

Tiu, C., and G.S. Low. 1981. Momentum and heat transfer of dilute polymer solutions in plate exchangers. AIChE 77 (208): 132-138.

Toms, B.A. 1948. Some observations on the flow of linear polymer solutions through straight tubes at large Reynolds numbers. In Proc. of 1st Int. Congress on Rheology, vol.2, 135-141. Amsterdam: North Holland Pub. Co.

_____. 1977. On the early experiments on drag reduction by polymers. The Physics of Fluids 20 (10): S3-S5.

Tsay, S., and C. Chou. 1983. Laminar convection to rotating disks in non-newtonian power-law fluids. Int. Com. Heat Mass Transfer 10:377-383.

Tulin, M.P. 1966. Hydrodynamic aspects of macromolecular solutions. In Proc. 6th Symp. on Naval Hydrodynamics, 3-18. Office of Naval Research report No. ONR ACR-136. Washington, D.C.: U.S. Department of Navy.

Tung, T.T., K.S. Ng, and J.P. Hartnett. 1978. Pipe frictions factors for concentrated aqueous solutions of polyacrylamide. Letters in Heat and Mass Transfer 5:59-69.

Van Driest, E.R. 1956. On turbulent flow near a wall. J. Aeronaut. Science (November): 1007-1036.

Van Vliet, T., and A.C. Van Hooijdonk. 1984. The gel properties of some beverages. In Advances in Rheology, vol. 4, 115-122. Eds.: B. Mena, A. Garcia-Rejon, and C. Rangel-Nafaile. Mexico: Universidad Nacional Autonoma de Mexico.

Vanoni, V.A., and G.N. Nomicos. 1959. Resistance properties of sediment-laden streams. J. of the ASCE Hydraulics Division paper No. 2020.

Vargas-Jarillo, C. 1984. A discrete model for the recovery of oil from a reservoir. In Advances in Rheology, vol. 4, 421-428. Eds.: B. Mena, A. Garcia-Rejon, and C. Rangel-Nafaile. Mexico: Universidad Nacional Autonoma de Mexico.

Vaseleski, R.C., and A.B. Metzner. 1974. Drag reduction in the turbulent flow of fiber suspensions. AIChE J. 20 (2): 301-306.

Veatch, R.W. 1982. Current hydraulic fracturing treatment and design technology. Society of Petroleum Engineers report No. SPE 10039. Dallas, Texas: Society of Petroleum Engineers.

Virk, P.S. 1975. Drag reduction fundamentals. AIChE J. 21 (4): 625-656.

Virk, P.S., and H. Baher. 1970. The effect of polymer concentration on drag reduction. Chemical Engineering Science 25:1183-1189.

Virk, P.S., H.S. Mickley, and K.A. Smith. 1970. The ultimate asymptote and mean flow structure in Toms phenomenon. ASME paper No. 70-APM-HH. New York, NY: American Society of Mechanical Engineers.

Vleggaar, J., W.R. Dammers, and M. Tels. 1968. The diameter effect in drag reduction. Chemical Engineering Science 23:1159-1169.

Wat, J., and V. Sarohia. 1982. Frictional characteristics and heat transfer of antimisting fuel in tubes. Federal Aviation Administration

report No. DOT/FAA/CT-82/20. Washington, D.C.: U.S. Department of Transportation.

White, A. 1976. Drag reduction by additives - review and bibliography. Cranfield, England: BHRA Fluid Engineering.

White, F.M. 1974. Viscous fluid flow. New York: McGraw-Hill.

Yavrouian, A.H., M. Sarboluki, and V. Sarohia. 1983. Influence of liquid water and water vapor on antimisting kerosene (AMK). Federal Aviation Administration report No. DOT/FAA/CT-82/18. Washington, D.C.: U.S. Department of Transportation.

Yavrouian, A.H., J. Ernest, and V. Sarohia. 1984. Antimisting kerosene: base fuel effects; blending and quality control techniques. Federal Aviation Administration report No. DOT/FAA/CT-83/36. Washington, D.C.: U.S. Department of Transportation.

Yoo, S.S. 1974. Heat transfer and friction factors for non-newtonian fluids in turbulent pipe flow. Ph.D. Thesis. University of Illinois, Chicago.

Zaba, J., and W. Doherty. 1956. Practical petroleum engineers' handbook, 4th ed. Houston: Gulf Publishing Co.

Zandi, I. 1967. Decreased head losses in raw-water conduits. J. AWWA (February): 213-226.

Appendix A.

HEAT TRANSFER EQUATIONS AND BALANCES

A.1. Computation of Temperature Difference between the Outside and Inside Wall

The heat transfer in the present experiments is obtained by Joule heating of the wall, which produces an approximately constant heat flux. As a consequence, the bulk temperature of the fluid and both the outside and inside wall temperatures increase about linearly with the distance.

Slight non-linearities will be caused by variations in material properties due to these temperature increases, however. As the temperature of the fluid increases during its passage in the tube, its viscosity will change, along with the local Reynolds and Prandtl numbers. The heat transfer coefficient depending on these numbers, the temperature difference between wall and bulk will thus vary because of the constant heat flux constraint. The effect of the temperature increase on the specific heat capacity and the thermal conductivity of the fluid is usually smaller than the effect on the viscosity. With non-newtonian fluids the deviations from linearity can be larger if additional phenomena such as viscoelasticity, shear thickening, or thixotropy are present.

The heat flux itself is not quite constant either, because the temperature of the tube wall increases between entry and exit, thereby also increasing the thermal conductivity and the electrical resistivity of the metal. The heat generated in the wall will thus be a function of the axial

location, and the temperature difference between inside and outside wall will vary as well. In fact, the heat generated in the wall and the metal's conductivity vary also with the radius because of the radial gradient of temperature in the wall.

An expression for the temperature difference between the inside and outside wall of the tube may be developed, assuming no heat loss (see app. A.4.). With this value it is a simple matter to compute the difference between the inside wall and the fluid temperature. Indeed, the outside wall temperature is directly measured by thermocouples and the bulk temperature of the fluid is readily computed from bulk temperature probes and power (see app. A.2.).

To obtain the temperature difference across the tube wall, heat conduction has to be considered there. Assuming steady conditions and angular symmetry, and using cylindrical coordinates, the general energy equation reduces to

$$\nabla \cdot (k(r,x)\nabla T) = -Q(r,x) \tag{A.1}$$

or

$$\nabla k(r,x)\cdot\nabla T + k(r,x)\nabla^2 T = -Q(r,x) \tag{A.2}$$

where Q is the heat source per unit volume. Both k and Q may be functions of r and x, as explained above. As a further simplification, let us assume that the radial gradients of temperature are much larger than the axial ones. Typical numbers support this assumption in fully-developed flow: 2 $^{\circ}C$ for the length of the tube or 0.4 $^{\circ}C/m$ vs at least

0.2 $°C$ across the wall or about 200 $°C/m$. The equation is then reduced further to

$$\frac{\partial k}{\partial r}\frac{\partial T}{\partial r} + k\frac{\partial^2 T}{\partial r^2} + k\frac{1}{r}\frac{\partial T}{\partial r} = -Q \quad . \tag{A.3}$$

However, in this equation we have k = k(T) = k(r,x) and Q = Q(T) = Q(r,x). These dependences complicate considerably the situation, turning this traditionally benign equation into a heavily non-linear one. Rather than attempting to solve this equation analytically , let us first evaluate how significant the non-linearities may be with respect to the degree of accuracy needed.

As a first approximation, the equation may be solved for constant k and Q. It is then reduced to

$$\frac{\partial^2 T}{\partial r^2} + \frac{1}{r}\frac{\partial T}{\partial r} = -\frac{Q}{k} \quad . \tag{A.4}$$

This is easily solved by expressing that the outside wall ($r = r_0$) is insulated, and that all the heat produced in the wall goes to the fluid radially at the inside wall ($r = r_i$). The resulting solution is

$$T - T_o = \frac{Q}{4k}\left[r_0^2 - r^2 + 2r_0^2 \ln\left(\frac{r}{r_0}\right)\right] \tag{A.5}$$

which gives the temperature profile across the wall as a function of the outside wall temperature (T_o). If the heat generation is expressed in terms of the total heating power (P) and volume of metal in the pipe, the difference in temperature between the outside and inside wall may be written as

$$T_o - T_i = \frac{P}{2\pi(r_0^2 - r_i^2)L\,k}\left[r_0^2 \ln\left(\frac{r_0}{r_i}\right) + \frac{r_i^2 - r_0^2}{2}\right] \qquad (A.6)$$

which is the expression normally used for this type of configuration. For a maximum heating power of 3500 W, with

$$r_0 = 4.776\,10^{-3}\,m$$

$$r_i = 3.930\,10^{-3}\,m$$

$$L = 4.853\,m$$

$$k\ (W/m\,°K) = 13.8 + 0.0225\,T\,(°C)$$

$$\rho_{el}(ohm\ m) = 75.9\,10^{-8} + 0.118\,10^{-8}\,T\,(°C)$$

and with the assumption that the average temperature of the wall is 30 $°C$, the temperature difference $T_o - T_i$ is about 1 $°C$. This temperature difference would cause a variation across the wall of only 0.15% for both k and ρ_{el}. This is certainly a sufficiently small variation to allow the use of linear approximations of the effect of variations in k and ρ_{el} with radius on the expression for the temperature difference (A.6).

The expressions for the thermal conductivity and electrical resistivity as a function of the temperature can be written as

$$k = \alpha\,(1 + \alpha' T) \qquad (A.7)$$

and

$$\rho_{el} = b(1 + b'T) . \tag{A.8}$$

First a constant heat flux per unit length (P/L) along the pipe will be considered. As a first approximation, a value of k determined at the average temperature between inside and outside wall will be used, and this value will be expressed as a function of the outside wall temperature. The temperature difference at any axial location along the pipe is then equal to

$$T_o - T_i = \xi \left[1 + \left(\frac{aa'\xi}{2k_o}\right)\right] \tag{A.9}$$

with

$$\xi = \frac{\frac{P}{L}\left[r_o^2 \ln\left(\frac{r_o}{r_i}\right) + \frac{r_i^2 - r_o^2}{2}\right]}{2\pi k_o (r_o^2 - r_i^2)} . \tag{A.10}$$

The thermal conductivity, k_o, is estimated at the outside wall temperature for the particular location considered.

Next the resistivity and the heat flux is computed as a function of the location, assuming as a first approximation that the temperature of the wall increases linearly with x. It is also assumed that the current density averaged over the cross-section of the wall is a constant independent of x. Then

$$p_{\ell,x} = \frac{P}{L} + \left[\frac{I^2}{\pi(r_0^2 - r_i^2)} bb'(T_{o,x} - T_{o,m})\right] \tag{A.11}$$

where $T_{o,m}$ is the outside wall temperature of the pipe at mid-length, $T_{o,x}$ the outside wall temperature at the axial location considered, $p_{\ell,x}$ the

heat production per unit length at that location, and I the intensity of current.

In conclusion, in order to account for the variation of temperature across the wall of the test tube and along its length, with the approximations outlined above, one finds

$$T_{o,x} - T_{i,x} = \xi \left[1 + \frac{a a'}{2 k_{o,x}} \xi \right] \tag{A.12}$$

with

$$\xi = \frac{r_o^2 \ln \left(\frac{r_o}{r_i} \right) + \left[\frac{r_i^2 - r_o^2}{2} \right]}{2 \pi k_{o,x} (r_o^2 - r_i^2)} \zeta \tag{A.13}$$

where

$$\zeta = \frac{P}{L} + \left[\frac{I^2}{\pi (r_o^2 - r_i^2)} b b' (T_{o,x} - T_{o,m}) \right] , \tag{A.14}$$

$$k = a (1 + a' T) \tag{A.15}$$

and

$$\rho_{el} = b (1 + b' T) . \tag{A.16}$$

It turns out that the inner/outer temperature difference computed with this expression is not as dissimilar from that computed with the simple version (A.6) (which assumed k and ro constant everywhere) as might have been expected. The reason for this is that although the power dissipated may increase measurably between the beginning and end of the pipe, the thermal conductivity will do likewise, and these effects cancel one another to a certain extent.

However, the variations in power with the distance along the axis will have a direct influence on the bulk temperature of the fluid. The increase of bulk temperature with distance may thus deviate from a straight line, and this in turn may have a disproportionately large effect on the heat transfer coefficient if the difference between bulk and inside wall temperature is small. It is thus important to evaluate the expression for the bulk temperature of the fluid as a function of the distance along the pipe (see next section).

A.2. **Bulk temperature of the fluid**

As mentioned in the previous section, it is not correct to assume that the bulk temperature of the fluid increases linearly with distance if one desires a computation of the heat transfer coefficients as accurate as possible. This problem arises from the variation in the amount of heat generated in the wall that is due to the increase in its temperature with distance along the test tube.

As an example, it is supposed that the total bulk temperature increase of the fluid is 2 $^{\circ}C$, and that a local bulk temperature deviates by 0.1 $^{\circ}C$ from the temperature computed assuming a linear increase between entry and exit. If the heat transfer coefficient had been computed from an inner wall/bulk temperature difference of 0.5 $^{\circ}C$, say, this 0.1 $^{\circ}C$ deviation would then correspond to a 20% error which is unacceptable. In practice, whereas differences between inner wall and bulk temperature of less than 1 $^{\circ}C$ are common for the newtonian fluids tested, this is not the case for the drag-reducing fluids for which the

error generated would thus be proportionally smaller.

An expression for the computation of the bulk temperature that would take this problem into account must also be evaluated. With the usual assumptions, the first law gives us for the entire pipe

$$P = \dot{m}\ Cp\ (T_{b,ex} - T_{b,ent}) \tag{A.16a}$$

and locally

$$p_{\ell,x} = \dot{m}\ Cp\ \left.\frac{\partial T_b}{\partial x}\right|_x \quad . \tag{A.17}$$

But it was found earlier that

$$p_{\ell,x} = \frac{P}{L} + \left[\frac{I^2}{\pi\,(r_o^2 - r_i^2)}\, bb'(T_{o,x} - T_{o,m})\right] \quad . \tag{A.18}$$

It is thus possible to compute the bulk temperature of the fluid at any location, if its specific heat and the total power are known, with the relation

$$T_{b,x} - T_{b,ent} = \int_o^x \frac{1}{\dot{m}\ Cp}\left[\frac{P}{L} + \frac{I^2}{\pi\,(r_o^2 - r_i^2)}\, bb'(T_{o,x} - T_{o,m})\right] dx \quad . \tag{A.19}$$

This expression can be simplified assuming a linear increase for the wall temperature and an average specific heat (which varies very little with temperature). The final relationship for the local bulk temperature becomes then

$$T_{b,x} = T_{b,ent} + \left[\frac{x}{\dot{m}\ Cp}\left[\frac{P}{L} + \frac{I^2 bb'(T_{o,ex} - T_{o,ent})}{\pi\,(r_o^2 - r_i^2)2L}(x - L)\right]\right] \tag{A.20}$$

which is also expressed in terms of the outside wall temperature (the

one actually measured during the experiments). It is apparent from this formula that the actual bulk temperature at all locations is lower than that which would have been estimated using the constant heat flux approximation. This results from the lower than average heat flux at the beginning of the pipe.

This simpler expression is best for fully-developed flow, because in the entrance region the outside wall temperature will not follow a linear increase pattern. In the computation programs, this problem was circumvented by determining the integral in a piecewise fashion, using the actual outside wall temperatures.

It is important to note that the computation of the bulk temperature at any location is conducted using only the measured entrance temperature and the electrical power. The fact that no direct measurements of the exit bulk temperature are involved in the computations is crucial for most of the non-newtonian fluids. Indeed, the exit bulk temperature could not be measured reliably in certain cases for these fluids.

Both the electric power and the mass flow rate being measured very accurately, the largest error in this expression will thus arise from the lack of information on the specific heat. In some cases, one also may want to include viscous dissipation in the computation of the bulk temperature (see next section).

A.3. **Viscous dissipation**

The increase in temperature due to viscous dissipation may also be evaluated. This value can be approximated by considering an adiabatic system and expressing the conservation of enthalpy. This temperature increase may be expressed as

$$\Delta T = \frac{\Delta p}{\rho Cp} \tag{A.21}$$

where Δp is the overall pressure drop along the pipe. This should be a good approximation even for non-newtonian fluids, although one could argue that the viscoelastic solutions could store energy elastically, or that fibers could be ruptured.

A typical value of pressure drop for water, at the largest flow rates, would be approximately 3.5 atm. With $\rho = 1000 kg/m^3$ and $Cp = 4180\ J/kg°K$, we obtain an increase in temperature of 0.08 $°C$ over the whole length of the pipe. This amounts at the most to 4% for the case of the minimum heating power (2 $°C$ increase in bulk temperature). For the drag-reducing fluids and the high viscosity suspensions used at a lower flow rate, this number would be smaller. In all cases, this correction can be easily taken into account in the computations of the bulk temperature of the fluid.

A.4. **Evaluation of thermal losses**

The test tube has been thermally insulated to prevent losses to the atmosphere. Additionally, there may also be losses due to conduction at the tube ends and in the fluid itself. An estimate of these losses may be made assuming rather extreme conditions.

- Axial conduction in the tube

An average temperature of the tube of 40 $°C$ (k=14.8 $W/m°K$) and a difference in temperature between its ends of 2 $°C$ (or about 0.4 $°C/m$) may be assumed. The cross-sectional area is 2.31 $10^{-5} m^2$. The heat loss is then about 1.4 10^{-4} W, which is certainly negligible.

- Conduction through the Teflon ends

The copper electrodes forming the ends of the tube (which can be assumed to be at the same temperature as the local wall temperature), are abutted to Teflon disks for thermal and electrical insulation. The value of the thermal conductivity for the Teflon is about 0.16 $W/m\,K°$ and the temperature difference across the disks about 5 $°C$. The Teflon disks are approximately 0.15 m in diameter and 0.015 m thick. The corresponding loss for the two disks would then be about 2 W.

- Conduction in the water

An average temperature of 30 $°C$ (k=0.6 $W/m°K$), with an increase in temperature of 2 $°C$ over 5 m may be assumed. The inner diameter of the tube is 7.86 $10^{-3} m$. The heat conducted away would then be approx-

imately 10^{-5} W.

- The generator copper leads

Using k=380 W/m °K, 0.01 m diameter leads, and assuming that the electrode at the end of the tube is 20 °C above the atmosphere and also that the lead is at room temperature 2 m from the electrode (it is heavily insulated), the power lost would then be 0.3 W.

- Thermal insulation around the test tube

Thermal insulation foam (2.5 cm thick) was added around the test tube, electrodes, leads, supply and exhaust lines, and mixing chamber. It is assumed that there is no convection or radiation loss and that the insulating foam has a thermal conductivity equivalent to air (k =0.025 W/m °K). The test tube is 9.553 10^{-3} m outside diameter and 5 m long. Under these conditions, if the tube is 20 °C hotter than the atmosphere it will lose at the most 3 W in that fashion.

- Total loss

The maximum total loss would thus amount to approximately 5.5 W. The heating power used varied between 500 and 10000 W. Therefore, in the worst case, the error generated by all those losses would be 1% of the value of the electric power used in the computation. This is acceptable when compared to the other sources of error involved in the procedure. The assumptions used in the computations of bulk temperature and wall temperature profile appear thus justified.

As a matter of fact, this estimate has been confirmed by direct measurement during the water tests. The heat capacity of the water is well-known, and the measurement of its bulk temperature in the mixing chamber does not present any problem. The ratio between the electric power and the measured increase of enthalpy could therefore be computed in those cases, and was found to be no more than 1 or 2% off from unity.

Appendix B.

MEASUREMENTS, CALIBRATIONS, AND HARDWARE

B.1. Measurement and Calibration of Mass Flow Rate

The piston in the main cylinder has a ball screw rod which is actuated by an electric motor through a gear box and a recirculating ball system. With this system, it is easier to measure than it is to compute the ratio between the speed of the motor (RPM) and the linear displacement of the rod. The motor speed is measured before the gear box, directly on the motor shaft. This location allows a good accuracy for the speed measurements (see app. B.2.).

There are two possible procedures for the calibration of the mass flow rate. The first consists of measuring the ratio between the motor rotation speed and the linear displacement of the rod, and then computing the volumetric flow rate on the basis of the diameter of the cylinder. The problem with this method is, firstly that the "cylinder" is not perfectly cylindrical and being very thin it might also deform substantially under stress; and secondly that there might very well be leaks around the rings under high pressure.

The second method consists of directly measuring the mass flow rate discharged from the cylinder as a function of the motor speed. This method was thought to be potentially more accurate given the availability of high-precision scales and timers for the calibration, provided a careful purge of any air present in the cylinder is conducted before each

run (air vents were fitted to the cylinder for that reason). A series of tests covering the whole range of RPM were conducted with water. The temperature of the water was measured (for density evaluation), as were the RPM, weight of water delivered and duration of the runs.

A series of runs was initially conducted before the pressurized hydraulic system was connected to the back side of the piston (see section 4.2.1.). The results, presented in Fig. B.-1 show that above a speed of 300 rpm, the coefficients between the flow rate and the speed decreased substantially, an indication of a leak from the front (live) side of the piston to the back. The existence of a leak at high RPM was also verified by the visual observation of an accumulation of water on the back side of the piston. The same graph shows that if an equal pressure is maintained on the back side, the leaks disappear. This pressurization procedure had to be used throughout the tests.

During the first tests, it was noticed that under high pressure the whole piston/rod assembly would start spinning because of the nature of the rotary-to-linear displacement transmission (ball recirculation and ball screw rod). This slippage had to be prevented by a system of casters and guiding rails in order to obtain a true linear relationship between the motor speed and the piston motion.

The final expression obtained from these calibration runs and used for all the tests is

$$\dot{Q} = 7.050\,10^{-7}\,RPM \qquad \text{(B.1)}$$

where $\dot{Q}\,(m^3/s)$ is the volumetric flow rate.

The error on this calibration coefficient is estimated to be less than 0.5%. Indeed, subsequent measurements, conducted during and after the actual heat transfer tests in order to check the constancy of this coefficient, also showed a repeatability of better than 0.5%. This good repeatability, made possible by the use of equalized back pressure, seems to disprove the possibility that rings wear and the associated leak increase were of importance during these tests.

It is interesting to note that the use of the first calibration method described above gave a relationship between the RPM and the linear displacement of the rod (in m/s) of

$$\dot{L} = 1.388\,10^{-5}\,RPM \quad . \qquad \text{(B.2)}$$

This value, with an average measured diameter of the cylinder of 0.2545 m would give

$$\dot{Q} = 7.061\,10^{-7}\,RPM \qquad \text{(B.3)}$$

or a difference of only 0.2 % with respect to the value of the coefficient established by the second calibration method.

It should be emphasized here that the accuracy obtained by this method of flow rate measurement is likely to be far better than that obtained by any other method involving such devices as Venturis, orifices, or propellers. All these devices have indeed been shown to exhibit unusual behaviors with non-newtonian fluids that could prevent their

use, or at the very least make a recalibration necessary for each batch of fluid used, because of possible differences in mixing or degradation.

B.2. **Measurement of the Rotational Speed of the Motor**

Several methods had to be tried before satisfactory measurements of the motor speed could be achieved with frequency counters. At first a magnetic pick-up was positioned next to the final gear on the recirculating ball system. (This gear is the only one exposed, the motor and gear box being a single enclosed unit in the configuration used.) This procedure was not adequate because of the low speed of the gear after the reduction box (ratio 14.45, max speed of motor 1750 rpm). These low speeds induced signals of a small amplitude that was also dependent on the RPM, and were very sensitive to interferences from the nearby motors and electrical systems. Several minutes of averaging were also necessary to achieve a good repeatability. At low speeds the accuracy of this method could not be made better than 5% and it was consequently abandoned, the flow rate being the most important measurement in these tests.

The second method used involved a photoelectric system placed on the final gear as well. A large disk pierced by 100 holes was attached to the gear and spun between a LED and a photodiode. An electronic circuit with DC power supply and IC comparators was built to generate a square wave from the photodiode signal. The main advantages of this method are that the amplitude of the final signal could be adjusted and kept constant regardless of the speed, and also that various filters could be

added.

These are important points because the counters used, both the independent ones and that in the A/D converter, all work with a discrete threshold trigger and between fixed limits of amplitude (they measure the wave length by counting triggerings during a preset interval). The capacitor filters are also important because at low speeds the presence of high-frequency parasitic signals could generate large errors. Finally, although this method worked better than the previous one, the limiting factor was still the low frequency of the generated signal (between 2 and 50 Hz).

Consequently, to overcome this last problem, a gear was mounted directly on the shaft of the motor with a corresponding magnetic pick-up. The RPM measured were large enough for the signals generated (by a circuit similar to that described above) to have frequencies larger than 50 Hz, which seemed to be the lowest value giving a good enough accuracy. Through careful shielding of the cables, use of filters and attenuators, the accuracy (as estimated by comparison with manual counting of gear revolutions) finally turned out to be better than 0.1% for motor speeds larger than 50 rpm. This was also verified by the simultaneous use of several counters with different trigger and attenuation settings.

For the actual tests, the signal was measured directly by a frequency counter board in the A/D converter. During these tests, the instantaneous displacement speed of the piston may not have been constant within 0.1%, possibly because of slight variations of the back pressure or of the

ring's friction. The averaging of several sets of measurements taken during the same run likely took care of that problem, however.

It was also initially noticed that slight oscillations of pressure could be measured in the tube; these had a frequency between 0.01 and 0.5 Hz, and were proportional to the speed of the motor. These oscillations were probably induced by a mechanical non-constancy of displacement speed, as suggested by the accompanying cyclic variation in motor noise. This problem was eliminated by the back-pressurization of the piston.

B.3. **Test Tube Dimensions**

The test tube chosen is nominally of 3/8 in. (9.525 mm) outside diameter with a wall thickness of 0.035 in. (0.889 mm). A large number of measurements of the outside diameter (OD) gave an average value of 9.553 mm, whereas the average wall thickness (WT) for several samples was estimated at 0.8465 mm, indicating an inside diameter (ID) value of 7.860 mm. All the previous measured values are estimated to be accurate within approximately 0.5%. The inside diameter was also computed using water and mercury fillings, but these measurements were found somewhat less reliable. The difference between measured and nominal values are +0.3% for the OD, and +1% for ID, which is adequate for industrial-type tubing. The smoothness of the tube was judged to be excellent.

The total length of the tube was found to be 4.853 m. The locations of the thermocouple stations were, expressed in terms of inside diameters:

0, 35.55, 74.12, 151.6, 229.3, 306.7, 390.6, 475.8, 559.4, 610.6, 617.4. The pressure taps were located respectively at 264.4, 348.4, 432.5, 517.0, and 600.9 inside diameters. This disposition ensured that the thermocouples were positioned about half-way between pressure taps. In this fashion, the average pressure drop measurement could be assumed to be representative of the localized pressure drop at the location of the intermediate thermocouple. All lengths measurements were conducted with no more than 1 mm error.

B.4. **Test Tube Properties**

The test tube used was chosen made of stainless steel because this metal has the highest electrical resistivity among the commonly available type of tubings. Accordingly, for a given heating power, the intensity of current necessary would thus be lowest for that case. The potential problem of corrosion is also taken care of with these tubes.

The tube used in this study has a nominal outside diameter of 9.525 mm and a wall thickness of 0.889 mm. (The measured dimensions are described in app. B.3.) This wall thickness was the smallest available, therefore conducive to a high total electrical resistance of the tube and a low temperature drop between the outer and inner wall, both desirable features.

This is an annealed seamless tubing made of AISI 347 stainless steel (columbium stabilized chrome-nickel steel) according to military specifications MIL-T-8808 and to ASTM A-269 for aircraft hydraulic qual-

ity tubing. The values of thermal and electrical conductivity published in the literature for this metal include k=13.8 $W/m°K$ at 0 $°C$, k=16.1 at 100 $°C$, and k=19.0 at 300 $°C$ for the thermal conductivity, and ρ_{el} = 73 10^{-8} Ohm m at 20 $°C$ for the electrical resistivity. (See for example,

- Parr J.G. and A. Hanson. An introduction to stainless steel. Metals Park, Ohio: American Society for metals.
- Hoyt, S.L. 1954. Metals properties (ASME handbook). New York: McGraw-Hill.
- Eckert, E.R. and R.M. Drake. 1972. Analysis of heat and mass transfer. New York: McGraw-Hill.
- Bolz, R.E. and G.L. Tuve. 1984. Handbook of tables for applied engineering science. Boca Raton, Florida: CRC Press Inc.)

The electrical conductivity of the tube was also directly measured as a function of the temperature by immersing a piece of tube in a distilled water bath set at various temperatures. Its electrical resistance was measured (the water conductivity can be neglected) with a milliohmmeter using silver soldered leads (whose resistances were also measured and taken into account). The expression found for the electrical resistivity using the measured values for the inner and outer diameters is:

$$\rho_{el} = 75.9\,10^{-8} + 0.118\,10^{-8}\,T \qquad \text{(B.4)}$$

where ρ_{el} is expressed in Ohm m and the temperature in $°C$. This measured value is slightly larger than the published one, and its accuracy is

estimated at 2%.

However, Yoo (1974) during measurements of a similar tube found the expression

$$\rho_{el} = 70.6\,10^{-8}(1 + 1.481 0^{-3}\,T) \qquad (B.5)$$

where the temperature is expressed in $°F$. A comparison of the 2 expressions at 21 $°C$ shows the present results to give a value of the electrical resistivity of $78.4\,10^{-8}$ Ohm m whereas Yoo's would be $78.0\,10^{-8}$, the difference between the two results being only 0.5%. Accordingly, equation B.4 for the electrical resistivity of the tube was judged acceptable and was used for the computations.

One way of checking the adequacy of this expression is to compare the value it would give for the resistance of the whole tube to the actual measured value of this resistance. One run was chosen at random and showed a voltage drop of 11.69 V for a current intensity of 75.10 A at an average tube temperature of 35 $°C$. To this temperature corresponds a value of $\rho_{el} = 80.0\,10^{-8}$ Ohm m from the expression chosen for the resistivity. It is then possible to evaluate whether this resistivity would give a value of the tube diameter close to the one measured.

The total resistance of the tube is thus 0.155 Ohms. The inside diameter being $7.86\ 10^{-3}\,m$, and using the expression

$$R_{el} = \rho_{el}\,\frac{L}{A_t} \qquad (B.6)$$

where R_{el} is the total resistance of the tube, and A_t its wall cross-sectional area, we end up with a computed outside diameter of

$9.678\,10^{-3}m$. The measured value being $9.553\,10^{-3}m$, the difference between the two is 1.3%, which is acceptable. The measured values for the electrical resistivity are thus probably adequate.

It should also be verified that the electrical resistance of the tube during the heat transfer tests is much smaller than that of the water column in its center, because otherwise some current might be diverted in the water, thereby invalidating the power computations. The resistivity of tap water is estimated to have a value between 1 and 10^6 Ohm m depending on its degree of purity. Using 1 Ohm m as a worst estimate, if the column of water is $7.86\ 10^{-3}m$ in diameter and 4.8 m long, the total resistance found is approximately 10^5 Ohms. Even if the actual suspension or solution used exhibits a lower resistivity than this, the margin between the resistance of the tube and that of the water seems large enough for very little current to be diverted in the fluid in any case.

The measurement of the thermal conductivity of the steel is a much more complex problem, and requires sophisticated equipment. Whereas the tables give us an approximate expression of

$$k_{ss} = 13.8 + 0.0225\,T \qquad \text{(B.7)}$$

(where the thermal conductivity is expressed in $W/m°C$ and the temperature in $°C$, Yoo's expression was

$$k_{ss} = 14.2 + 0.0185\,T \qquad \text{(B.8)}$$

The difference between the two results at 20 $°C$ is only 2%. Accordingly, it was chosen to use equation B.7 for the computations involving the

thermal conductivity of the tube.

B.5. **Calibration of the Thermocouples**

All the thermocouples used in this study were manufactured and calibrated at the Jet Propulsion Laboratory (California Institute of Technology). They were built from a single spool of chromel-constantan wire by an inert gas-arcing technique. No extension wires were used, the thermocouple leads being one piece from the bead to the A/D converter. The beads were approximately 1 mm in diameter. E-type thermocouples were chosen because they have a high output (60 $\mu V/°C$) therefore permitting a good resolution, and also have a low thermal conductivity. Special techniques such as guarding, tree switching, normal mode filtering, and integration were nevertheless used in the data logger to avoid system noise.

The thermocouples were calibrated in oil baths. The results of the calibrations are expressed below as a correction in μV with respect to the standard NBS 125 / IPTS 68 tables.

T(°C)	0	23	70	90
Cor.(μV)	0	-2	-22	-30

These values were used in the data acquisition programs to correct the voltages measured across the thermocouples.

In the A/D converter, the thermocouples were connected to copper leads on an isothermal board. The temperature of this board is measured by a high-accuracy thermistor, and it is then possible to compute

the voltage generated by these extra junctions of known characteristics. Using this software compensation of the measured voltages, it is possible to find the genuine thermocouple emf without using an ice reference. The corrected voltages are then converted to temperatures in the data acquisition programs by high-order polynomials that are best fits of the NBS standard thermocouple tables over the range of temperature desired.

The polynomial fit error may be as high as 0.05 $^{\circ}C$. However, because only temperature differences for the critical measurements are used, this error as well as the wire error is probably eliminated. The repeatability of the measurement by different thermocouples was outstanding. Tests showed that if two thermocouples were immersed in thermal grease or water, the temperatures measured would be within 0.01 $^{\circ}C$ of each other. It is estimated that a temperature difference could be measured accurately with these thermocouples within 0.02 $^{\circ}C$, assuming no drift in their characteristics. For practical purposes, these errors are probably smaller than those introduced by all the problems inherent to the experimental setup such as local variations in the thickness of the tube wall or in positioning of the thermocouples, conduction in the leads etc.

B.6. **Measurement of Densities**

The densities of all the fluids used were measured as a function of the temperature. This was done with calibrated containers and with pyktometers, using thermocouples and electronic scales. These

measurements proved very repeatable and the difference between average densities measured by the two methods was shown to be of the order of 0.1%.

B.7. **Properties of Water**

The properties of water used in the computations are reproduced here in table form for reference:

$T(°C)$	$\rho(kg/m^3)$	$\nu(m^2/s)$	$Cp\,(J/kg\,°K)$	$k\,(W/m\,°K)$	Pr
10	999.7	$1.307\ 10^{-6}$	4192	.5794	9.40
15	999.1	1.140	4186	.5884	8.03
20	998.2	1.004	4182	.5971	7.00
25	996.9	.8930	4180	.6056	6.13
30	995.4	.8010	4178	.6132	5.42
35	993.9	.7237	4178	.6202	4.82
40	992.4	.6580	4179	.6272	4.33
45	990.2	.6019	4180	.6342	3.92
50	988.1	.5534	4181	.6403	3.57

B.8. **Viscometers and Calibration of Capillary Tubes**

In order to determine the viscosity functions of the various fluids studied, two capillary viscometers were built and calibrated. The first one was designed on the basis of the pressurized tank concept. It consists of a plexiglas cylinder of 4.5 in. (0.114 m) ID and 6 in. (0.152 m) high, mounted under compression between aluminium flanges (see fig. 4.-4.). The tank is fitted with a relief valve, compressed air and pressure trans-

ducer hoses, and filling valve. The bottom plate has a central threaded orifice permitting easy interchangeability of the capillary test tubes used. These glass tubes of various lengths and diameters had a threaded nipple fitted at one end to engage in the bottom of the tank. The entry angle on all tubes is 180° and the tops of the tube and nipple were kept flush with the bottom of the tank.

The pressure or vacuum in the tank was measured with a pressure transducer similar to those used for the friction experiments. The pressure transducers were changed according to the range of pressure or vacuum necessary for the tests, in order to obtain the best accuracy. The compressed air and vacuum were maintained constant with regulators. The plexiglas cylinder was inscribed with a scale to permit easy reading of the level in the tank.

It was found unnecessary and impractical to build a constant temperature system around the viscometer, tests having shown that, with thermal insulation, the temperature variations during the experiments could be easily limited to 0.5 $°C$ if necessary, an adequate accuracy for these purposes. The temperature was measured in both the tank and receiving container with thermocouples connected to the computer. The fluid discharged from the vertical capillary was weighed on a laboratory scale (Mettler H20T, resolution 10 μg) and the duration of this collection timed with an electronic chronometer (resolution 0.01 s).

The tubes were calibrated by direct filling with mercury and water, and also indirectly by friction measurement with distilled water in the

laminar regime. The difference between the diameters found with the 2 methods could be as high as 2%. Accordingly, it was thought preferable to calibrate the diameters using the friction method. In this manner, even if an error is introduced by the viscometer or by the procedure used for the measurements (such as entrance effects for example), the measured viscosity of an unknown fluid may nevertheless turn out to be accurate because the same measurement method was used for the calibration with distilled water of well-known viscosity. In other words, the calibrated value of the diameter might not be physically the correct one, but it will nevertheless likely give accurate results for the viscosity if the formulas and procedure are kept the same, because the errors will probably cancel out.

The scatter on the viscosity during tests with identical fluids is usually of the order of 0.5%, which is the estimated accuracy of the method. Precautions have to be taken, however, regarding the zeroing of the transducers, the constancy of the temperature, and the proper mixing of the fluid in the tank to avoid sedimentation and temperature gradients.

The formula used for the calibration of the diameters and for the subsequent determination of viscosities is obtained from a simple balance of pressure drops:

$$p_t - p_a + (\rho g\,(H_t + L_c)) - (1.12\rho V^2) = \frac{\tau_w 4 L_c}{D_c} \qquad \text{(B.9)}$$

where p_t is the pressure in the tank, p_a the atmospheric pressure, H_t the

level of fluid in the tank, and D_c and L_c respectively the diameter and length of the vertical capillary.

The "1.12 ρV^2" term represents the kinetic energy plus the viscous loss at the entrance (see also app. C.2.). This correction was determined by tests to be adequate because it gave values of the diameter that were independent of the flow rate. (Other factors sometimes used for flush entrances, such as 1.25 ρV^2 or simply 1.0 ρV^2, did not.)

If the flow is laminar and the fluid is newtonian, we have

$$\tau_w = \eta \dot{\gamma}_w \tag{B.10}$$

where $\dot{\gamma}_w$ is the wall shear rate (eq. 3.9a), and η is the dynamic viscosity. It is then easy to find an expression involving only measured quantities with only one unknown, either D_c or η, depending on whether it is used for calibration of the diameter or actual measurement of viscosity

$$p_t - p_a + \rho g (H_t + L_c) - 1.12 \frac{\dot{m}^2 4}{\rho \pi D_c^2} = \frac{\eta\ 128\ L_c \dot{m}}{\rho \pi D_c^4} . \tag{B.11}$$

These calibrations were conducted with tubes of various diameters and lengths. The constraints on the viscosity measurements are that the flow must be laminar, that the range of shear rate covered must correspond to that of the heat transfer experiments, and that the diameter of the capillary used should be large with respect to the size of any particles or fibers present in the fluid.

The calibration results for the several tubes used in this study are

Tube	L_c	D_c	L_c / D_c
T-1	.0100 m	1.025 mm	9.75
T-2	.7207	2.134	337
T-3	.7223	1.676	431
T-4	.7223	.8524	847
T-10	.6017	1.025	587
T-11	1.214	.5402	2247
T-11B	.6358	.5402	1177
T-12	1.214	.5400	2248
T-13	1.211	1.038	1166
T-20	.3026	.6448	469

Using the small diameter tubes and the maximum allowable pressure for the tank, it is possible to reach shear rates as high as 100000 s^{-1} (for water). Using vacuum, on the other hand, shear rates as low as 50 s^{-1} can be measured reasonably fast.

The problem with this viscometer is that it is difficult to make measurements at the same shear rate for fluids of different viscosities. This is because the adjustment of the flow rate is done indirectly through the pressure in the tank. The most important parameter for studies of non-newtonian viscosities being the shear rate, however, it was decided to build a viscometer that would allow a more accurate control of this quantity. This was done using a single-action cylinder and piston arrangement actuated by a variable speed electric motor (fig. 4.-5.).

The capillary tubes are placed horizontally in this case, connected to the main reservoir at mid-height by a quick-disconnect coupling. The pressure in the reservoir is measured also at mid-height by a pressure transducer. The dimensions of the piston are known and the displacement of its rod is measured against a ruler and timed. In this fashion, there is no need to collect the fluid in order to measure the mass flow rate (as was the case for the other viscometer).

The same formula as that mentioned above (eq. B.11) is used, except for the absence of the hydrostatic pressure term, because the tube is horizontal. Calibrations and measurements are performed in a similar fashion but the accuracy was found to be better for this device, it is estimated to be about 0.2% on the viscosity for newtonian fluids. For certain non-newtonian fluids, because of problems such as sedimentation, non-homogeneity, or degradation, the repeatability might be slightly worse.

The diameter of the piston is 0.02578 m, therefore we have

$$\dot{m} = 5.220\,10^{-4}\,\rho\,\dot{x}_p \qquad \text{(B.12)}$$

where $\dot{x}_p$ is the displacement speed of the piston. For this expression to be valid, the reservoir has to be carefully purged of all air, which was done before each run. The course of the piston is about 0.10 m. The variable speed DC motor used is a Bodine NSH34RH with a 10:1 reducer (1/15 hp, 17 in lbs of torque at 173 rpm), which activates the helical screw rod through a concentric worm gear unit.

The cylindrical reservoir is 4 in. (0.102 m) in diameter and 3 1/2 in. (0.0889 m) long. It is fitted with drain and filling valves. The range of shear rate covered with this configuration and a 0.6 mm inside diameter tube is from 50 to 30000 s^{-1}.

B.9. **Hardware**

- Milliohmmeter: Hewlett-Packard model HP4328A (used for measurement of electrical resistivity of stainless steel tube).

- Generators:

The 2 DC generators used are motor-driven arc welders (Lincoln SAE-400 and SAE-600). These are respectively rated at 500 and 750 A with 40 arc Volts. For most of the experiments the smaller generator which allowed adjustments of the power from 0 to 3500 W was used. This range covered the desired 2 $^{\circ}C$ increase in bulk temperature for all necessary flow rates. Typically, at 3500 W, this generator would give a current of 150 A for about 23 V of voltage drop across the tube (of average temperature 40 $^{\circ}C$. The bigger generator, under the short-circuit configuration used, could not deliver less than 9000 W, and accordingly was only used for a few high power tests.

Both generators were modified and fitted with remote controls for the tests. The leads delivering the current to the test tube are heavy duty copper welding cables of about 1/2 in. (1.27 mm) core. It is to be noted that the voltage drop was measured directly from the electrodes located at the extremities of the tube, therefore circumventing any drop in the

supply leads.

- Computer

The computer used for the data acquisition and processing was a Hewlett-Packard HP85F with memory extension, mass storage ROM, I/O ROM, plotter/printer ROM, and HP-IB interface. It was connected to a printer (HP82905B), disk drives (HP9121D), and plotter (HP7225A). All the programs were written in Basic, and the instructions to the data logger in machine language. All the computations were conducted in full precision (10 bytes per variable).

- Data logger

The data acquisition unit (HP3497A) was connected directly to the computer. The latter was in charge of controlling the experiment and organizing the data collection by the A/D converter. The data acquisition unit features a real-time clock and a digital voltmeter assembly providing 5 and 1/2 digit resolution and 1 μV sensitivity. For these tests, it was also equipped with a 20-channel relay multiplexer, a 19-channel relay multiplexer with thermocouple compensation, and a reciprocal counter assembly. The standard accuracy for the microvoltmeter is of the order of 0.01% of the reading.

The thermocouple compensation is based on a high-accuracy temperature sensor mounted on the isothermal connector board to which all the thermocouples are directly connected. The temperature of the junctions being known, it is possible to correct for the extra emf they

create through software adjustment. This technique eliminates the need of ice references for the thermocouples.

The whole electrical system had to be carefully grounded and all the leads shielded and connected to guards to avoid additional errors due to differences of potential or induced currents.

- Pressure transducers

A large number of pressure transducers were used, most of them manufactured by Statham (e.g. PM385 and PM8142). The ranges of pressure they cover varied from 0.5 to 100 psid. All these transducers were periodically recalibrated using high-precision equipment at the transducer calibration lab of the Jet Propulsion Laboratory. It is believed that the accuracy of the calibration and polynomial fit is better than 0.1%. These transducers were connected to bridge supplies (Dynamics 6343A) for excitation and the bridges themselves directly connected to the A/D converter for measurement of their output. The excitation and zeroes can be adjusted within 0.1% as well, and these adjustments were conducted systematically before each test.

- Counters

The frequencies measured by the counter board in the data logger were checked against two other counters set with different trigger levels and attenuations (General Radio GR1192 and DANA 8010B), and with function generators (HP3300A). The IC signal processor had a variable power supply (HP721A) for optimum signal triggering. The magnetic

pick-up mounted on the main motor is a Boston Gear MPA140TC.

- Digital voltmeter

Other independent digital voltmeters (DANA 5330, 1 μV resolution) were used to check the measurements of the data logger, to adjust the bridge supplies, to perform various checks with the thermocouples, and to conduct viscometer tests.

- Oscilloscopes

Oscilloscopes (Tektronix 555) were used for all the experiments dealing with the RPM circuits, in order to evaluate the cleanliness of the electric signals.

- Heating current intensity

The current circulating through the test tube was measured with a calibrated resistor (General Electric GE50-140034SNAA). This shunt-type resistor was put in series in the main electric heating circuit. It is rated at 100 mV for 800 A. The voltage across its extremities was measured directly by the microvoltmeter in the data logger. The calibrated accuracy of this resistor is 0.25%.

- Cylinder, piston, and driving train

The cylinder and piston assembly was manufactured by Sheffer (model 10AFB34CRAKW). The shunt winding DC variable speed electric motor driving the piston is a Boston Gear B6-R29594 (1 hp at 1750 rpm), connected to a 14.45:1 reducer (Boston Gear F226D-PH-14G7, 494 in. lbs

of torque). Its control is a Minarik BCR290.

- Thermocouple epoxy

The epoxy used to affix the thermocouples on the test tube is a high thermal conductivity epoxy manufactured by Emerson and Cuming (Stycast 2850 FT). It was verified experimentally that a layer of epoxy of less than 0.5 mm did effectively isolate electrically the thermocouples from the test tube (the difference of potential between tube and ground was never more than about 25 V DC). A layer of epoxy encircling the tube was used to average out possible circumferential variations in temperature, although these were verified to be negligible in most cases. It was necessary, however, to experiment with the thickness and width of the epoxy layers and with the positioning of the thermocouples before repeatable and satisfying results were obtained. This was ascertained by tests involving variable configurations of multiple thermocouples set in thermal grease at the desired locations.

Appendix C.

RELATED PUBLICATIONS

Appendix C.1: "A method of predicting the 'diameter-effect' for heat transfer and friction of drag-reducing fluids." (Matthys, E.F., and R.H. Sabersky. 1982. International Journal of Heat and Mass Transfer 25 (9): 1343-1351.)

Int. J. Heat Mass Transfer. Vol. 25, No. 9, pp. 1343–1351, 1982
Printed in Great Britain

0017-9310/82/091343-09 $03.00/0
Pergamon Press Ltd.

A METHOD OF PREDICTING THE 'DIAMETER EFFECT' FOR HEAT TRANSFER AND FRICTION OF DRAG-REDUCING FLUIDS

E. F. MATTHYS and R. H. SABERSKY
California Institute of Technology, Pasadena, CA 91125, U.S.A.

(*Received* 29 *March* 1982)

Abstract—A multilayered velocity profile has been assumed to exist for 'drag reducing' fluids flowing in a pipe. The profile is characterized by a logarithmic portion offset by an increment Δu^+ from that pertaining to a Newtonian fluid. For a given fluid Δu^+ is assumed to be determined by the shear velocity u_τ. On this basis a method is proposed by which one may predict the effect of changes in diameter on the friction and heat transfer coefficients.

NOMENCLATURE

A, intersection point of viscous and asymptotic layers (Fig. 3);
B, intersection point of asymptotic and logarithmic layers (Fig. 3);
C, concentration of solution [ppm];
C_F, friction coefficient, $\tau_w/[(\rho u_m^2)/2]$;
C_H, heat transfer coefficient, $q_w/[\rho C_p u_m(T_w - T_m)]$;
C_p, specific heat [J kg^{-1} K^{-1}];
D, pipe diameter [m];
k, thermal conductivity [W m^{-1} K^{-1}];
P, parameter characterizing the nature of the solution;
Pr, Prandtl number evaluated at T_m, $(\mu C_p)/k$;
Pr_ε, 'turbulent' Prandtl number, $(\nu + \varepsilon_M)/(\alpha + \varepsilon_H)$;
q, heat flux [W m^{-2}];
q_w, heat flux at wall [W m^{-2}];
R, pipe radius [m];
R^+, dimensionless radius, $(Ru_\tau)/\nu$;
Re, Reynolds number, $(u_m D)/\nu$;
T, temperature [K];
T^+, dimensionless temperature, $(T\rho C_p u_\tau)/q_w$;
T_m, average temperature in pipe [K];
T_w, wall temperature [K];
T_m^+, dimensionless average temperature, $(T_m \rho C_p u_\tau)/q_w$;
T_w^+, dimensionless wall temperature, $(T_w \rho C_p u_\tau)/q_w$;
u, velocity (average of turbulent fluctuations) [m s^{-1}];
u^+, dimensionless velocity, u/u_τ;
u_m, average velocity in pipe [m s^{-1}];
u_m^+, dimensionless average velocity, u_m/u_τ;
u_τ, friction velocity, $(\tau_w/\rho)^{1/2}$ [m s^{-1}];
y, coordinate distance normal to wall [m];
y^+, dimensionless distance from the wall, $(yu_\tau)/\nu$;
y_B, coordinate of point B (Fig. 3) [m];
y_B^+, dimensionless coordinate of point B, $(y_B u_\tau)/\nu$;
y_m, distance from wall at which $u = u_m$ and $T = T_m$ [m];
y_m^+, dimensionless y_m, $(y_m u_\tau)/\nu$.

Greek symbols

α, thermal diffusivity, $k/(\rho C_p)$ [m^2 s^{-1}];
α_ε, total turbulent heat diffusivity, $\alpha + \varepsilon_H$ [m^2 s^{-1}];
Δu^+, shift of logarithmic layer, equation (10);
ε_H, turbulent heat exchange coefficient [m^2 s^{-1}];
ε_M, turbulent momentum exchange coefficient [m^2 s^{-1}];
μ, dynamic viscosity [kg m^{-1} s^{-1}];
ν, kinematic viscosity, μ/ρ [m^2 s^{-1}];
ν_{H_2O}, kinematic viscosity of water [m^2 s^{-1}];
ν_ε, total turbulent momentum diffusivity, $\nu + \varepsilon_M$ [m^2 s^{-1}];
ρ, density [kg m^{-3}];
τ, shear stress [N m^{-2}];
τ_w, wall shear stress [N m^{-2}];
$\tau_{w,0}$, wall shear stress at onset of drag reduction [N m^{-2}].

1. INTRODUCTION

IN THE last decade considerable attention has been paid to the field of non-Newtonian fluids in general and in particular to a special category of these fluids, the dilute polymer solutions of the drag-reducing type. These fluids are of great interest in many applications as they frequently lead to striking reductions in friction and heat transfer as well as in mass transfer.

These characteristics may be of importance in a number of applications including for example pipe-line transport, drag reduction for ships and submarines, firefighting, oil well drilling, and irrigation. Less frequently mentioned but perhaps even more important are industrial processes treating fluids which naturally exhibit strong non-Newtonian behavior such as fibers suspensions, pastes and gums. Such substances may well have to be processed in the preparation of foods or the manufacture of certain chemical products.

The complete and detailed description of the interaction of the molecules or fibers with the flow is, of course, most complex and even a complete formal solution may not always be directly suitable for engineering use, because it may require detailed information on the behavior of the molecules, information which in practice may not really be available.

These considerations have led us to limit our goal to developing a method by which heat transfer and friction coefficients may be predicted for pipes of any size, on the basis of test data obtained in a single pipe. This approach is to some extent equivalent to the common practice of presenting friction and heat transfer coefficients for smooth tubes in terms of Re and Pr. The data for these presentations are also obtainable from tests in a single pipe, which, of course, reduces the required experimental work tremendously. Nevertheless, the proposed approach will still be applicable only for a given solution, that is a solution characterized by such factors as the type of polymer, concentration, and the state of degradation.

2. SUMMARY OF PREVIOUS WORK

Polymer solutions of the drag-reducing type have been studied intensively, and are covered by an extensive literature. For a basic approach of the problem, we refer the reader to the reviews [1, 2] for friction and heat transfer [3, 4].

The drag-reduction phenomena can be described briefly as follows. The Newtonian fluids can be adequately represented by the well-known universal laws

$$C_F = \frac{16}{Re} \tag{1}$$

for laminar flow [curve (1), Fig. 1] and

$$C_F^{-1/2} = 4.0 \log_{10}(Re\, C_F^{1/2}) - 0.4 \tag{2}$$

for turbulent flow [curve (2), Fig. 1].

This is not the case for viscoelastic drag-reducing fluids however. In fact the typical friction curve for the latter will be located in a domain bounded by the Newtonian friction law on the upper side and by the so-called 'maximum drag-reduction asymptote' on the lower side [Virk's asymptote, curve (3), Fig. 1]. Note that in Fig. 1 as well as in the subsequent development, we have used a simplified Reynolds number as defined for Newtonian fluids. The extension to a Reynolds number corrected on the basis of a 'power law' [5, 6] should present little difficulty as the method remains unchanged in that case. Also, the correction will most probably be small for the dilute solutions of polymers in a Newtonian solvent generally used for drag-reduction purposes. The experimental asymptote has been found to be remarkably insensitive to polymer nature, concentration and solvent, constituting a seemingly 'absolute' limitation to the decrease in friction made possible by the presence of a drag-reducing agent. Virk's equation [2] for the asymptote is

$$C_F^{-1/2} = 19.0 \log_{10}(Re\, C_F^{1/2}) - 32.4. \tag{3}$$

The actual position of the friction curve between those limits is unknown *a priori* and will depend on all the factors previously mentioned. An example of such a curve is shown in Fig. 1 and designated by curve (4).

In particular, it has been often noted that there is a rather strong influence of the diameter of the pipe on the friction law, all other factors being constant, as clearly illustrated in Fig. 2 based on ref. [7] whose data we will subsequently use for comparison with the values predicted from our approach.

The problem of the diameter effect is of particular importance as it would be most valuable to predict the friction (and heat transfer) in large scale pipes (which may be required in actual industrial applications) from data obtained with relatively small sizes in the laboratory. Accompanying the reduction in friction, a corresponding decrease in heat transfer takes place. The two phenomena cannot however be directly related by a simple law. The C_H vs Re curves will have for upper bound the Newtonian relationship described by the traditional Colburn analogy

$$C_H Pr^{2/3} = C_F/2 \tag{4}$$

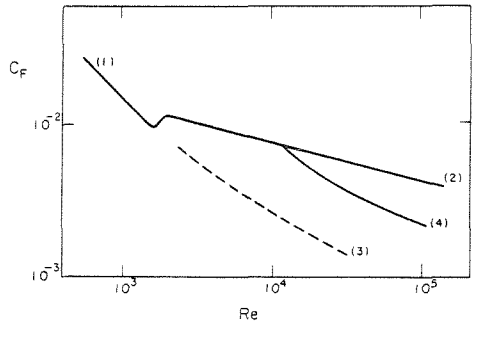

FIG. 1. Typical friction laws: friction coefficient (C_F) vs Reynolds number (Re). Curve (1): laminar flow; (2): Newtonian turbulent flow; (3): Virk's maximum drag reduction asymptote; (4): typical drag reducing fluid.

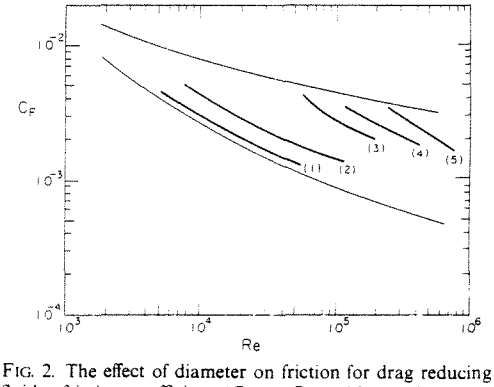

FIG. 2. The effect of diameter on friction for drag reducing fluids: friction coefficient (C_F) vs Reynolds number (Re). Solution: 500 ppm guar gum in water [7]. Curve (1): 4.1 mm dia. pipe; (2): 10 mm; (3): 52.5 mm; (4): 104.7 mm; (5): 208 mm.

and for lower bound the minimum heat transfer asymptote, an expression for which has been proposed as [4]

$$C_H Pr^{2/3} = 0.03\, Re_a^{-0.45} \tag{5}$$

where Re_a is a Reynolds number based on the apparent viscosity at the wall.

It is significant that the data and studies of heat transfer are much scarcer than the corresponding friction data for this kind of fluids. From those available, it is important to note, as has been suggested for fiber suspensions as well as for polymer solutions [4] that the often assumed Reynolds analogy ($\varepsilon_M = \varepsilon_H$) is most probably not applicable in general for any viscoelastic drag-reducing solutions. Furthermore, when taking or evaluating the experimental data, one has to take into account radical departures from Newtonian behaviour such as greatly lengthened entrance regions [4] and the anomalous readings by classical instruments (e.g. hot wire, pitot tubes). The study of heat transfer data, however, is often doubly rewarding as it may not only be helpful in providing information for design purposes, but it may also lead to a better understanding of the turbulent transport mechanism for heat and momentum transfer.

Various models have been proposed for the representation of the velocity profile in terms of the non-dimensional quantities u^+ and y^+ as used in the classical turbulent universal profile. These models are related to expressions that have been designed in the case of Newtonian fluids to represent the smooth transition between the laminar sublayer

$$u^+ = y^+, \tag{6}$$

the logarithmic profile [9]

$$u^+ = 2.5 \ln y^+ + 5.5 \tag{7}$$

and the outer wake defect law [10]. A good example is [11]

$$y^+ = u^+ + e^{-5.5K}\left[e^{Ku^+} - 1 - Ku^+ - \frac{(Ku^+)^2}{2} - \frac{(Ku^+)^3}{6}\right] \tag{8}$$

with $K = 0.4$.

3. THE DIAMETER EFFECT ON THE FRICTION COEFFICIENT

3.1. *The velocity profile*

In the present proposed approach, we will, for the sake of simplicity, use Virk's 3-layers model [2] which consists of the classical viscous sublayer [equation (6), layer 1 in Fig. 3], an 'ultimate' (or 'asymptotic') profile

$$u^+ = 11.7 \ln y^+ - 17.0 \tag{9}$$

(layer 2, Fig. 3) and a logarithmic layer

$$u^+ = 2.5 \ln y^+ + 5.5 + \Delta u^+ \tag{10}$$

(layer 3, Fig. 3). The logarithmic portion will be parallel to the Newtonian one (layer 4, Fig. 3) but

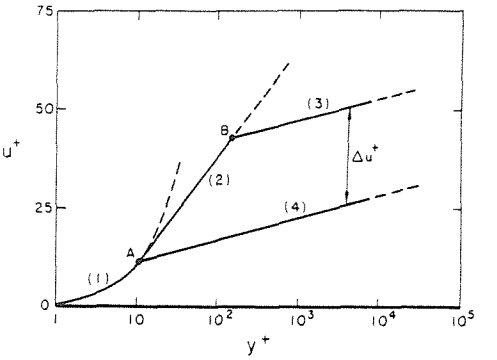

FIG. 3. Virk's velocity profile model: Dimensionless law of the wall velocity ($u^+ = u/u_*$) vs dimensionless distance from the wall ($y^+ = (yu_*)/\nu$). Curve (1): viscous sublayer; (2): Virk's elastic sublayer (3): logarithmic layer; (4): Newtonian logarithmic layer.

displaced by an amount Δu^+ which is assumed to be a function of the nature of the polymer solution, its concentration, state of degradation, flow conditions etc. Some authors have proposed that the logarithmic portions of the velocity profiles are not exactly parallel to each other and certain corrections have been suggested [12]. These are generally small, however, and we will neglect them in this first approach. We will also neglect the outer wake layer as is often done for pipe flow without adverse pressure gradient, and simply suppose that the logarithmic layer extends to the center of the pipe. We will assume that those conditions exist for the flow of our solutions and re-examine this point as we continue with the development.

The limits of the different layers are then: the triple intersection between the viscous laminar sublayer, the asymptotic profile and the Newtonian logarithmic profile (point A in Fig. 3), and the intersection of the ultimate profile with that of the central core (point B). The triple intersection (point A) is approximated by $y^+ = 12$, and point B is a function of the displacement Δu^+ of the logarithmic portion of the velocity profile with respect to the Newtonian one. This intersection is determined by

$$y_B^+ = \exp\left(\frac{\Delta u^+ + 22.5}{9.2}\right). \tag{11}$$

We will hereafter consider the increment Δu^+ as a typical number characterizing the degree, or in a sense the effectiveness, of the drag reduction. Indeed, if $\Delta u^+ = 0$, the profile collapses to the classical Newtonian one and if Δu^+ is such that $y_B^+ > R^+$, (R^+, non-dimensionalized radius), the profile will consist only of the laminar sublayer and the asymptotic interactive layer. In that case, one would expect to obtain the case defined by Virk's asymptote.

The parameters governing Δu^+ may be derived by following general dimensional analysis and the concepts of the law of the wall. The quantity Δu^+ should

then depend on the type and condition of the polymer described by P and the concentration C. Appropriate forms of this parameter P could be $(u_\tau L)/\nu$ or $u_\tau^2 T/\nu$ where L is a characteristic length of the polymer and T a characteristic time. Many studies have been dedicated to finding expressions for L or T in terms of classical rheological parameters for the polymer solution such as molecular weight, number of chain links in the macromolecules, intrinsic viscosity, radius of gyration or relaxation times. For the purpose of the present study as outlined in the introduction, however, L or T may be regarded as fixed quantities for any particular solution. As a consequence Δu^+ becomes a function of u_τ only.

Making use of the velocity profiles as illustrated in Fig. 3, it is now possible to integrate numerically these profiles to find a relationship between C_F, Re and Δu^+.

Comparing these calculated values of C_F and Re to the corresponding measured values, the appropriate Δu^+ can be determined. Since for a given pipe C_F and Re also fix the value of u_τ, a relation between u_τ and Δu^+ is established. Through repeated tests in the same pipe, the desired range of Δu^+ vs u_τ may be established for each solution. Thus a curve of Δu^+ vs u_τ may be prepared which may be regarded as a basic characteristic of the particular solution.

3.2. *Numerical integration of the velocity profiles*

The steps outlined in Section 3.1 will now be described in some more detail.

Integrating the velocity from the wall ($y = 0$) to the centerline ($y = D/2$), we define an average velocity

$$u_m = \frac{4}{\pi D^2} \int_0^{D/2} 2\pi \left(\frac{D}{2} - y\right) u \, dy \tag{12}$$

and, using the usual relations

$$u_m^+ = (2/C_F)^{1/2}, \tag{13}$$

$$u_\tau = (\nu/D)\, Re\, (C_F/2)^{1/2} \tag{14}$$

with

$$Re = (\rho u_m D)/\mu \tag{15}$$

we find

$$C_F = 2\left[\frac{8}{D^2}\frac{y^2}{u_\tau^2} \int_0^{R^+} (R^+ - y^+) u^+ \, dy^+\right]^{-2} \tag{16}$$

and

$$Re = \frac{8}{D}\frac{y}{u_\tau} \int_0^{R^+} (R^+ - y^+)\, u^+ \, dy^+, \tag{17}$$

equations which give us C_F and Re in terms of u_τ and Δu^+. The value of Δu^+ appears through the logarithmic velocity profile expression and in the determination of the intersection of the asymptotic and logarithmic layers.

Carrying out the computations as indicated by equations (16) and (17) we obtain a series of curves for C_F vs Re, each curve corresponding to a different value of Δu^+. The results are shown in Fig. 4. These curves represent the relationship between C_F, Re and Δu^+ which was mentioned in Section 3.1, and which for convenience we might call the 'general C_F–Re–Δu^+' curve.

Any point on these curves is representing, for that particular 'effectiveness of drag reduction' (i.e. given Δu^+), a certain wall shear stress for a known diameter and viscosity, as

$$\tau_w = \rho[(\nu/D)\, Re (C_F/2)^{1/2}]^2. \tag{18}$$

We have represented only the turbulent flow region since, for the type of fluids under consideration, drag reduction is known to be relevant only to that case.

It is interesting to note the very smooth tangential blending of the constant Δu^+ curves with the maximum drag reduction asymptote. This corresponds to the transition from the asymptotic to the logarithmic layer of the velocity profile.

It is also apparent that, unless u_τ and Δu^+ are such that $R^+ < y_B^+$ (i.e. the flow is still in the region of the drag reduction asymptote), the logarithmic part of the profile very soon exerts a major influence on the Re–C_F curves, as the parallelism to the Newtonian law seems to imply.

It is important to recall that for different diameters, the same value of u_τ will occur at different positions on the curve for a constant Δu^+, thus determining different pairs of the values C_F–Re. Indeed, we know that for the same Re, a given solution in different diameters of pipe will show different values of C_F (the so-called 'diameter effect').

As mentioned before, it is believed that for a given solution there is a unique relationship between u_τ and Δu^+. The value of u_τ will then be sufficient to describe the velocity in the region close to the wall, which is the one probably most responsible for the phenomena considered here. A similar proposition has been well

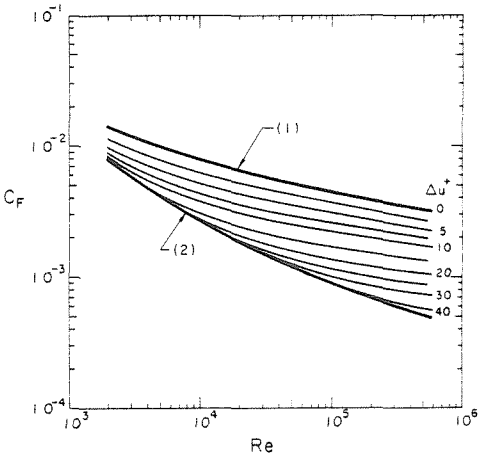

FIG. 4. General C_F–Re–Δu^+ graph (turbulent flow): Friction coefficient (C_F) vs Reynolds number (Re) for various values of Δu^+, (shift from Newtonian logarithmic velocity profile). Curve (1): Newtonian turbulent friction law; Curve (2): Virk's asymptote for maximum drag reduction.

demonstrated by the success of the classical Newtonian universal velocity profile ('law of the wall'). Thus, if the assumption that the wall region effects are predominant is correct, u_τ should be adequate to describe the whole flow and Δu^+ should be only weakly dependent on the diameter. Indeed, this has been indicated experimentally.

It is now possible therefore, after experimental measurements of the C_F vs Re law in a single pipe for a particular solution, to plot these results on our general C_F–Re–Δu^+ graph and to associate a value of Δu^+ with every combination of C_F–Re, that is for every u_τ [equation (14)]. That one-to-one relationship between Δu^+ and u_τ may in fact be regarded as a principal characteristic of a given polymer solution, as pointed out earlier.

3.3. *Prediction of the friction coefficients for different diameters*

The next step now is to apply the previous computation so as to be able to predict for a given solution the drag reduction in a pipe of any diameter from data taken in a single pipe (usually a size conveniently handled in the laboratory). It is important to repeat at this point that we are assuming that the solution to be considered in a pipe of arbitrary size will in all respects be the same as that in the test pipe.

Measurement in a test pipe of a given diameter will, by the procedure explained in the previous section, give us the relation between Δu^+ and u_τ for that particular solution.

The basic assumption we will use is that, as has been suggested before, this relationship Δu^+–u_τ is fairly independent of the diameter of the pipe for a given solution. Experiments have shown that this proposition is acceptable [13]. This assumption, as well as other types of correlations [14–16] have been used, and studies have been conducted [17–20] in an attempt to isolate and understand the nature of the diameter effect.

Using the 'general C_F–Re–Δu^+' graph (Fig. 4) together with the appropriate relationship between u_τ and Δu^+ which is applicable to the solution in question, it is now possible to predict the friction coefficient for the flow in a pipe of any desired diameter.

The computations can be summarized as follows:

Select an arbitrary C_F corresponding to the Re desired for the pipe under consideration.
Compute the associated u_τ [equation (14)].
Evaluate Δu^+ from the experimental graph Δu^+–u_τ.
For the same Re, locate the pair of values C_F–Re specified by the value of Δu^+ on the 'general C_F–Re–Δu^+' graph (Fig. 4).
Find the corresponding value of C_F. This is a new estimate for C_F.
Compute a new u_τ, etc., until the values of C_F converge to the one which then becomes our prediction for the new pipe at the specified Re.

The same procedure for different Re will give us a complete relationship between C_F and Re for that given pipe. Note that the process usually converges rapidly and 2 or 3 iterations are generally enough for each point.

4. THE 'DIAMETER EFFECT' ON THE HEAT TRANSFER COEFFICIENT

4.1. *Basic relationships*

The usual turbulent relations for shear flow may be expressed as

$$\frac{\tau}{\rho} = (\nu + \varepsilon_M)\frac{du}{dy} \tag{19}$$

and

$$q/(\rho C_p) = -\left[\frac{k}{\rho C_p} + \varepsilon_H\right]\frac{dT}{dy}. \tag{20}$$

Now, with

$$T^+ = T/[q_w/(\rho C_p u_\tau)] \tag{21}$$

and

$$\nu_\varepsilon = \nu + \varepsilon_M, \tag{22}$$

$$Pr_\varepsilon = \frac{\nu + \varepsilon_M}{\alpha + \varepsilon_H}, \tag{23}$$

$$\alpha = \frac{k}{\rho C_p}, \tag{24}$$

if we assume fully developed flow, no viscous dissipation, no axial conduction and similar variations of τ/τ_w and q/q_w, we find

$$\frac{dT^+}{dy^+} = -Pr_\varepsilon\frac{du^+}{dy^+}. \tag{25}$$

We can then integrate from $y^+ = 0$ to $y^+ = y_m^+$ where y_m^+ is the position of the average velocity u_m^+ and is also assumed to be corresponding to the average temperature T_m^+ (this should not introduce a large error for smooth tubes).

Let

$$C_H = -\frac{q_w}{\rho C_p u_m (T_m - T_w)}. \tag{26}$$

Then [21]

$$T_m^+ - T_w^+ = -(C_F/2)^{1/2}(1/C_H). \tag{27}$$

Also, with

$$u_m^+ = \int_0^{y_m^+}\left[\frac{du^+}{dy^+}\right]dy^+ \tag{28}$$

we finally find that the combination of terms which is sometimes called the Dipprey number is given by

$$[(0.5C_F/C_H) - 1](C_F/2)^{-1/2} = \int_0^{y_m^+}(Pr_\varepsilon - 1)\left(\frac{du^+}{dy^+}\right)dy^+. \tag{29}$$

Note that we did not need to make any assumption regarding the value of Pr_ε and that the Reynolds analogy, in particular, did not have to be introduced.

Supposing again, as mentioned earlier in Section 3.1, that the polymer solution can be described by the parameters C and P, for a given solution the phenomena will be characterized by u_τ only. We can write then

$$\frac{du^+}{dy^+} = f_1(C, P, y^+) = f'_1(u_\tau, y^+). \tag{30}$$

Assuming also as before a unique relationship between Δu^+ and u_τ for each solution, it follows that

$$y_m^+ = f_2(\Delta u^+, u_\tau) = f'_2(u_\tau). \tag{31}$$

For heat transfer, the Prandtl number of the solution will also have to be included as a parameter. The way in which P has been defined, the possibility that it depends on temperature must be considered too. A given temperature, however, will fix the value of Pr and the dependence on temperature of P, so that for a particular solution and temperature, we have

$$Pr_\varepsilon = f_3(Pr, C, P, y^+) = f'_3(u_\tau, y^+). \tag{32}$$

Finally, after integration with respect to y^+ in equation (29), we find

$$[(0.5C_F/C_H) - 1](C_F/2)^{-1/2} = F(u_\tau). \tag{33}$$

We can thus with the experimental data for C_F–Re and C_H–Re in a single pipe, compute the previous function [equation (33)] which is a characterization of the combined heat transfer and friction reduction induced by that particular solution.

The procedure of predicting heat transfer coefficients for pipes of different diameters may now be summarized.

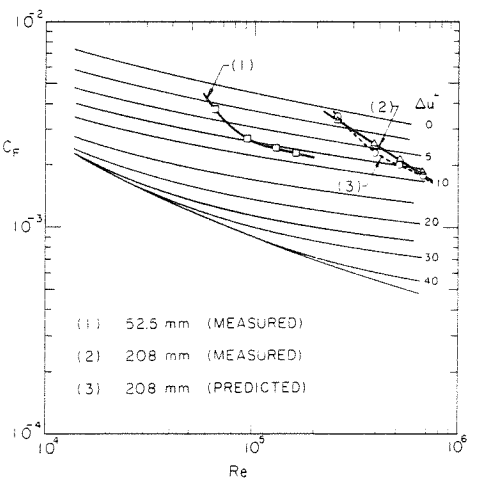

FIG. 5. Prediction of the diameter effect on friction: Friction coefficient (C_F) vs Reynolds number (Re). Solution: 500 ppm guar gum in water [7]. Curve (1): experimental data for 52.5 mm pipe; Curve (2): experimental data for 208 mm pipe; Curve (3): prediction for 208 mm pipe on basis of 52.5 mm data.

After obtaining friction and heat transfer data experimentally in a single test pipe, we can predict the C_F–Re law for another diameter by first computing the Δu^+–u_τ function as explained in Section 3.

We next also compute

$$[(C_F/2C_H) - 1]/(C_F/2)^{1/2} = F(u_\tau) \tag{34}$$

from those data, where $F(u_\tau)$ is a function of u_τ only and is not directly dependent on the diameter. For a desired Re and the predicted C_F, we can compute u_τ [equation (14)]. With these values of u_τ and C_F, C_H is obtained from the previously found relation [equation (34)], which will usually be given in graphical or numerical form.

5. EXAMPLES

5.1. *Prediction of the friction coefficient*

Let us try to predict friction coefficients for a pipe of 208 mm dia from the experimental data for a 52.5 mm one, for a guar gum solution of 500 ppm in water. The experimental data are taken from ref. [7]. In Fig. 5 we have plotted the experimental data for the 52.5 mm pipe on the general 'C_F–Re–Δu^+' graph, the curve is designated (1). From the intersection of the experimental curve with the constant Δu^+ curves, we can compute the relation Δu^+ vs u_τ (Fig. 6). In so doing we have used the expression

$$\nu = \nu_{H_2O}(1 + 4.73\,10^{-4} C_1^{1.157})$$

(where C_1 is the concentration in ppm) for the viscosity.

This curve of Δu^+ vs u_τ is considered to be a unique characteristic of this solution. The shape of this curve is also typical in that it shows a rather rapid increase in Δu^+ after u_τ reaches the 'onset' value (the minimum for which any drag reduction is noted) and more gradual increase of Δu^+ for large values of u_τ.

Incidentally this relationship between Δu^+ and u_τ may be used to address a problem often encountered by engineers working in this field. The fluids we are concerned with do degrade with use and there have been difficulties in quantifying in a convenient way the extent of degradation they experience. Also sometimes the relative effectiveness of different additives has to be

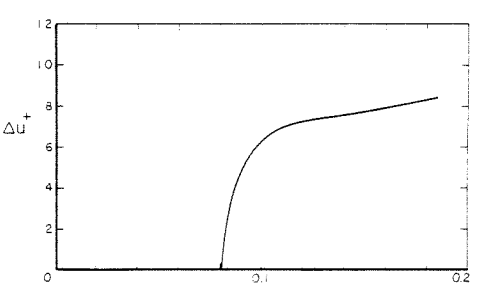

FIG. 6. Characteristic curve for drag reducing fluid: Shift from Newtonian logarithmic velocity profile (Δu^+) vs friction velocity [$u_\tau = (\tau_w/\rho)^{1/2}$]. Solution: 500 ppm guar gum in water [7]. Computed from data in 52.5 mm tube.

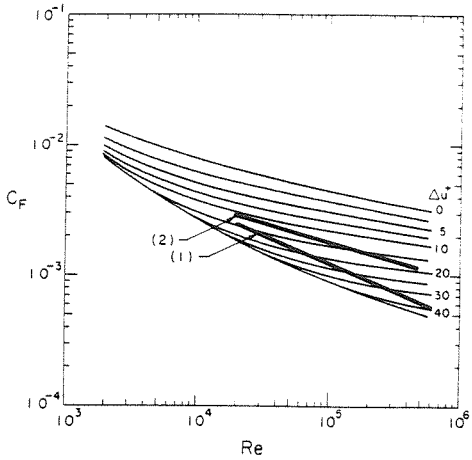

FIG. 7. Prediction of the diameter effect on friction: Friction coefficient (C_F) vs Reynolds number (Re). Solution: 50 ppm polyethylene oxide in water, Pr = 6.16, [22]. Curve (1): experimental data for 0.95 cm dia. pipe; Curve (2): prediction for 5 cm pipe.

evaluated. It may be suggested that the use of the $\Delta u^+ - u_\tau$ relationship might prove convenient for such purpose by enabling us to compute typical ratios of wall shear stress at onset and comparisons of Δu^+ for given u_τ.

Following the steps outlined in Section 3.3, we may now predict the curve of C_F vs Re for a 208 mm pipe with the same gum solution [curve (3), Fig. 5]. We have plotted for comparison the actually measured data for a 208 mm pipe as given in ref. [7] (curve 2, Fig. 5).

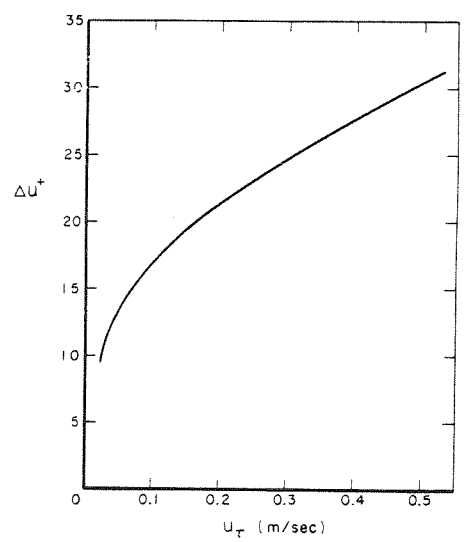

FIG. 8. Characteristic curve of drag reduction: Shift from Newtonian logarithmic velocity profile (Δu^+) vs friction velocity [$u_\tau = (\tau_w/\rho)^{1/2}$]. Solution: 50 ppm polyethylene oxide in water. Pr = 6.16 [22]. Computed from data in 0.95 cm tube.

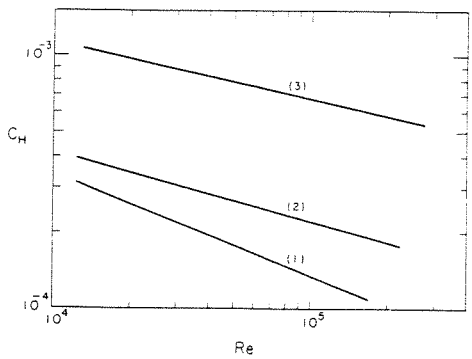

FIG. 9. Prediction of the diameter effect on heat transfer: Heat transfer coefficient (C_H) vs Reynolds number (Re). Solution: 50 ppm polyethylene oxide in water Pr = 6.16 [22]. Curve (1): experimental data for 0.95 cm pipe; Curve (2): prediction for 5 cm pipe; Curve (3): Newtonian heat transfer law.

The agreement is rather good, suggesting that the proposed method might be based on a reasonable concept of the transfer processes.

5.2. *Prediction of the heat transfer coefficient*

We have not been able so far to find suitable data in the literature mentioning explicity heat transfer results for different diameters and providing all the necessary information. We were thus not able to actually compare the prediction for heat transfer with actual experimental data.

However, for a better illustration of the method, we will use here data from ref. [22]. From measurements of a solution of 50 ppm of polyethylene oxide in water in a 0.95 cm dia. tube, at a temperature corresponding to Pr = 6.16, we will try to predict friction and heat transfer for a hypothetical 5 cm dia. tube in the same conditions.

In Fig. 7, we show the measured friction data for a

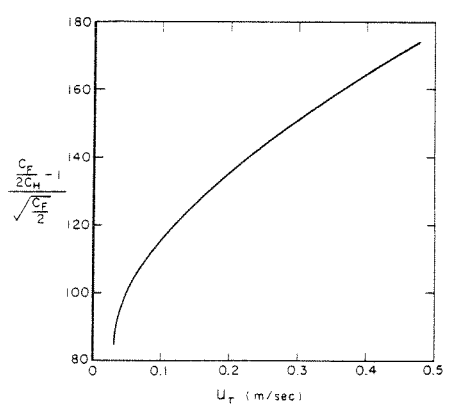

FIG. 10. Characteristic combined heat transfer and friction curve for drag reducing fluid: Dipprey number $\{[(0.5C_F/C_H) - 1]/(C_F/2)\}^{1/2}$ vs friction velocity [$u_\tau = (\tau_w/\rho^{1/2})$]. Solution: 50 ppm polyethylene oxide in water, Pr = 6.16 [22]. Computed from data in 0.95 cm tube.

0.95 cm pipe [curve (1)] and the predicted data for a 5 cm pipe [curve (2)]. The predictions were obtained as described in Section 5.1, and the Δu^+ vs u_τ curve used in the process is shown in Fig. 8.

To obtain the heat transfer coefficient, it is now first necessary to plot the parameter $\{[(0.5C_F/C_H) - 1]/(C_F/2)^{1/2}\}$ vs u_τ which can be done from the data for the 0.95 cm tube. The curve is shown in Fig. 10, with the aid of which, C_F and u_τ being already computed, the appropriate value for C_H can be easily obtained. The resulting graph of C_H vs Re for the 5 cm tube is shown in Fig. 9, together with the data for the smaller pipe. For reference the heat transfer coefficient for a Newtonian fluid with $Pr = 6.16$ [curve (3)], computed from Colburn analogy, is also shown

Although it is not possible at this time to compare these results with actual data, they are likely to give a valid estimate for the illustration of the importance of the diameter effect on heat transfer, an effect usually far from negligible.

Indeed, it has been shown that the heat transfer is usually reduced even more than the friction by the drag-reducing additive. Studies have been conducted (for example [4]) to estimate the values of heat and momentum transport coefficients that would lead to the observed heat transfer and drag reduction, and it has been shown that the heat transport coefficient can be much lower close to the wall than the momentum one for certain solutions.

6. SUMMARY AND CONCLUSIONS

We have reported here a proposed method of predicting the diameter effect for drag-reducing solutions.

A simplified model of the velocity profile is assumed which includes a shift, Δu^+, of the logarithmic layer. This velocity profile is numerically integrated to compute a 'general C_F–Re–Δu^+' graph. We can then obtain for the solution considered a relationship between this shift Δu^+ and the friction velocity u_τ using data obtained for experiments in a single pipe.

This relationship is taken as a major characteristic describing the behavior of the drag-reducing fluid and is assumed to be valid regardless of the diameter of the pipe. It is then possible to make predictions for the friction in pipes having different diameters.

Rather analogous assumptions could be made in analyzing the heat transfer problem. As a result it was shown that the Dipprey number $[(0.5C_F/C_H) - 1]/(C_F/2)^{1/2}$ for a given solution should be a function of the friction velocity u_τ only.

The use of this last function allows us to make predictions for heat transfer in a pipe of any diameter, on the basis of a set of heat transfer experiments taken in a single pipe with the fluid to be examined.

Experimental data for friction were available for comparison with the values predicted by the proposed method. The agreement was considered quite satisfactory.

REFERENCES

1. J. W. Hoyt, The effect of additives on fluid friction, *Trans. Am. Soc. Mech. Engrs*, Series D, *J. Bas. Engng* **94**, 258–285 (1972).
2. P. S. Virk, Drag reduction fundamentals, *A.I.Ch.E. Jl* **21**, 625–656 (1975).
3. Y. Dimant and M. Poreh, Heat transfer in flows with drag reduction, in *Advances in Heat Transfer*, Vol. 12, pp. 77–113 (1976).
4. Y. I. Cho and J. P. Hartnett, Non-Newtonian fluids in circular pipe flow, in *Advances in Heat Transfer*, Vol. 15, pp. 59–139 (1981).
5. A. B. Metzner and J. C. Reed, Flow of non Newtonian fluids, correlation of the laminar, transition and turbulent flow regions; *A.I.Ch.E. Jl* **1**, 434–440 (1955).
6. D. W. Dodge and A. B. Metzner, Turbulent flow of non-Newtonian systems, *A.I.Ch.E. Jl* **5**, 189–204 (1959).
7. J. P. De Loof, B. De Lagarde, M. Petry and A. Simon, Pressure drop reduction in large industrial ducts by macromolecular additives, *2nd Int. Conf. on Drag Reduction*, BHRA Pub., paper B2 (1977).
8. A. L. Moyls and R. H. Sabersky, Heat transfer and friction coefficients for dilute suspensions of asbestos fibers, *Int. J. Heat Mass Transfer* **21**, 7–14 (1978).
9. J. Nikuradse, Gesetz mässigkeiten der turbulenten strömung in glatten Rohren, *V. D. I., Forsch.* **356** (1932).
10. D. E. Coles, The law of the wake in turbulent boundary layer, *J. Fluid Mech.* **1**, 191–226 (1956).
11. D. B. Spalding, A single formula for the law of the wall, *J. Appl. Mech.* **28**, 455–457 (1961).
12. D. C. Bogue and A. B. Metzner, Velocity profiles in turbulent pipe flow; *I/EC Fundamentals* **2**, 143–149 (1963).
13. T. T. Huang, Similarity laws for turbulent flow of dilute solutions of drag reducing polymers, *Physics Fluids* **17**, 298–309 (1974).
14. J. G. Savins and F. A. Seyer, Drag reduction scale-up criteria, *Physics Fluids* **20**, S78–S84 (1977).
15. P. Katsibas, C. Balakrishnan, D. White and R. J. Gordon, Drag reduction correlations; *Int. Conf. on Drag Reduction*, September 1974, BHRA Pub., paper B2 (1974).
16. P. S. Granville, Scaling-up of pipe flow frictional data for drag-reducing polymer solutions; *2nd Int. Conf. on Drag Reduction*, BHRA Pub., paper B1 (1977).
17. R. Y. Ting, Diameter dependence on the cutoff molecular weights of drag reducing polymers; *J. Appl. Polym. Sci.* **20**, 3017–3023 (1976).
18. C. S. Wells, Use of pipe flow correlations to predict turbulent skin friction for drag reducing fluids, *J. Hydronautics* **4**, 22–26 (1970).
19. J. H. Elliott and F. S. Stow Jr., Solutions of drag reducing polymers: diameter effect and rheological properties, *J. Appl. Polym. Sci.* **15**, 2743–2748 (1971).
20. D. D. Taylor and R. H. Sabersky, Extrapolation to various tube diameters of experimental data taken with dilute polymer solutions in a smooth tube, *Lett. Heat Mass Transfer* **1**, 103–108 (1974).
21. R. L. Webb, E. R. Eckert and R. J. Goldstein, Heat transfer and friction in tubes with repeated rib roughness, *Int. J. Heat Mass Transfer* **14**, 601–617 (1971).
22. P. M. Debrule and R. H. Sabersky, Heat transfer and friction coefficients in smooth and rough tubes with dilute polymer solutions, *Int. J. Heat Mass Transfer* **17**, 529–540 (1974).

Résumé—Un profil de vitesse multi-couches est supposé exister pour les fluides du type 'réducteurs de friction' lors de leur écoulement en tube.

Le profil est caractérisé par une portion logarithmique rehaussée d'un incrément Δu^+ par rapport à celle représentant les fluides Newtoniens. Pour une certaine solution, Δu^+ est supposé être déterminé par la 'vitesse de cisaillement' u_τ.

Sur ces bases, une méthode est proposée à l'aide de laquelle il est possible de prédire l'effet d'une variation de diamètre sur les coefficients de friction et de transfert de chaleur.

EINE METHODE ZUR BESTIMMUNG DES "DURCHMESSER-EFFEKTS" BEI WÄRMEÜBERGANG UND DRUCKABFALL VON WIDERSTANDSVERMINDERNDEN FLÜSSIGKEITEN

Zusammenfassung—Die Existenz eines vielschichtigen Geschwindigkeitsprofils wird für die Rohrströmung widerstandsvermindernder Fluide angenommen. Das Profil wird durch einen logarithmischen Bereich, der um das Inkrement Δu^+ gegenüber dem für ein newton'sches Fluid geltendem Profil verschoben ist, charakterisiert. Für ein gegebenes Fluid wird angenommen, daß Δu^+ durch die Schergeschwindigkeit u_τ bestimmt wird. Auf dieser Grundlage wird eine Methode vorgeschlagen, mit deren Hilfe man den Einfluß von Änderungen im Durchmesser auf die Reibungs- und Wärmeübergangskoeffizienten bestimmen kann.

МЕТОД ПРЕДСКАЗАНИЯ "ЭФФЕКТА ДИАМЕТРА" НА ТЕПЛОПЕРЕНОС И ТРЕНИЕ ЖИДКОСТЕЙ, СНИЖАЮЩИХ СОПРОТИВЛЕНИЕ

Аннотация—Предполагается, что снижающие сопротивление жидкости имеют многослойный профиль скорости при течении в трубе. Логарифмическая часть профиля получает приращение на величину Δu^+ по сравнению с характерным для ньютоновской жидкости значением. Для рассматриваемой жидкости предполагается, что величина Δu^+ определяется скоростью сдвига u_τ. На основании этого предложен метод, позволяющий предсказать влияние изменения диаметра на трение и теплоперенос.

Appendix C2.: "A viscometric study of the gelation phenomenon for polymer solutions in kerosene." (Matthys, E.F. 1984. Advances in Rheology (*Proceedings of the 9th International Congress on Rheology*); Eds.: B. Mena, A. Garcia-Rejon, and C. Rangel-Nafaile; vol. 2, 117-125. Mexico: Universidad Nacional Autonoma de Mexico.)

A VISCOMETRIC STUDY OF THE GELATION PHENOMEMON FOR POLYMER SOLUTIONS IN KEROSENE

ERIC F. MATTHYS

California Institute of Technology
Division of Engineering and Applied Science
Pasadena , CA 91125 , USA

ABSTRACT

Certain polymer solutions in laminar capillary flow exhibit an abrupt increase in viscosity if a critical shear rate is exceeded. This behavior is related to the gelation phenomenon which has been shown to depend on the magnitude of the shear rate as well as on the duration of exposure. We have investigated this behavior for the case of a polymer designed to reduce misting when dissolved in jet fuel. In these experiments the influence of several parameters on the critical shear rate and on the extent of the viscosity increase was studied. In particular the effect of temperature, concentration, light-induced aging, and thermal degradation were examined. Some results characterizing this gelation phenomenon are presented here. Their analysis in the light of cone and plate rheometer data suggest a thickening mechanism developing along the tube. Capillaries of various lengths were used in order to evaluate the importance of the end effects and to illustrate the mechanical degradation influence at high shear rates. Similar measurements in a short tube were conducted to provide an estimate of the contribution of the extensional entrance flow on the pressure drop and the thickening of the solution.

KEYWORDS

Gelation, polymer solutions, viscosity, shear-thickening, capillary, viscoelasticity, end effects, antimisting kerosene.

INTRODUCTION

In the past few years studies have been conducted on polymer solutions in kerosene with the intention to develop an additive which, when dissolved in jet fuel, would provide fire protection during survivable crash landings of airplanes. This "antimisting kerosene" (AMK), as its name implies, is designed to reduce the possibility of having very fine mists develop from ruptured fuel tanks. These mists are a major cause of fire when ignited by hot engine parts or sparks.

It has been shown that after addition of small quantities of special polymers to the fuel, a high air velocity will induce the creation of fairly large filaments and blobs of material rather than the usual dispersion of very small droplets that is much easier to ignite. This phenomenon is usually credited to high extensional viscosities or viscoelastic effects introduced in the otherwise newtonian jet fuel by the presence of the polymer. The polymer used in this study, *FM-9*^{TM}, has been developed by Imperial Chemical Industries and has been the subject of various studies in the past. Mannheimer (1983), among several detailed analyses of the rheological characteristics of this polymer and of quality control and degradation techniques, has successfully related measurements in packed tubes and capillaries to flammability tests in a spinning disc atomizer. Flammability tests from various sources were also correlated

by Peng and Landel (1983) with their thorough investigation of the gelation behavior of FM-9 in a cone-and-plate rheometer. Several large scale fire tests have also been conducted (Miller and Wilford, 1973; Salmon, 1981; San Miguel and Williams, 1978).

Our present work is dedicated to a systematic study of the shear-dependent thickening or "gelation" phenomenon exhibited by this AMK in laminar capillary flows. We have attempted to isolate the various parameters having an influence on this behavior and to characterize their effects in terms of viscosities. Some of the factors studied were concentration, temperature, exposure to light, cold storage, thermal and mechanical degradation, end effects and orifice flows. In this article we will limit ourselves to characterizing the gelation phenomenon and to presenting a few results illustrating its manifestations in laminar capillary and short tube flows.

EXPERIMENTAL SET-UP AND FORMULATION OF RESULTS

Our set-up is based on the capillary pressure drop method for measurement of the viscosity. It includes a tank that can be either pressurized or connected to a vacuum pump in order to cover the largest possible range of shear rates (for the tubes used in this study we can typically control the shear rate from 100 to 100000 sec^{-1} for fluids such as water or kerosene while maintaining the flow in the laminar regime). This tank is connected to a vertical capillary freely discharging to the atmosphere.

The mass flow rates were measured by the weight/time method while the pressure in the tank was obtained from a calibrated pressure

transducer. The level of fluid in the tank was measured visually during the experiments and the temperature monitored by thermocouples. All measurements were taken in the "once-through" mode during the steady state phase. The diameters of the tubes were calibrated using distilled water and the well-known laminar newtonian friction laws. The density and viscosity of AMK have been measured as a function of temperature from $-20°C$ to $80°C$. We are using here for the density the expression $\rho = 821.4 - 0.7317\,T$ where T is expressed in degrees Celsius and ρ in kg/m^3.

With these various measurements it is then possible to compute the pressure drop and the wall shear stress ($\tau_w = D\Delta p / 4L$) along the pipe. It is to be noted that this indirect method for evaluating the pressure drop implies the usual newtonian fluid assumption that the pressure of the fluid at the end of the tube is atmospheric. Because of the presence of large normal stress differences this may not be true for viscoelastic fluids, however, and indeed in our case the presence of the associated characteristic die swells was noticed under certain conditions. The computed pressure drop will thus be overestimated, but this error can be reduced to a certain extent by taking measurements in tubes of various lengths. In a similar fashion, one may account for the influence of the entrance effects.

We have also subtracted in all cases $1.12\,\rho\,V^2$ (where V is the average velocity in the pipe) from the computed pressure drop, which is a common correction for entrance effects in newtonian fluids. The remaining difference serves to emphasize the non-newtonian behavior of the solutions.

We present here our results in terms of an apparent viscosity at the wall ($\tau_w/(\rho 8V/D)$) as a function of the associated newtonian laminar wall shear rate ($8V/D$). The use of the correction factor "$(3n+1)/4n$" for power law fluids was abandoned since the exponent n is not computable everywhere in the case of our fluids and, where it is computable, the correction factor turns out to be close to one.

The fluids used in this study were prepared in-situ from a master batch of slurry (*AVGARD*^{TM}) provided by Imperial Chemical Industries, using an in-line blending technique developed at the Jet Propulsion Laboratory by Yavrouian, Ernest and Sarohia (1984). This technique enables us to prepare solutions of consistent quality, but handling precautions have to be observed, the solutions being degradable by exposure to light or agitation.

TYPICAL EXPERIMENTAL RESULTS AND INTERPRETATION

Some results are presented here for a solution of 0.3% by weight of FM-9 in Jet A (a type of kerosene commonly used by commercial aviation). The solution in question was one and a half day old. It was stored at room temperature in a dark location. The effect of degradation due to light exposure and the post-blending transient history will be discussed elsewhere but let us just mention here that these conditions correspond to a fully stabilized, least degraded solution.

A typical viscosity/shear rate curve (Fig. 1) covers 3 basic regimes. For the lower shear rates the viscosity is almost constant. Once the shear rate exceeds a certain value (which is sometimes called the "critical

shear rate"), the viscosity increases very abruptly and will typically jump from 3 10^{-6} to 20 10^{-6} m^2/s at 26.5°*C*. If the shear rate is increased still further, the viscosity will level off and remain roughly constant at the higher value until finally it will slightly decrease again. The critical shear rate is usually observed around 3000 sec^{-1}. The thickening of the solution, even if not always conducive to the formation of an actual gel, is often called "gelation" for simplicity.

An explanation for this characteristic viscosity-shear rate relationship may be proposed as follows. Peng and Landel (1983) in their work on FM-9 solutions found these to be threshold-type time-dependent thickening fluids. Their results show that, when subjected to a constant shear in a cone and plate rheometer, the solution's viscosity will increase with time. The larger the shear, the faster the viscosity increase. Considering our capillary experiments results, it appears then that the lower viscosity region might correspond to shear rates that are not large enough to cause the solution to thicken appreciably during the given residence time of the fluid in the pipe. On the other hand, the data points in the high viscosity region could pertain to shear rates that are sufficient to almost instantaneously thicken the fluid as it enters the pipe. The intermediate points would then result from the averaging over the length process inherent in the capillary pressure drop method, say if it took half the length of the tube before the fluid gelates, the capillary would show a viscosity roughly halfway between the entry and exit ones.

For the tube considered here, L=0.6017 m and D=1.025 mm, the residence times for 8V/D= 2000 and 3000 sec^{-1} respectively are 2.3 and 1.6 sec. An examination of Peng's cone and plate data shows that at

2000 sec^{-1} it takes roughly 10 sec before the viscosity doubles while at 3000 sec^{-1}, in less than a second the viscosity can increase by a factor of ten. A comparison of these numbers with our residence times shows that at 2000 sec^{-1} there probably is not enough time for the material to have a chance to thicken before it reaches the end of the tube. Above 3000 sec^{-1} on the other hand, the viscosity of the fluid could well have reached its highest value soon after the entrance of the tube. In addition to the strong correlation of the two sets of data, a visual examination of the exiting jet also supports the hypothesis of progressive thickening development along the length of the tube. Indeed, the presence of die swells becomes apparent only if the shear rate is increased beyond the critical value.

It is interesting to note that for shear rates slightly larger than the critical one, the viscosity of the fluid reaches a maximum and then remains almost constant. This fact might result from the adoption of a "preferential" state by the fluid through a molecular rearrangement of some sort, possibly as a consequence of a dynamic balance between thickening and break-up of bonds or molecules. This "constancy" seems to support the assumption that the fluid does gelate at the beginning of the tube for that range of shear rates. Otherwise, if the shear rate were increased, the gelation would likely take place earlier in the tube and that, in turn, would be translated into a higher measured viscosity. The decrease in viscosity observed at high shear rates is probably due to mechanical degradation. Indeed, if the material is collected after one high shear rate run through the tube and retested, it will then show a permanent partial loss of viscosity with respect to the first measurement. For shear rates

lower than or slightly larger than the critical one, no degradation is observed.

It is still somewhat unclear what mechanisms at the molecular level are involved in this gelation phenomenon but studies of shear-thickening materials (Eliassaf and Silverberg, 1962; Savins, 1968) have suggested that a shift from intra- to intermolecular hydrogen bonding could possibly be responsible for this type of behavior.

L/D AND END EFFECTS

In Fig. 2 we have reproduced the results obtained in 2 tubes, one of L/D=587 (D=1.025 mm) and one of L/D=1166 (D=1.038 mm). For pre-gelation values of the shear rate, the viscosities measured by the two capillaries are identical. The value of the critical shear rate, as expected, is about the same for the two tubes. For larger values of shear rate, however, a difference between the measured viscosities is apparent. This difference is likely to reflect the influence of end effects and degradation. The degradation, being a function of the residence time, will result in a lower length-averaged viscosity measurement for the longer tube at the same shear rate. This effect, probably more pronounced at higher shear rates, would also explain the faster decrease in viscosity with shear rate observed for the longer tube. If the fluid exhibits viscoelastic properties, it is possible that both the extensional convergent flow at the entrance (all tubes used in this study have a 180° entry angle) and the normal stress differences at the exit of the tube will play an important role in our overestimation of the pressure drop. Intuitively though,

if our hypothesis about the progressive development of the gelation in the tube is correct, the effects would be proportionally more important at the exit where the viscosity and probably the viscoelasticity are higher. In order to test this assumption, we built a short tube of the same diameter but of only about L/D=10.

We assume then as a first approximation that for past-critical shear rates, the total pressure drop along the short tube is representative mainly of the extensional entrance flow in the full length ones. Indeed, the entrance flows should be very similar and, on a proportional basis, the exit effects and the friction along the wall should be much smaller in the short tube because the fluid probably does not have time to thicken before it reaches the exit (characteristically, there was no observation of die swell for the short tube).

The pressure drop measured in the two long tubes and in the short one are presented in Fig. 3 as a function of the shear rate. All these results, as in the previous graphs, have been corrected already to a certain extent for kinetic energy and the newtonian entrance pressure loss by subtracting $1.12\rho V^2$ from the total pressure drop. It is apparent from this graph that the pressure drop in the short tube is negligible with respect to the total pressure drop in the long ones and small compared to the presumed total end effects. At 5000 sec^{-1} for example, where the viscosities are maxima and where no mechanical degradation has been measured, we find for L/D=1166 a total pressure drop of approximately 3.7 bars while for L/D=587 we have roughly 2 bars. Therefore, if we assume the same entrance and exit flows for the two tubes, this implies an excess of about 0.3 bars that could be ascribed to ends effect. At the

same shear rate, the short tube shows only a total pressure drop of 0.02 bar. If the friction along its wall were the same as in the longer tubes, this term only would be approximately 0.03 bars. The fact that the total pressure drop is smaller than this, seems to support the assumption that the fluid has not had time to gelate yet in the short tube thus also implying that probably the exit effects are comparatively small.

In first approximation then, the end effect corrections, estimated at roughly 8% of the total pressure drop for the L/D=1166 tube, could be further subdivided into 10% for the entrance (including $1.12\rho V^2$) and 90% for the exit. If the 0.3 bars difference is caused not only by end effects but also in part by degradation, the correction to be attributed to the entrance would be proportionally larger with respect to the exit. But in any case, we see that on an absolute basis, it would probably amount to no more than 0.02 bars out of 3.7 or 0.5% of the total for the L/D=1166 tube. In order to find out how the "entrance losses" vary with shear rate, we measured the total pressure drop in our short tube for shear rates up to 50000 sec^{-1} . These results are shown in Fig. 4 where we have plotted $1.12\rho V^2$ and the corrected total pressure drop versus shear rate. We see that as the shear rate increases, the residual pressure drop after subtraction of $1.12\rho V^2$, initially larger than this last term, becomes later smaller and then actually tends to zero. The 1.12 factor is empirical and thus probably more adequate for certain Reynolds numbers than others, but we see that for the range of shear rate covered here, it is a fairly good approximation, better than would have been expected a priori.

A correction for end effects will not be applicable for shear rates much larger than the critical one due to the permanent mechanical

degradation influence on the viscosity and accordingly, we have not presented the corrected viscosity curves here.

These results clearly seem to suggest that the viscoelasticity in the extensional entrance flow has very little influence on the pressure drop for this kind of fluid. Also, since the capillary critical shear rate seems to be in agreement with the pure shear (cone-and-plate) data, it is probable that the entrance region has little or no effect on the triggering of the thickening phenomenon.

SUMMARY AND CONCLUSIONS

We have presented here some basic results illustrating the shear-thickening or "gelation" behavior of a FM-9 polymer solution in kerosene as evidenced by viscometric measurements in laminar capillary flow. The effect is clearly seen in the graphs of viscosity vs shear rate, each curve showing an abrupt increase in viscosity at a critical shear rate. These results were examined in the light of cone and plate rheometer data and suggest a mechanism of shear thickening which develops along the tube. A study of the flow in capillaries of various lengths illustrates the mechanical degradation effect for high shear rates and the influence of the end effects on the pressure drop. Similar measurements in a very short tube seem to indicate that the entrance flow correction to the pressure drop is very small.

These phenomena constitute an interesting manifestation at the global flow level of the intricate molecular mechanisms characteristic of these polymer solutions. Information as to the onset of gelation and the extent

of the changes in effective viscosity may thus be of importance in itself. In addition, however, these characteristics may possibly serve as sensitive tools for an evaluation of the solution's condition. Such factors as light-induced aging, concentration, and thermal degradation are indeed readily reflected in a decrease in overall viscosity or a shift in critical shear rate. An analysis of the viscous behavior of the fluid might, therefore, also provide a practical means of predicting the effectiveness of a given solution in preventing mist formation.

ACKNOWLEDGMENTS

This work was partially supported by the Department of Transportation, Federal Aviation Administration, contract DTFA03-80-A-00215. I would also like to express my thanks to Professor R. Sabersky and Doctor V. Sarohia for their continuous support and encouragements throughout this research project and to Professor G. Leal and Mr. A. Yavrouian for many stimulating discussions.

REFERENCES

Eliassaf, J. and A. Silverberg (1962). The gelation of aqueous solutions of polymethacrylic acid. *Polymer*, *3*, 555-564.

Mannheimer, R. J. (1983). Rheological and mist ignition properties of dilute polymer solutions. *Chemical Engineering Communications*, *19*, 221-241.

Miller, R.E. and S.P. Wilford (1973). Fire resistance of some thickened

aircraft fuels under simulated crash conditions. RAE Technical Report No.72167.

Peng, S. T. and R.F. Landel (1983). Rheological behavior of FM-9 solutions and correlation with flammability tests results and interpretations. *Journal of Non-Newtonian Fluid Mechanics*, *12*, 95-111.

Salmon, R.F. (1981). Wing spillage tests using antimisting fuel. Federal Aviation Administration Report No. FAA-CT-81-11.

San Miguel, A. and M.D. Williams (1978). Antimisting fuel spillage and air shear tests at the Naval Weapons Center. Federal Aviation Administration Report No. FAA-RD-78-50.

Savins, J. G. (1968). Shear thickening phenomena in poly(vinyl) alcohol-borate complexes. *Rheologica Acta*, Band 7,Heft 1, 87-93.

Yavrouian, A.H.; J. Ernest and V. Sarohia (1984). Antimisting kerosene: base fuel effects; blending and quality control techniques. Federal Aviation Administration Report No. FAA/CT-83-96

LIST OF FIGURES

Fig. 3: Effect of L/D. Pressure drop along the tube minus $1.12\rho V^2$ vs shear rate. T = 26.5°C, 0.3% FM-9-SD in Jet A. Curve 1: L/D = 1166, D = 1.038 mm. Curve 2: L/D = 587, D = 1.025 mm. Curve 3: L/D = 9.76, D = 1.025 mm.

Fig. 4: Orifice flow. Pressure drop vs shear rate. T = 26.5°C, L/D = 9.76, D = 1.025 mm, 0.3% FM-9-SD in Jet A. Curve 1: $1.12\rho V^2$. Curve 2: pressure drop minus $1.12\rho V^2$.

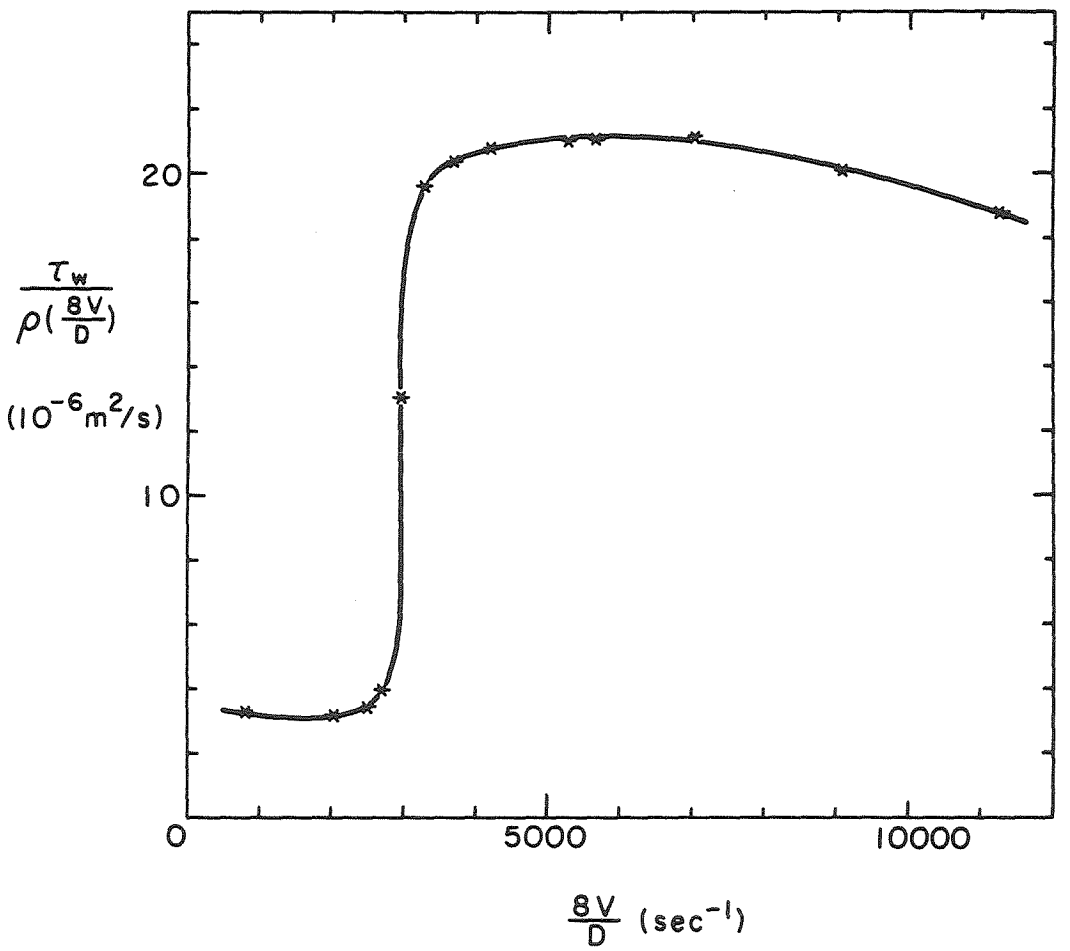

Fig. 1

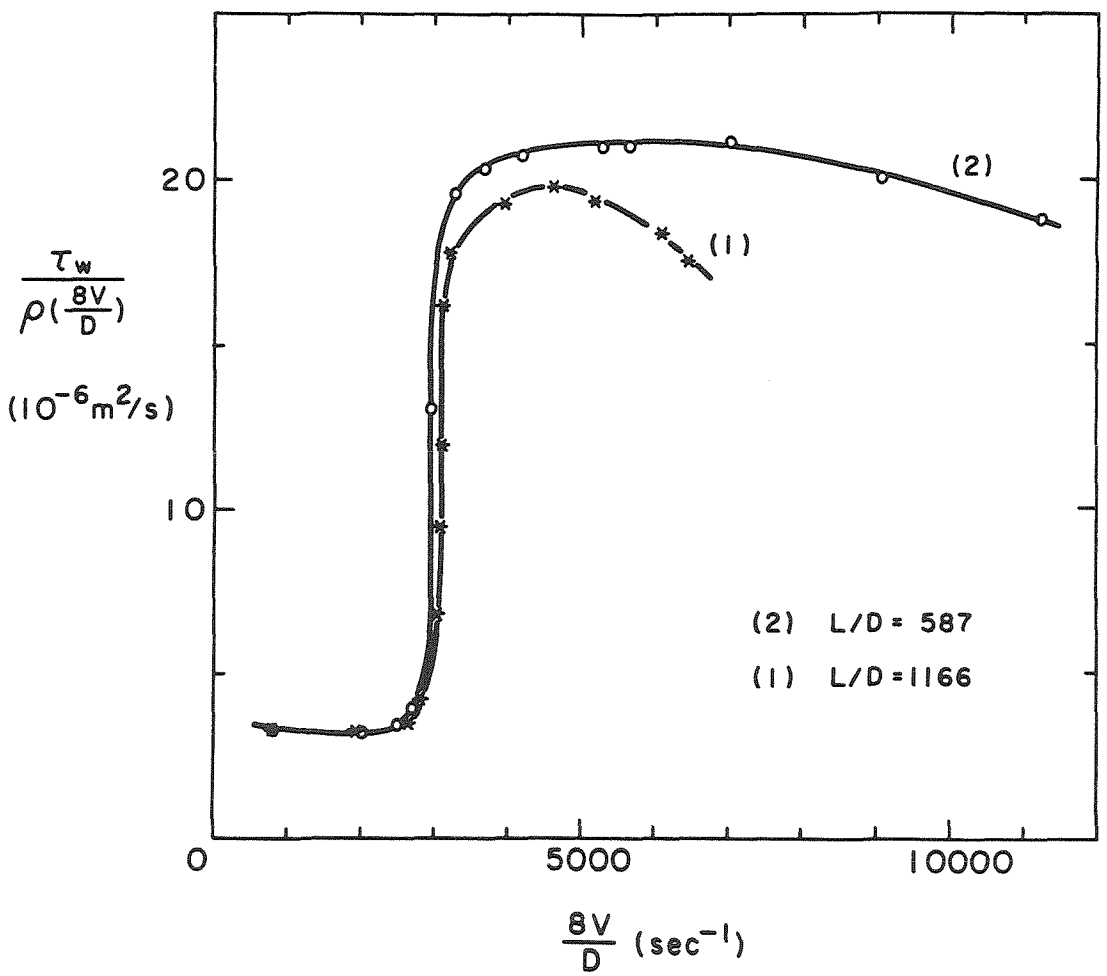
$\frac{\tau_w}{\rho(\frac{8V}{D})}$
$(10^{-6}m^2/s)$
20
10
0
5000
10000
$\frac{8V}{D}$ (sec^{-1})
(2)
(1)
(2) L/D = 587
(1) L/D = 1166

Fig. 2

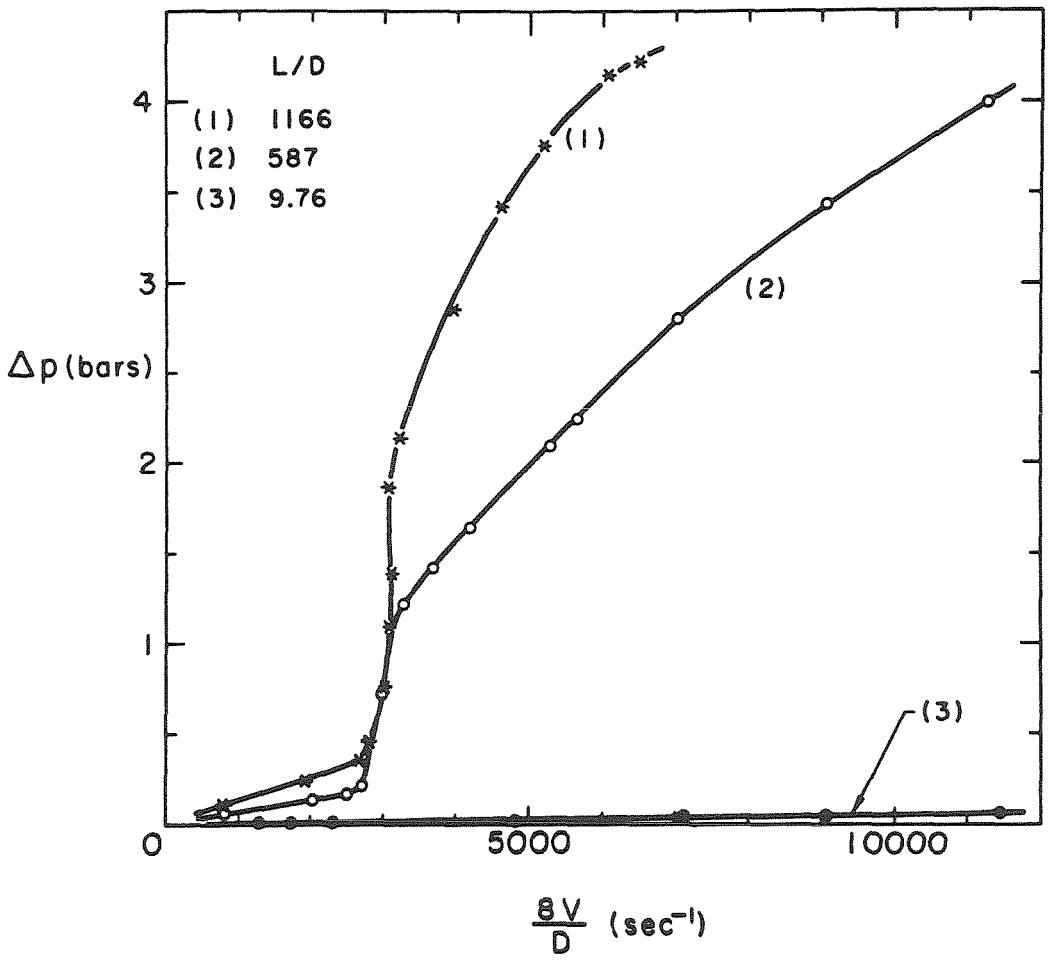

Fig. 3

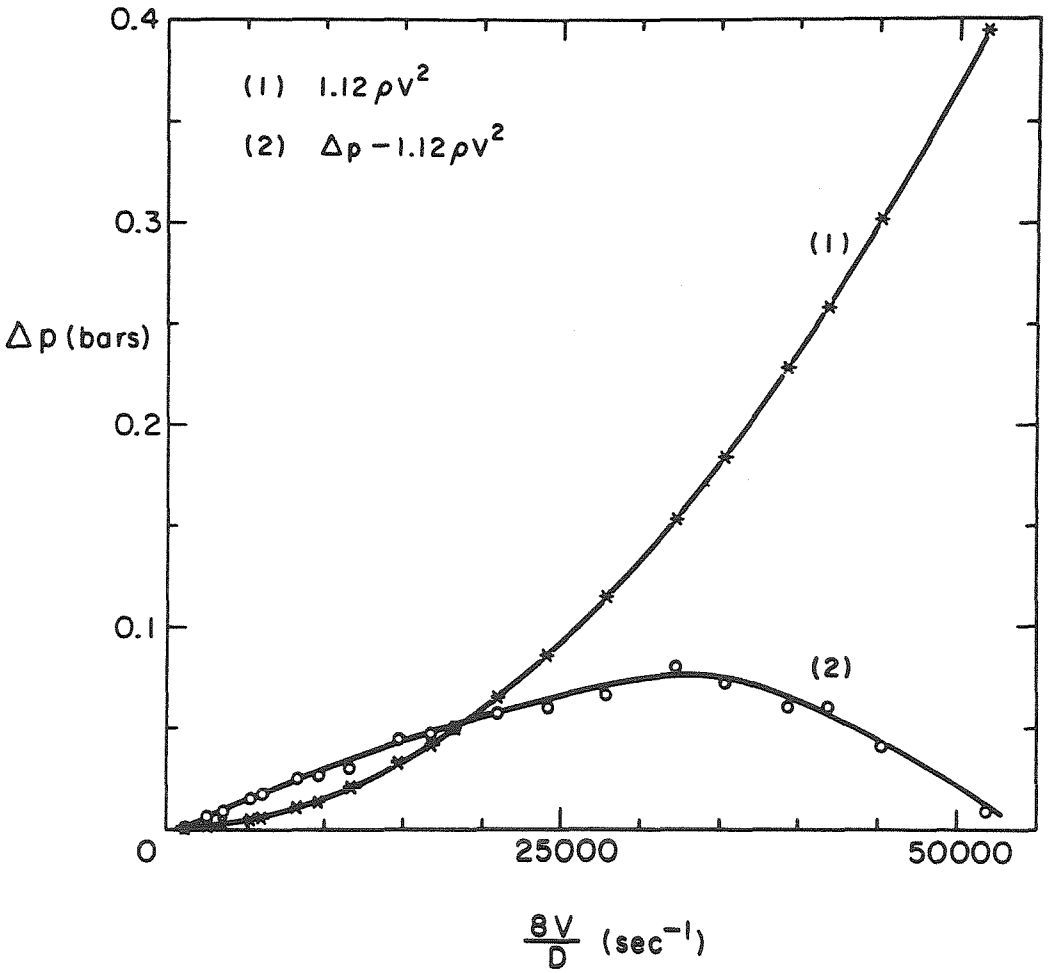
0.4
0.3
0.2
0.1
0
Δp (bars)
(1) 1.12ρV²
(2) Δp − 1.12ρV²
(1)
(2)
25000
50000
8V/D (sec⁻¹)

Fig. 4

Appendix C.3: "Influence of photodegradation and aging on the viscosity of antimisting polymer solutions." (Matthys, E.F. 1985. Journal of Non-Newtonian Fluid Mechanics-in press.)

INFLUENCE OF PHOTODEGRADATION AND AGING ON THE VISCOSITY OF ANTIMISTING POLYMER SOLUTIONS

E.F. MATTHYS

Division of Engineering and Applied Science, California Institute of Technology, Pasadena, California 91125 (U.S.A.)

SUMMARY

The effect of aging and exposure to light on the viscosity of an antimisting polymer solution was investigated in laminar capillary flows. A particular feature of this solution is the abrupt increase in its viscosity that occurs if a critical shear rate is exceeded. Whereas storage in the dark induced only slight modifications of the viscous characteristics of the samples, exposure to light was found to increase the value of the critical shear rate, substantially decrease the maximum post-gelation viscosity and reduce the susceptibility to high shear mechanical degradation.

1. INTRODUCTION

Several polymeric additives have been developed during the past few years in order to reduce the possibility of fire during crash landing of airplanes. When added to kerosene, these polymers inhibit the formation of small droplets in developing mists. Some of these solutions experience a characteristic time-dependent thickening once a threshold shear rate is exceeded. The antimisting kerosene (AMK) examined here is of this type and is based on the *FM*-9^{TM} polymer developed by Imperial Chemical Industries.

This particular polymer has been the subject of several recent studies: Peng and Landel [1] have related measurements in a cone-and-plate rheometer to flammability tests results, Mannheimer [2] has investigated techniques for the measurement of shear and normal stresses, and Yavrouian et al [3] have perfected procedures for quality control and blending.

In an earlier article [4], the viscous behavior of this polymer solution was characterized in terms of a pseudo-viscosity at the wall, $\tau_w/(\rho 8V/D)$, itself expressed as a function of an associated laminar wall shear rate, 8V/D. These results were obtained by means of steady-state laminar pressure drop measurements in capillary tubes of various lengths.

The viscosity of the solution was shown to be approximately constant -usually slightly decreasing- until a "critical shear rate" $\dot{\gamma}_c$ was exceeded. At this point, the viscosity increased sharply by a factor of ten. For shear rates larger than $\dot{\gamma}_c$, the viscosity reached a maximum and then slowly decreased.

This behavior is believed to be related to a shear-induced thickening developing along the length of the tube, that is a function of both the shear rate and the residence time. The permanent decrease in viscosity experienced at high shear rates is thought to be caused by mechanical degradation.

It is known that these polymer solutions are photosensitive and may be degraded to some extent when exposed to light for long periods of time. The purpose of this work was to evaluate the effect of light

exposure on the viscous characteristics of the solutions.

2. EXPERIMENTAL RESULTS

All the samples used in this study were prepared by in-line blending with a master slurry (*AVGARD*^{TM} from Imperial Chemical Industries) using commercial aviation kerosene (Jet A) as solvent. The properties of the fluid and characteristics of the set-up were described in [4]. In order to differentiate the influence of light exposure from aging, reference tests were conducted with samples kept in the dark for 15 days (note that the solution is fully stabilized in approximately one day after blending).

Typical results are presented in Fig. 1. The two curves corresponding to a 1 day old (curve 1) and 15 days old (curve 2) solutions, both stored at room temperature and in the dark, show fairly similar characteristics. The low shear rate viscosities, the critical shear rates, and the maximum post-gelation viscosities were respectively about the same for both cases. For high shear rates, however, the viscosity of the older solution was slightly smaller than the original one and the difference seemed to increase with the shear rate, showing a greater susceptibility to mechanical degradation.

The influence of exposure to light on the viscosities was far more significant. In Fig. 1 - curve (3), data are shown for a fluid exposed for 15 days to both natural light (through common glass windows) and fluorescent light, while stored in a translucent plastic container. The 'pre-gelation' viscosity (i.e. for shear rates lower than $\dot{\gamma}_c$) was slightly smaller

for the light-exposed solution. Its critical shear rate was larger, and the thickening was less abrupt than for the solution aged in the dark. The maximum value of the viscosity in the post-gelation region was noticeably smaller, evidence of a smaller thickening potential. The high shear rate viscosity of the fluid, however, when compared to that of the fluid aged in the dark, demonstrated a reduced susceptibility to mechanical degradation.

Fig. 2 shows the viscosity of solutions exposed to light for 15 days (curve 2) and 50 days (curve 3), as well as that of a freshly blended fluid (curve 1) for reference. The overall changes in viscous characteristics induced by light exposure were, as expected, greater for the 50-days old solution than for the 15-days old one, but the photodegradation influence appeared to become proportionally less important as the duration of exposure increased.

Preliminary experiments were also conducted on storage at high and low temperatures. Whereas the higher temperatures caused thermal degradation, extended storage at -10°C subsequently induced lower critical shear rates and higher post-gelation viscosities than were obtained for the case of room temperature aging.

3. CONCLUSIONS

It is thought that the thickening exhibited by these AMK solutions corresponds to a shear-induced transition from intramolecular to intermolecular hydrogen bonding. The decrease in viscosity associated with mechanical degradation at high shear rate, on the other hand, is probably caused by rupture of the covalent bonds. Additionally, a review of several patents (US4396398, GB2045778, GB2048937) on antimisting jet fuel additives indicated that the example structures of many of these additives would also favor chain scission processes under exposure to light [5]. This latter scission mechanism is probably responsible for the decrease in viscosity shown by the photodegraded samples. Indeed, one would expect that, the molecules having already been broken before being subjected to shear, the intermolecular hydrogen bonding would be responsible for a less extensive network, thereby decreasing the post-gelation viscosity. This initial scission of the molecules would also lower the solution's susceptibility to subsequent mechanical degradation.

In summary, aging alone did not decrease the thickening capability of the fluid, but caused the solution to become more sensitive to mechanical degradation. Light exposure, on the other hand, did seem to greatly decrease this thickening capability and resulted in a reduced susceptibility to mechanical degradation. Exposure to light also increased significantly the critical shear rate.

ACKNOWLEDGMENTS

Financial assistance by the Department of Transportation - Federal Aviation Administration (contract DTFA03-80-A-00215) is gratefully acknowledged. The author would also like to thank Prof. R. Sabersky, Dr. V. Sarohia, and Mr. A. Yavrouian for their support throughout this project, and Dr. R. Liang for valuable discussions on photodegradation.

REFERENCES

1. S.T. Peng and R.F. Landel, Rheological behavior of FM-9 solutions and correlation with flammability tests results and interpretations, J. Non-Newt. Fluid Mech., 12 (1983) 95-111.

2. R.J. Mannheimer, Shear and normal stress measurements of antimisting kerosene at high shear rates, in: Advances in Rheology (Proceedings of the 9th International Congress on Rheology), B. Mena, A. Garcia-Rejon, and C. Rangel-Nafaile (Eds), U.N.A.M. Pub., 1984, vol. 2, pp 1-16.

3. A.H. Yavrouian, J. Ernest and V. Sarohia, Antimisting kerosene: base fuel effects; blending and quality control techniques, Federal Aviation Administration report No. FAA-CT-83-96 (1984).

4. E.F. Matthys, A viscometric study of the gelation phenomenon for polymer solutions in kerosene, in: Advances in Rheology (Proceedings of the 9th International Congress on Rheology), B. Mena, A. Garcia-Rejon, and C. Rangel-Nafaile (Eds), U.N.A.M. Pub., 1984, vol. 2, pp 117-125.

5. B.G. Ranby and J.F. Rabek, Photodegradation, Photo-oxidation and Photostabilization of Polymers, Wiley, London, 1975.

LEGENDS TO THE ILLUSTRATIONS

Fig. 1. Viscosity vs shear rate. T=26.5°C, 0.3% FM-9 in Jet A, L/D=587, D=1.025 mm. Curve (1): fluid stored for 1 day in the dark at room temperature. Curve (2): fluid stored for 15 days in the dark at room temperature. Curve (3): fluid stored for 15 days exposed to light at room temperature.

Fig. 2. Viscosity vs shear rate. T=26.5°C, 0.3% FM-9 in Jet A, L/D=587, D=1.025 mm. Curve (1): fluid stored for 1 day in the dark at room temperature. Curve (2): fluid stored for 15 days exposed to light at room temperature. Curve (3): fluid stored for 50 days exposed to light at room temperature.

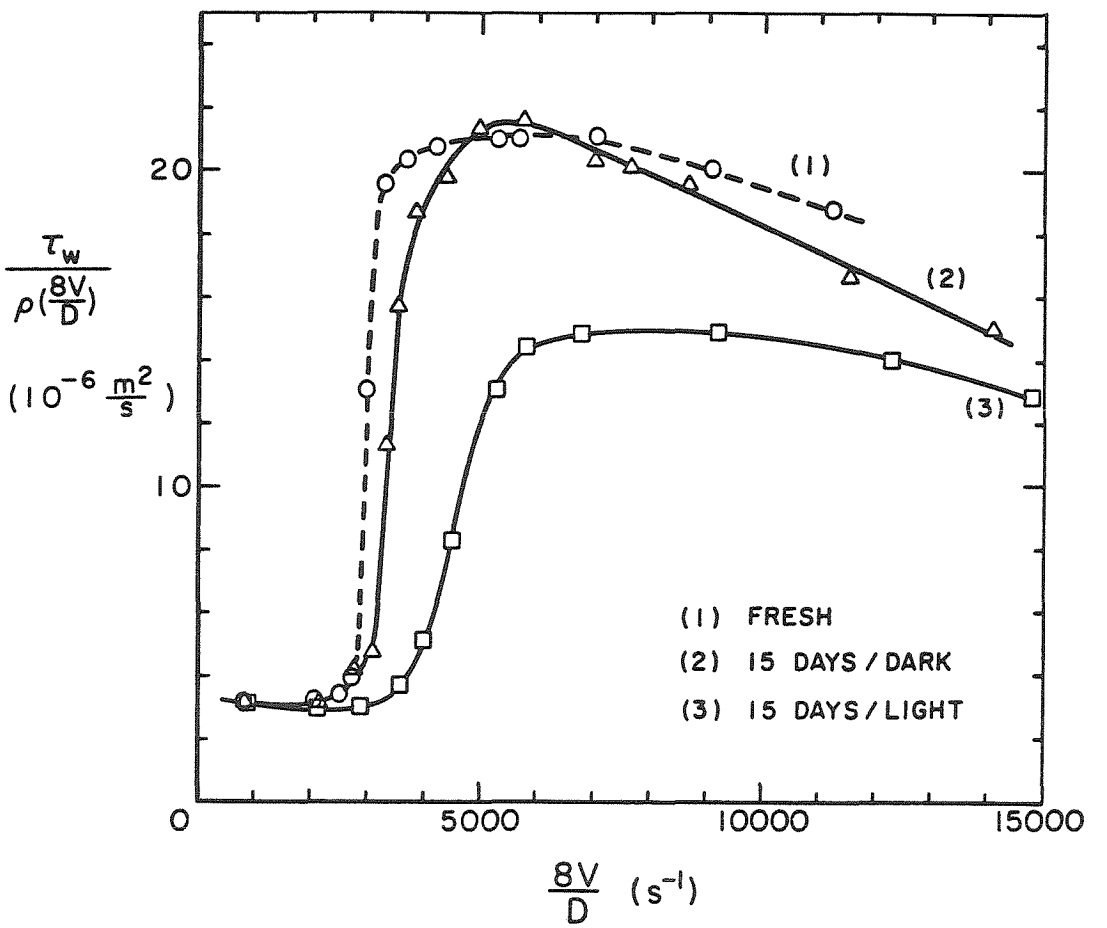
$\frac{\tau_w}{\rho(\frac{8V}{D})}$
$(10^{-6}\ \frac{m^2}{s})$
20
10
0
5000
10000
15000
$\frac{8V}{D}$ (s^{-1})
(1)
(2)
(3)
(1) FRESH
(2) 15 DAYS / DARK
(3) 15 DAYS / LIGHT

Fig. 1

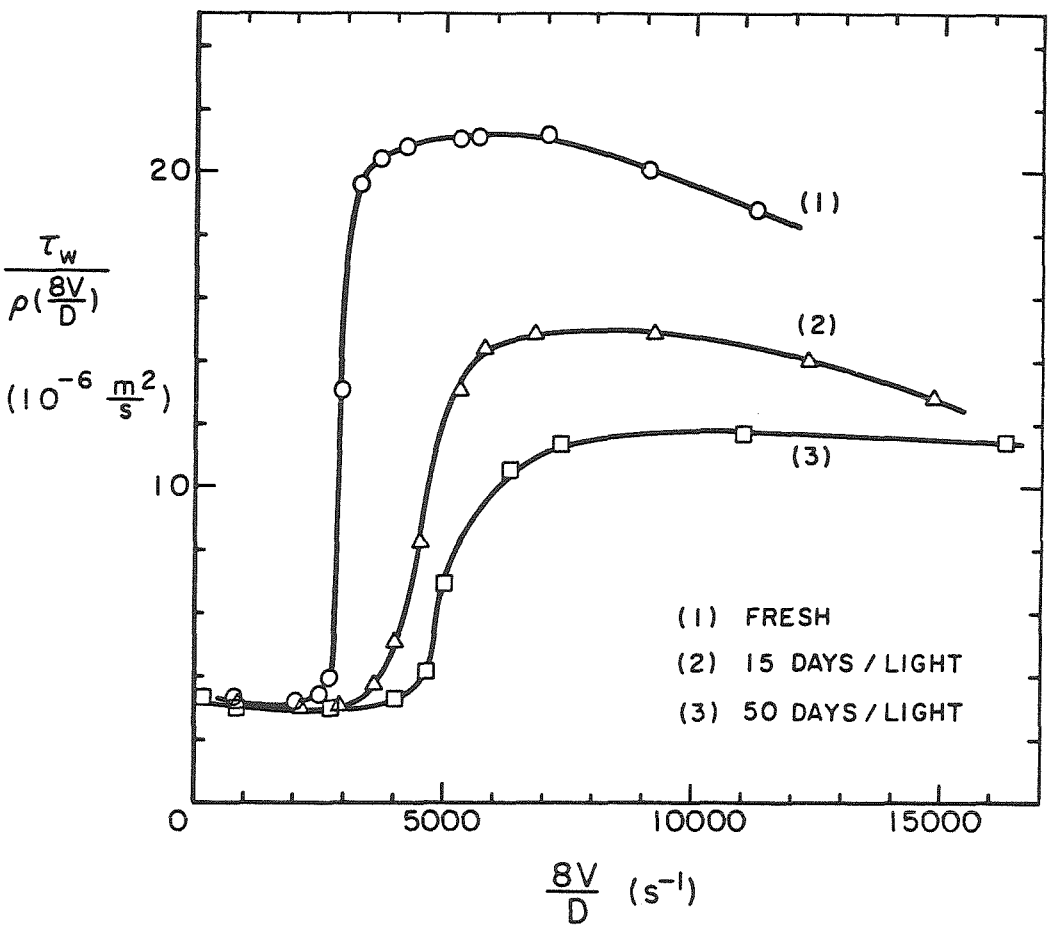
$\frac{\tau_w}{\rho(\frac{8V}{D})}$
$(10^{-6}\ \frac{m^2}{s})$
20
10
0
5000
10000
15000
$\frac{8V}{D}$ (s^{-1})
(1)
(2)
(3)
(1) FRESH
(2) 15 DAYS / LIGHT
(3) 50 DAYS / LIGHT

Fig. 2

Appendix D.

EXAMPLE OF DATA REDUCTION AND ERROR ESTIMATES

For a better understanding and illustration of the computations that are necessary to obtain the friction and heat transfer results, a numerical example is worked out in this section. The fluid chosen is the 200 ppm polyacrylamide solution, batch #3, with computations conducted for station x/D=560, and for a Reynolds number chosen at random. The procedure would be identical for all the other fluids, conditions and stations.

The estimated errors on the basic quantities and the sources of errors during the measurements have been mentioned in the text. The overall error on the results can be best estimated based on the operator's experience, the repeatability of data, and the nature of the measurement technique used. Indeed, some of the formulas used are approximations, and the programs rely on interpolations between best fit polynomials. Moreover, the errors may vary dramatically between different fluids, depending on the corresponding test conditions and nature of the fluid.

Accordingly, only the best estimate of the uncertainty on the final results will be given for the different fluids. As an illustration of typical measurement scatter (which is similar for all cases), the standard deviations for the measurements are shown for this particular example as well.

D.1. Basic quantities

Total length of the tube:	L= 4.853 m (estimated error: 0.05%)
Inner diameter of the pipe:	D_i= 7.860 10^{-3} m (e.e.: 0.5%)
Outer diameter of the pipe:	D_o=9.553 10^{-3} m (e.e.: 0.5%)
Thermocouple location:	x/D = 559.4
	x = 4.397 m (e.e.: 0.05%)
Adjacent pressure drop stations:	x/D= 517.0 and 600.9 (e.e.: 0.05%)
Equivalent average pressure drop measurement:	x/D = 559.0

D.2. Measurements

All the measurements quoted are averages of 5 sets of data taken during a period of 12.6 seconds after the establishment of steady-state. The standard deviation of the individual data measurements with respect to the average is quoted in percents (s.d.). For simplicity, the temperature measurements are already converted to $°C$ by the use of the calibration polynomials for the thermocouples and by software compensation. Similarly, the pressure transducer output in millivolts is already converted to Pascals, using its individual calibration function, and the voltage across the calibrated resistor has been converted to the intensity of current through the tube.

RPM = 253.8	(s.d. : 0.7%)
T_b (entry) = 24.02 $°C$	(s.d. : 0.05%)
T_b (exit) = 25.89 $°C$	(s.d. : 0.2%)

$T_o(x/D = 560)$ = 36.77 °C (s.d. : 0.05%)

Δp (between x/D = 517.0 and 600.9) = 3529 Pa (s.d. : 0.4%)

Voltage drop across the tube = 15.14 V (s.d. : 0.3%)

Current intensity = 97.2 A (s.d. : 0.3%)

D.3. **Computations**

Average bulk temperature:	T_b = 24.96 °C
Corresponding heat capacity:	Cp = 4180 J/kg °K
density:	ρ = 996.9 kg/m^3
water viscosity:	ν = 0.8940 10^{-6} m^2/s
Volumetric flow rate (eq. B.1):	Q = 1.789 10^{-4} m^3/s
Average mass flow rate:	$\dot{m}$ = 0.1784 kg/s
Power:	P = 1473 W
Theoretical bulk temperature increase (eq. A.16a):	ΔT_b = 1.98 °C
Measured bulk temperature increase:	ΔT = 1.87 °C

(As explained in the text, the measurements of the thermocouple probe at the exit proved sometimes unreliable for the viscoelastic fluids. For most of these fluids, this probe did not achieve a steady state until long after the rest of the set-up. There is no such problem at the entry because the fluid and the probe are at room temperature on that side. Consequently, the bulk temperature is computed using the entry temperature only (see app. A.2.). The discrepancy between bulk temperature increases is probably not related to inaccuracies of the values of the heat capacity and flow rate used. Indeed, at higher flow rates the value

of the ratio of bulk temperature increases becomes very close to one (within 1%). Thermal losses have also been shown to be small (see app. A.4).

Computed bulk temperature at x/D=560 (eq. A.20)	$T_b = 25.81\ ^\circ C$
Computed outer/inner wall temperature difference (eq. A.12):	$T_o - T_i = 0.34\ ^\circ C$
Inner wall temperature:	$T_i = 36.43\ ^\circ C$
Average film temperature:	$T_f = 31.12\ ^\circ C$
Difference inner wall/bulk:	$\Delta T = 10.62\ ^\circ C$
Heat flux per unit area:	$\dot{q}_w = 12290\ W/m^2$
Convective heat transfer coefficient:	h= 1157 $W/m^{2\circ}C$
Thermal conductivity of fluid	
at inner wall temperature:	k= 0.6222 W/m $^\circ C$
at average film temperature:	k= 0.6148 W/m $^\circ C$
at bulk temperature:	k= 0.6068 W/m $^\circ C$
Nusselt number at inner wall temperature:	Nu= 14.62
film temperature:	Nu= 14.79
bulk temperature:	Nu= 14.99
Viscosity of solvent at bulk temperature:	$\nu = 0.8781\ 10^{-6}\ m^2/s$
Density at bulk temperature:	$\rho = 996.7\ kg/m^3$
Velocity:	V= 3.688 m/s
Average solvent Reynolds number at bulk temperature:	$Re_s = 33010$
Average wall shear stress between x/D= 517.0	

and 600.9 (i.e. x= 4.064 m and 4.723 m): $\tau_w = 10.50\ N/m^2$

Friction velocity: $u_\tau = 0.1026$ m/s

The programs compute all the following values at bulk, film, and inner wall temperature; and with viscosity functions corresponding to fresh fluid, degraded exit fluid, and fluid with degradation interpolations based on the location and average shear rate. For simplicity, the computations presented here are based on wall temperature and degraded fluid viscosity (computed at x/D=560) only.

Equivalent laminar shear rate: $8V/D = 9763\ s^{-1}$

(This value of 8V/D corresponding to $\tau_w = 10.50\ N/m^2$ is obtained from the viscosity functions of the polymer solution samples, at the proper temperature and with interpolation (based on both shear rate and location) between the viscosity functions of the fresh fluid and the degraded samples.)

Density: $\rho = 993.5\ kg/m^3$

Heat capacity: $Cp = 4178\ J/kg\ ^\circ C$

Thermal conductivity: $k = 0.6222\ W/m\ ^\circ C$

Viscosity of solvent at wall temp.: $\nu_s = 7.049\ 10^{-7}\ m^2/s$

Power-law exponent (eq. 3.25): n= 0.9588

Wall shear rate (eq. 3.26): $\dot{\gamma}_w = 9867\ s^{-1}$

Consistencies (eq. 3.24 and 3.28): $K' = 1.570\ 10^{-3}\ N(s^{0.9588})/m^2$

$K = 1.554\ 10^{-3}\ N(s^{0.9588})/m^2$

Apparent viscosity (eq. 3.34): $\eta_a = 1.064\ 10^{-3}\ Ns/m^2$

Apparent Reynolds number (eq. 3.35): $Re_a = 27060$

Generalized Reynolds number (eq. 3.31): $Re' = 25740$

Solvent Reynolds number: $Re_s = 41120$

Apparent Prandtl number (eq. 3.73): $Pr_a = 7.15$

Generalized Prandtl number (eq. 3.72): $Pr' = 7.22$

Solvent Prandtl number: $Pr_s = 4.68$

Stanton number: $C_H = 7.561\ 10^{-5}$

Apparent Colburn factor: $C_H Pr_a^{2/3} = 2.803\ 10^{-4}$

Modified apparent Colburn factor: $C_H Pr_a^{0.5} = 2.021\ 10^{-4}$

Generalized Colburn factor: $C_H Pr'^{2/3} = 2.821\ 10^{-4}$

Modified generalized Colburn factor: $C_H Pr'^{0.5} = 2.032\ 10^{-4}$

Experimental friction coefficient: $C_f = 1.554\ 10^{-3}$

(Note: all the following comparisons are based on the "apparent" representation.)

Prandtl's C_f (eq. 3.12): $C_f = 6.020\ 10^{-3}$

ratio of measured C_f to Prandtl's: 0.258

Blasius's C_f (eq. 3.13): $C_f = 6.159\ 10^{-3}$

ratio of measured C_f to Blasius's 0.252

White's C_f (eq. 3.14): $C_f = 6.165\ 10^{-3}$

ratio of measured C_f to White's: 0.252

Petukhov's C_f (eq. 3.15): $C_f = 6.050\ 10^{-3}$

ratio of measured C_f to Petukhov's: 0.257

Virk's C_f (eq. 3.38): $C_f = 1.576\ 10^{-3}$

ratio of measured C_f to Virk's: 0.986

Cho's C_f (eq. 3.45): $C_f = 1.491\ 10^{-3}$

ratio of measured C_f to Cho's: 1.042

Experimental Nusselt number:	Nu= 14.62
Petukhov's Nu (eq. 3.61):	Nu= 197.7
ratio of measured Nu to Petukhov's:	0.0739
Sleicher and Rouse Nu (eq. 3.62):	Nu= 191.8
ratio of measured Nu to Sleicher's:	0.0762
Kays's Nu (eq. 3.63):	Nu= 197.8
ratio of measured Nu to Kays's:	0.0739
Dittus-Boelter's Nu (eq. 3.65):	Nu= 177.5
ratio of measured Nu to Dittus's:	0.0823
Kale's Nu (eq. 3.77):	Nu= 31.74
ratio of measured Nu to Kale's:	0.461
Cho's Nu (eq. 3.80):	Nu= 15.84
ratio of measured Nu to Cho's:	0.922
Drag reduction:	75%
Heat transfer reduction:	92%
Ratio of measured Colburn factor and $C_f/2$:	0.361

D.4. **Estimate of errors**

The estimated errors mentioned here are upper-bound margins within which the results are believed to fall with high probability.

(There should not be any significant difference in error with varying Reynolds number because the pressure transducers are changed between runs to insure their use in the most accurate part of their range, and because the power is adjusted to keep the temperature increases about the same for all flow rates. One limitation, however, is

the measurement of very low RPM for which the frequency data might be unreliable. These measurements have been discarded and were not presented in this report.)

For water, the error on the friction coefficient is estimated to be less than 5%, 3% for the Reynolds number, and 8% for the Nusselt number. (The error on the C_f is mainly due to the 5th power of the diameter in the relationships. The large error on Nu is due to the small difference in temperature between bulk and wall for newtonian fluid under the standard experimental conditions. The properties of the water are assumed to be correct within 2%.) Friction results, when compared to existing correlations were shown to fall within 2% of the latter in most cases. The Nusselt numbers were shown to be within 3% of the correlations believed most accurate and very close to the average of most existing correlations.

For the polymer solutions, the error margin on C_f is assumed to be 5% as well. The error on Re_a could be 5% (because of slightly larger uncertainty on the viscosity). The error on Nusselt is believed to be only 4%, however (the large temperature difference between fluid bulk and inner wall absorbs all errors on temperature). (The material properties except viscosity were assumed to be the same as for water, this should be a very good approximation because of the low concentration.) The computed friction coefficients are within about 10% of Virk's results. The Nusselt numbers corresponding to the heat transfer asymptote fall within 5% of Cho's results.

For kerosene, there could be 5% uncertainty on C_f, and 3% on Re_a. The error on the Nusselt number is estimated to be within 6% if the value of k and Cp used are correct. (These values were obtained from standard tables and were not measured directly. Accordingly, any large discrepancies between actual values and used ones would have to be added to the error estimate mentioned here.) No results are available for comparison of heat transfer, but the friction results were found to be within 2% of Blasius's expression for newtonian fluids.

For antimisting kerosene, there could be 5% error on C_f and 7% on Re_a (because of large variations in viscosity). The Nusselt number could be accurate within 3% if, as for the case of kerosene, the values used for k and Cp are correct. With the proper choice of computational parameters, the friction results for AMK were found to be within 5% of the friction asymptote for the polyacrylamide solutions. The heat transfer results were found to be within 15% of the heat transfer asymptote.

The fully-degraded AMK results should show the same errors as the kerosene, and gave friction results within 5% of those for Jet A, and heat transfer results within 2%.

For bentonite suspensions, there might be 5% uncertainty on C_f, 5% on Re_a, and 10% on Nu (the concentrations are small enough that we expect the values used for k and Cp to be within 4% or so of the actual values). The friction results were found to be within 2% of newtonian values with a proper representation, and the heat transfer results in the entrance region were within 10% of values given by existing relationships

for laminar flow.

For the mixture of bentonite and polymer, the error on Re_a might be as high as 10% (because of the strong susceptibility of the viscosity to degradation), but the Nusselt number is probably accurate within 6% (because of larger temperature differences). The upper-bound of error for C_f is the same as for all fluids: 5%.

For the tomato puree, the uncertainty could be 5% on C_f and 6% on Re_a if the viscosity measurements are meaningful. That is, if the viscosity measured in the capillary is representative of the flow in the test tube, barring large effects due to macroscopic heterogeneity in one but not the other tube. Although the laminar results differ somewhat from usual non-newtonian pipe correlations, it cannot be dismissed that other phenomena might be present besides pseudoplasticity, such as plug flow or thixotropy for example. Additionally, the turbulent results of the mixture of tomato puree and 200 ppm polymer were within 12% of the usual relationships for asymptotic drag reduction, apparently validating somewhat the viscosity measurements. The Nusselt numbers should be accurate within 5% if the values used for k and Cp are acceptable, and probably less for the batches mixed with polymer. (These properties were assumed to be the same as those of water, and any actual discrepancy should be added to this error estimate.)

In conclusion, it should be emphasized that the error estimates mentioned here are believed to be upper-bound margins, and that in most cases the results might be closer to the actual values. It must be

pointed out that the scatter of the experimental results is not due only to random errors, but also to variations in test conditions such as the temperature for example. Clearly, a similar fluid used for comparison in another laboratory may well give different results, because of inherent variations in composition, preparation, aging, or degradation. It is believed, however, that the computations methods used in this study are complete enough and based on a sound enough representation of the physical concepts to produce correlations of general applicability. This has been shown to be the case for various batches of (nominally) the same fluid but exhibiting largely different properties (see the case of AMK for example).

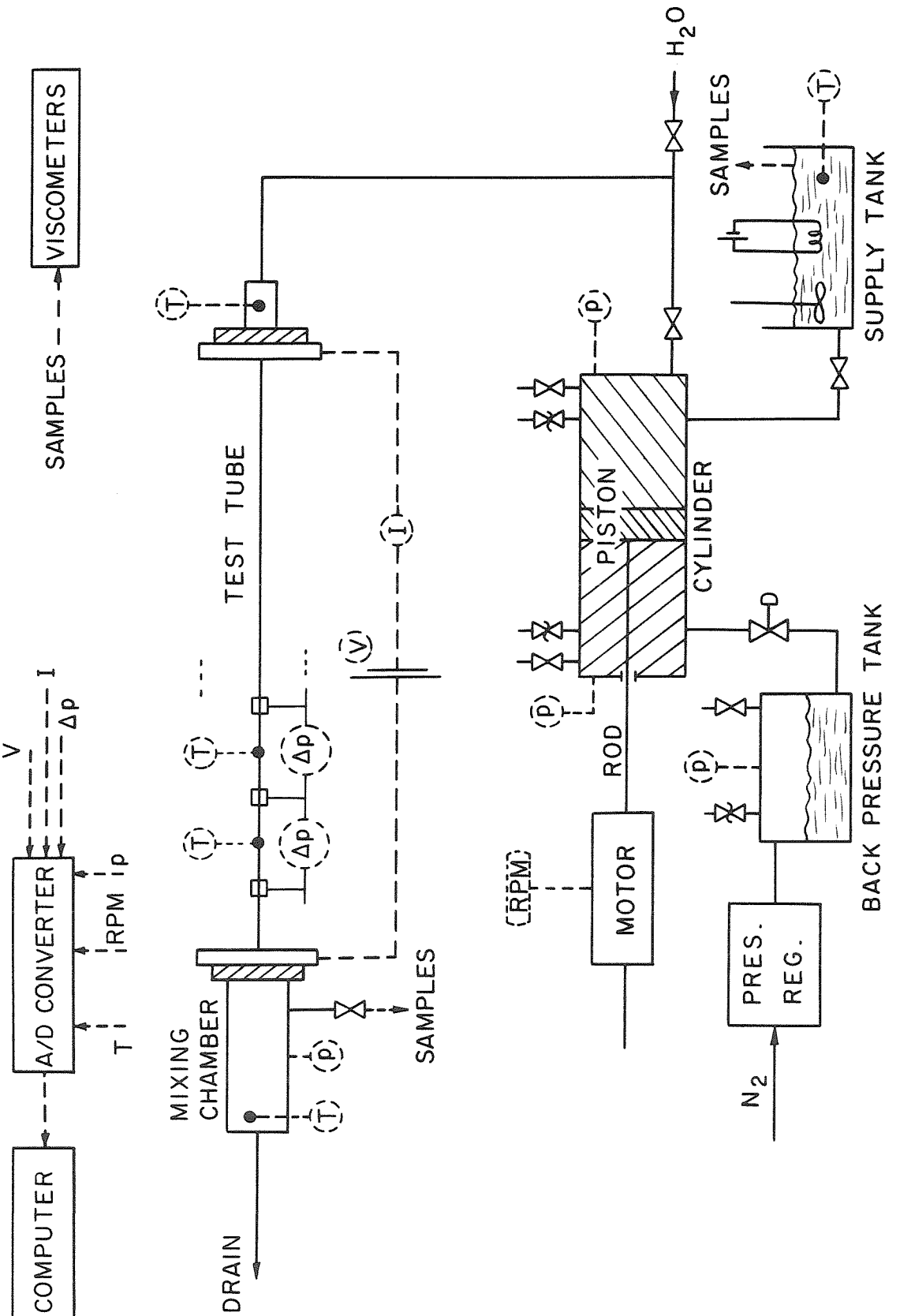

Figure 4.-1: Schematic of the experimental installation.

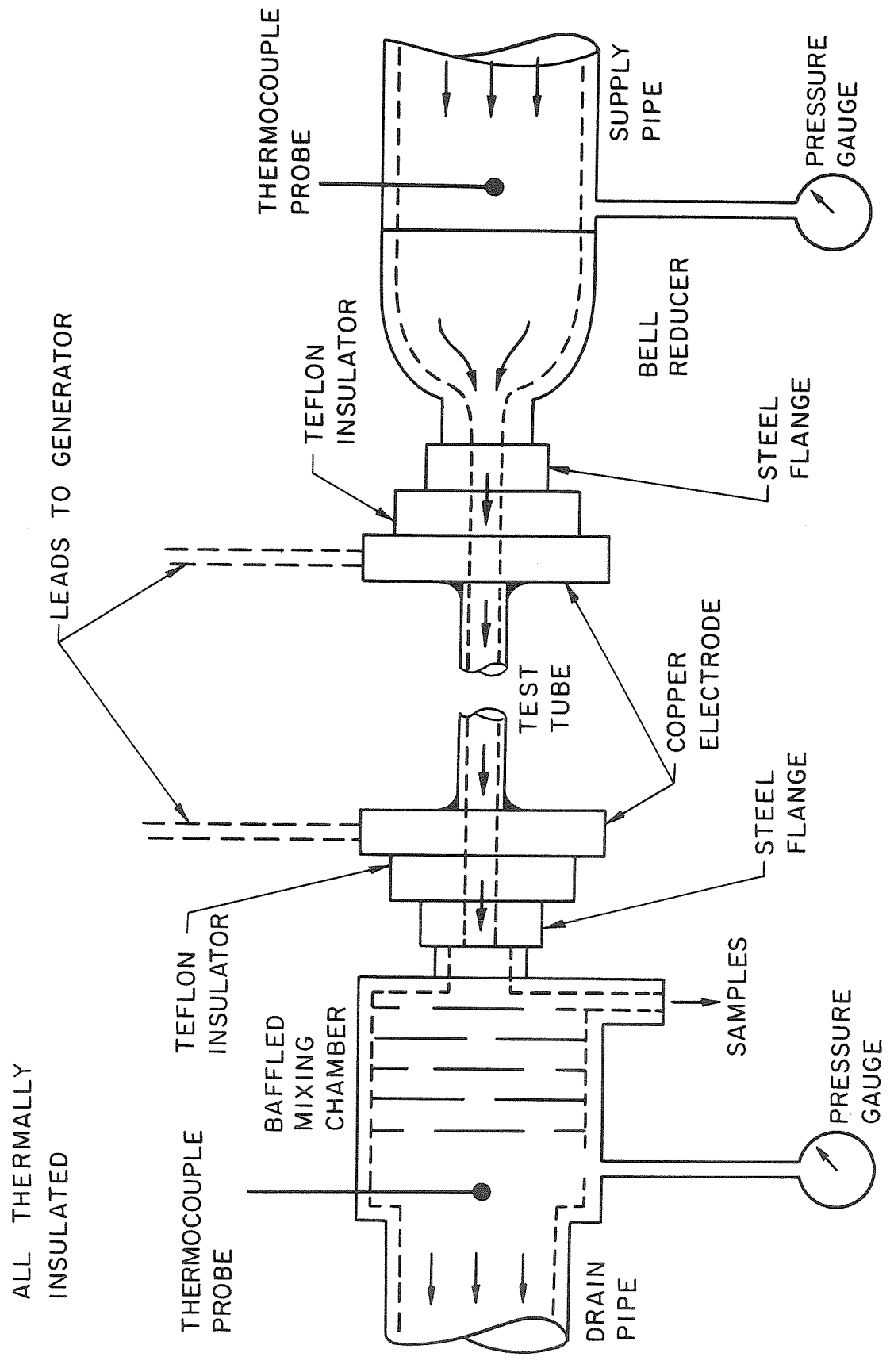

Figure 4.-2: Schematic of the test section.

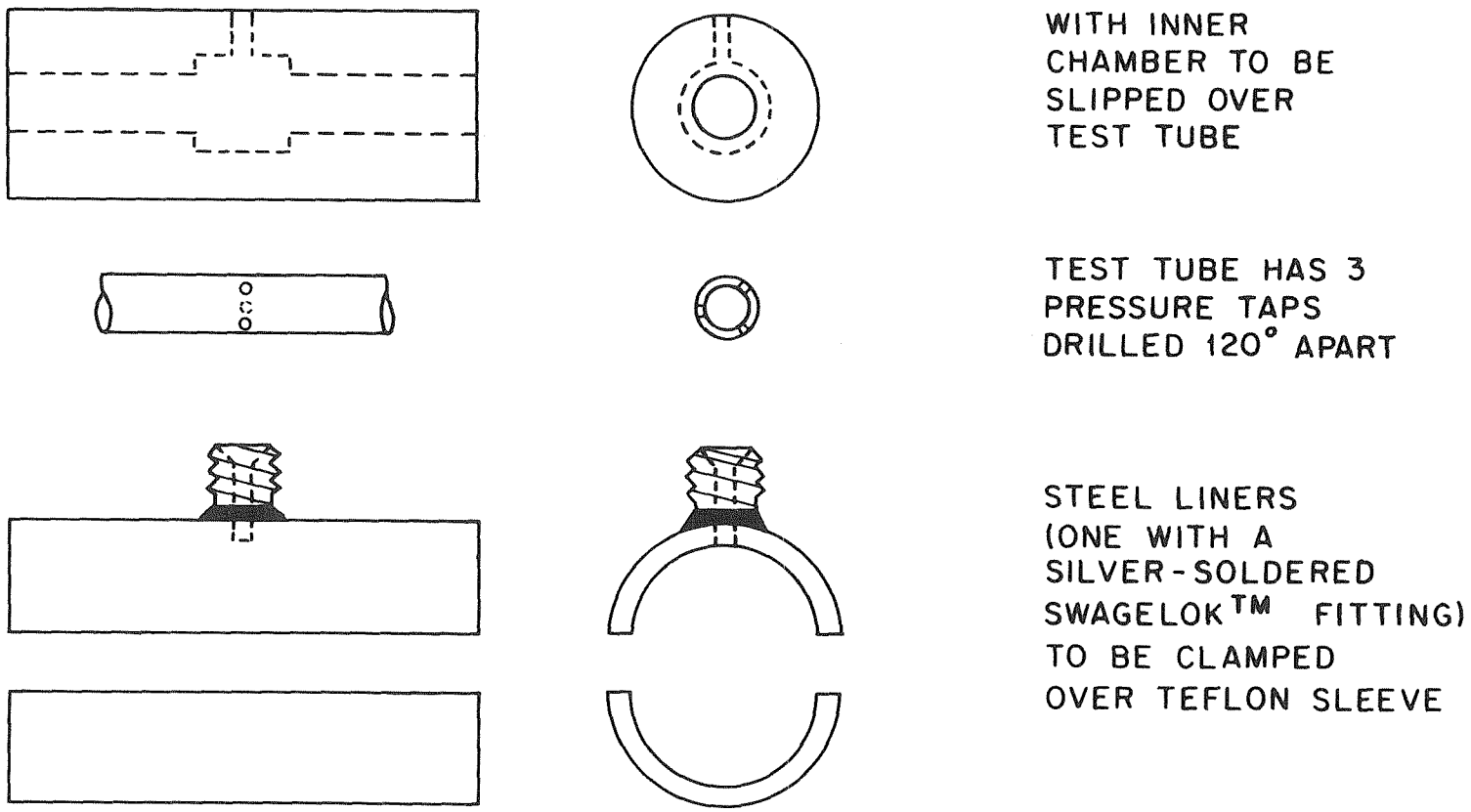

Figure 4.-3: Pressure taps configuration.

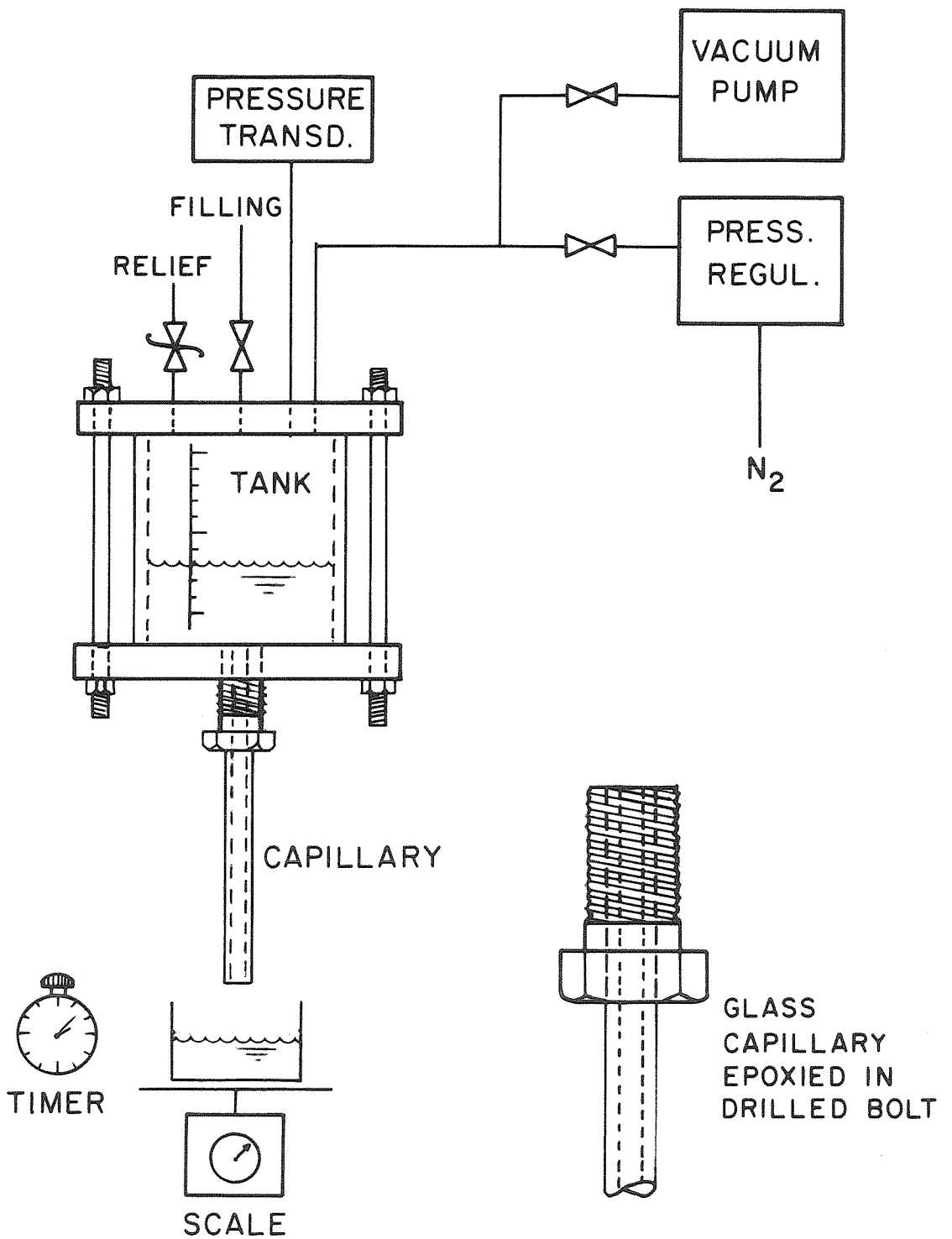

Figure 4.-4: Capillary viscometer schematic (pressurized/vacuum tank type).

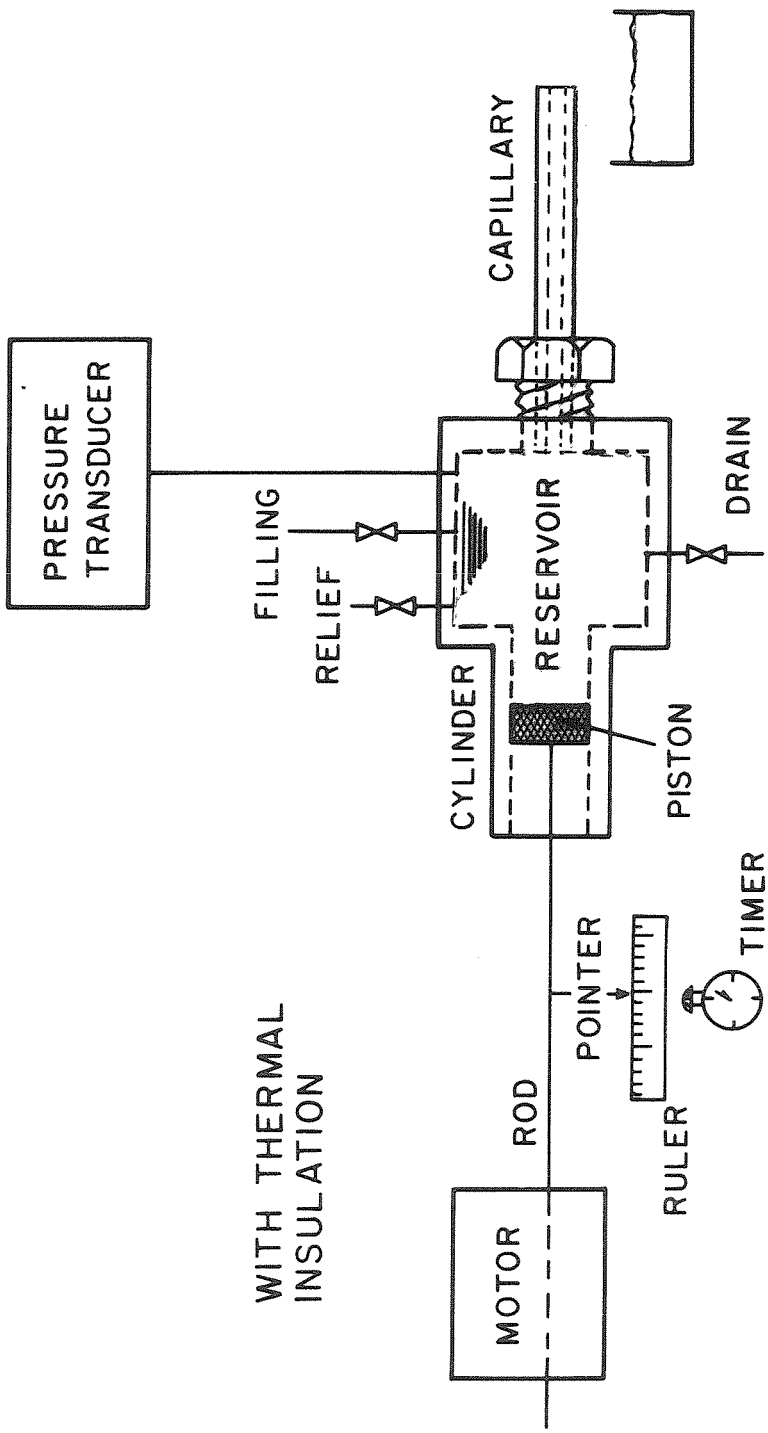

Figure 4.-5: Capillary viscometer schematic (hydraulic ram type).

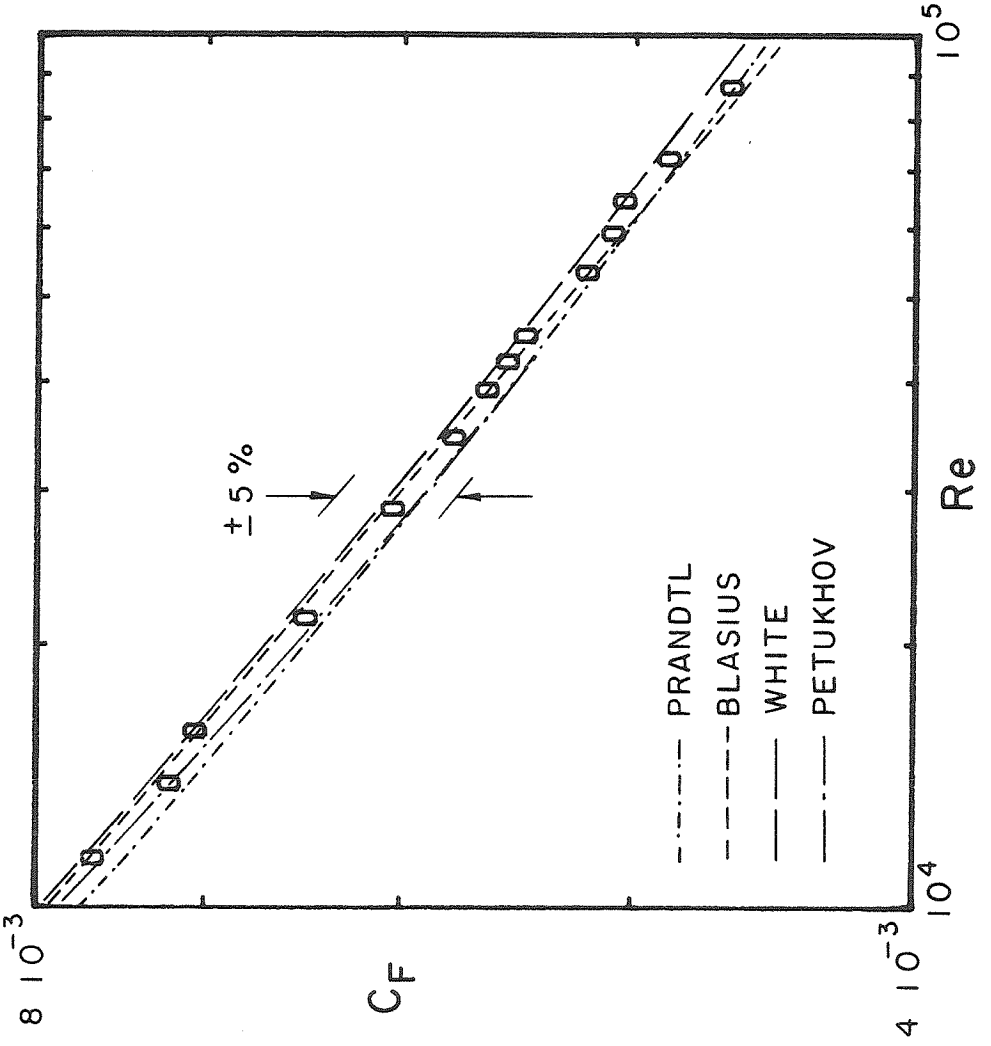

Figure 5.1.-1: Friction results for water.

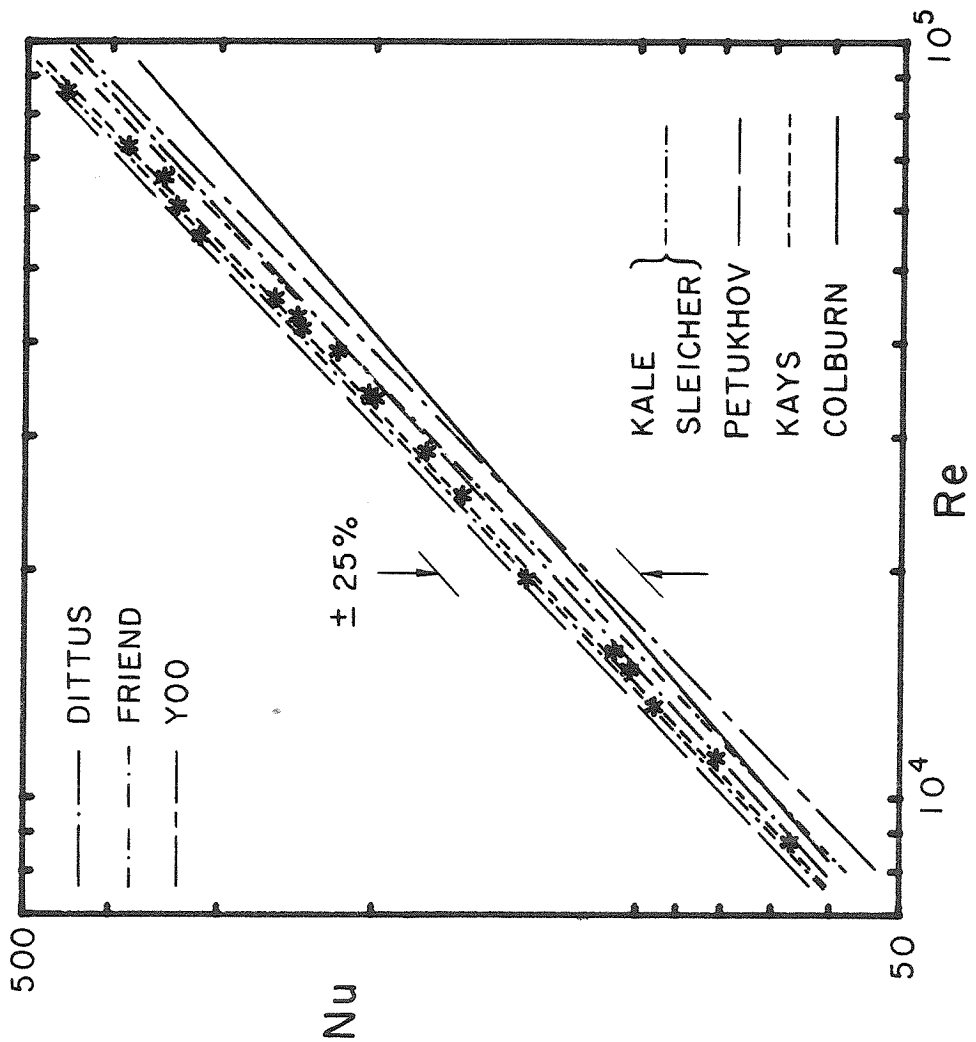

Figure 5.1.-2: Heat transfer results for water. Pr=5.55 +/- 6%.

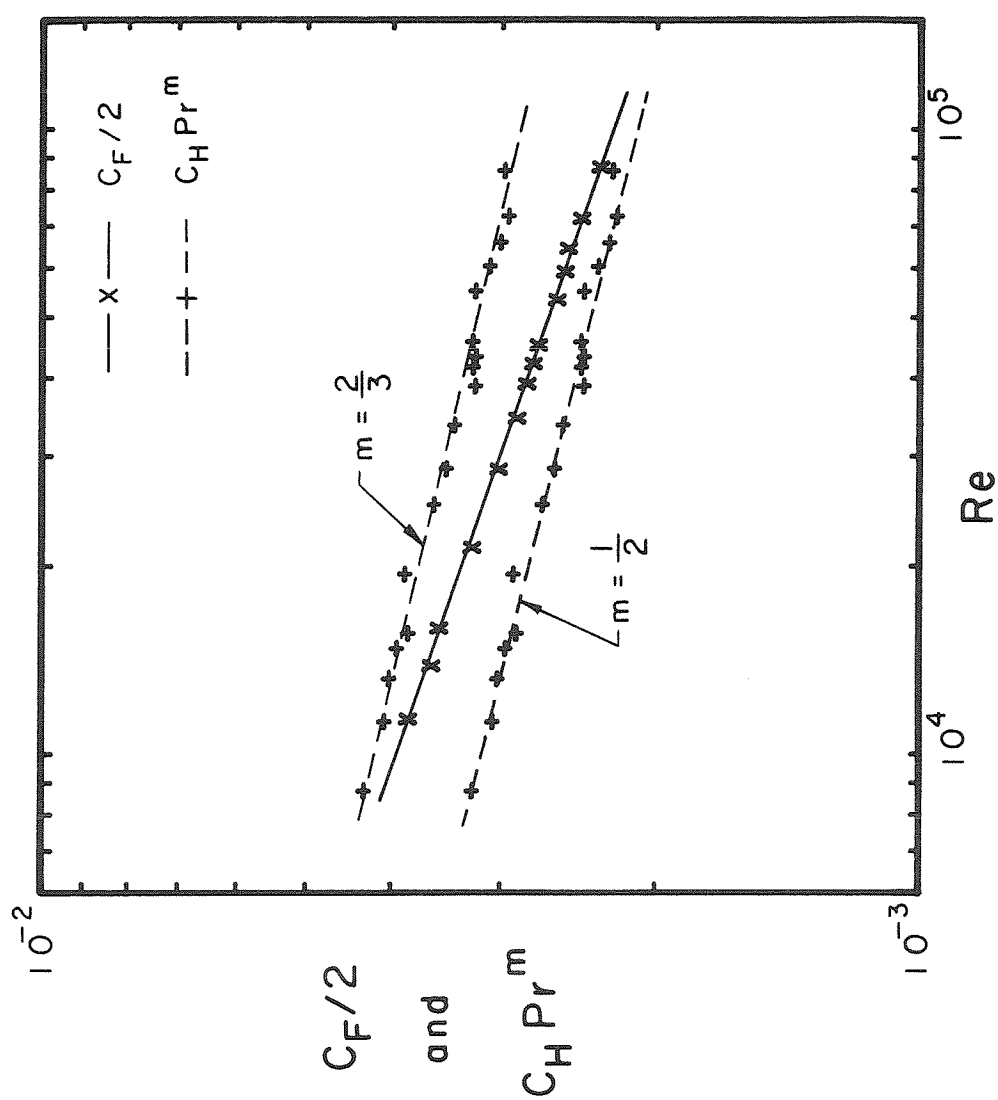

Figure 5.1.-3: Comparison of heat transfer and friction for water. Pr=5.55 +/- 6%.

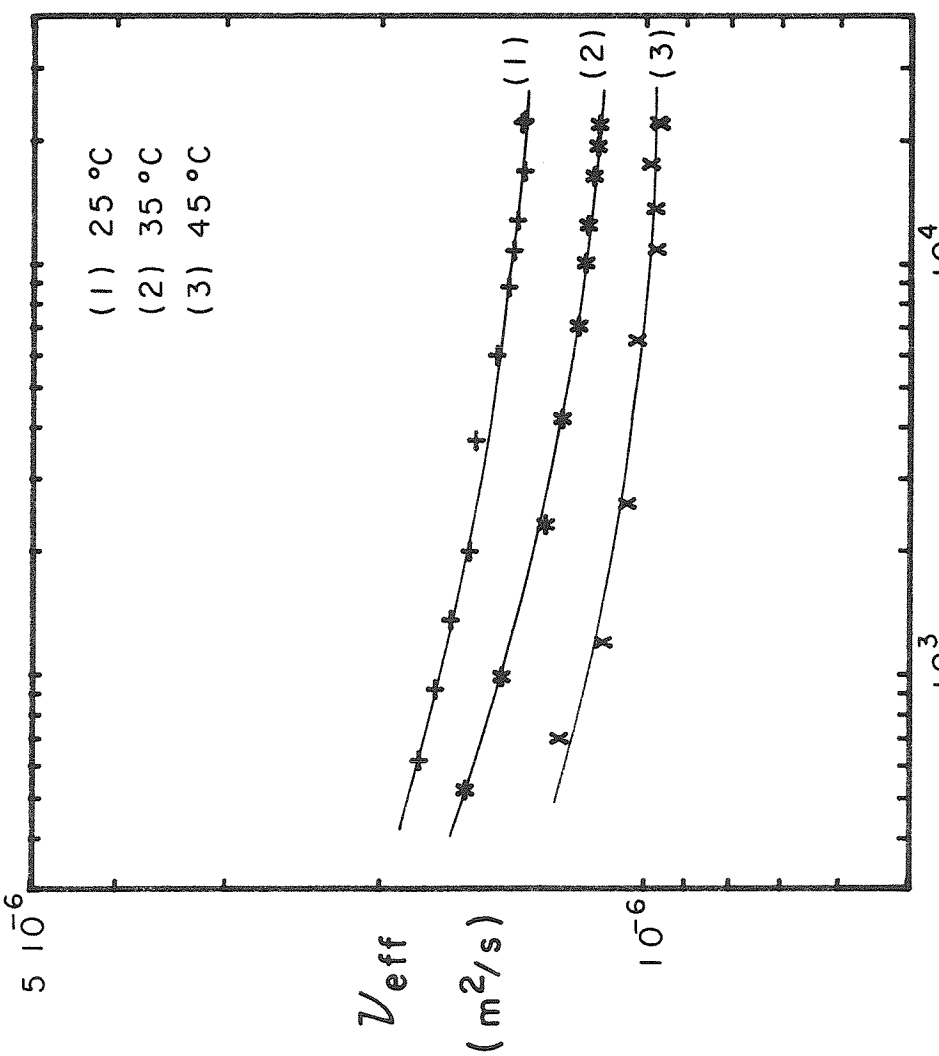

Figure 5.2.-1: Viscosity functions for asymptotic polymer solutions at various temperatures. (Unused 200 ppm AP-273, batch #3, T-20 capillary.)

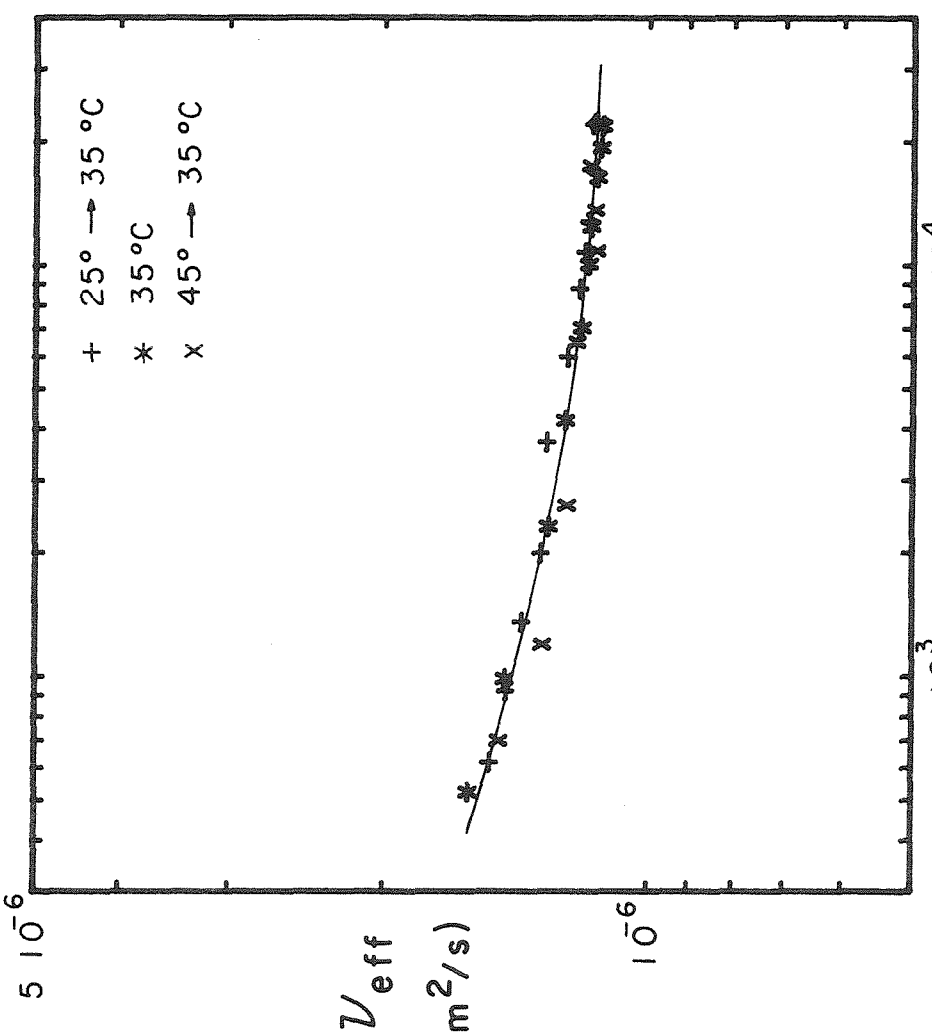

Figure 5.2.-2: Viscosity function for asymptotic polymer solutions. Correlation of temperature effect. (Unused 200 ppm AP-273, #3, T-20 capillary.)

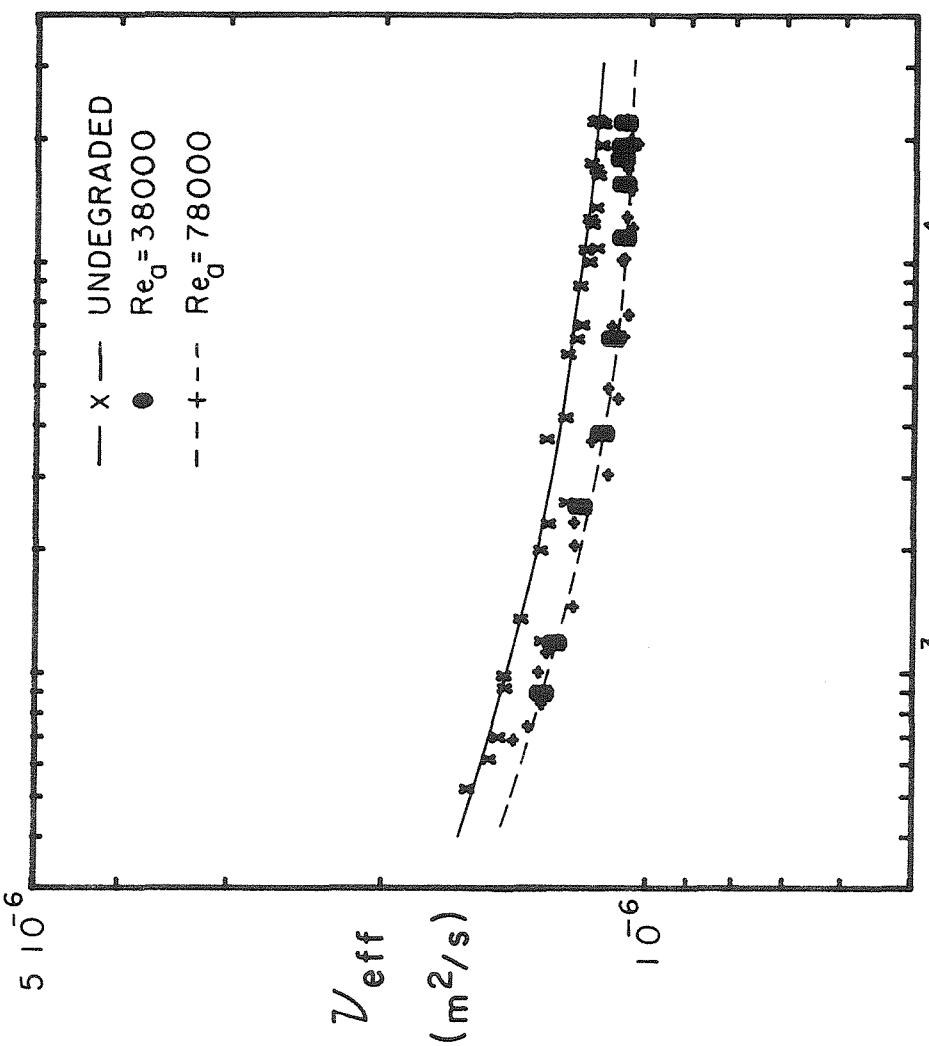

Figure 5.2.-3: Viscosity functions for asymptotic polymer solutions. Samples: unused; ran in test tube at $Re_a = 38000$ ($\dot{\gamma}_w = 15000 s^{-1}$); and at $Re_a = 78000$ ($\dot{\gamma}_w = 38000 s^{-1}$). (200 ppm #3, T-20 capillary, reduced to 35 °C.)

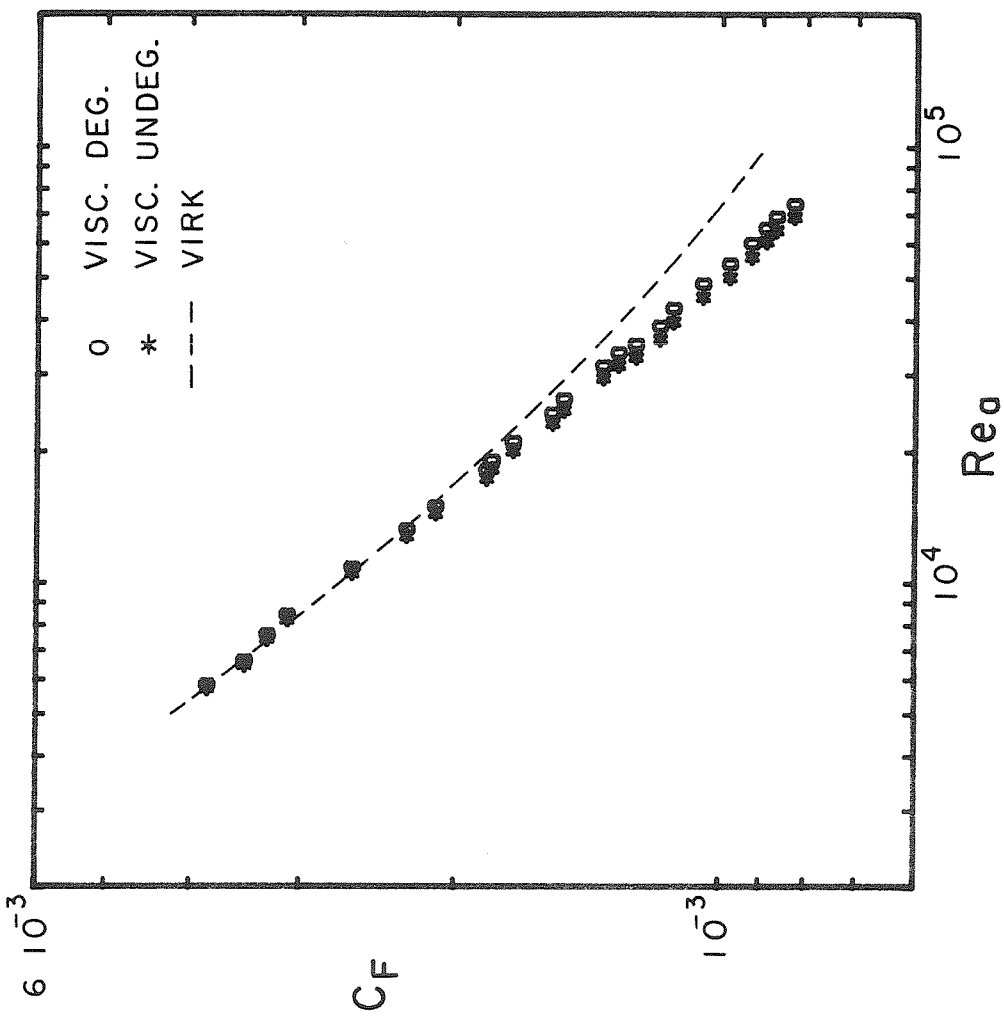

Figure 5.2.-4: Friction results for asymptotic polymer solutions. Computations based on undegraded and degraded viscosity functions. (200 ppm #3, x/D=560, film temperature reference.)

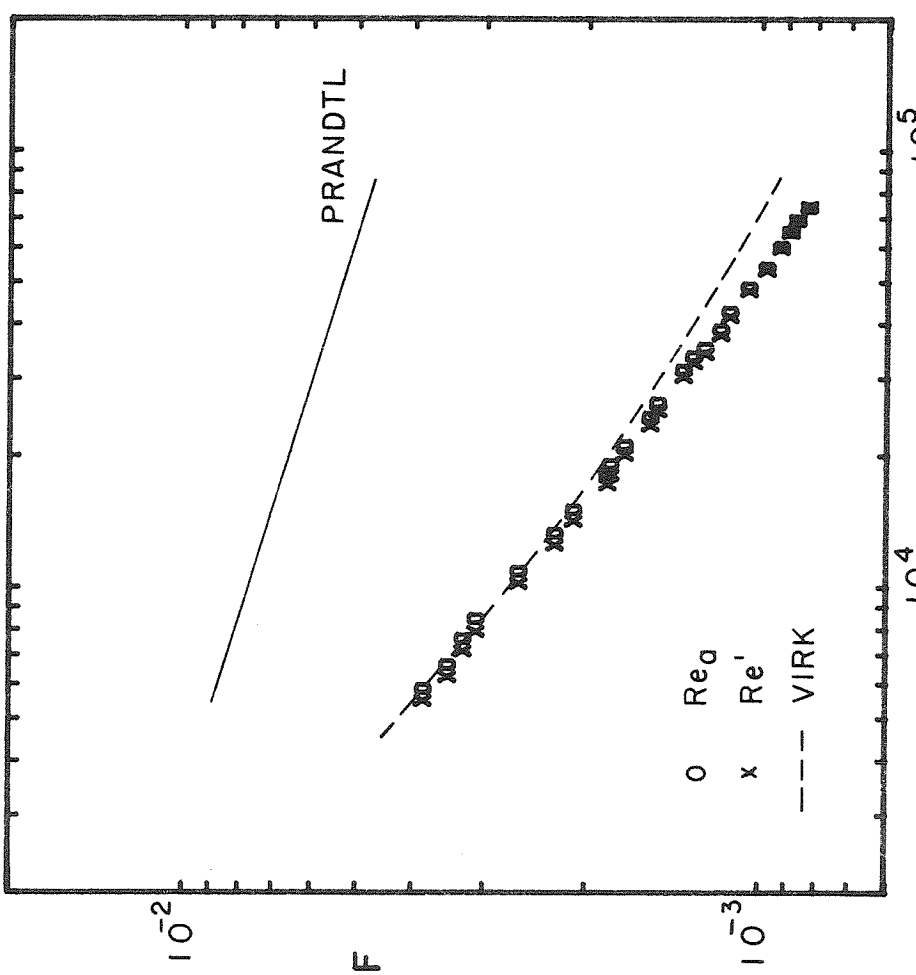

Figure 5.2.-5: Friction results for asymptotic polymer solutions. Apparent and generalized Reynolds number representations. (200 ppm #3, x/D=560, film temperature reference, degraded viscosity functions.)

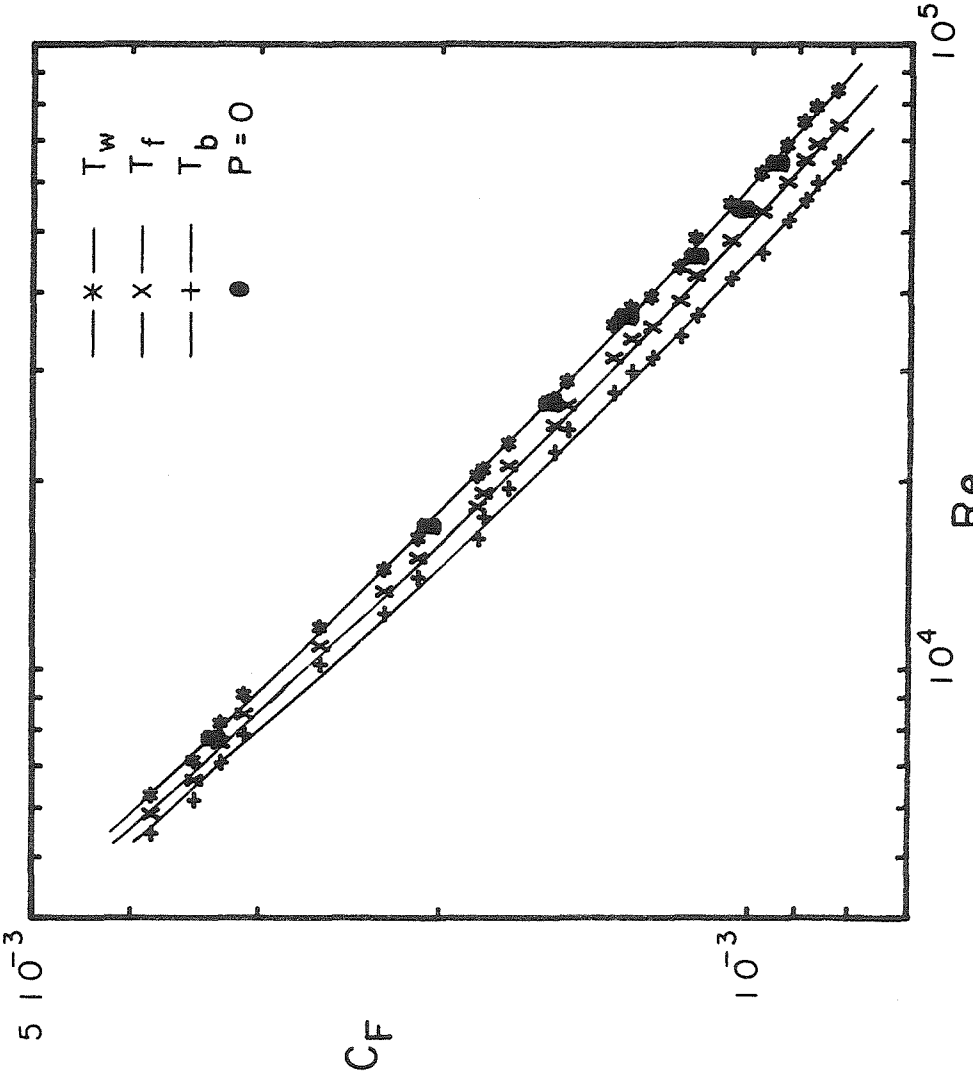

Figure 5.2.-6: Friction results for asymptotic polymer solutions. Computations conducted at bulk, film, and wall temperature for power-on runs. Also shown are isothermal runs. (200 ppm #3, x/D=560, degraded viscosity functions.)

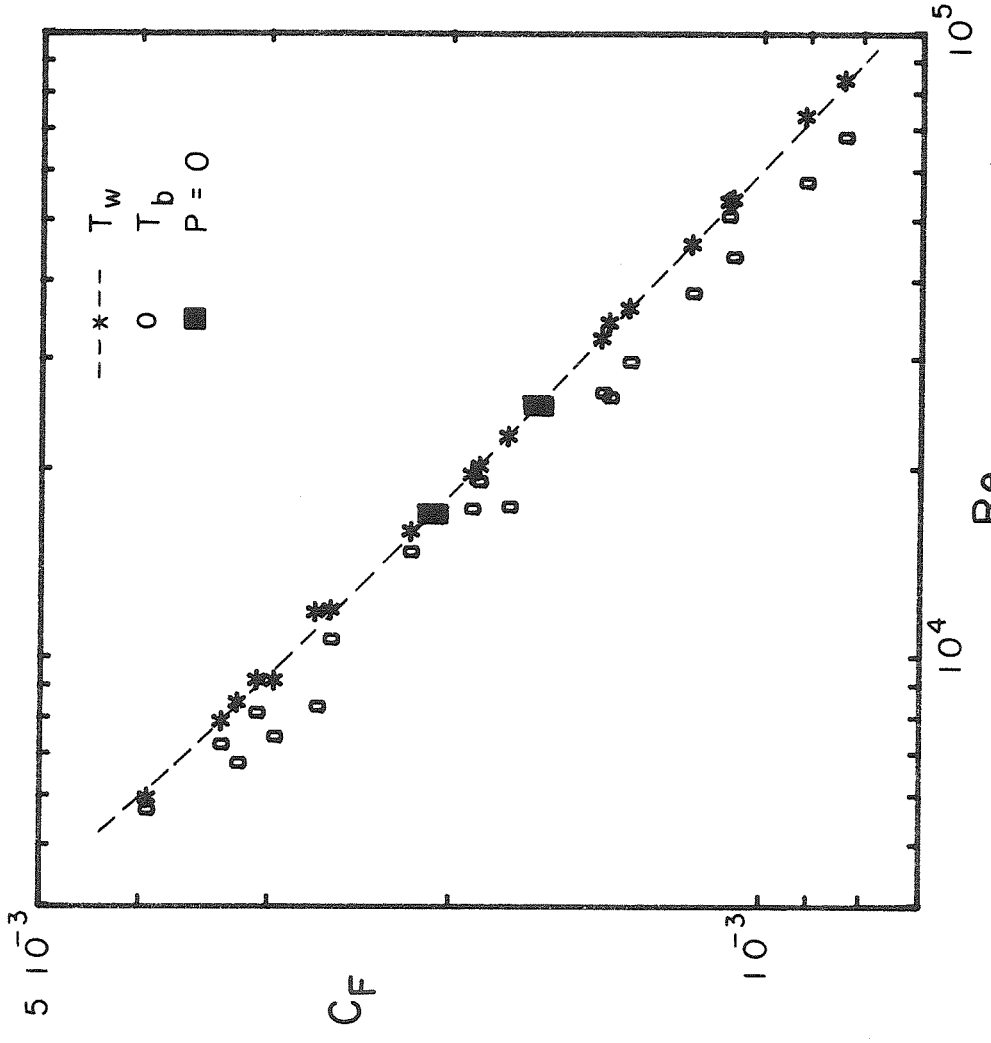

Figure 5.2.-7: Friction results for asymptotic polymer solutions (large power variations). Computations conducted at bulk and wall temperature for power-on runs. Also shown are isothermal runs. (200 ppm #1, x/D=560, degraded viscosity functions.)

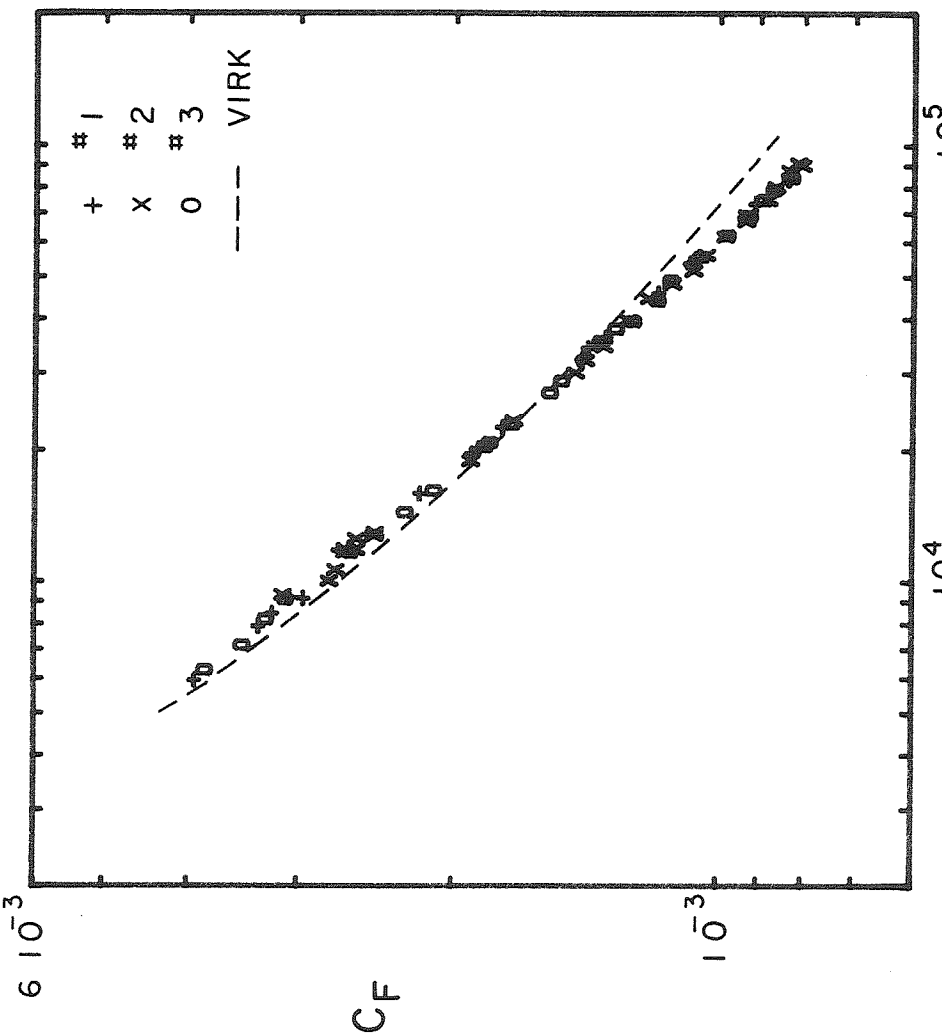

Figure 5.2.-8: Friction results for various asymptotic polymer solutions batches. (200 ppm #1, #2, and #3; x/D=560; wall temperature reference; degraded viscosity functions.)

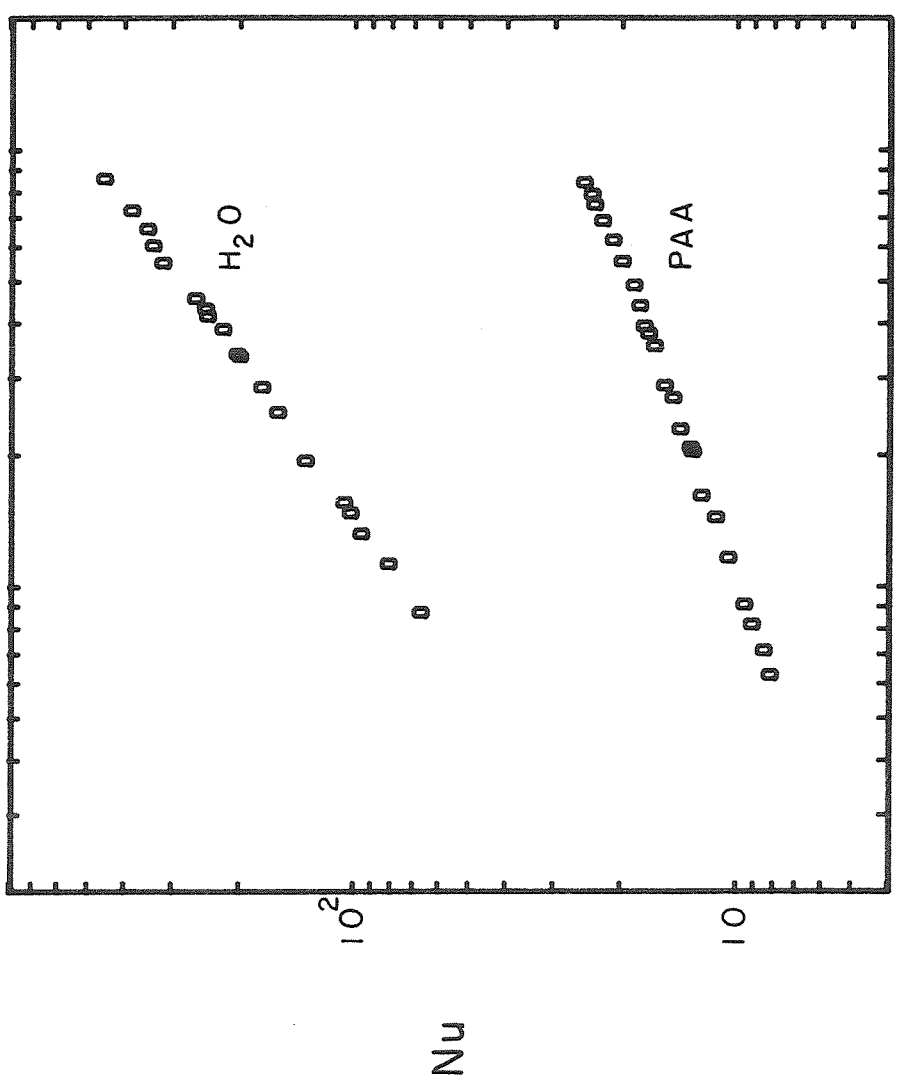

Figure 5.2.-9: Heat transfer results (Nusselt numbers) for asymptotic polymer solutions. (200 ppm #3, x/D=560, wall temperature reference, degraded viscosity functions.)

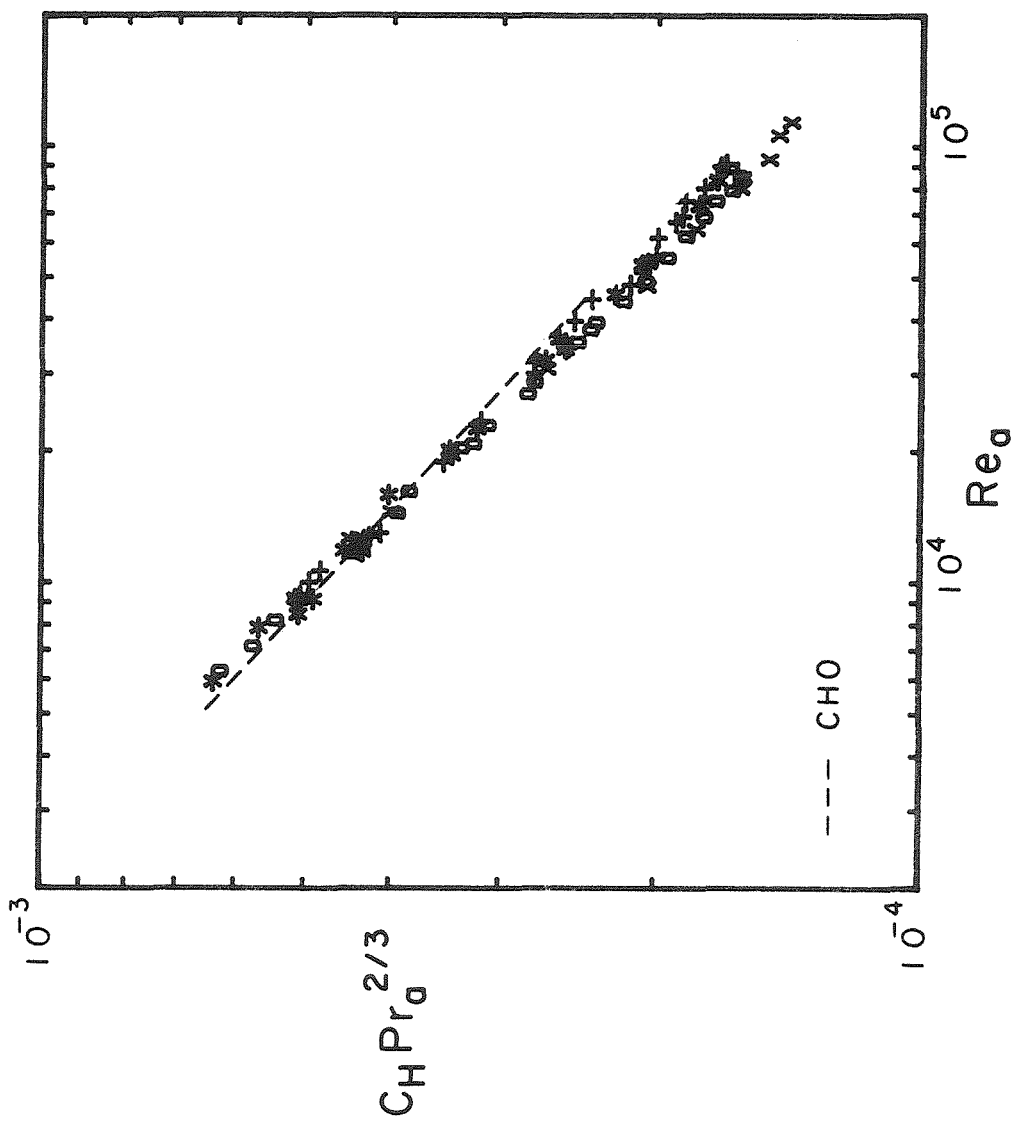

Figure 5.2.-10: Heat transfer results (Colburn factors) for various batches of asymptotic polymer solutions. (200 ppm #1, #2, and #3; x/D=560; wall temperature reference; degraded viscosity functions.)

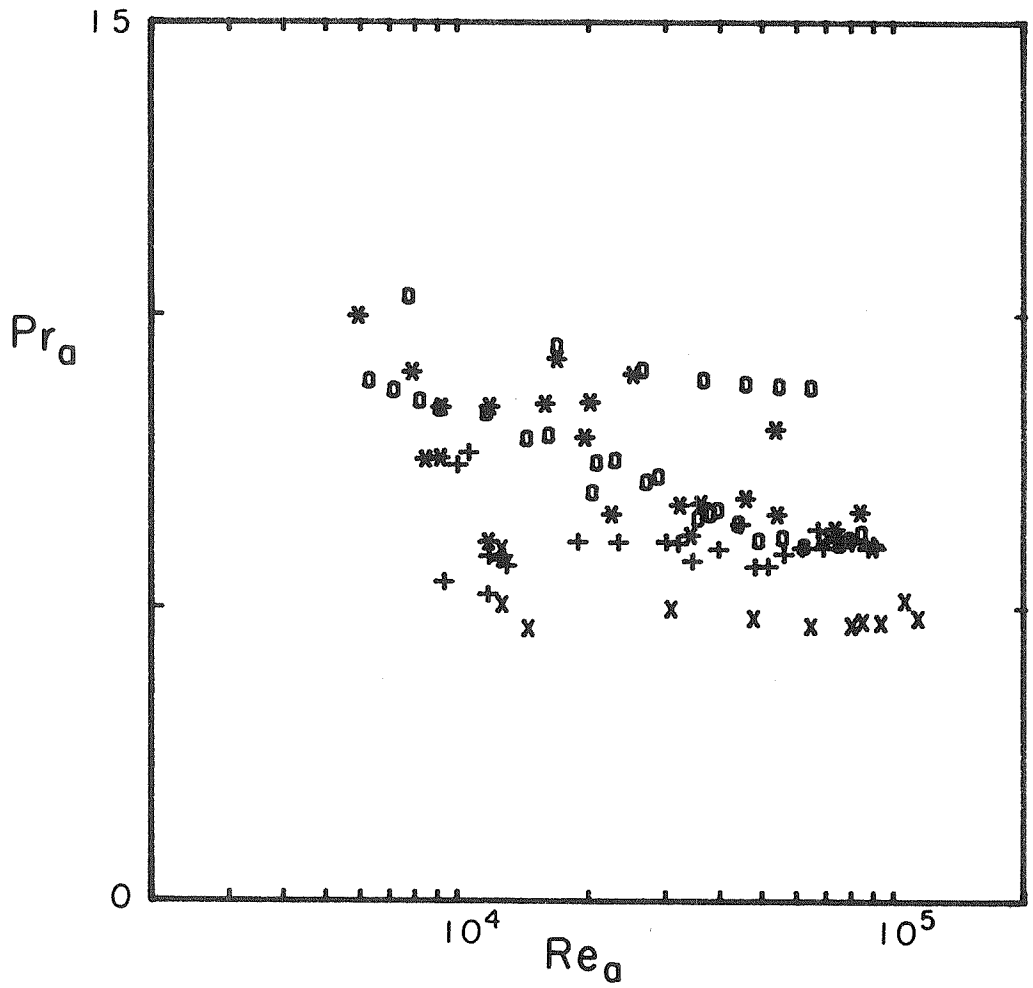

Figure 5.2.-11: Variations in Prandtl number for various batches of asymptotic polymer solutions. (200 ppm #1, #2, and #3; x/D=560; wall temperature reference; degraded viscosity functions.)

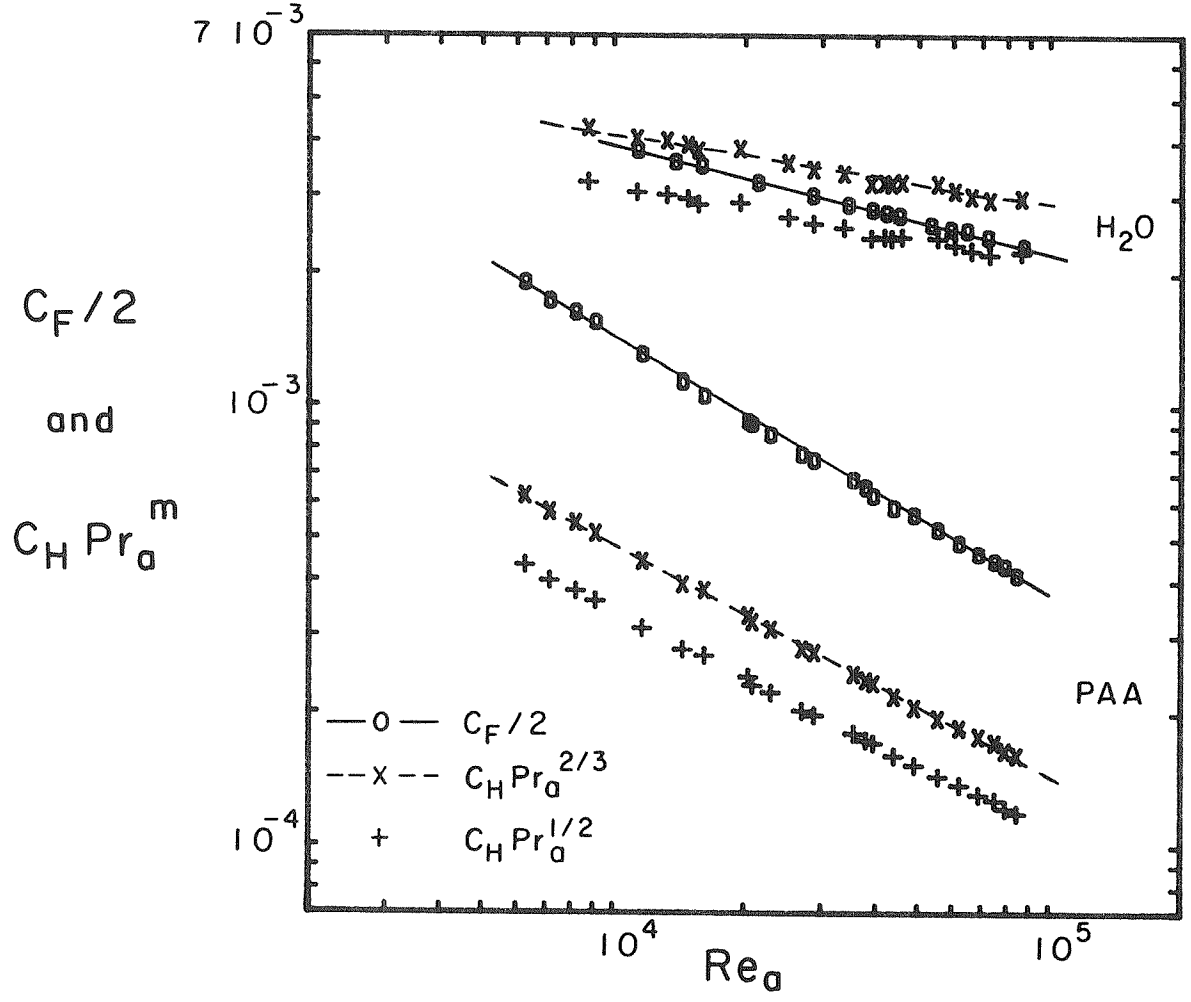

Figure 5.2.-12: Comparison of friction and heat transfer for asymptotic polymer solutions. (200 ppm #3, x/D=560, wall temperature reference, degraded viscosity functions.)

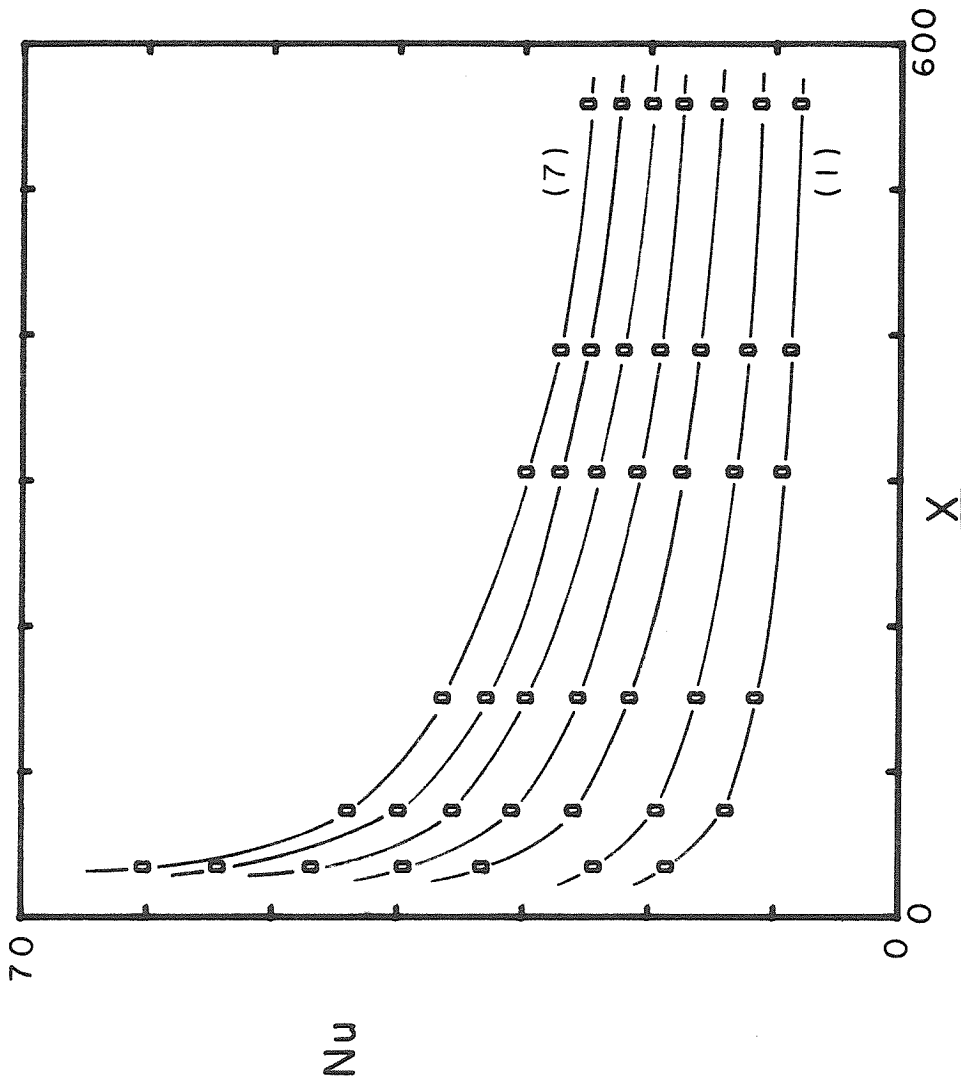

Figure 5.2.-13: Heat transfer results as a function of distance for asymptotic polymer solutions. Curve (1): Re_a=6280 (Pr_a=8.87), (2): 14400 (7.88); (3): 27100 (7.15); (4): 39500 (6.67); (5): 55600 (6.20); (6): 68900 (6.19); (7): 84300 (6.28). (200 ppm #3, wall temperature reference, degraded viscosity functions.)

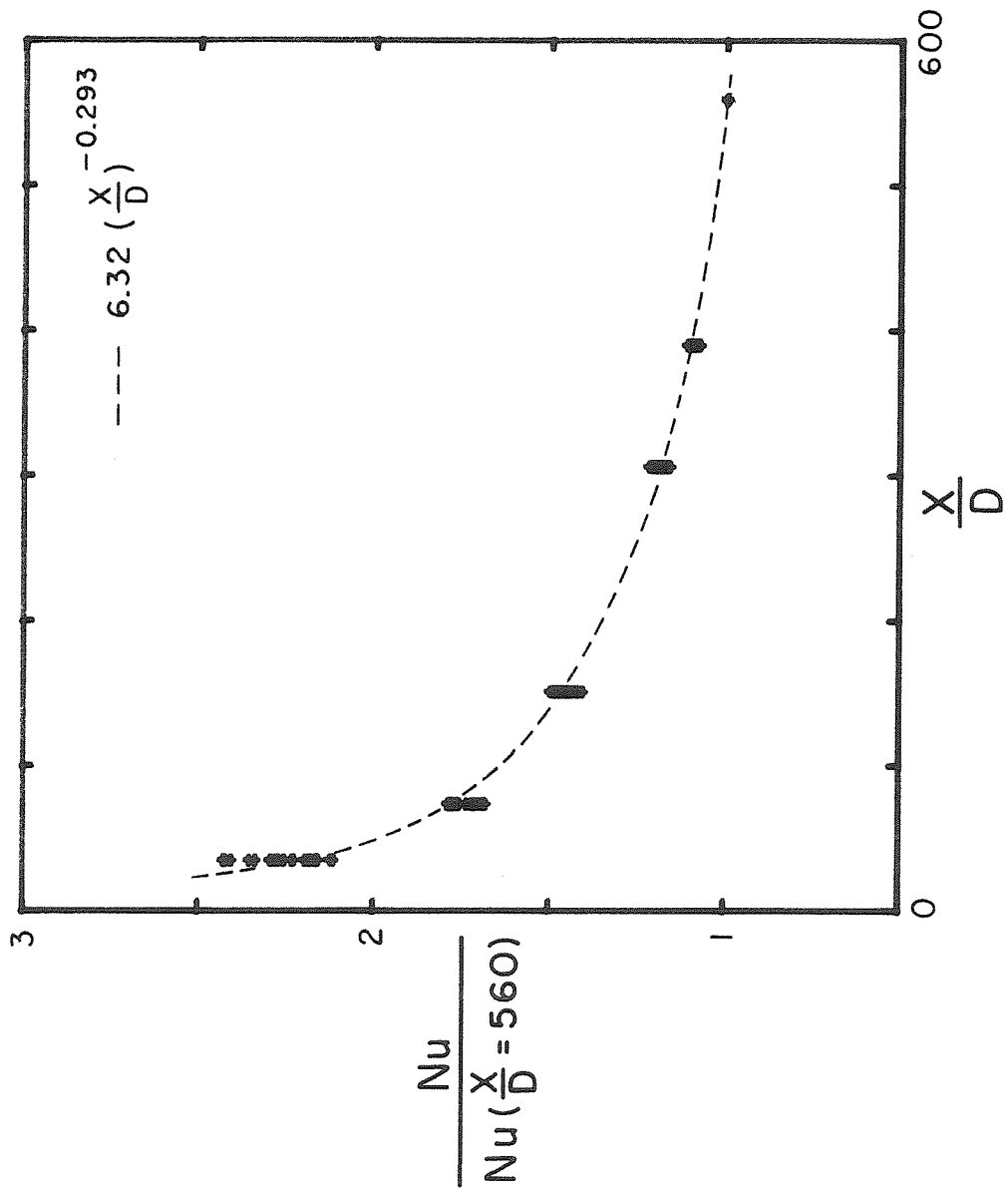

Figure 5.2.-14: Correlation of heat transfer results for asymptotic polymer solutions in the entrance region. (200 ppm #3, wall temperature reference, degraded viscosity functions.)

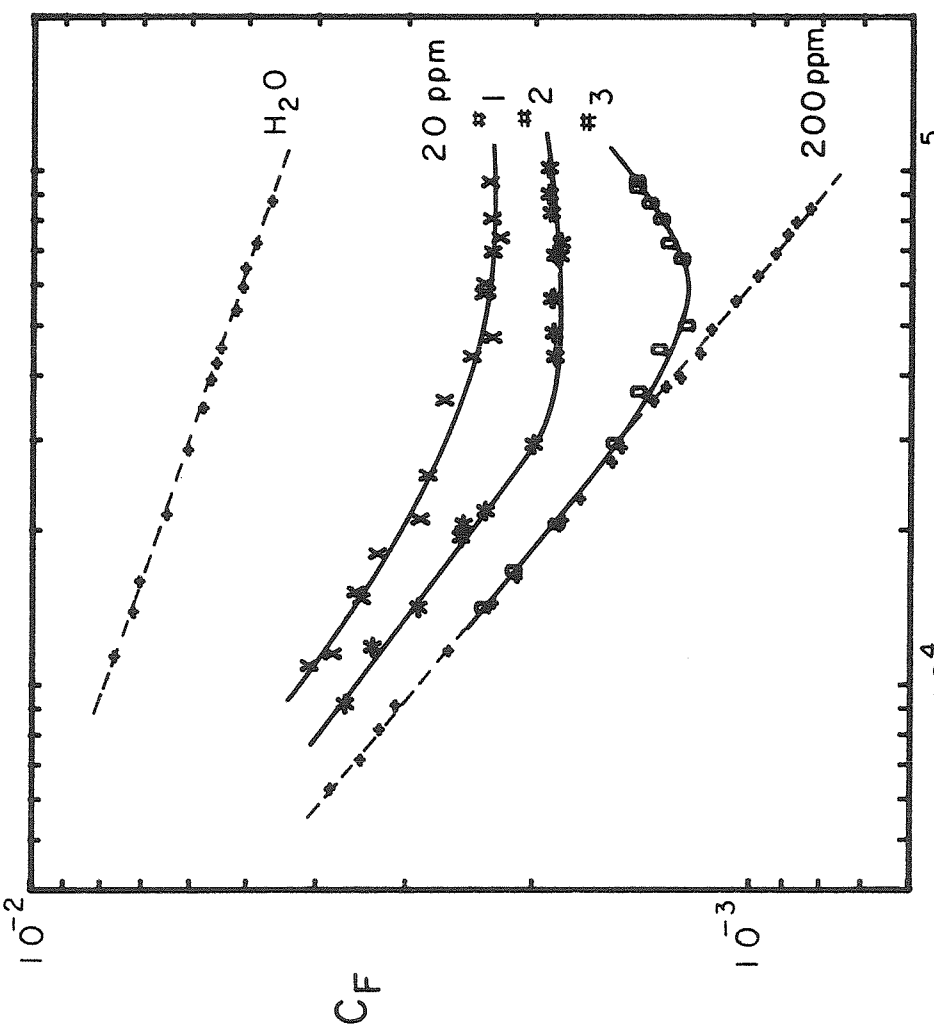

Figure 5.2.-15: Friction results for pre-degraded and asymptotic polymer solutions. (20 ppm #1, #2, and #3; 200 ppm #3; x/D= 560; wall temperature reference; degraded viscosity functions.)

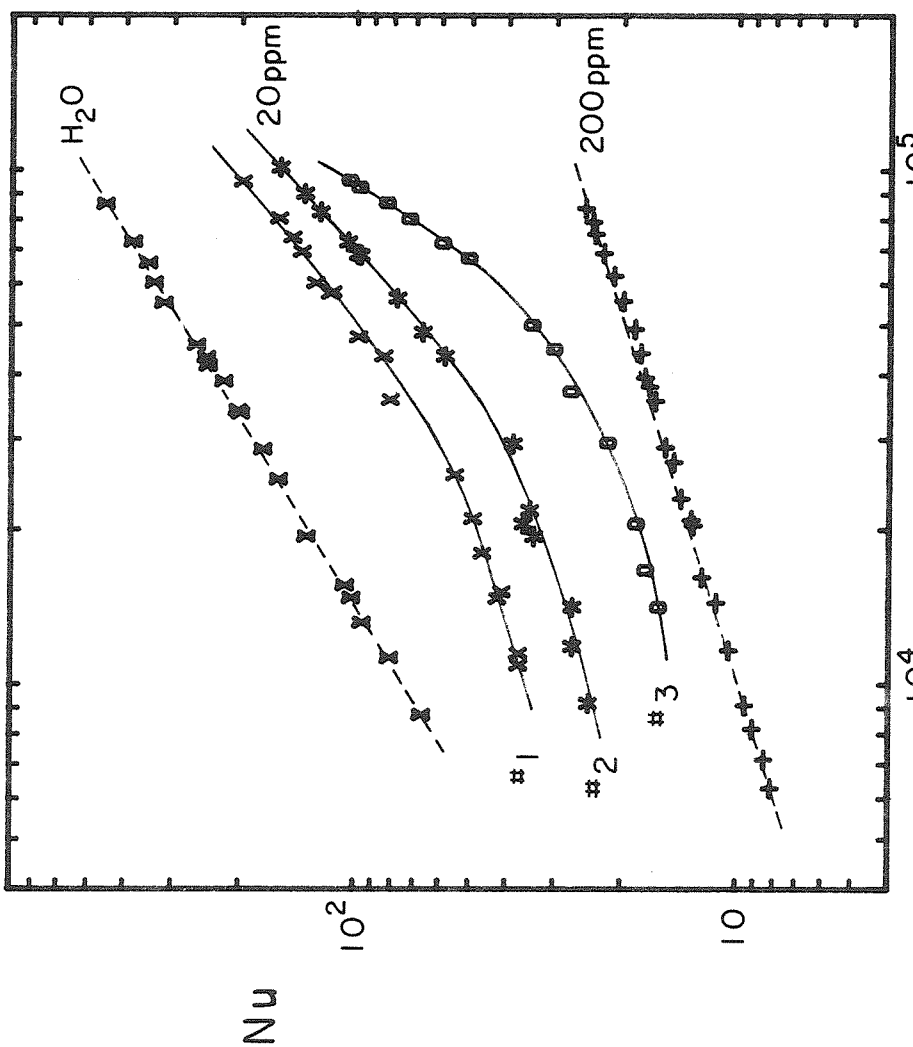

Figure 5.2.-16: Heat transfer results for pre-degraded and asymptotic polymer solutions. (20 ppm #1, #2, and #3; 200 ppm #3; x/D= 560; wall temperature reference; degraded viscosity functions.)

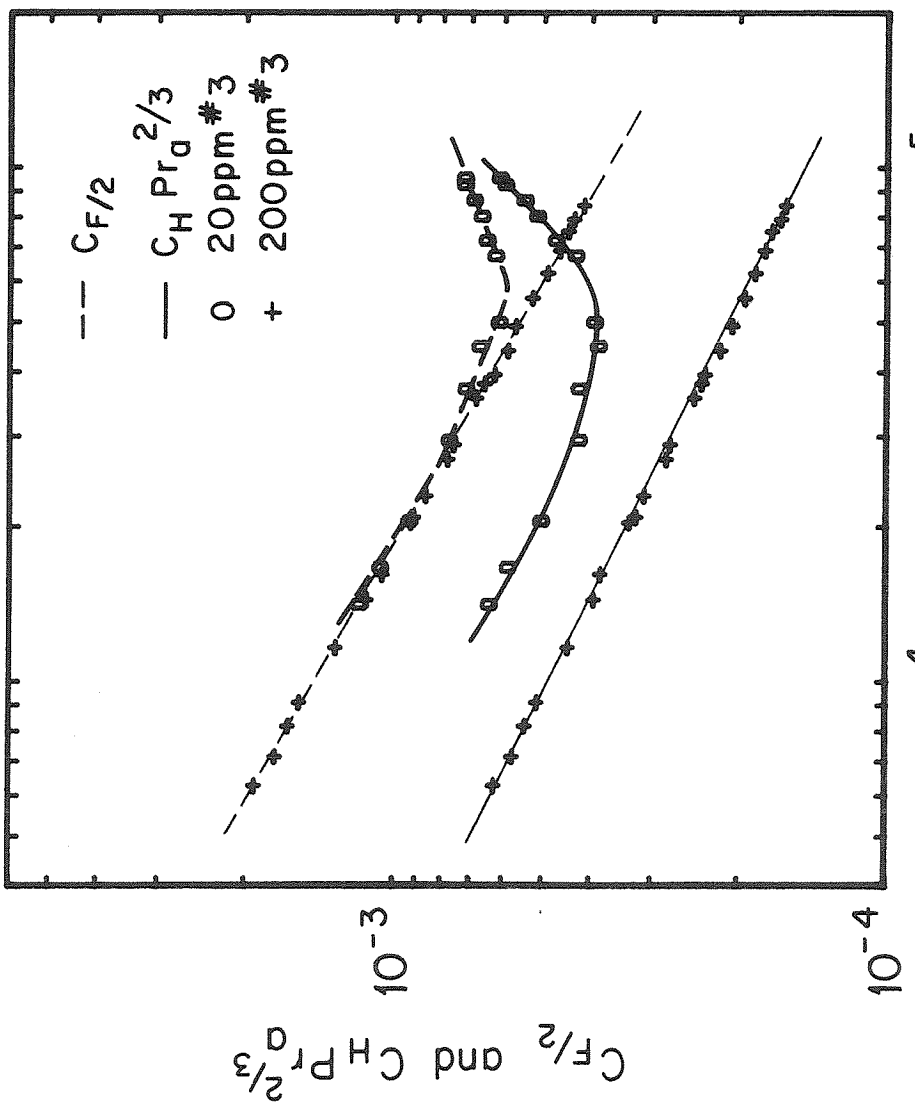

Figure 5.2.-17: Comparison of friction and heat transfer for predegraded and asymptotic polymer solutions. (20 ppm #3, 200 ppm #3, x/D= 560, wall temperature reference, degraded viscosity functions.)

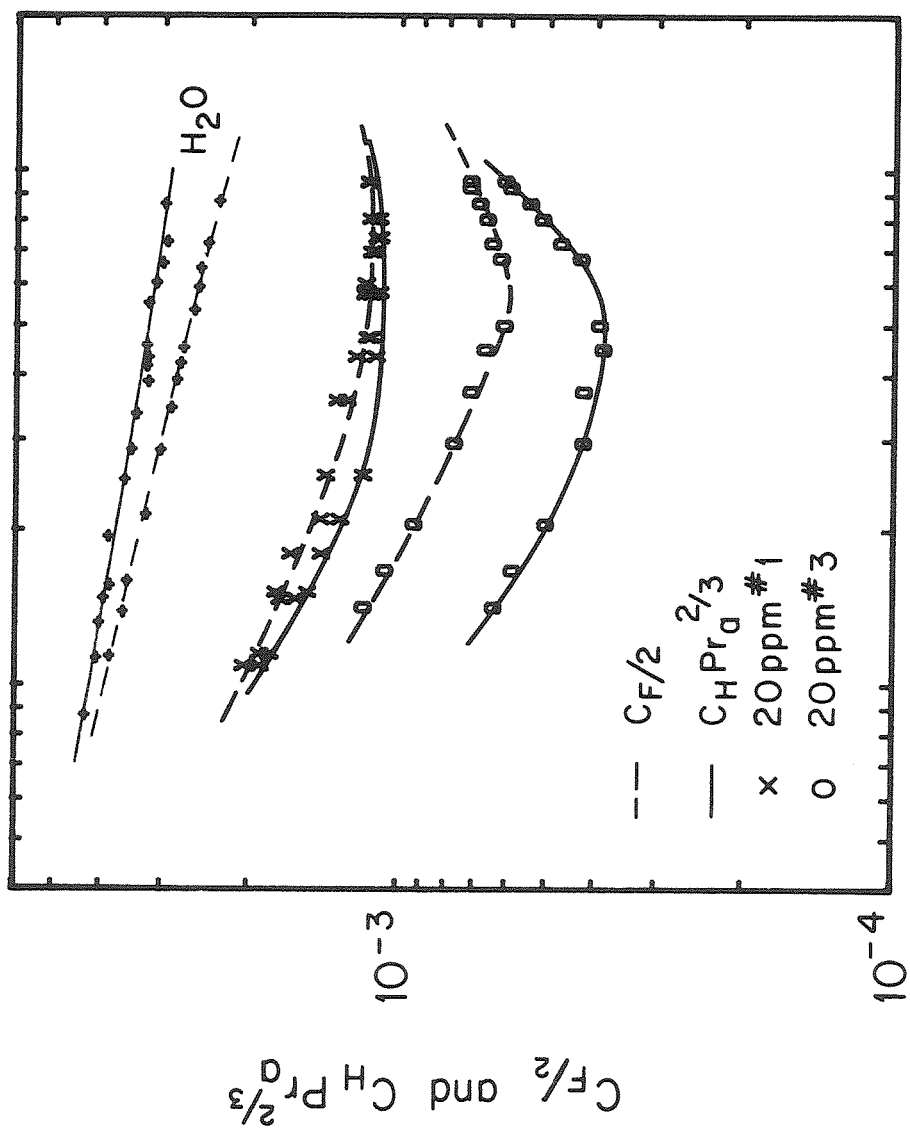

Figure 5.2.-18: Comparison of friction and heat transfer for various levels of pre-degradation for polymer solutions. (20 ppm #1 and #3, x/D= 560, wall temperature reference, degraded viscosity functions.)

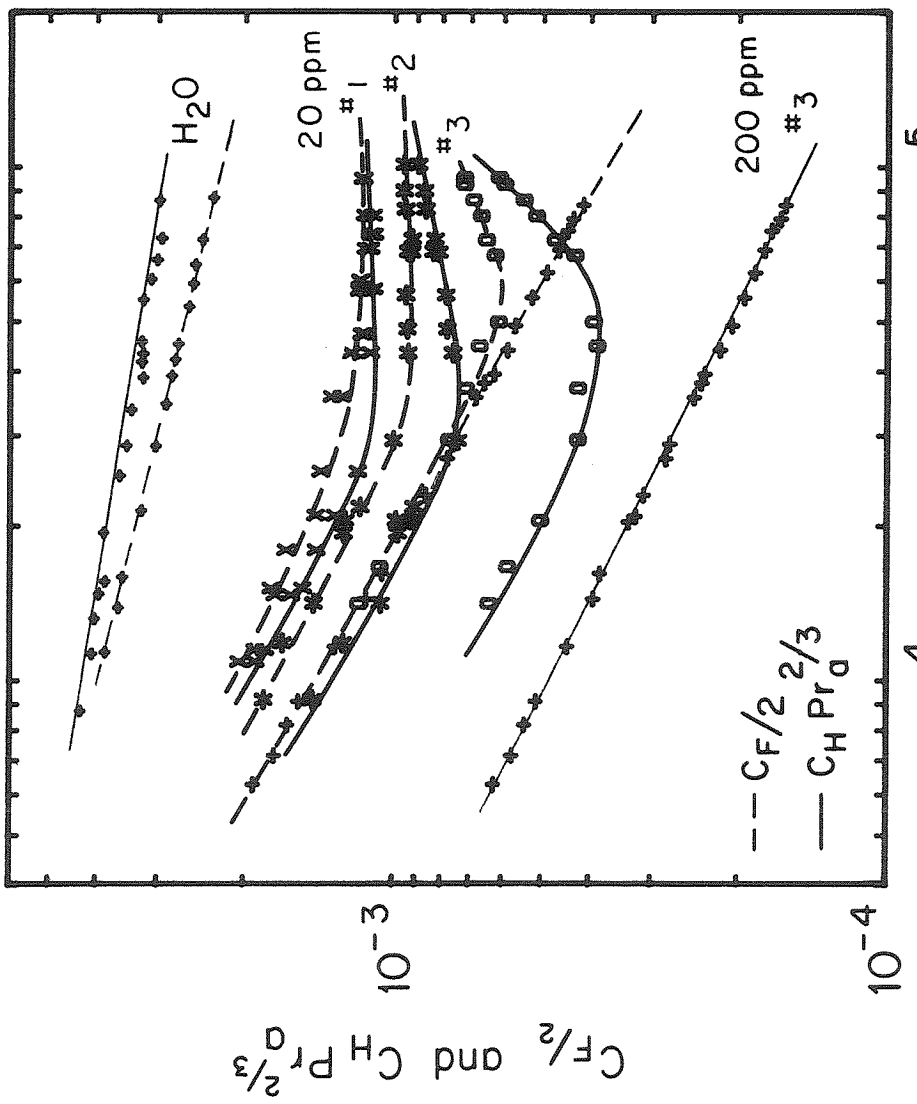

Figure 5.2.-19: Comparison of friction and heat transfer for pre-degraded and asymptotic polymer solutions. (20 ppm #1, #2, and #3; 200 ppm #3; x/D= 560; wall temperature reference; degraded viscosity functions.)

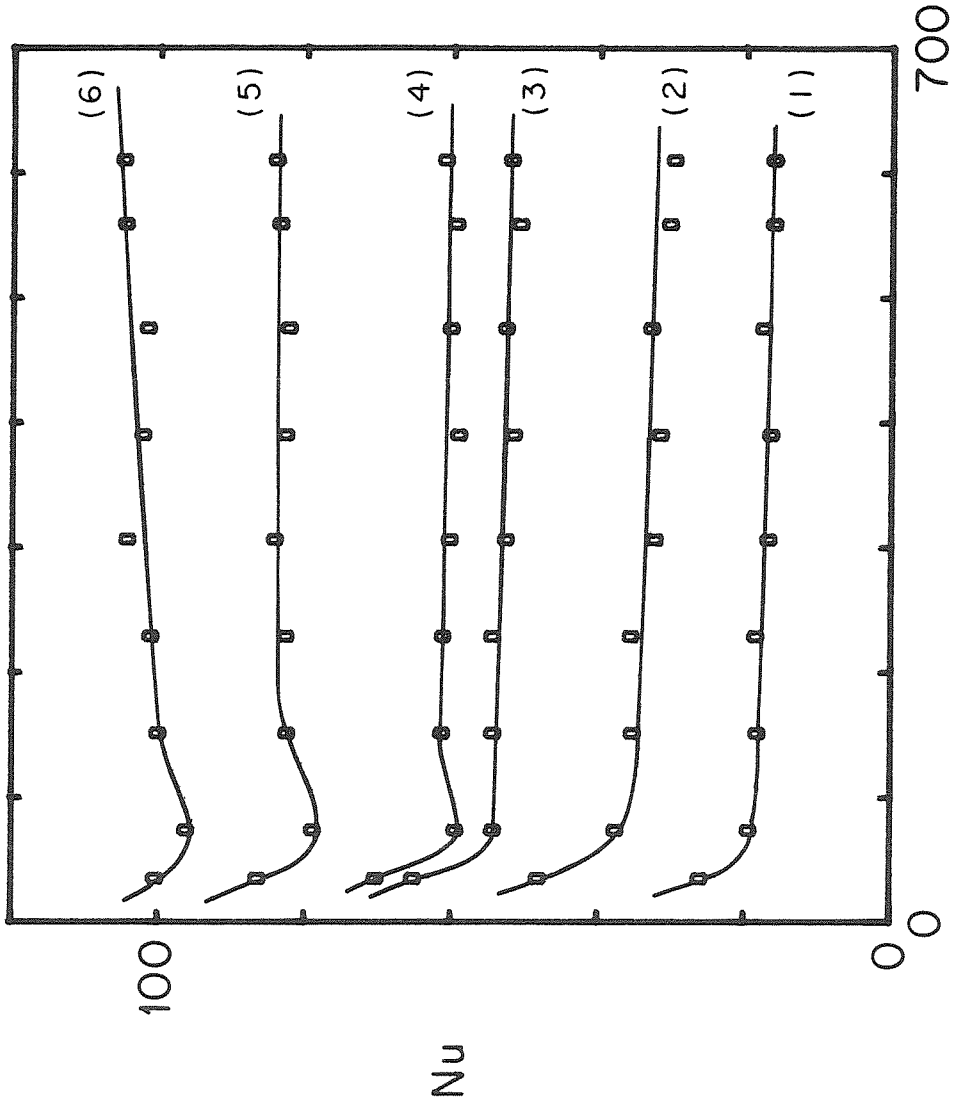

Figure 5.2.-20: Heat transfer results as function of distance for non-asymptotic polymer solutions. Curve (1): Re_a=14100 (Pr_a=5.56); (2): 44800 (5.27); (3): 67300 (5.33); (4): 72100 (5.33); (5) 86300 (5.46); (6) 95500 (5.59). (20 ppm #3; wall temperature reference; degraded viscosity functions.)

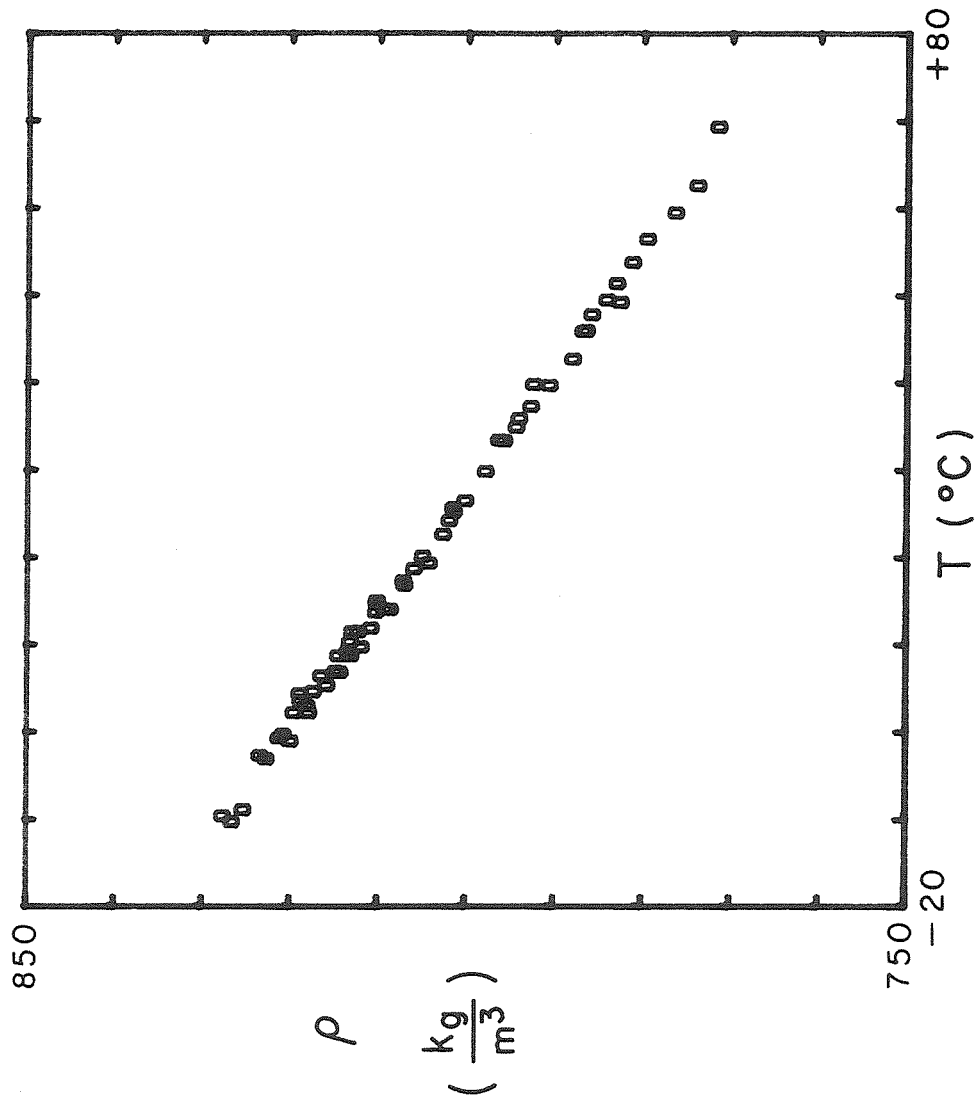

Figure 5.3.-1: Effect of temperature on density of kerosene.

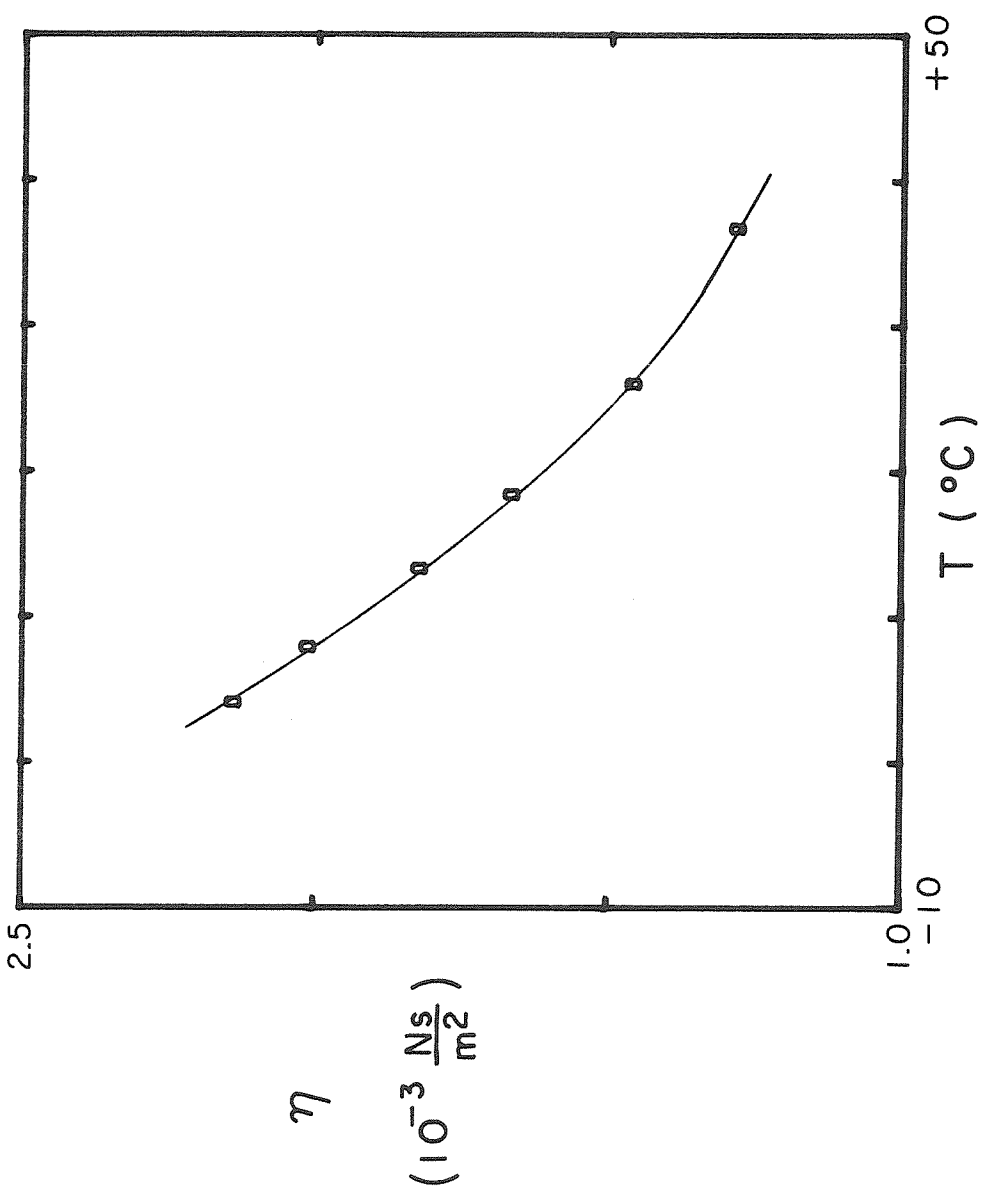

Figure 5.3.-2: Effect of temperature on viscosity of kerosene. (T-20 capillary.)

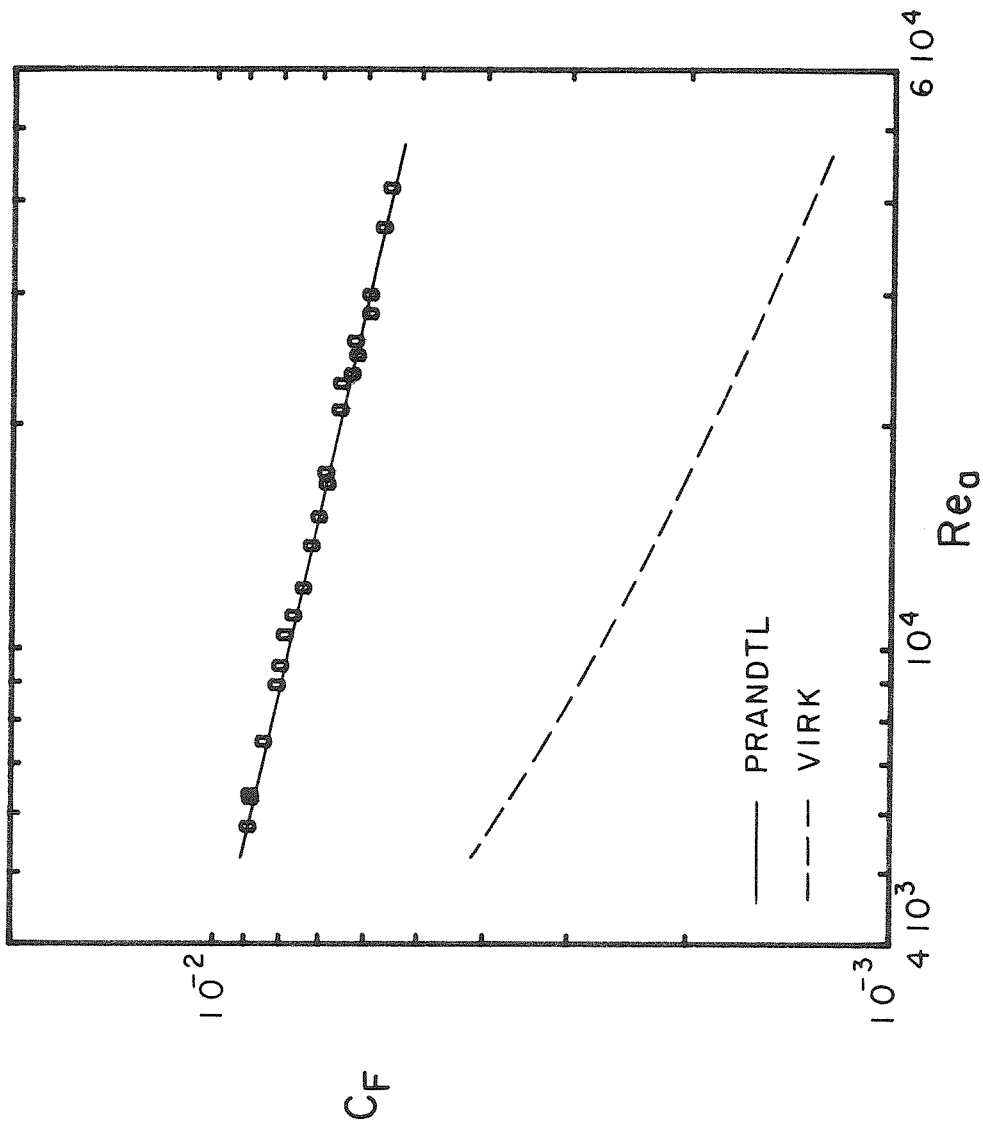

Figure 5.3.-3: Friction results for kerosene. (Averaged for $350 < x/D < 600$; wall temperature reference.)

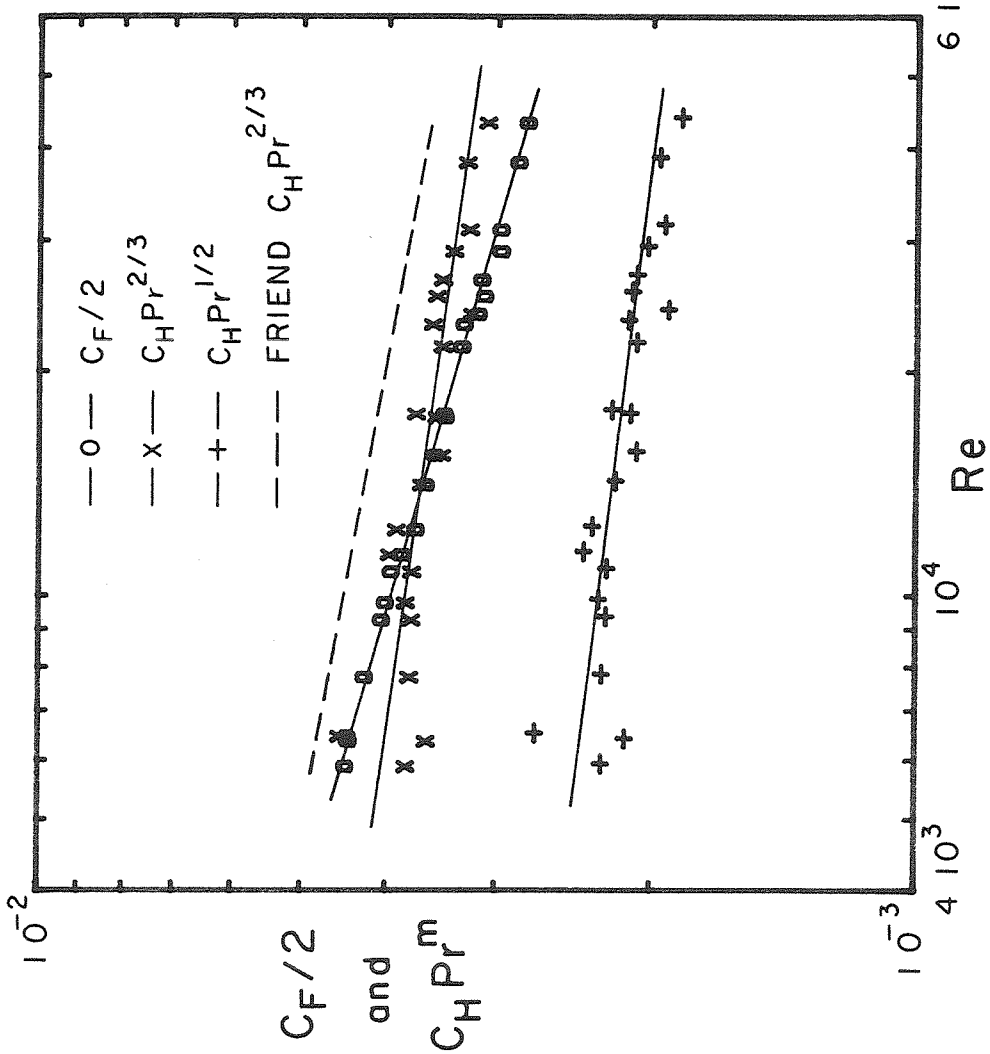

Figure 5.3.-4: Comparison of friction and heat transfer for kerosene.
(Averaged for $350 < x/D < 600$; wall temperature reference.)

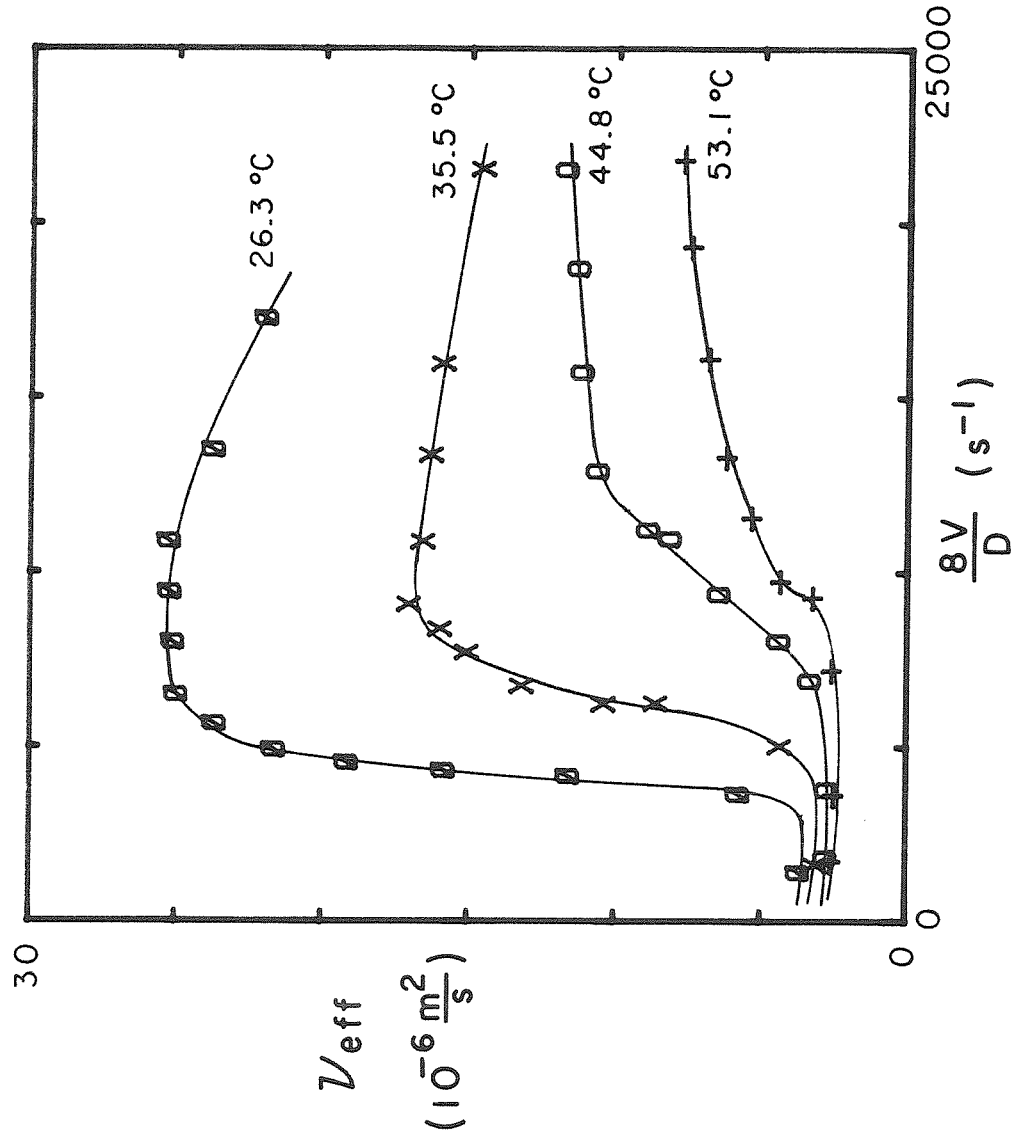

Figure 5.4.-1: Effect of temperature on the viscosity functions of antimisting kerosene. (Unused AMK #2, 2 days old, T-20 capillary.)

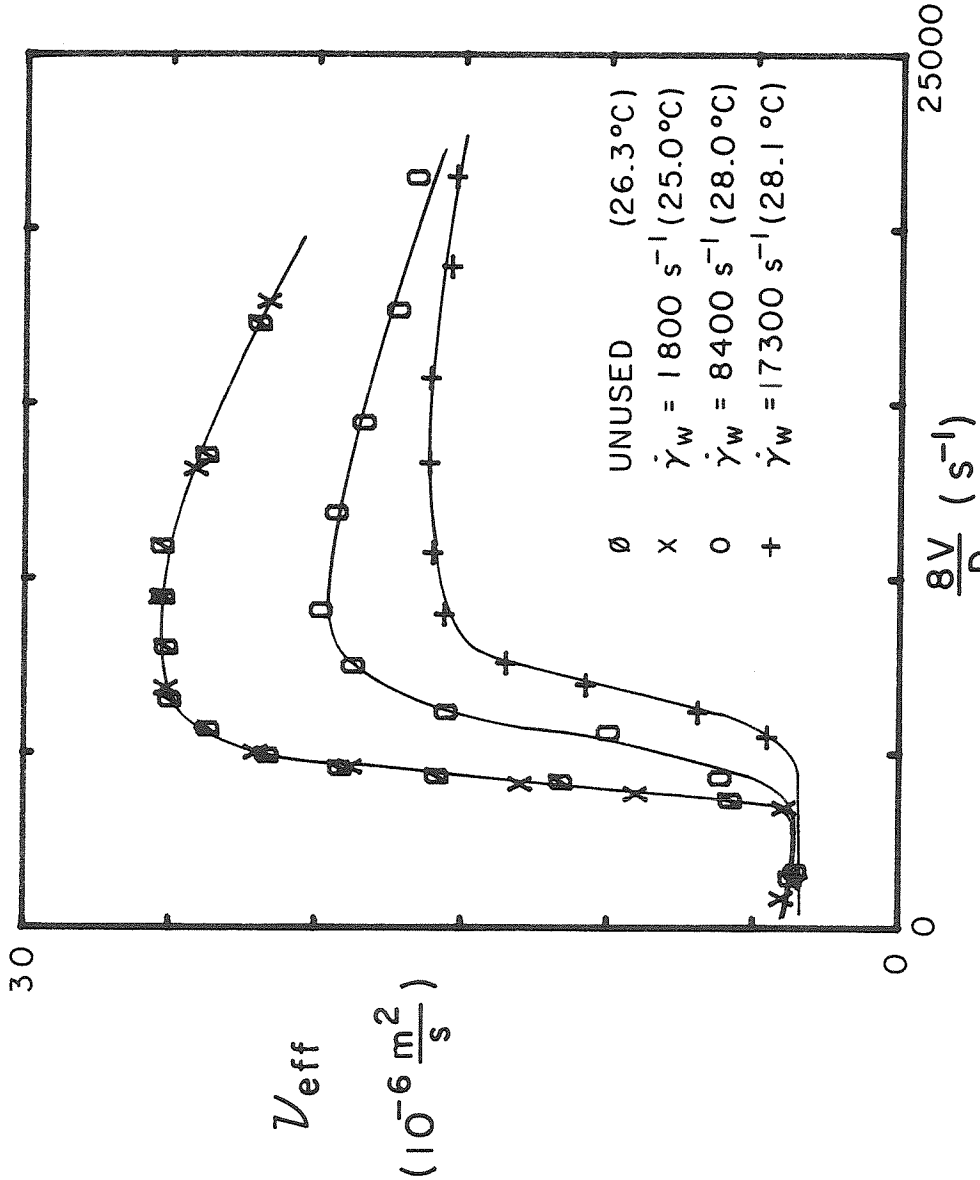

Figure 5.4.-2: Effect of degradation on the viscosity functions of antimisting kerosene. Samples ran at $\dot{\gamma}_w$ = 1800 s^{-1} (Re_a = 4000, τ_w = 3.5 N/m^2); $\dot{\gamma}_w$ = 8400 s^{-1} (Re_a = 11700, τ_w = 17.0 N/m^2); and $\dot{\gamma}_w$ = 17300 s^{-1} (Re_a = 13200, τ_w = 65.0 N/m^2). (AMK #2, 2 days old, T-20 capillary.)

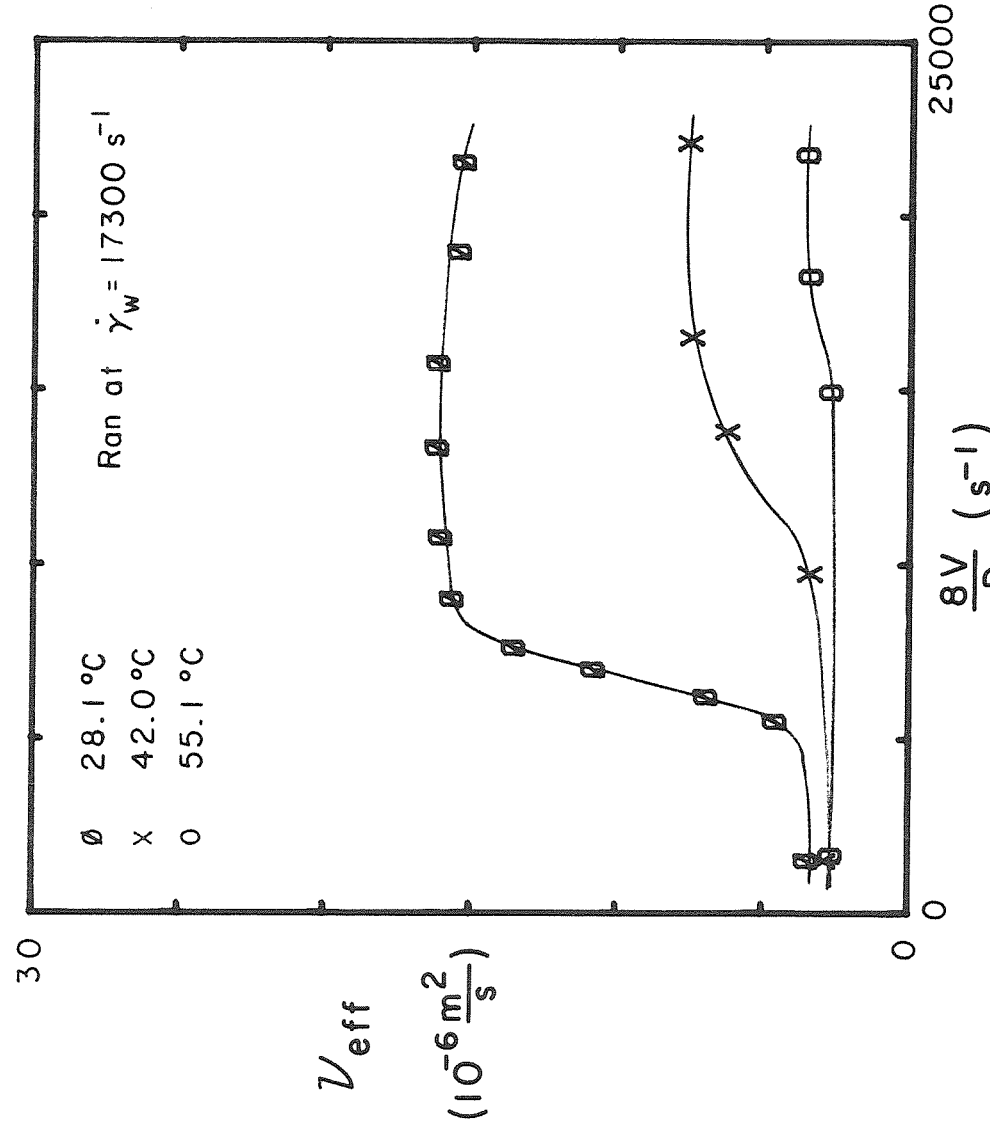

Figure 5.4.-3: Effect of temperature on the viscosity functions of degraded antimisting kerosene. Sample ran at $\dot{\gamma}_w$ = 17300 s^{-1} (Re_a = 13200, τ_w = 65.0 N/m^2). (AMK #2, 2 days old, T-20 capillary.)

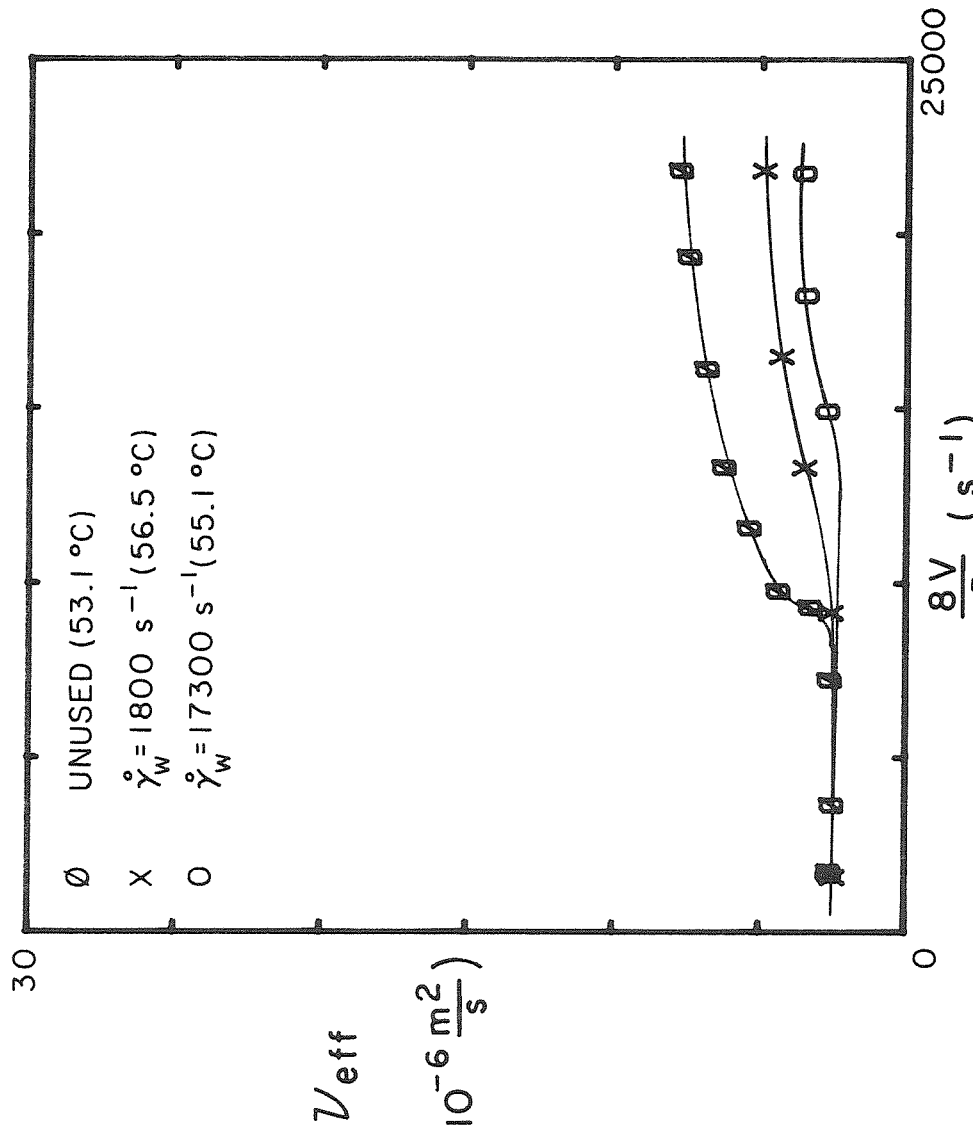

Figure 5.4.-4: Effect of degradation on the viscosity functions of antimisting kerosene at high temperature. Samples ran at $\dot{\gamma}_w$ = 1800 s^{-1} (Re_a = 4000, τ_w = 3.5 N/m^2) and $\dot{\gamma}_w$ = 17300 s^{-1} (Re_a = 13200, τ_w = 65.0N/m^2). (AMK #2, 2 days old, T-20 capillary.)

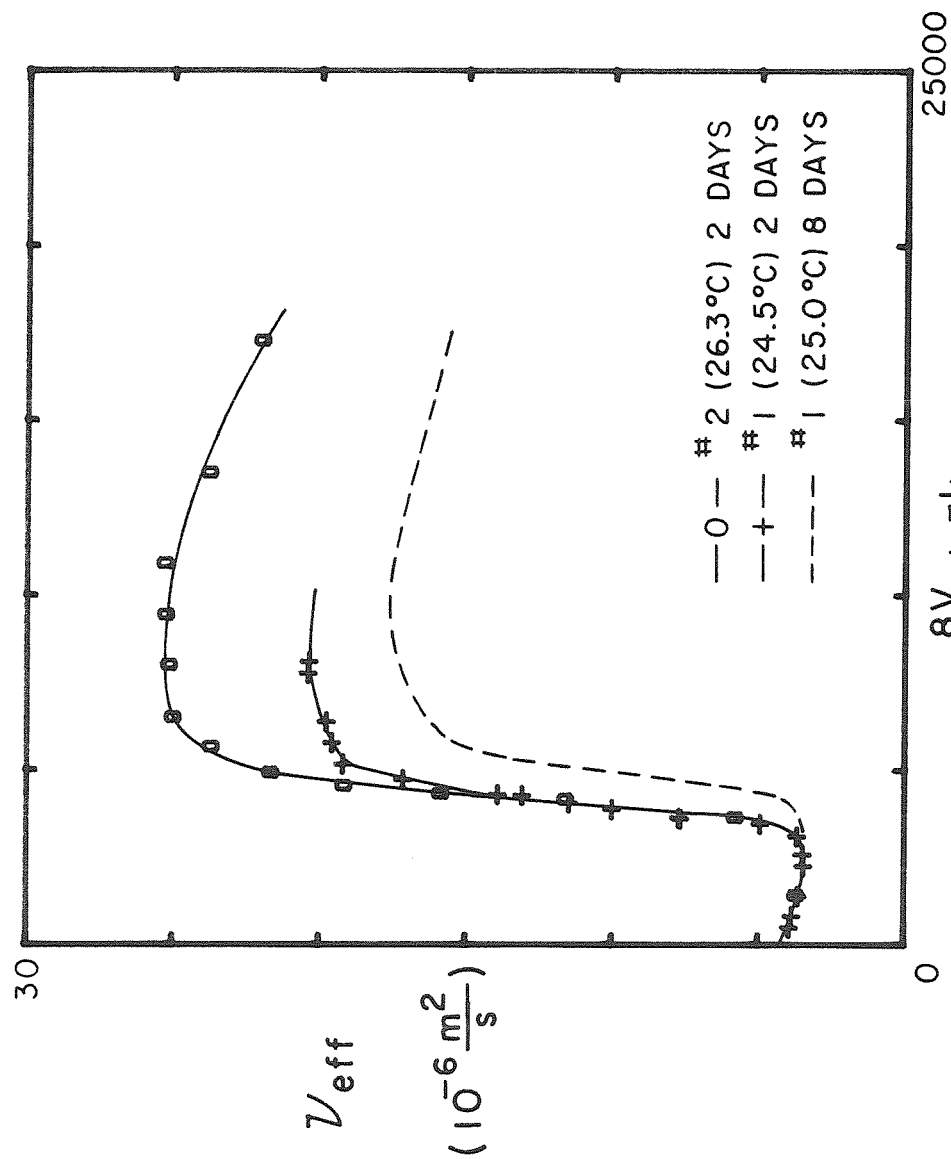

Figure 5.4.-5: Concentration and aging effect on the viscosity functions of antimisting kerosene. (AMK #1, 0.275 %, at 2 and 8 days; AMK #2, 0.315 %, at 2 days; T-20 capillary.)

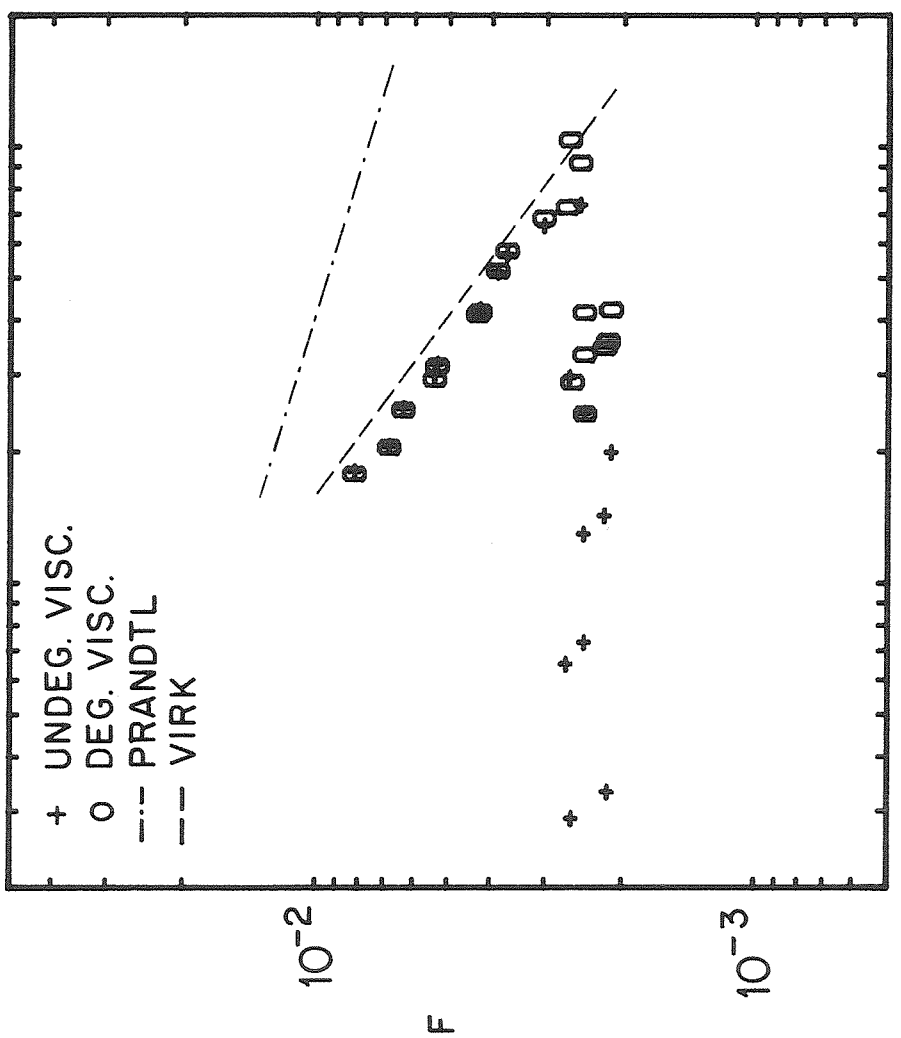

Figure 5.4.-6: Friction results for antimisting kerosene. Computations conducted with undegraded and degraded viscosity functions. (AMK #2, 2 days old, bulk temperature reference, averaged for $265 < x/D < 600$.)

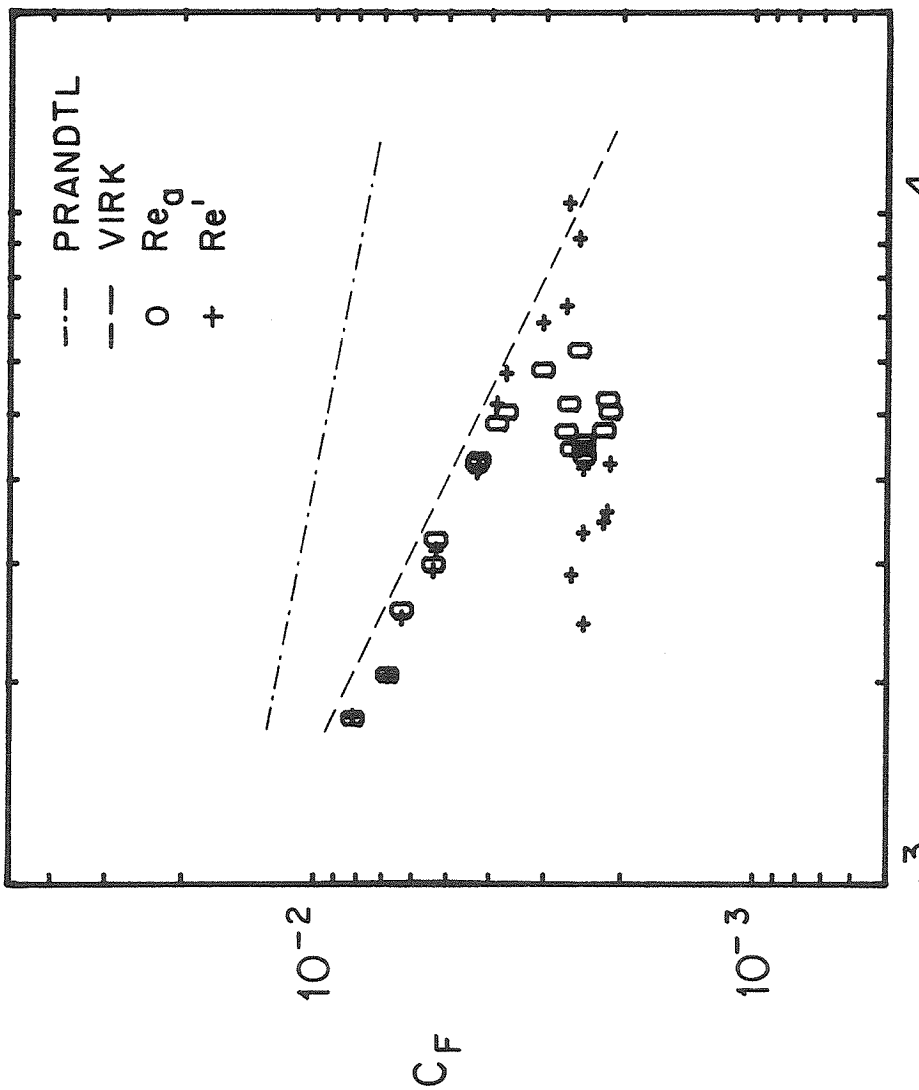

Figure 5.4.-7: Friction results for antimisting kerosene. Apparent and generalized Reynolds number representations. (AMK #2, 2 days old, bulk temperature reference, degraded viscosity functions, averaged for $265 < x/D < 600$.)

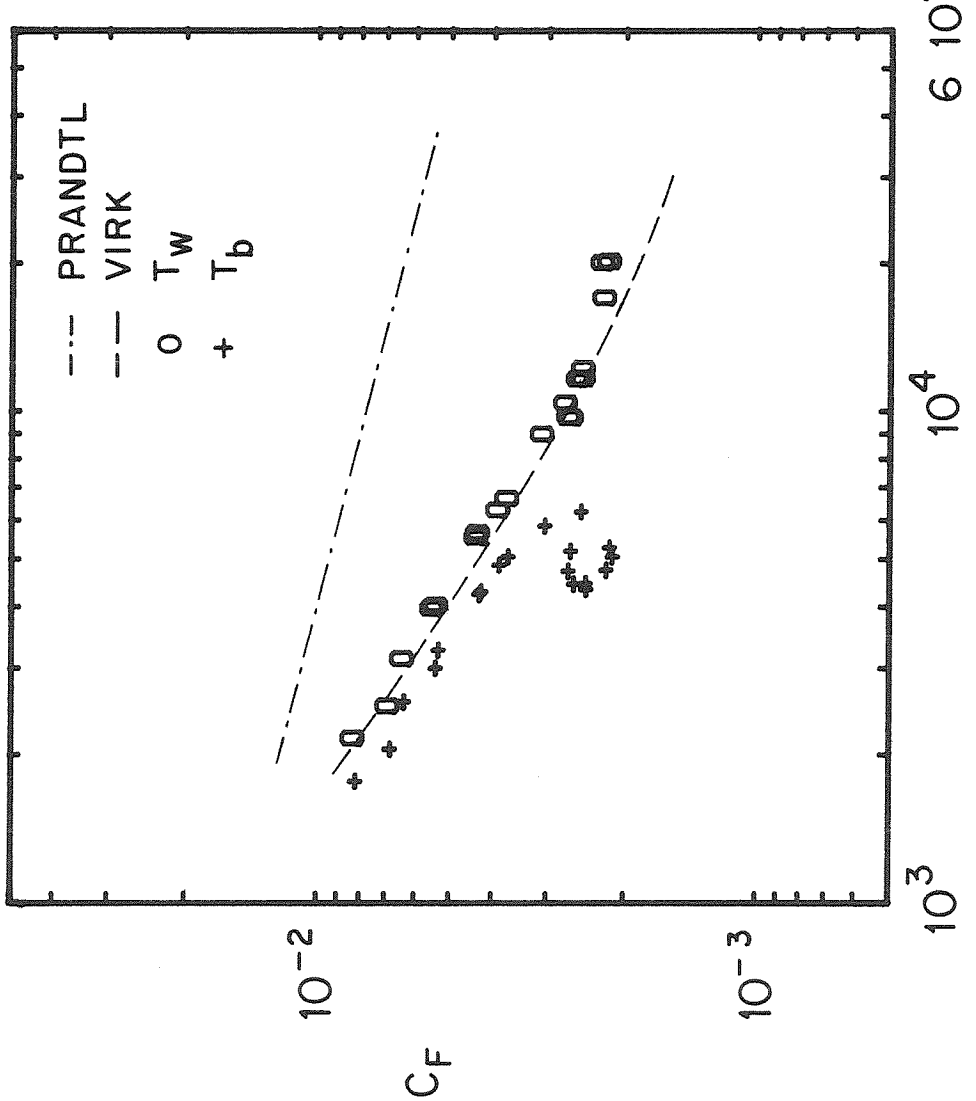

Figure 5.4.-8: Friction results for antimisting kerosene. Computations conducted at wall and bulk temperature. (AMK #2, 2 days old, degraded viscosity functions, averaged for $265 < x/D < 600$.)

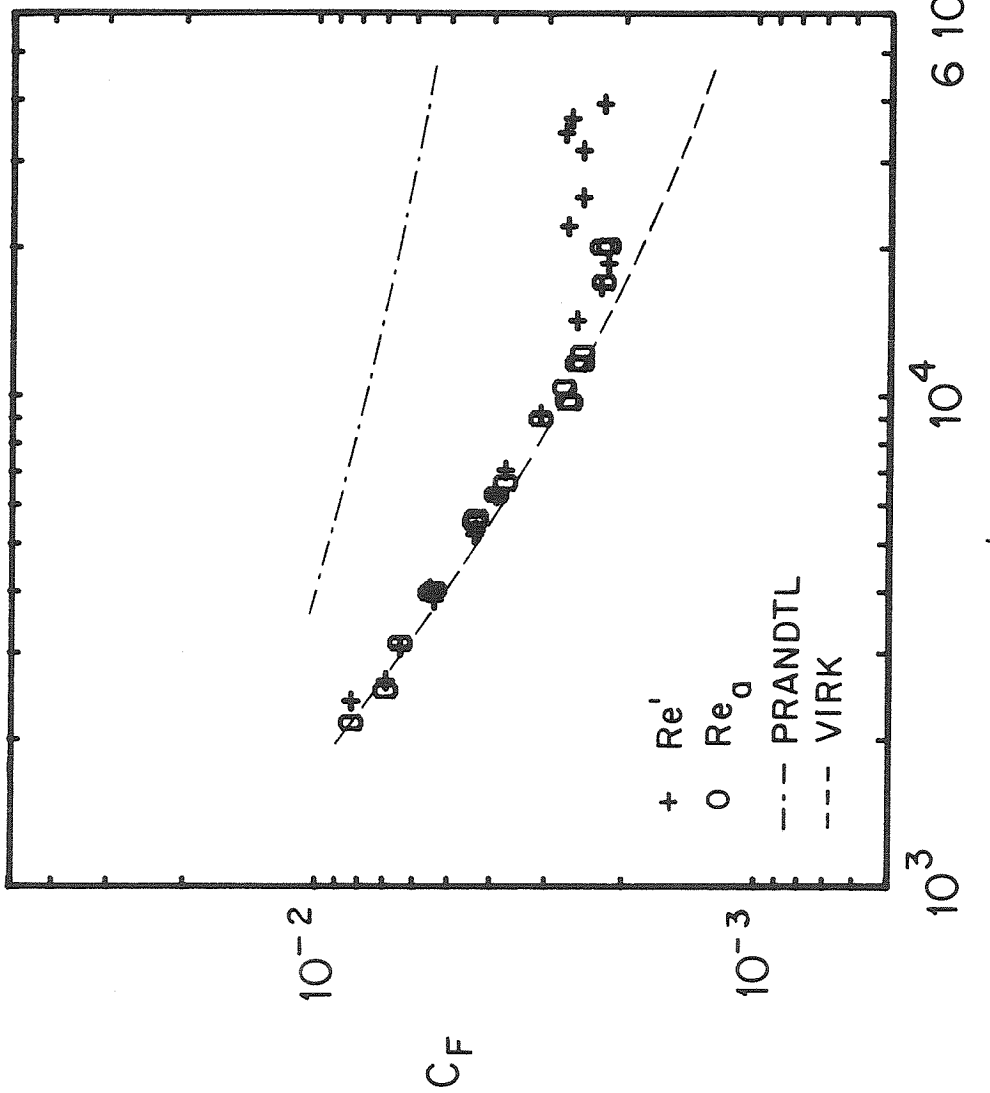

Figure 5.4.-9: Friction results for antimisting kerosene. Apparent and generalized Reynolds number representations. (AMK #2, 2 days old, wall temperature reference, degraded viscosity functions, averaged for $265 < x/D < 600$.)

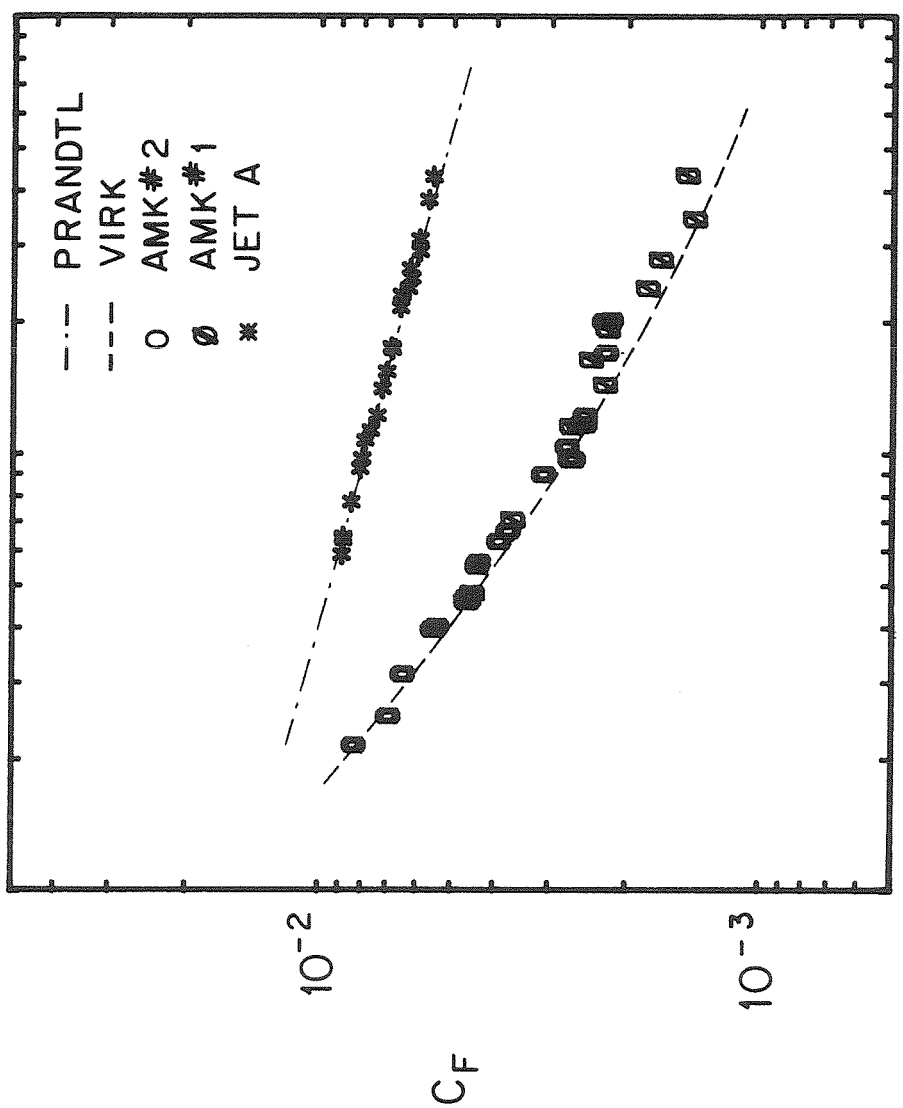

Figure 5.4.-10: Friction results for different batches of antimisting kerosene. (AMK #1, 8 days old; AMK #2, 2 days old; wall temperature reference; degraded viscosity functions; averaged for 265 < x/D < 600.)

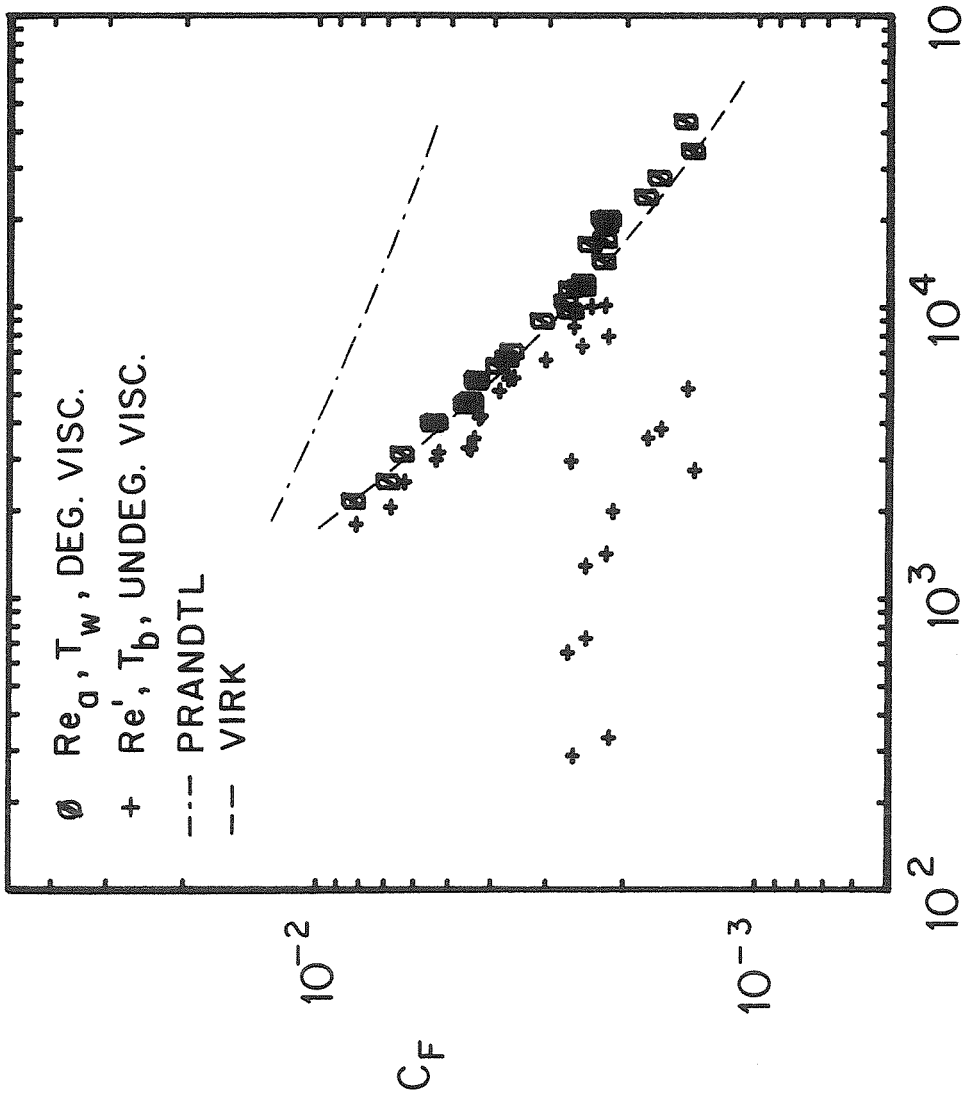

Figure 5.4.-11: Friction results for antimisting kerosene. Extreme computational configurations: (1) Apparent Reynolds number, wall temperature reference, degraded viscosity functions; and (2) generalized Reynolds number, bulk temperature reference, unused viscosity functions. (AMK #1, 8 days old; AMK #2, 2 days old; averaged for $265 < x/D < 600$.)

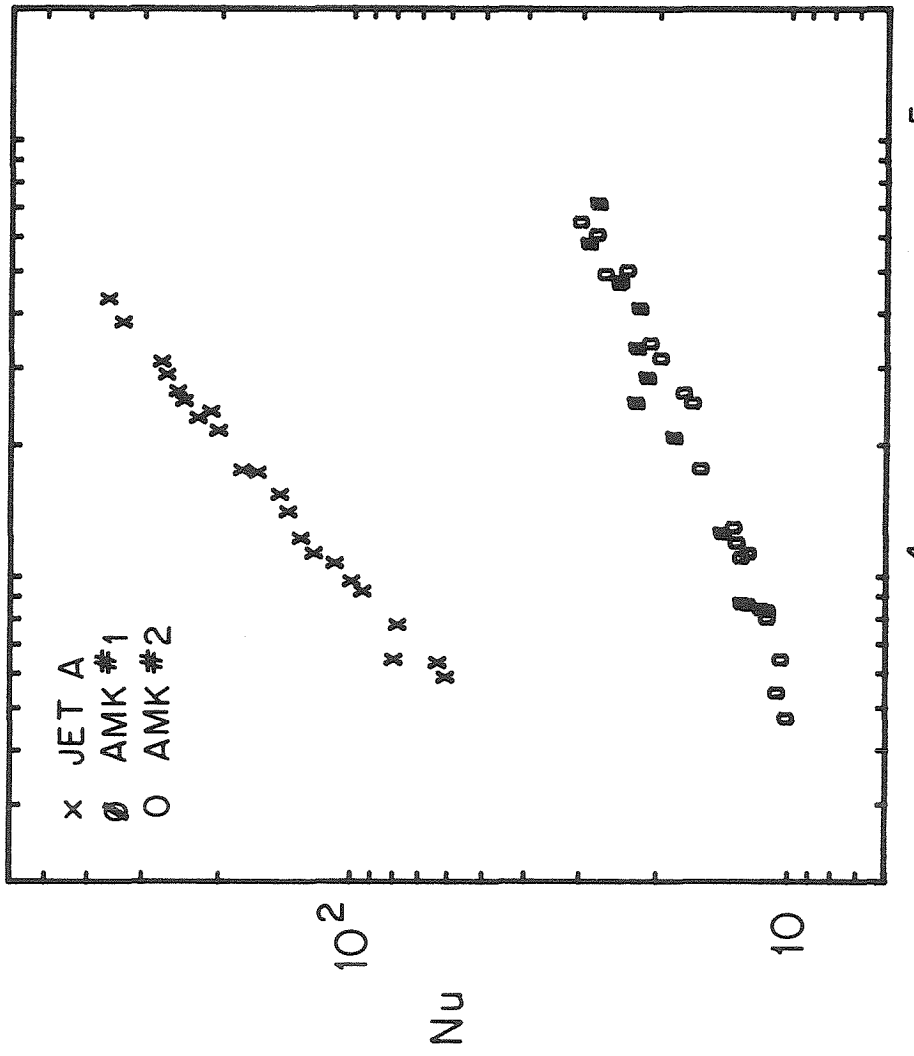

Figure 5.4.-12: Heat transfer results for antimisting kerosene. Solvent Reynolds number representation. (AMK #1, 8 days old; AMK #2, 2 days old; wall temperature reference; degraded viscosity functions; averaged for $307 < x/D < 560$.)

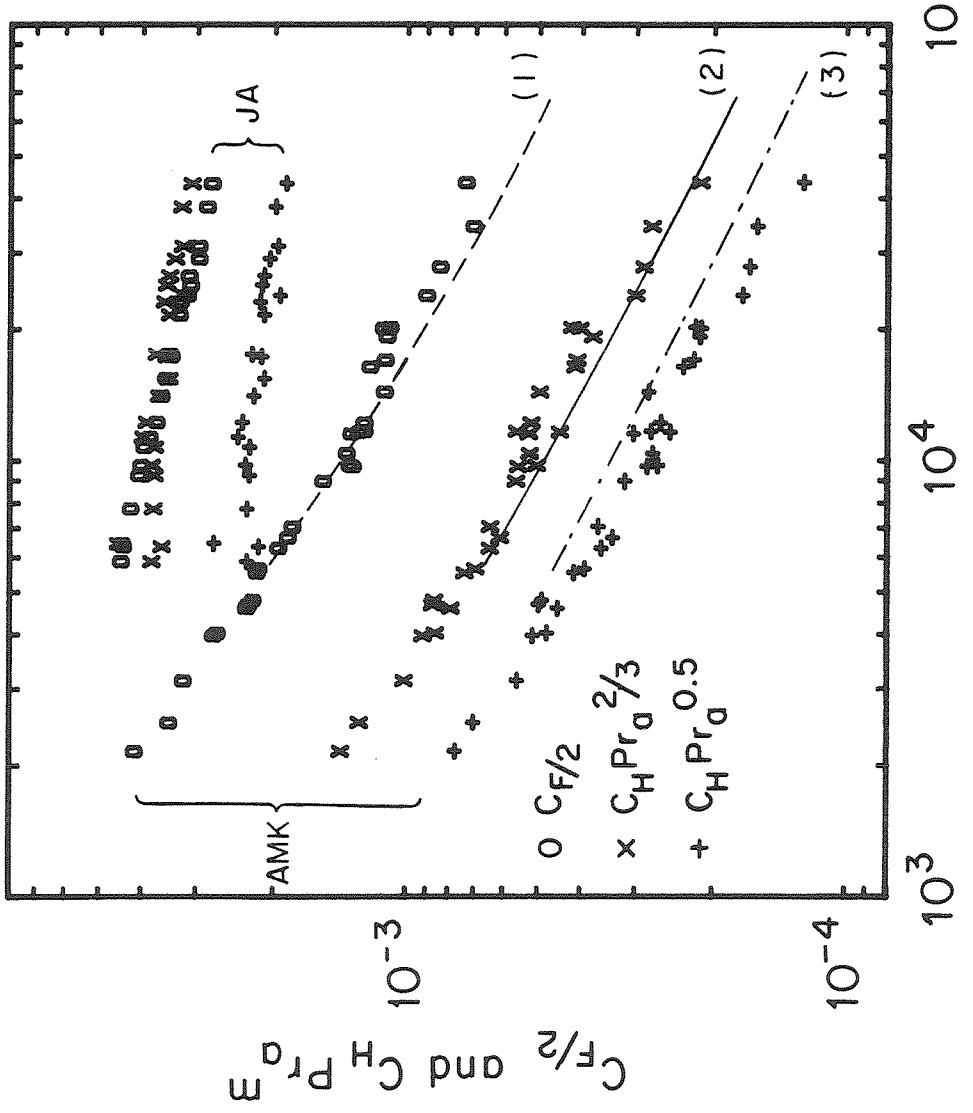

Figure 5.4.-13: Comparison of friction and heat transfer for antimisting kerosene. Curve (1) for asymptotic polymer solution: $C_f/2$; (2): $C_H Pr_a^{2/3}$; (3): $C_H Pr_a^{1/2}$. (AMK #1, 8 days old; AMK #2, 2 days old; wall temperature reference; degraded viscosity functions; averaged for 307 < x/D < 560.)

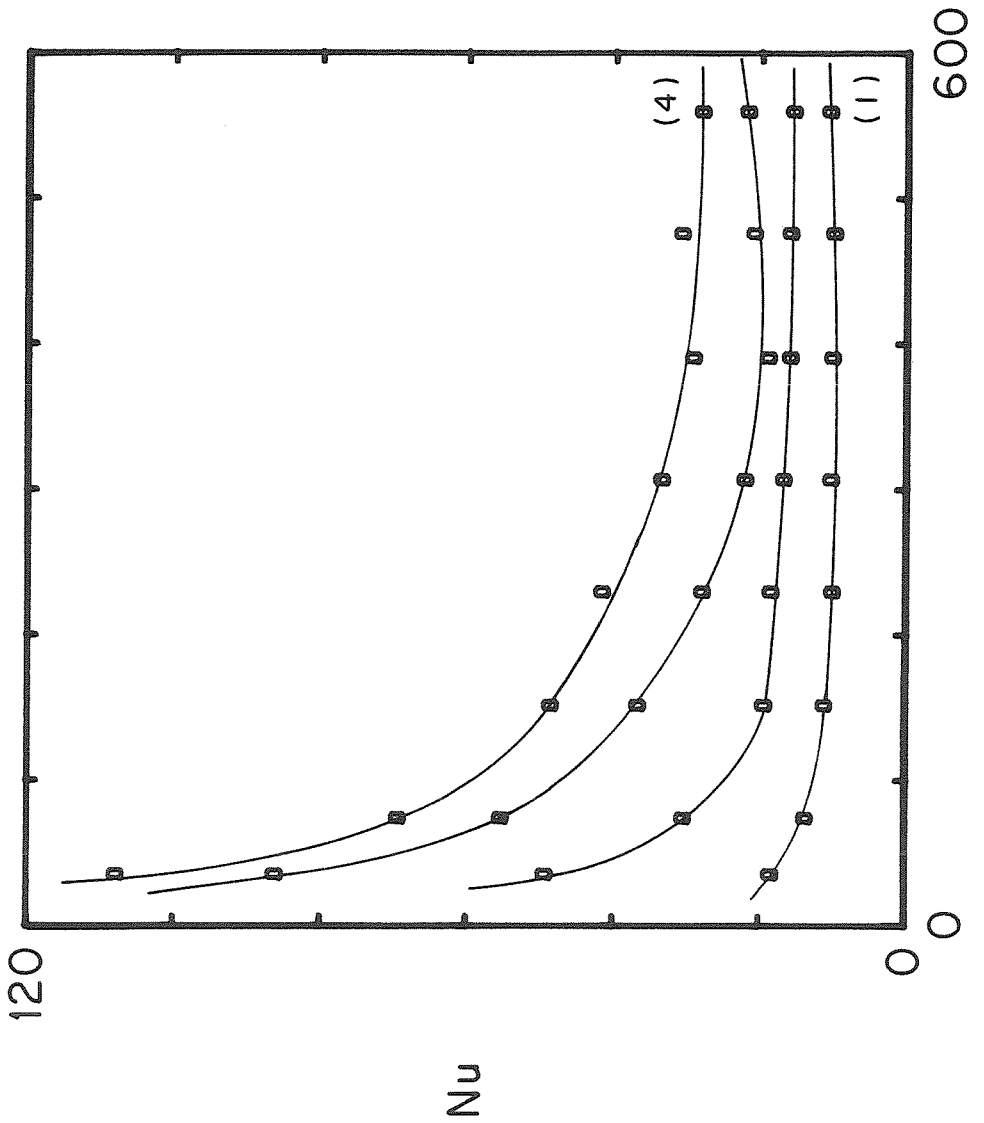

Figure 5.4.-14: Heat transfer results as a function of distance for antimisting kerosene. Curve (1): Re_a = 2220 (Pr_a = 36.3); (2): 9180 (30.8); (3): 8870 (64.3); (4) 25900 (37.9). (AMK #2, 2 days old, wall temperature reference, degraded viscosity functions.)

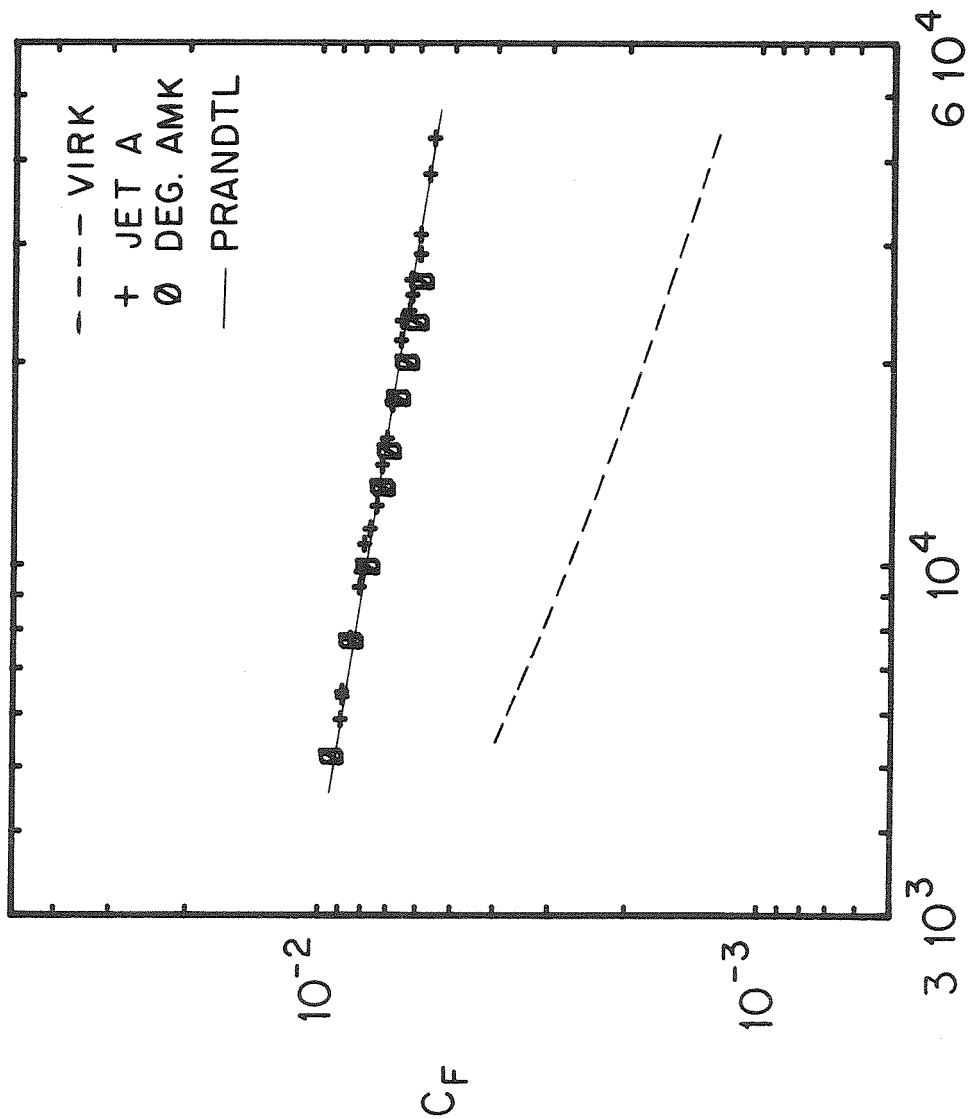

Figure 5.4.-15: Friction results for fully-degraded antimisting kerosene. (AMK #2, wall temperature reference; averaged for $265 < x/D < 600$.)

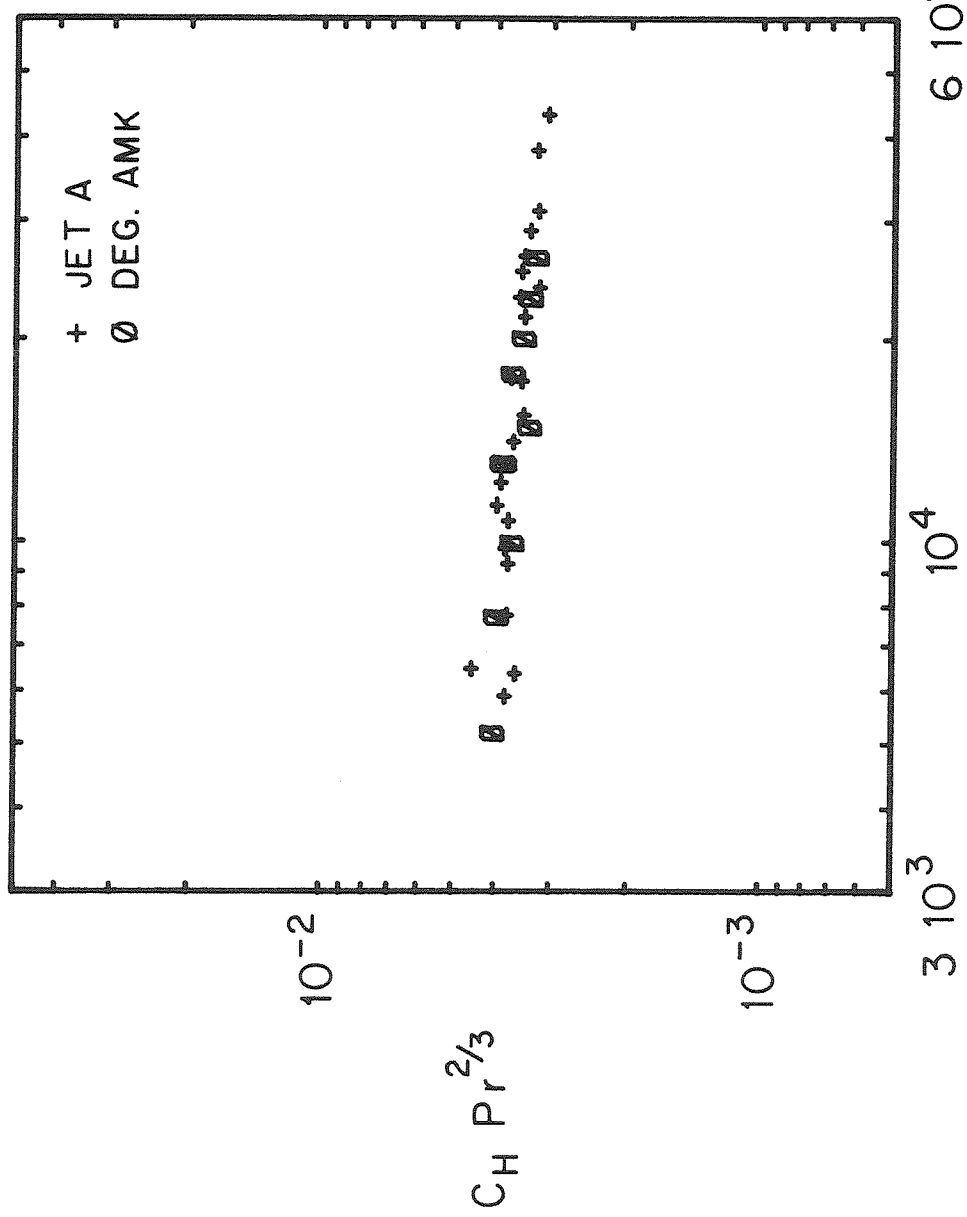

Figure 5.4.-16: Heat transfer results for fully-degraded antimisting kerosene. (AMK #2, wall temperature reference; averaged for $30? < x/D < 560$.)

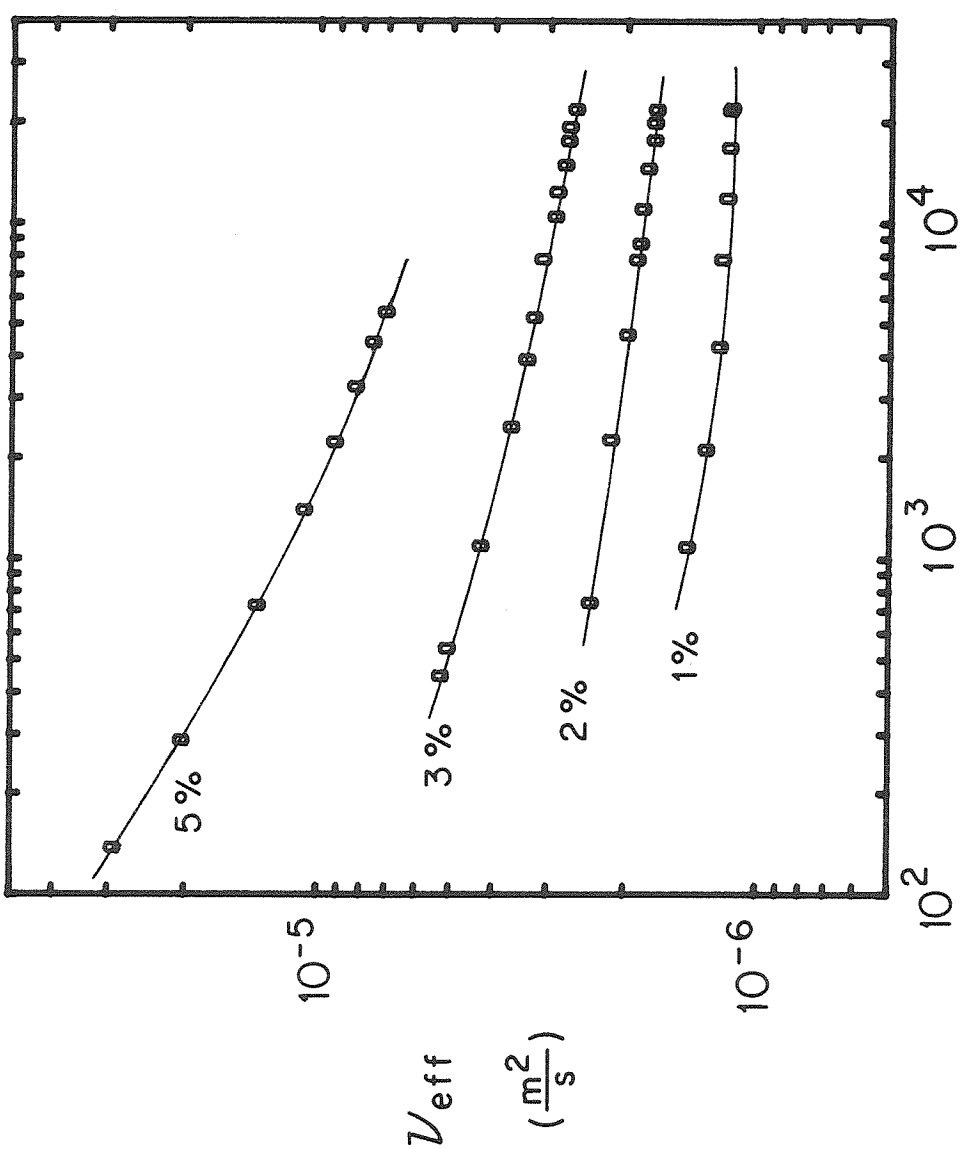

Figure 5.5.-1: Effect of concentration on the viscosity functions of bentonite suspensions. (T-20 capillary; 1% batch measured at 25.4 °*C*; 2% at 25.0 °*C*; 3% at 25.1 °*C*; and 5% at 25.2 °*C*.)

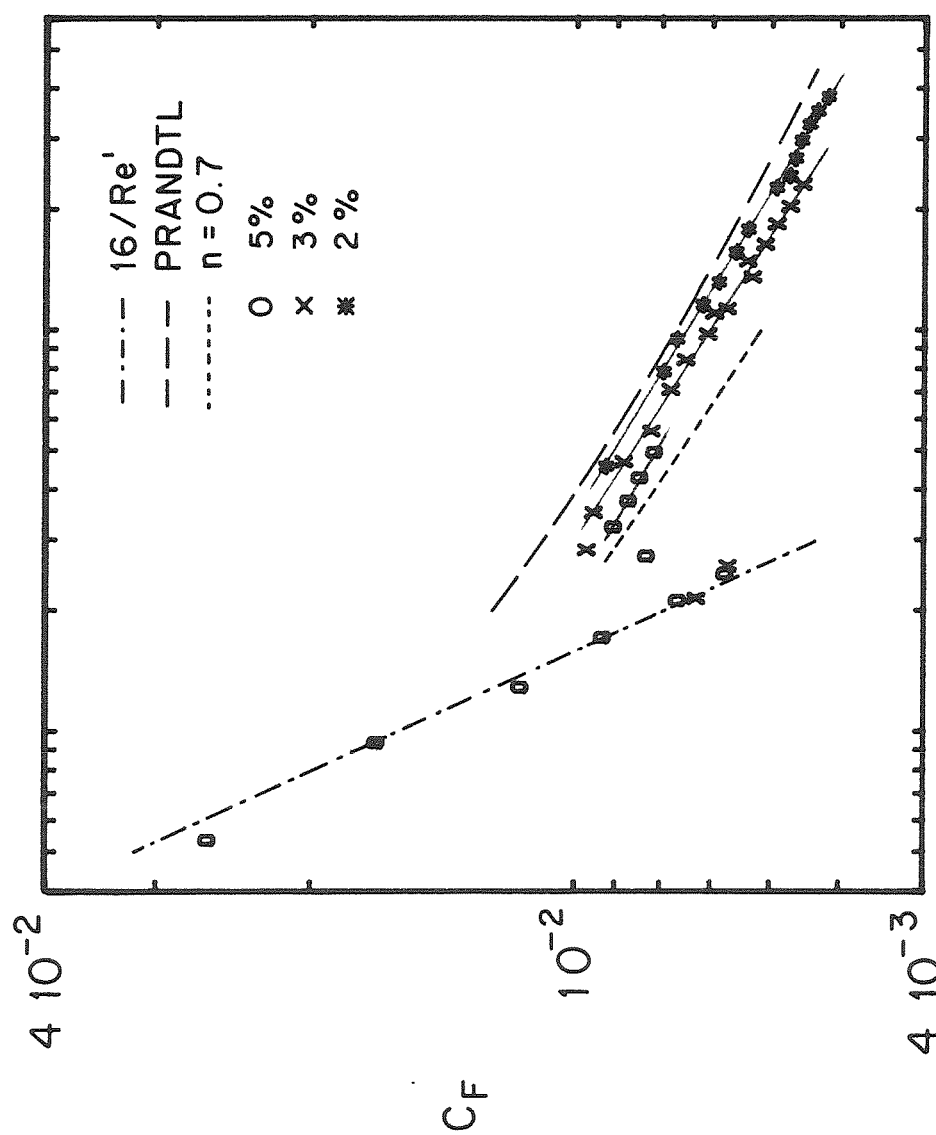

Figure 5.5.-2: Effect of concentration on the friction results of bentonite suspensions in the generalized Reynolds numbers representation. Also shown is Metzner's expression for n = 0.7. (Wall temperature reference; x/D=560; 2%, 3%, and 5%.)

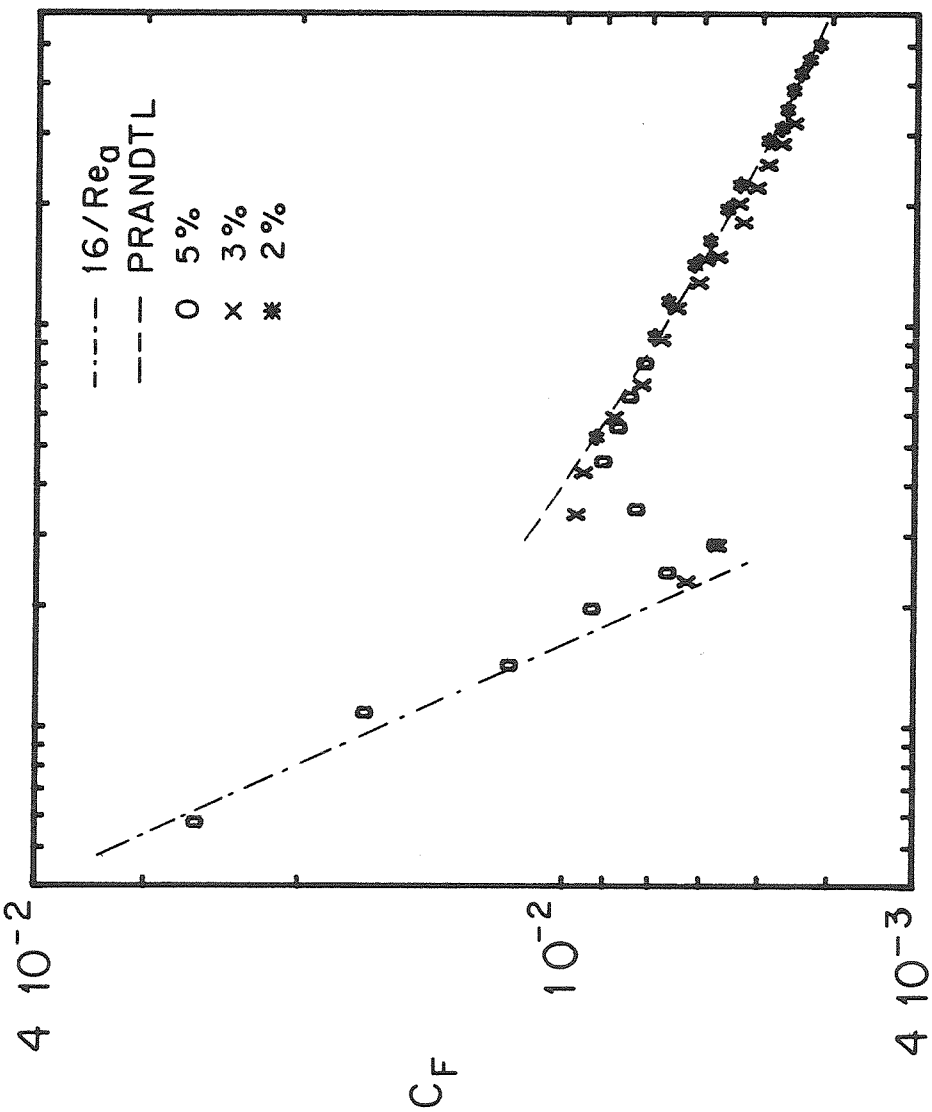

Figure 5.5.-3: Friction results of bentonite suspensions in the apparent Reynolds numbers representation. (Wall temperature reference; x/D=560; 2%, 3%, and 5% .)

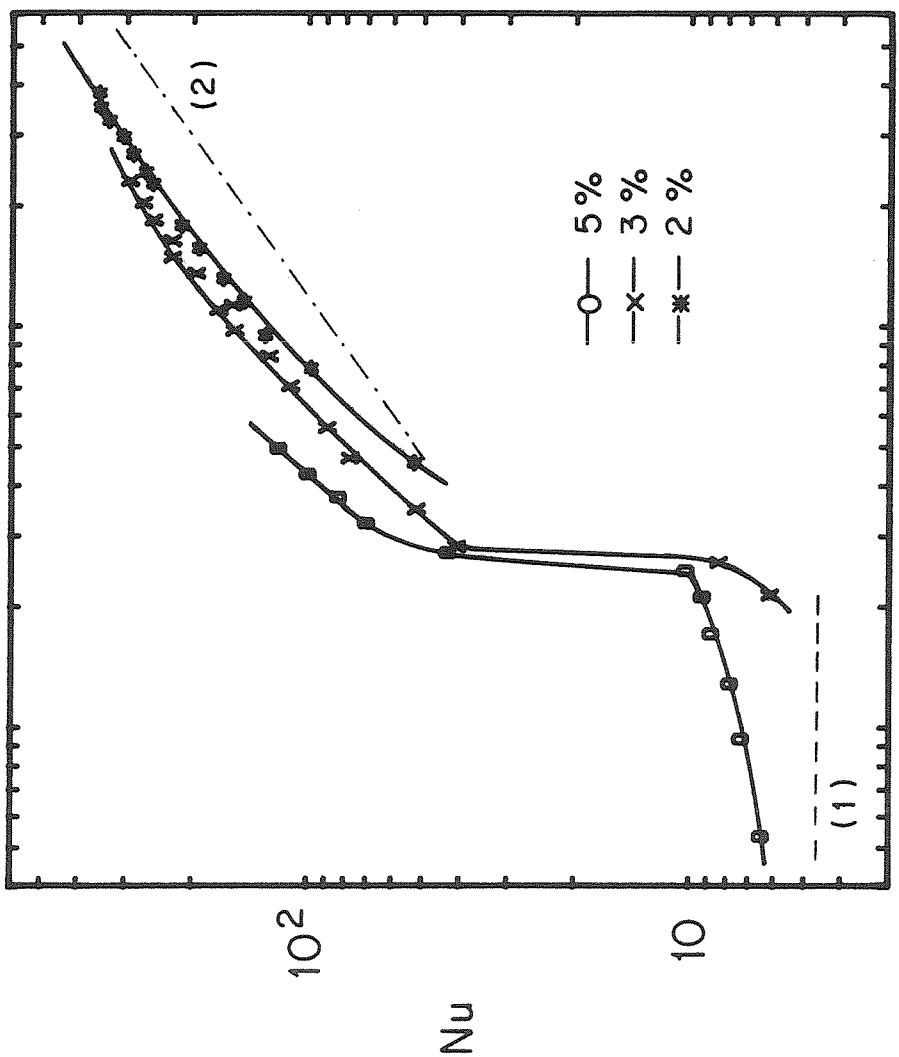

Figure 5.5.-4: Effect of concentration on the heat transfer results for bentonite suspensions. Curve (1): laminar fully-developed heat transfer. Curve (2): Metzner's expression of fully-developed turbulent heat transfer for the 2% suspension. (Wall temperature reference; x/D=560; 2%, 3%, and 5% .)

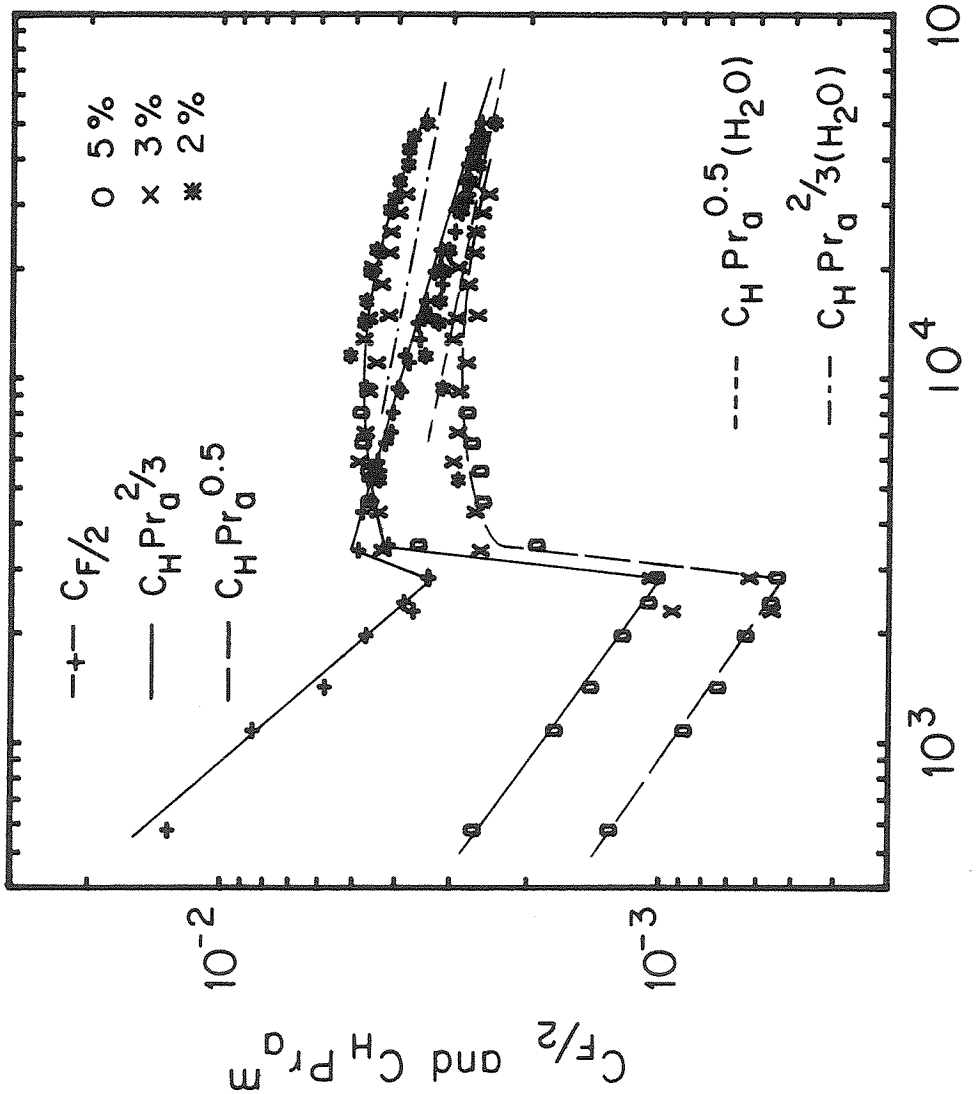

Figure 5.5.-5: Comparison of friction and heat transfer results for bentonite suspensions. (Wall temperature reference; x/D=560; 2%, 3%, and 5% .)

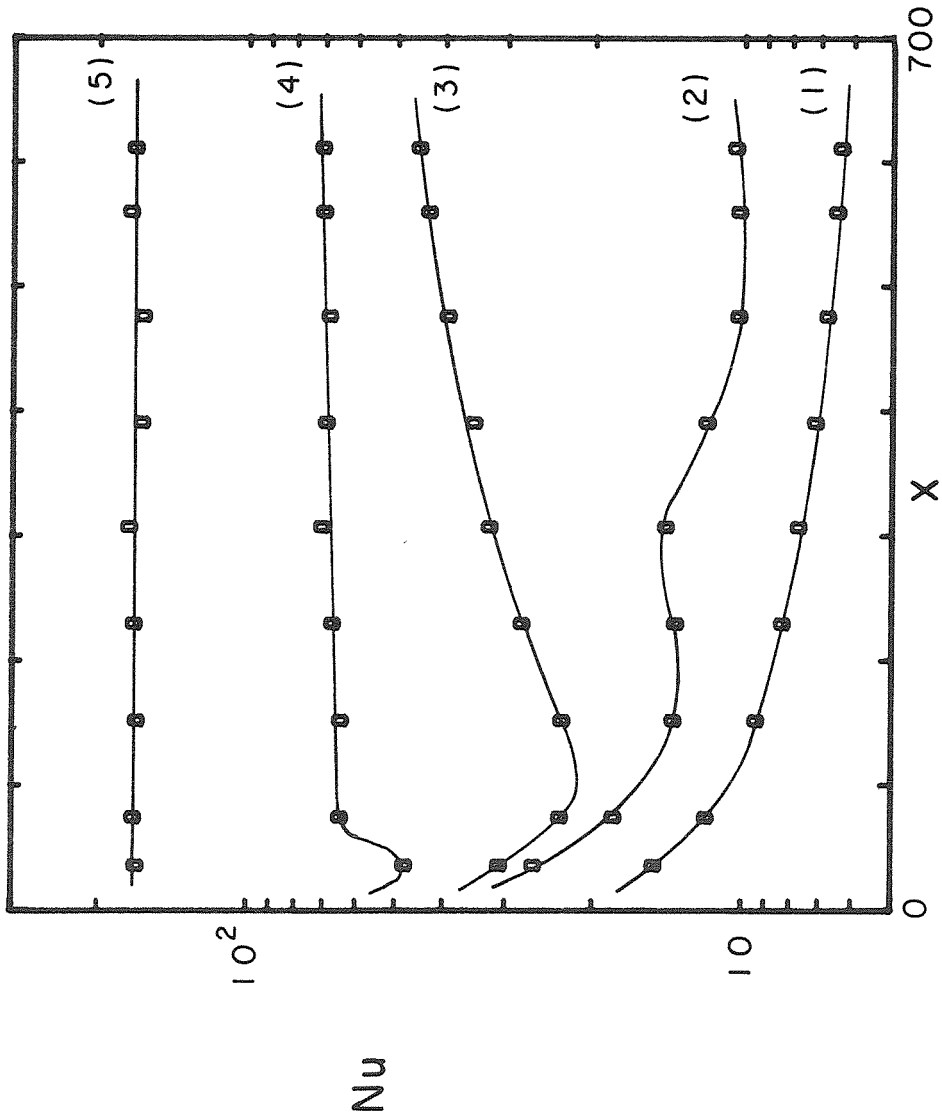

Figure 5.5.-6: Heat transfer results as a function of distance for bentonite suspensions. Curve (1): Re' = 530 (Pr' = 90); (2): 2460 (50); (3): 2730 (46); (4): 3230 (40); (5): 9650 (22). (Wall temperature reference, 5% .)

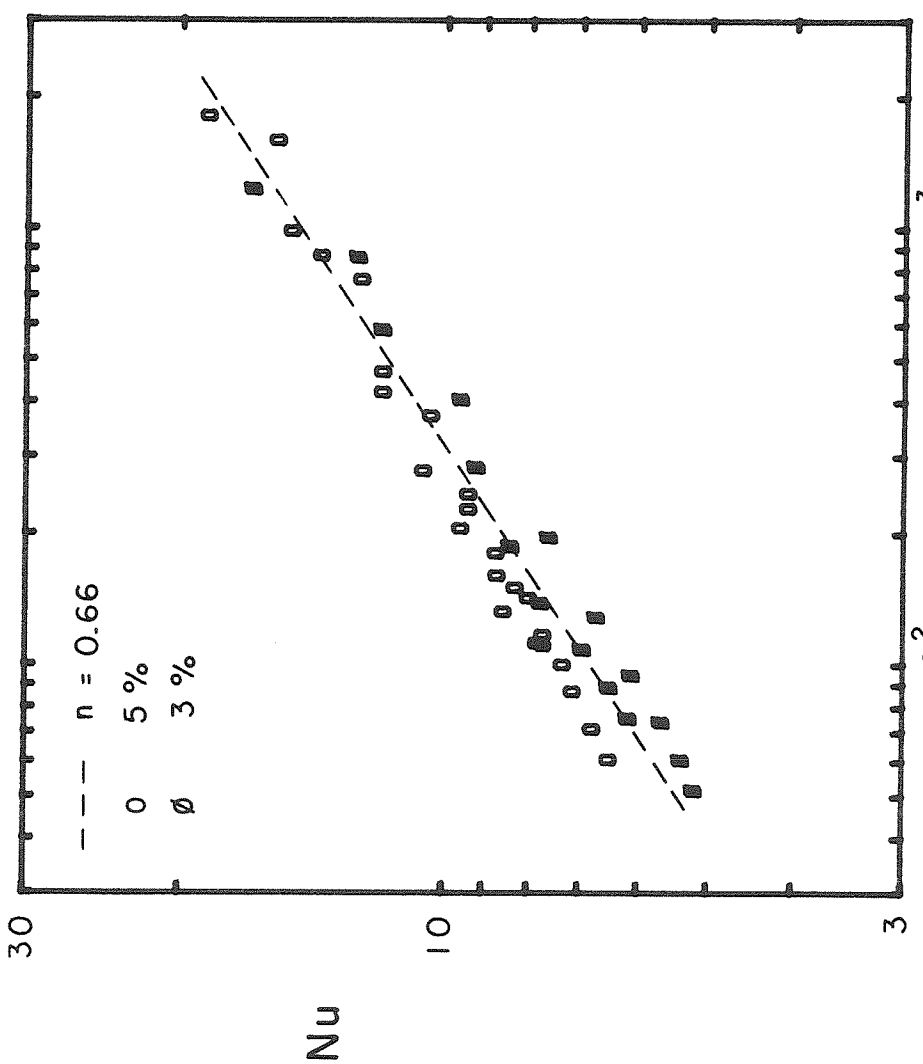

Figure 5.5.-7: Correlation of laminar heat transfer results for bentonite suspensions in the entrance region. Also shown is Bird's expression for n = 0.66. (Wall temperature reference, 3% and 5% .)

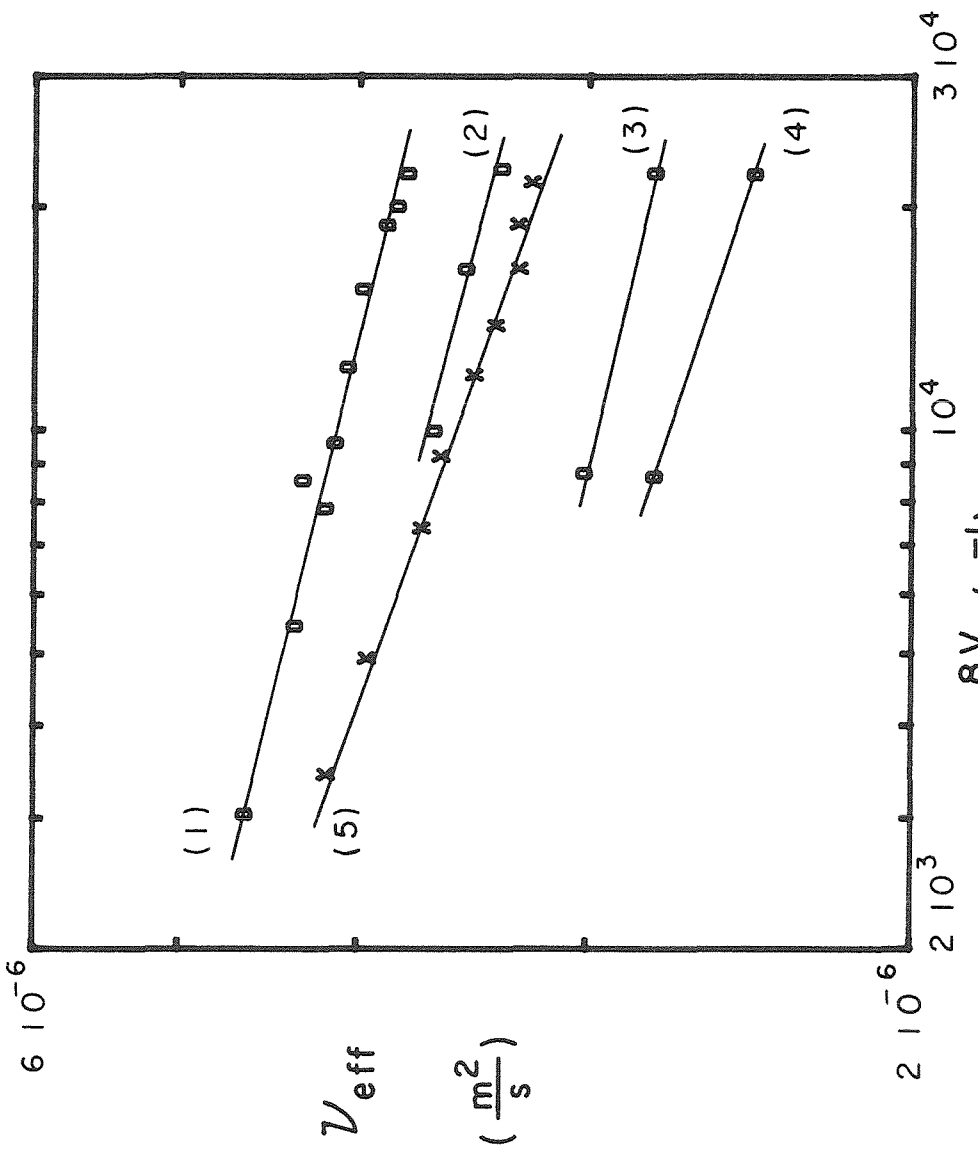

Figure 5.6-1: Viscosity functions of a combination of bentonite and polymer. Curve (1): unused sample (measured at 23.2 °C); (2), (3), and (4): manually degraded (23.2, 23.8, and 23.8 °C); (5): ran at Re_a = 17500 (23.5 °C). (T-20 capillary; 3% bentonite + 20 ppm AP-273.)

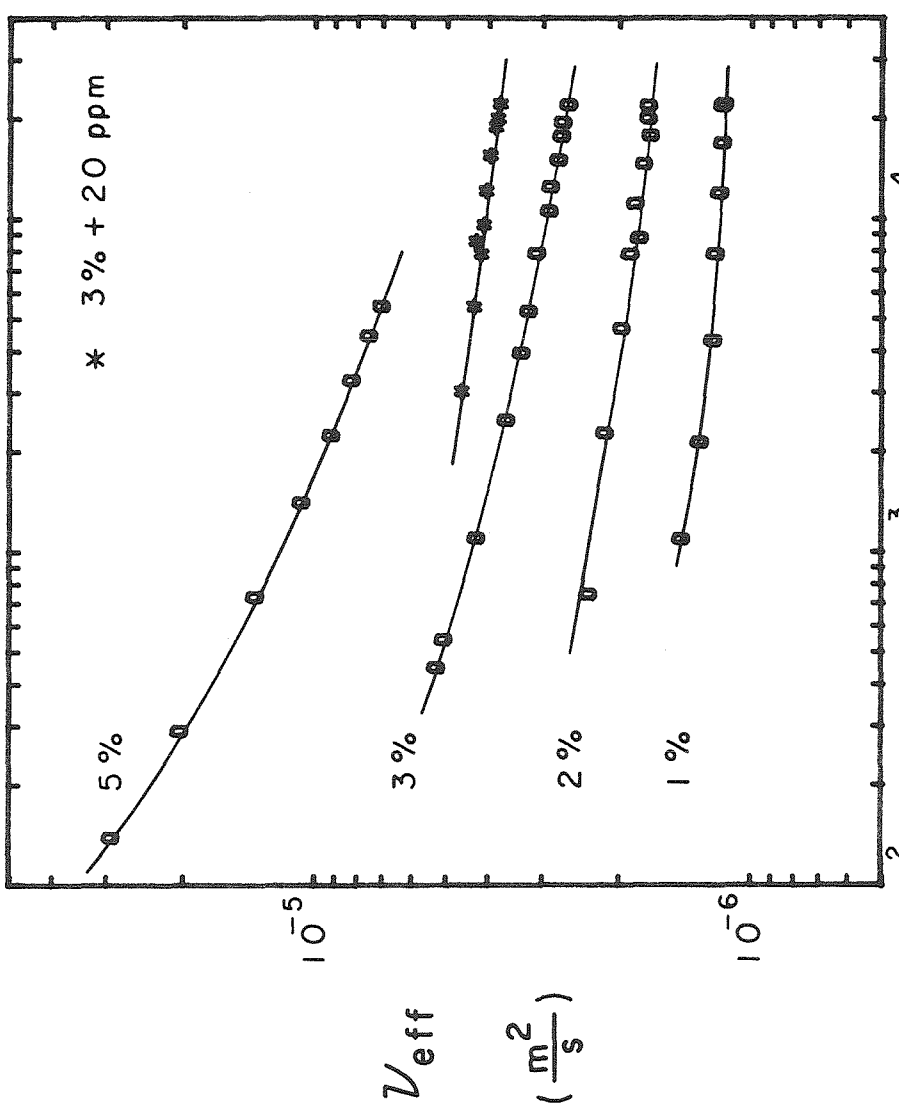

Figure 5.6-2: Comparison of viscosity functions for pure bentonite suspensions and unused combination of bentonite and polymer. Sample of 1% measured at 25.4 °C, 2% at 25.0°C, 3% at 25.1 °C, 5% at 25.2 °C, and 3%+20ppm at 23.2 °C. (T-20 capillary.)

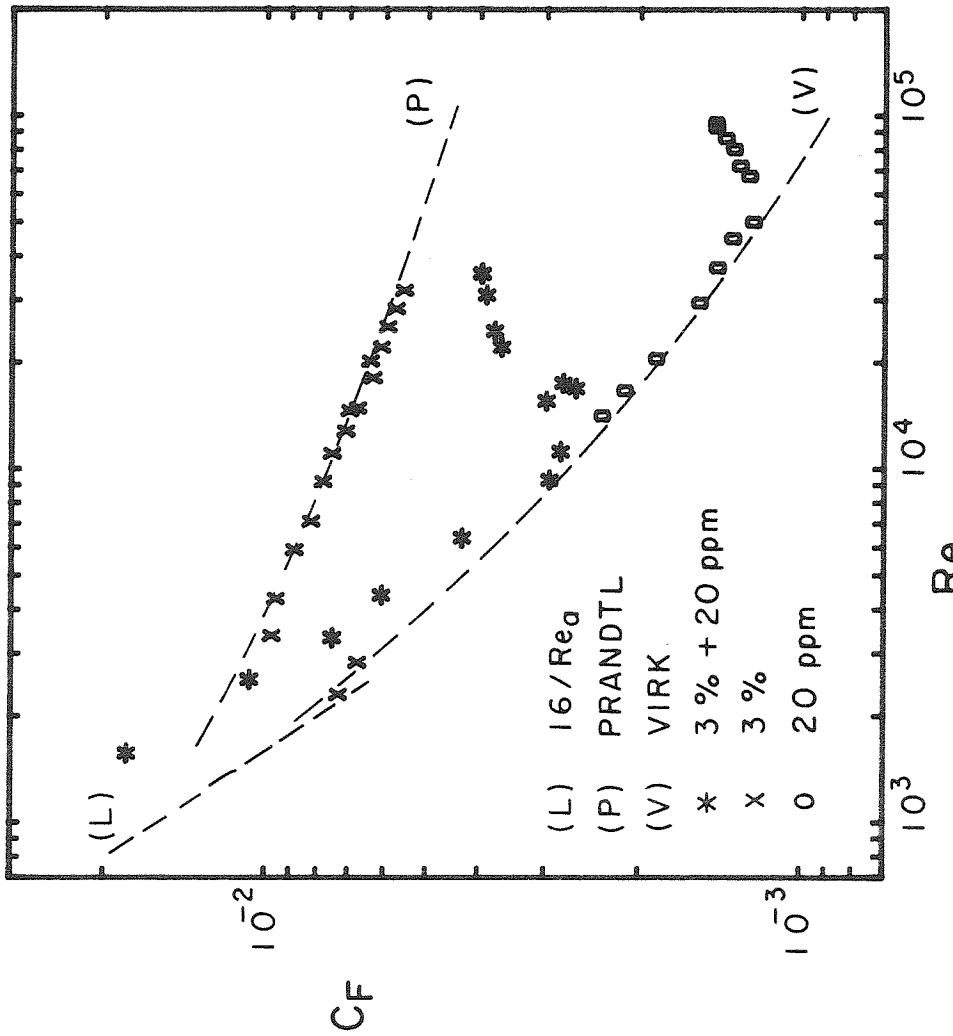

Figure 5.6-3: Comparison of friction results for a polymer solution, a bentonite suspension, and their combination. (Wall temperature reference, degraded viscosity functions, x/D= 560; 20 ppm, 3%, 3%+20ppm.)

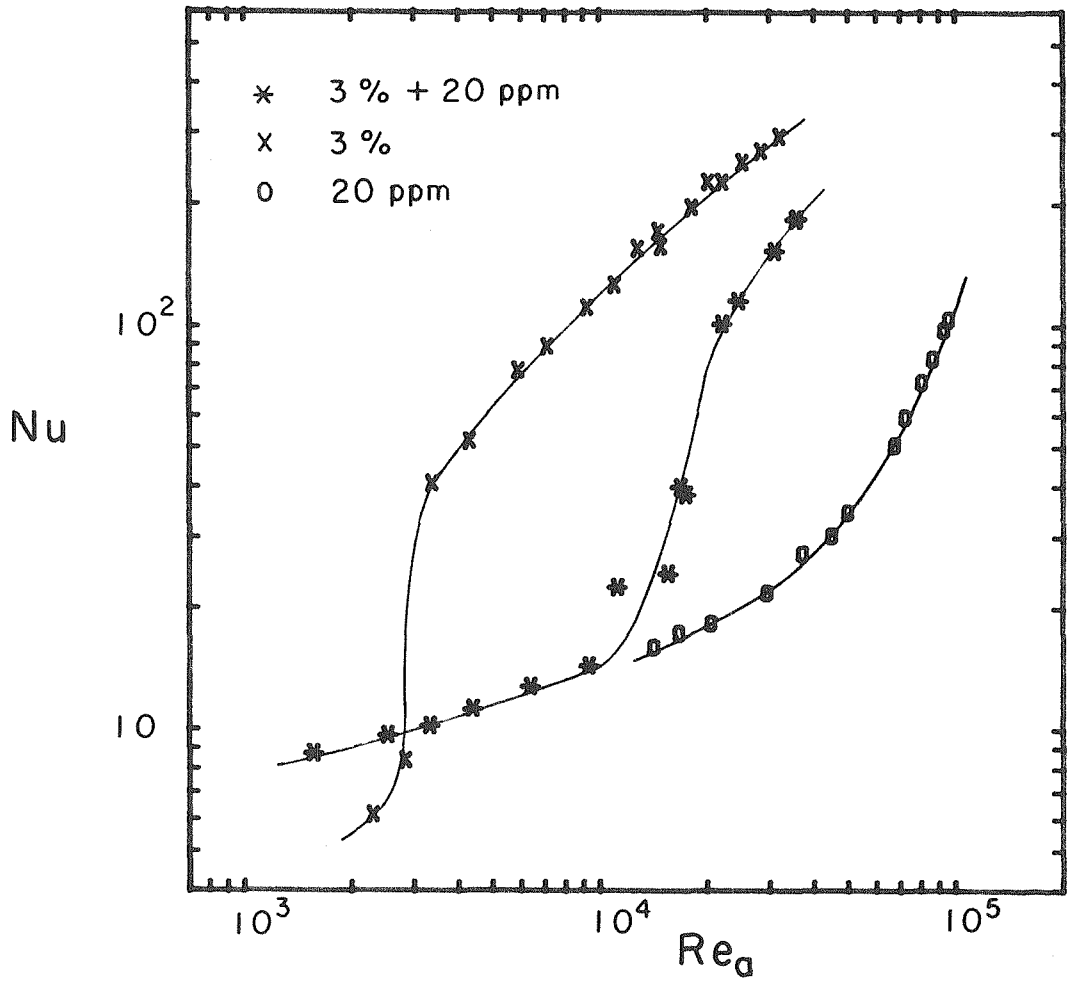

Figure 5.6-4: Comparison of heat transfer results for a polymer solution, a bentonite suspension, and their combination. (Wall temperature reference, degraded viscosity functions, x/D= 560; 20 ppm, 3%, 3%+20ppm.)

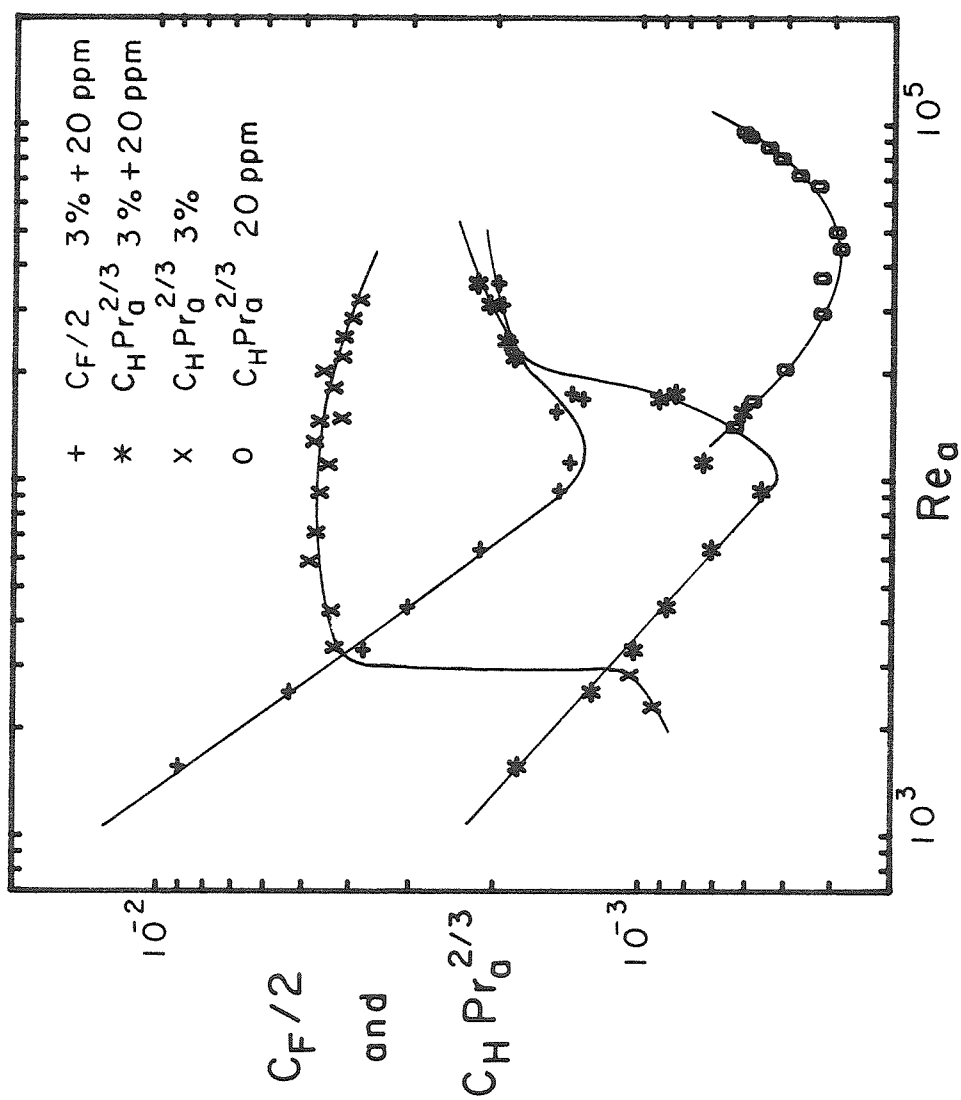

Figure 5.6-5: Comparison of friction and heat transfer results for a combination of polymer and bentonite. (Wall temperature reference, degraded viscosity functions, x/D= 560; 20 ppm, 3%, 3%+20ppm.)

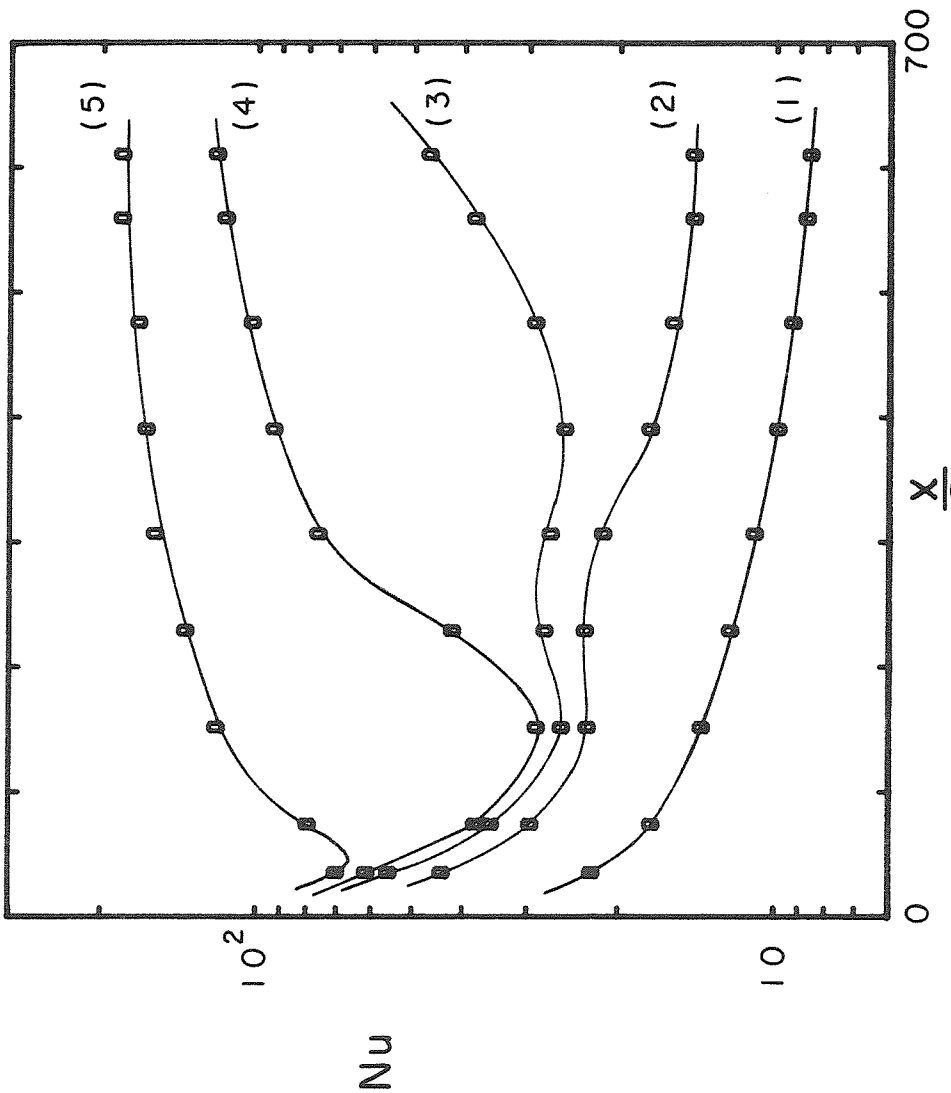

Figure 5.6-6: Heat transfer results as a function of distance for a combination of polymer and bentonite. Curve (1): Re_a = 1560 (Pr_a = 30.2); (2): 9300 (20.8); (3): 17500 (17.1); (4): 24500 (15.0); (5): 35600 (13.1). (Wall temperature reference, degraded viscosity functions, 3%+20ppm.)

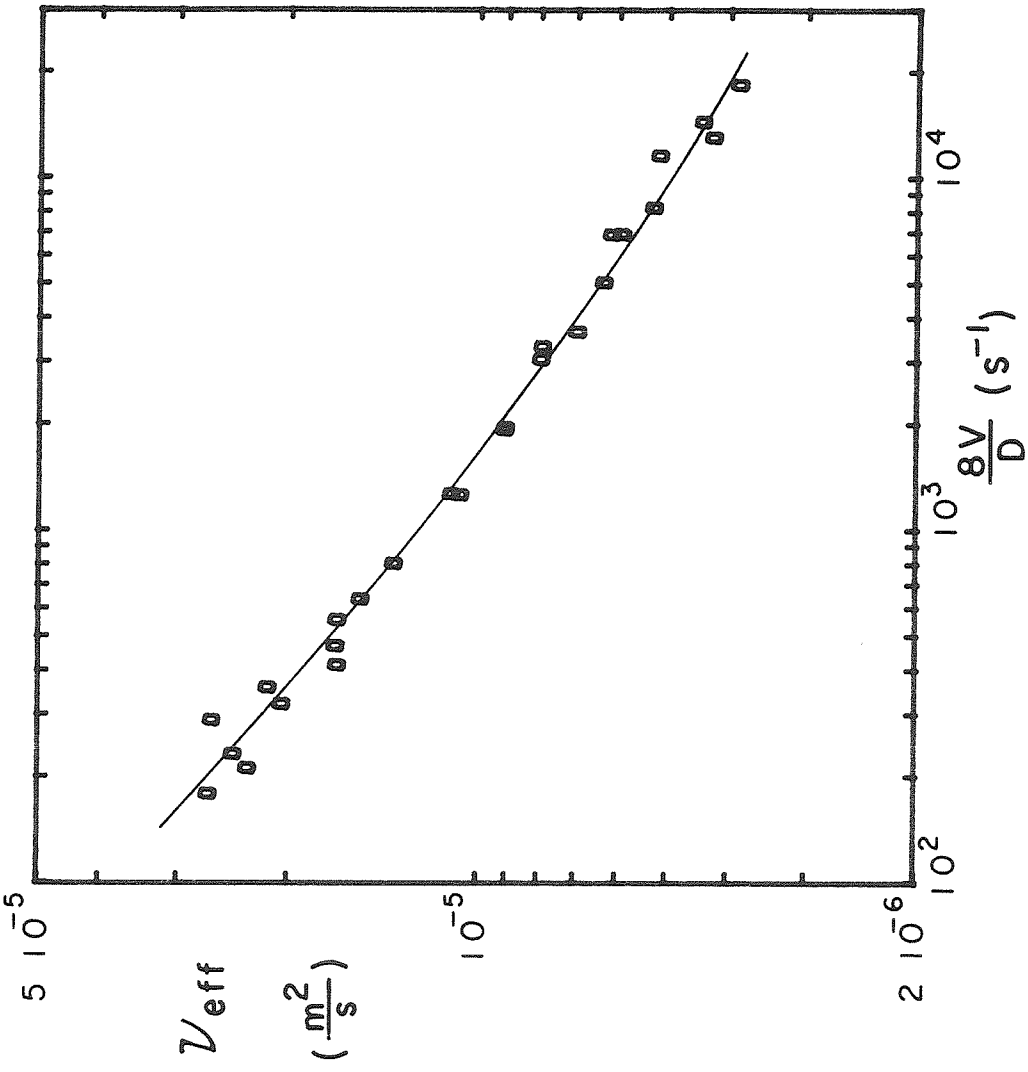

Figure 5.7.-1: Viscosity function of tomato puree. (T-2 capillary, 6% solids, reduced to 25 °C.)

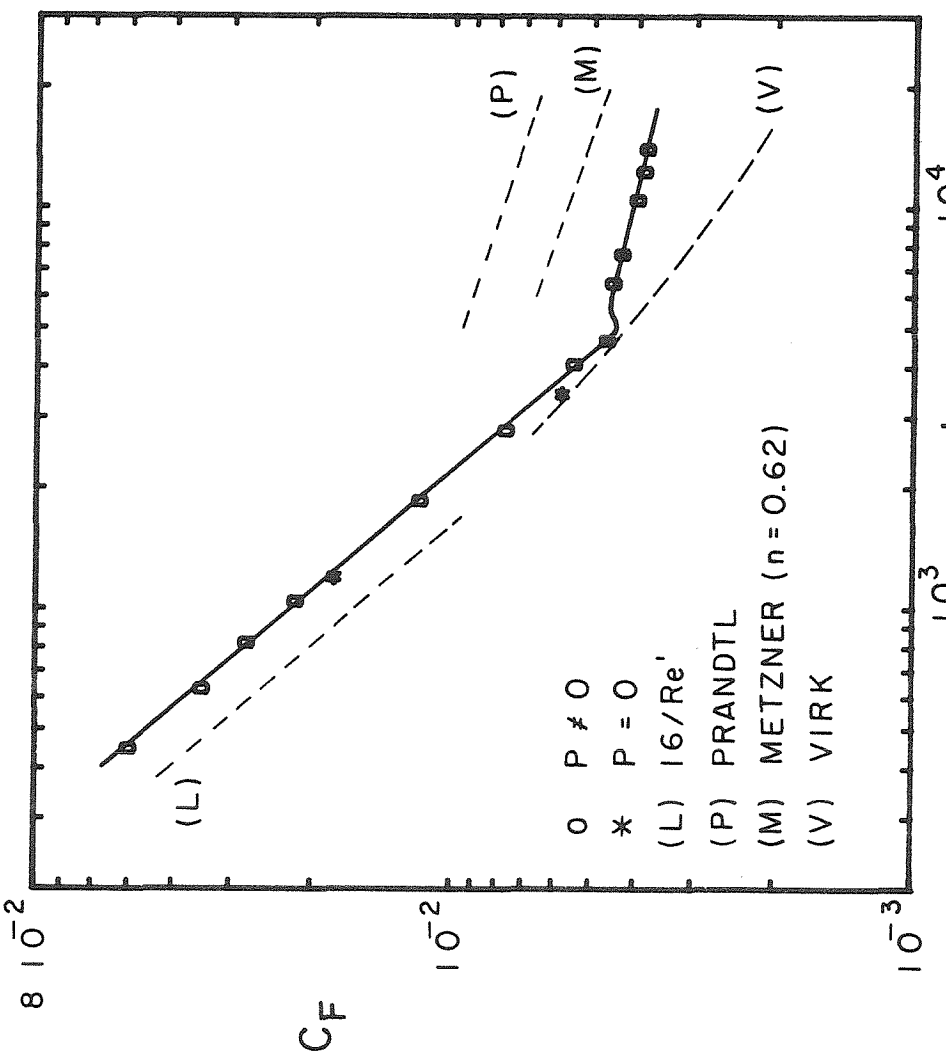

Figure 5.7.-2: Friction results for tomato puree in the generalized Reynolds number representation. Also shown are isothermal results. (Wall temperature reference, 6% solids, averaged over 430 < x/D < 600.)

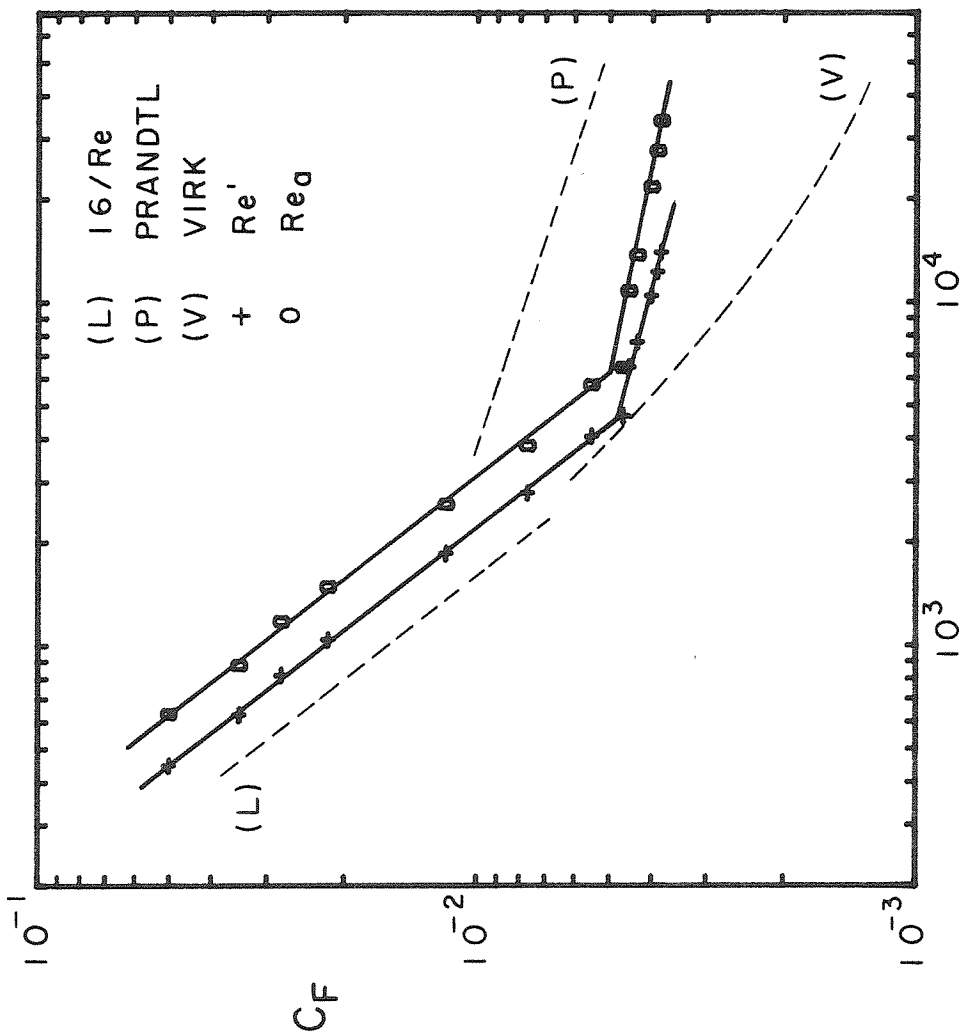

Figure 5.7.-3: Comparison of friction results for tomato puree in the generalized and apparent Reynolds number representations. (Wall temperature reference, averaged over $430 < x/D < 600$, 6% solids.)

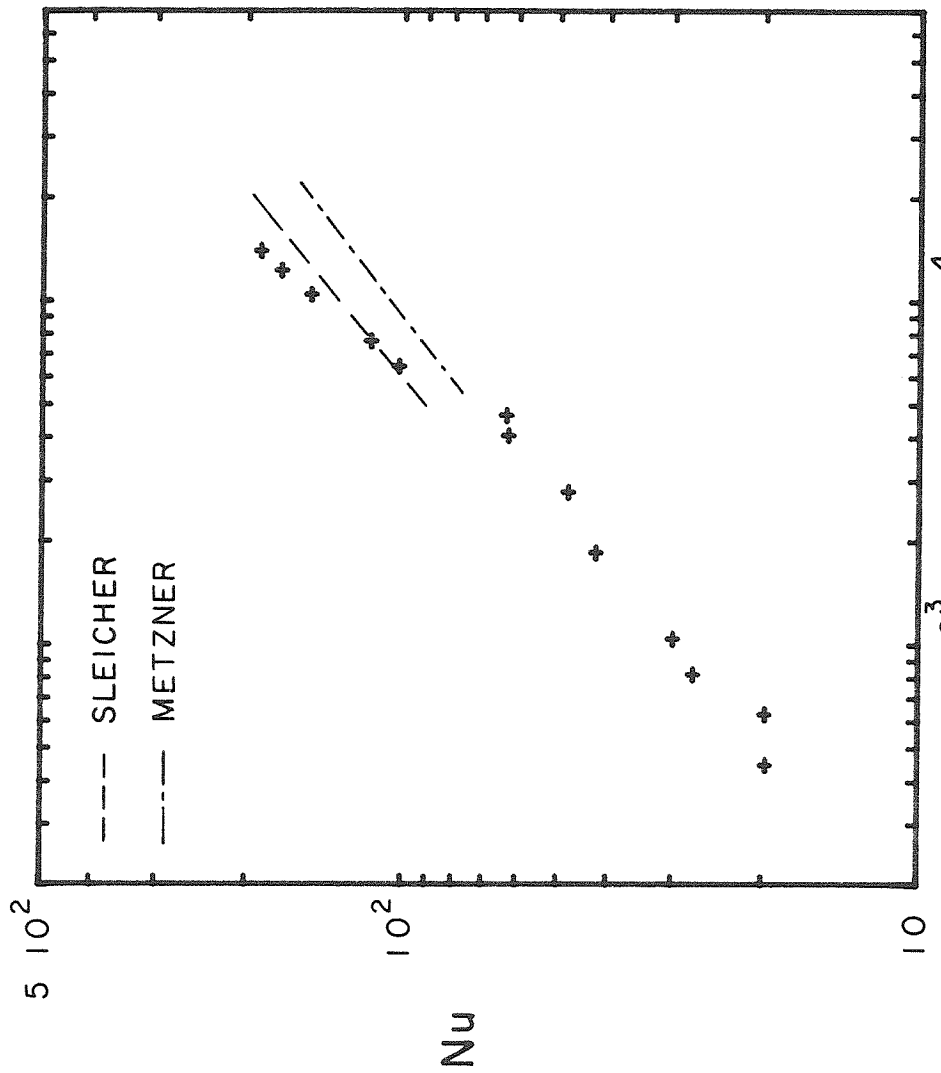

Figure 5.7.-4: Heat transfer results for tomato puree in the generalized Reynolds number representation. (Wall temperature reference, average of x/D= 475 and 560, 6% solids.)

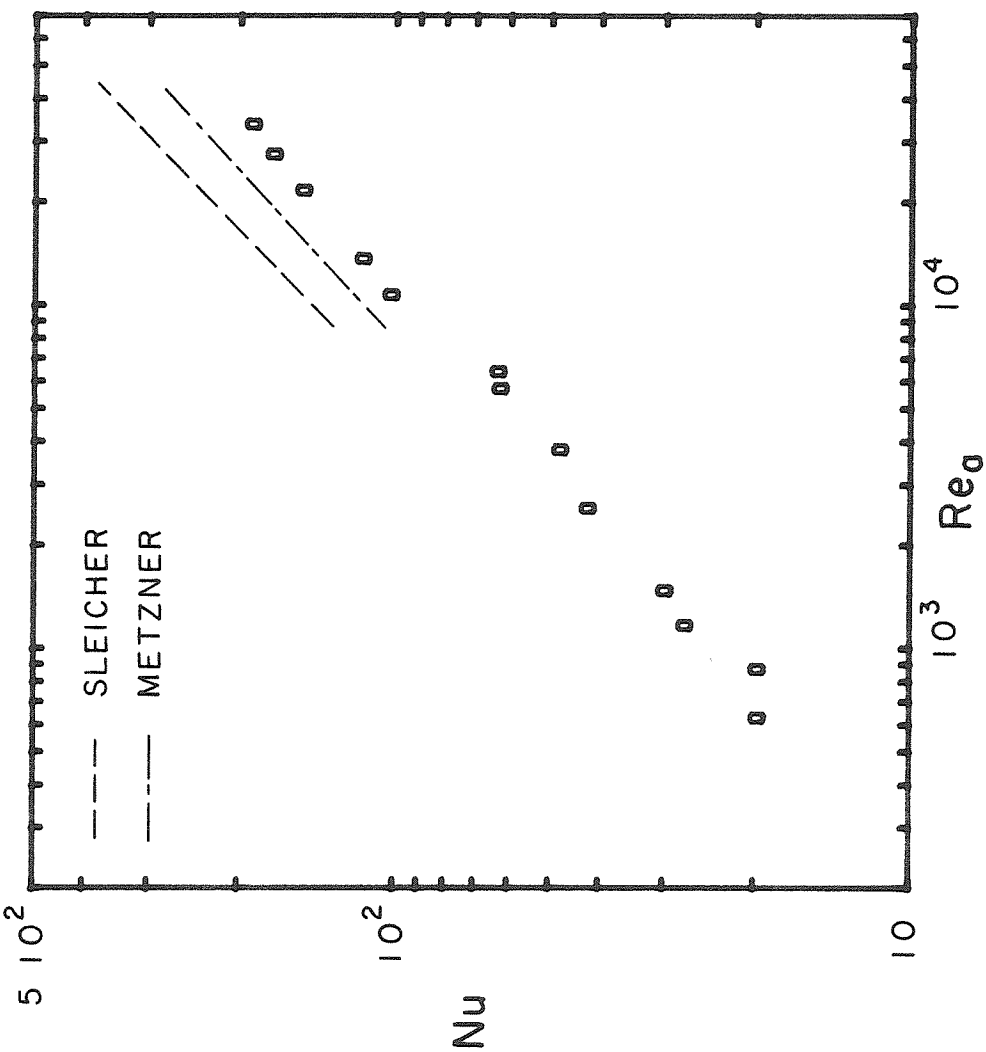

Figure 5.7.-5: Heat transfer results for tomato puree in the apparent Reynolds number representation. (Wall temperature reference, average of x/D= 475 and 560, 6% solids.)

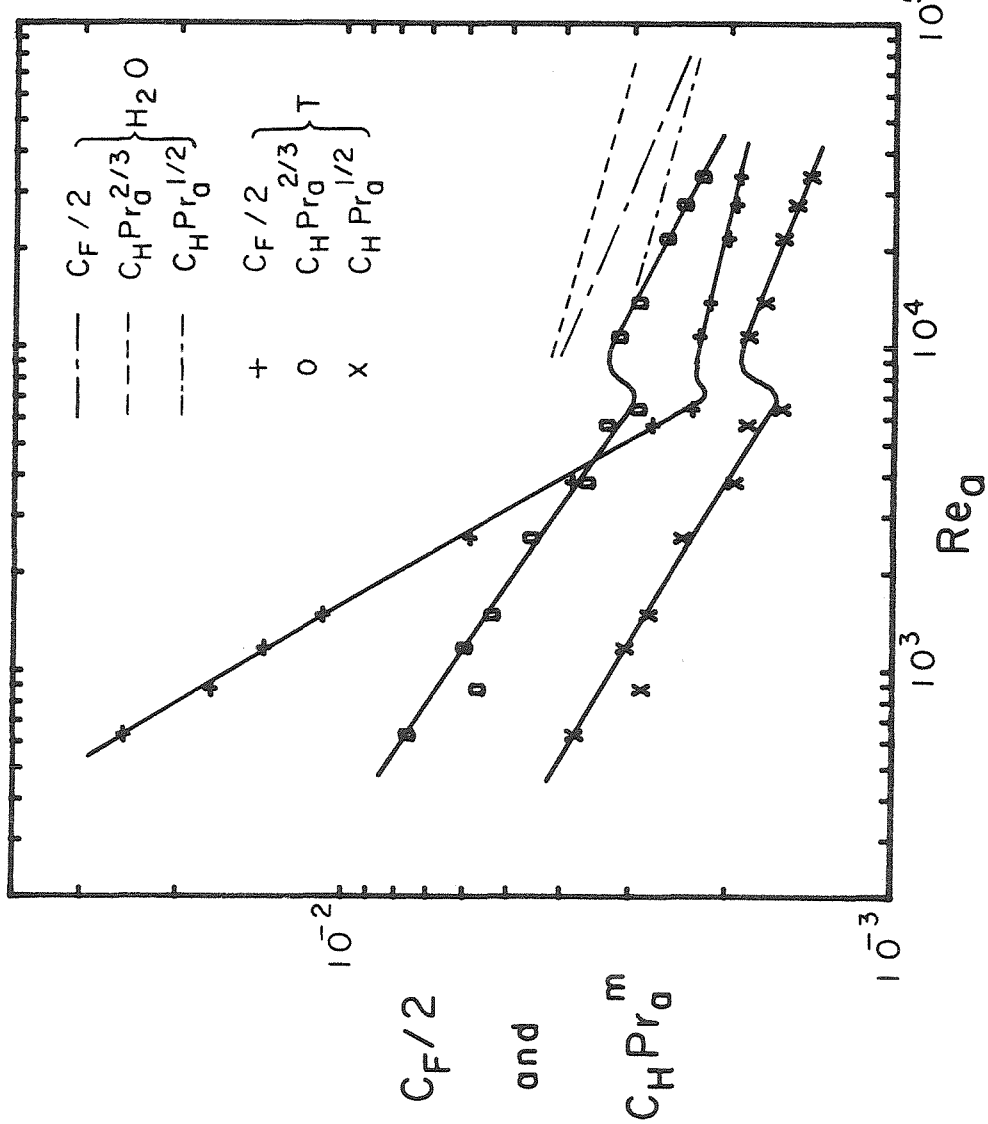

Figure 5.7.-6: Comparison of heat transfer and friction results for tomato puree. (Wall temperature reference, average of x/D= 475 and 560, 6% solids.)

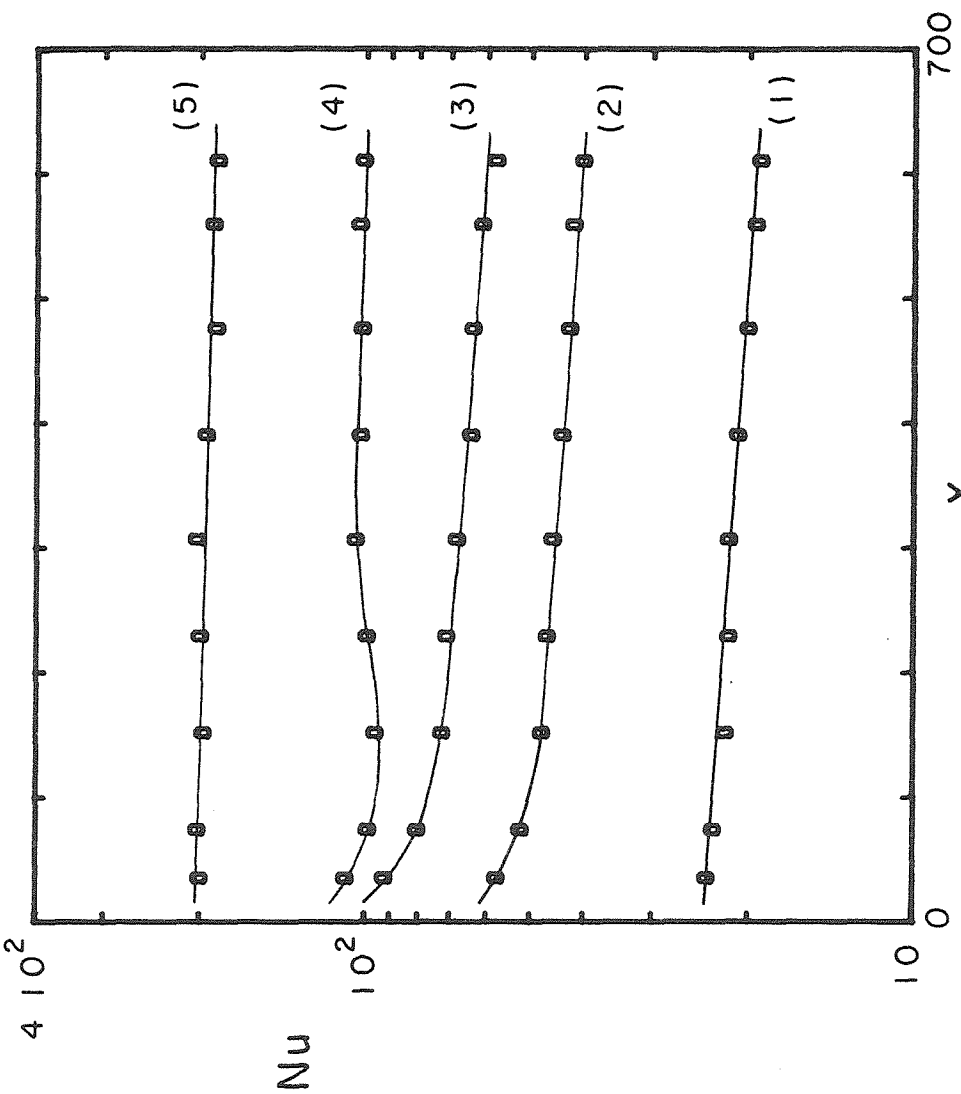

Figure 5.7.-7: Heat transfer as a function of distance for tomato puree. Curve (1): Re_a = 880 (Pr_a = 61.9), (2): 2590 (45.8), (3): 5810 (34.1); (4): 10900 (26.2); (5): 33800 (15.4). (Wall temperature reference, 6% solids.)

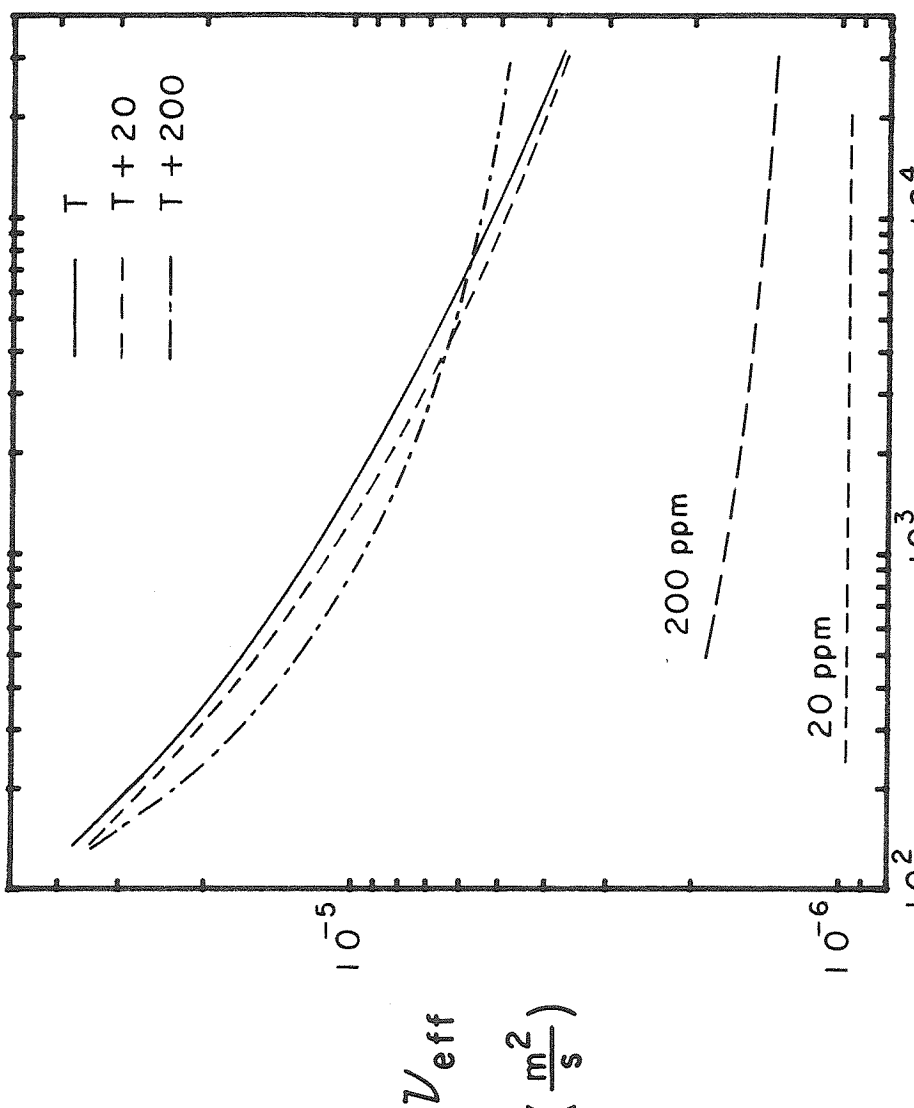

Figure 5.8.-1: Viscosity functions of combinations of tomato puree and polymer. (T-2 capillary; reduced at 25 °C; 6% solids, 6% + 20 ppm AP-273, 6% + 200 ppm.)

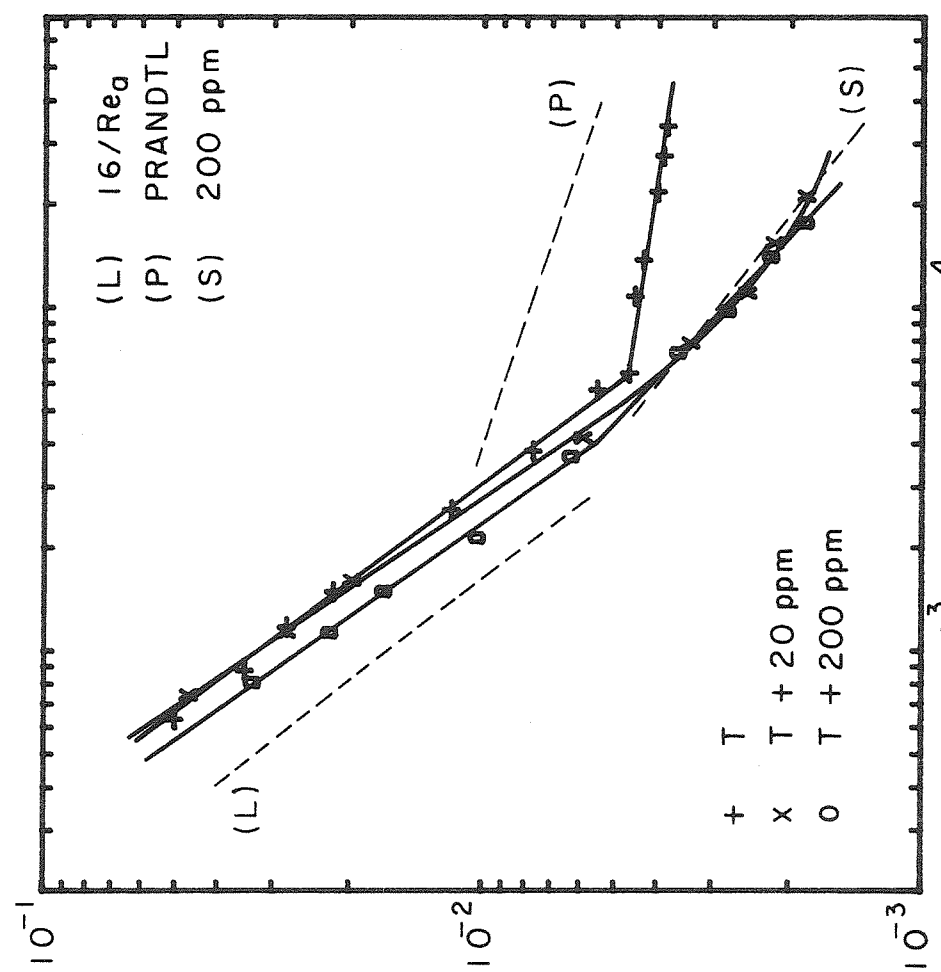

Figure 5.8.-2: Comparison of friction results for various combinations of tomato puree and polymer. (Wall temperature reference; averaged over $430 < x/D < 600$; 6%, 6%+20ppm, 6%+200ppm.)

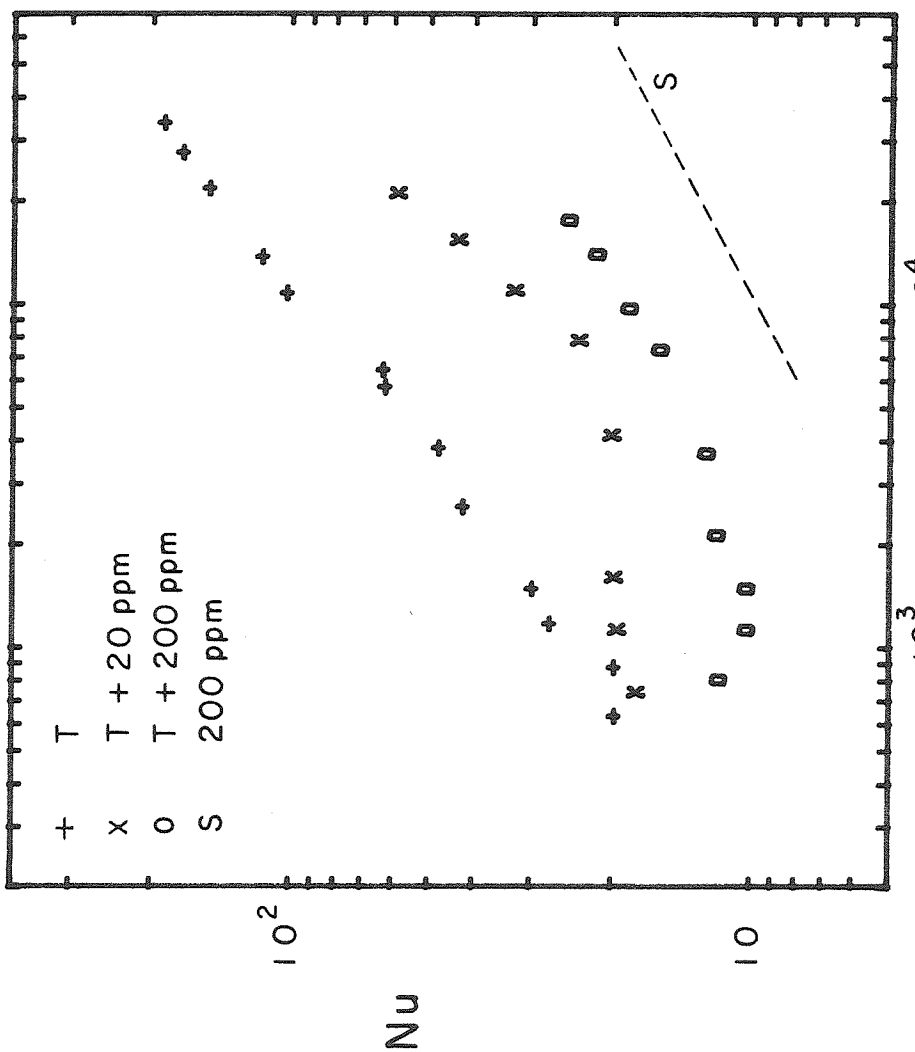

Figure 5.8.-3: Comparison of heat transfer results for various combinations of tomato puree and polymer. (Wall temperature reference; average of x/D= 475 and 560; 6%, 6%+20ppm, 6%+200ppm.)

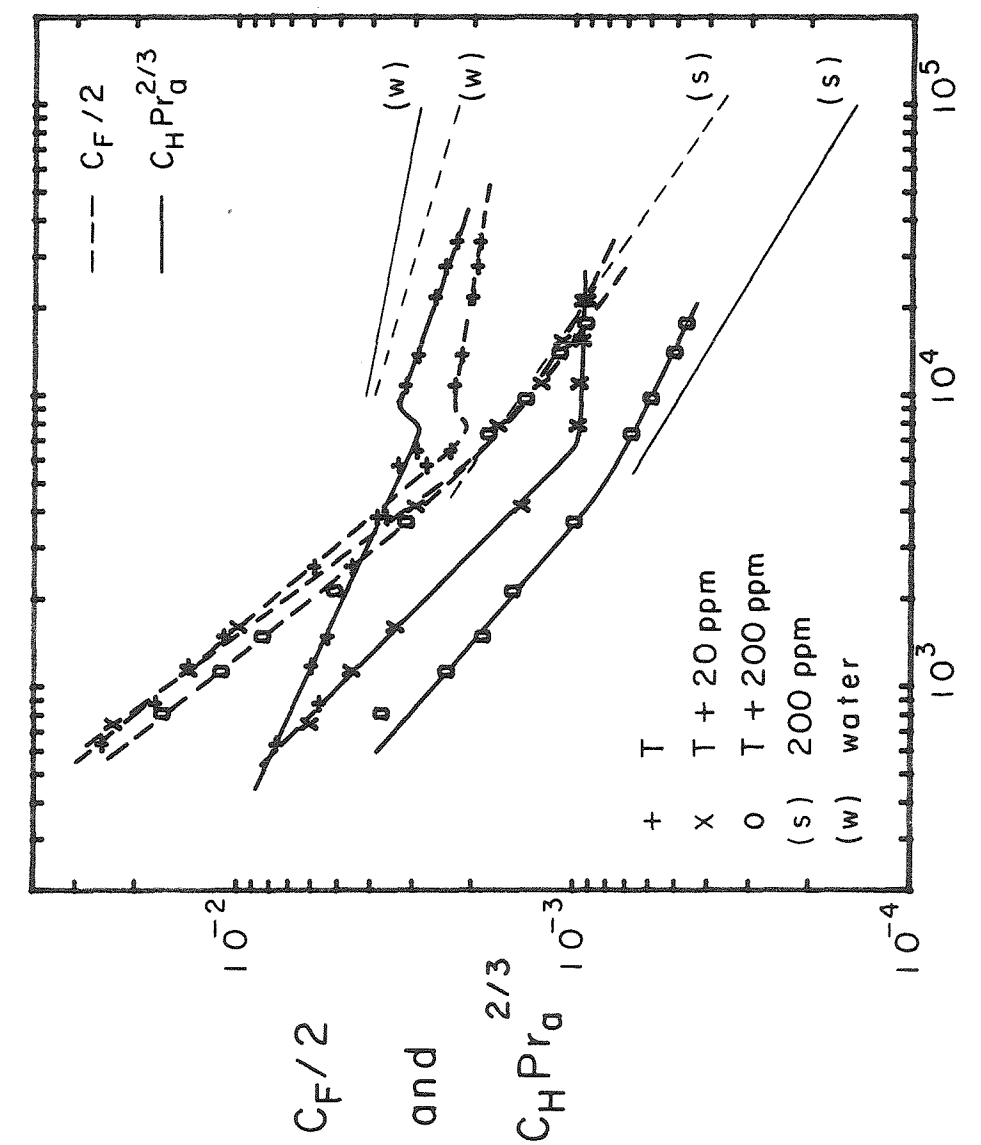

Figure 5.8.-4: Comparison of heat transfer and friction results for various combinations of tomato and polymer. (Wall temperature reference; average of x/D= 475 and 560; 6%, 6%+20ppm, 6%+200ppm.)

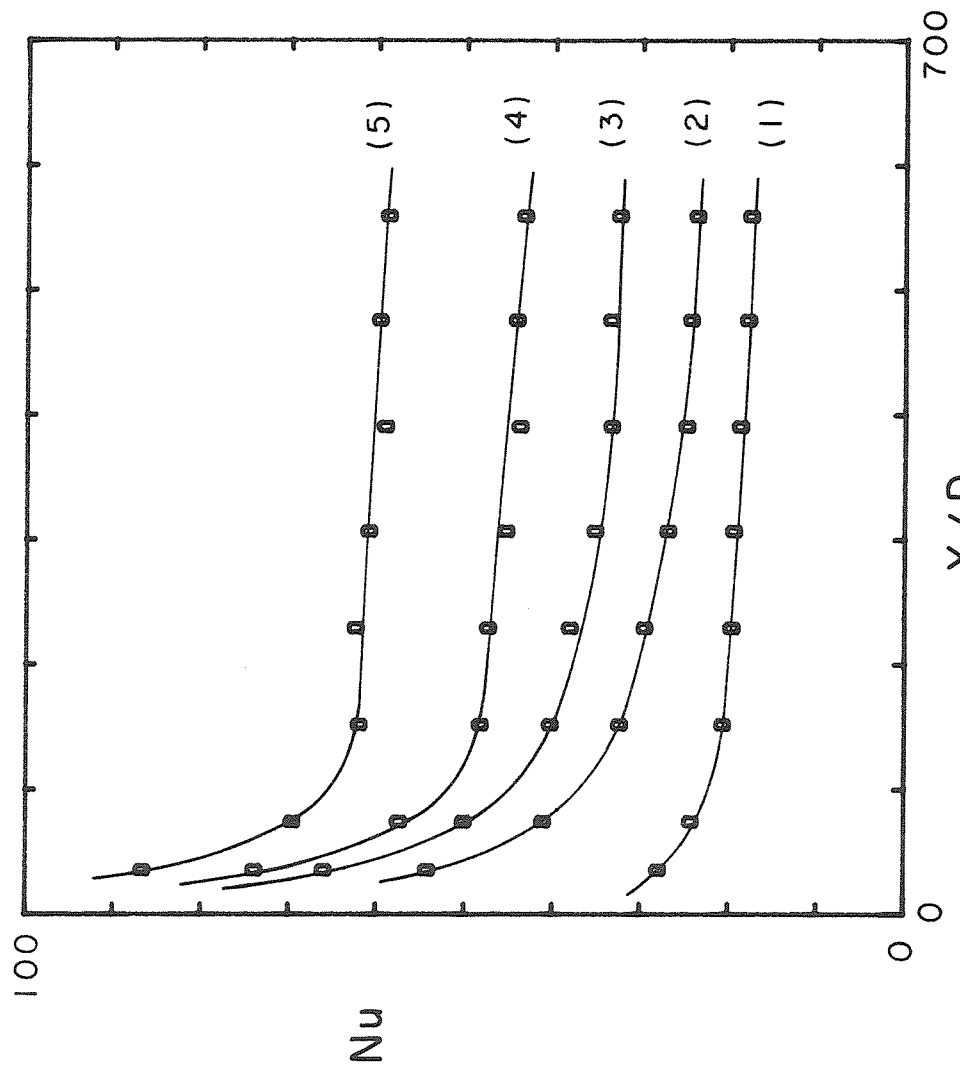

Figure 5.8.-5: Heat transfer as a function of distance for a combination of tomato puree and polymer. Curve (1): Re_a = 745, (Pr_a = 59.2), (2): 7890 (28.8); (3): 11000 (28.7); (4): 15500 (25.6); (5): 21100 (24.9). (Wall temperature reference; 6%+20ppm.)

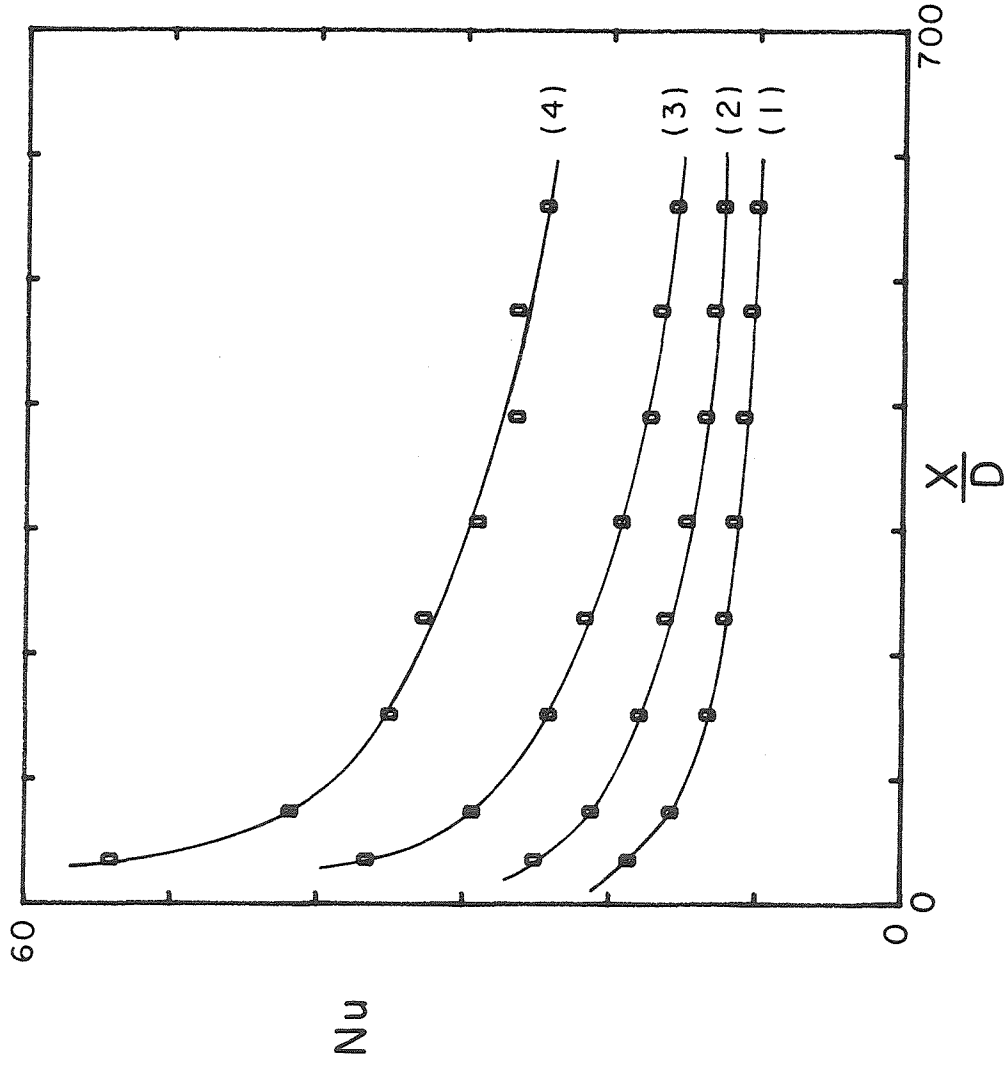

Figure 5.8.-6: Heat transfer as a function of distance for a combination of tomato puree and polymer. Curve (1): $Re_a = 1130$ ($Pr_a = 54.2$); (2): 3680 (38.8); (3): 7380 (31.3); (4): 17670 (27.6). (Wall temperature reference; 6%+200ppm.)

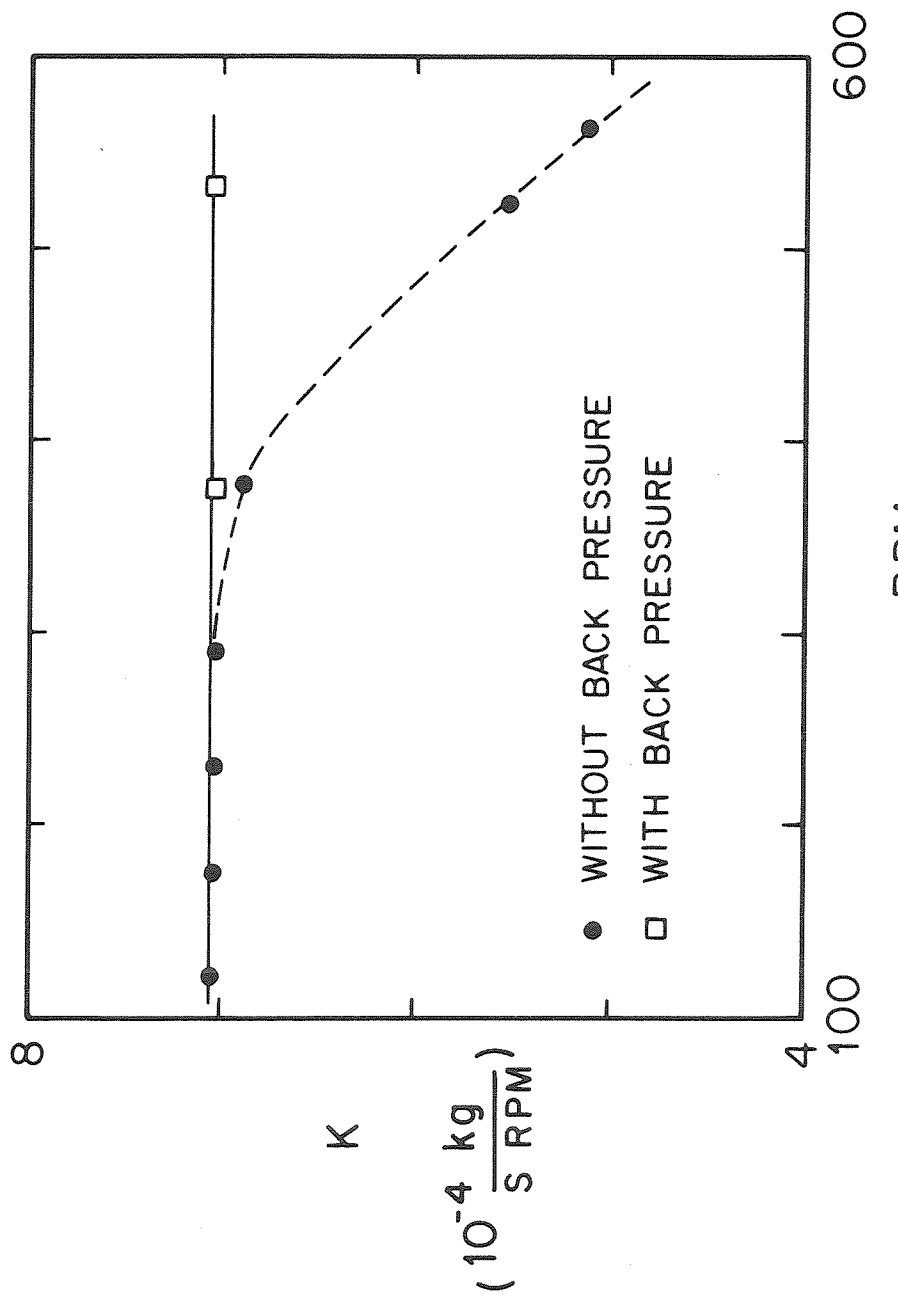

Figure B.1: Influence of back pressure on mass flow rate vs motor speed relationship.